

**STRUCTURAL INSIGHTS INTO THE
SELF-ASSEMBLY OF BIOINSPIRED
SPIDER SILK PROTEINS**

DISSERTATION

zur Erlangung des Grades einer
Doktorin der Naturwissenschaften
(Dr. rer. nat.)

in der Bayreuther Graduiertenschule
für Mathematik und Naturwissenschaften (BayNAT)
der Universität Bayreuth

vorgelegt von
MERISA SARIC
aus Bayreuth

Bayreuth 2023

This doctoral thesis was prepared at the department of Biomaterials at the University of Bayreuth from April 2017 until December 2022 and was supervised by Prof. Dr. Thomas Scheibel.

This is a full reprint of the dissertation submitted to obtain the academic degree of Doctor of Natural Sciences (Dr. rer. nat.) and approved by the Bayreuth Graduate School of Mathematical and Natural Sciences (BayNAT) of the University of Bayreuth.

Form of thesis:	Cumulative thesis
Date of submission:	21.04.2023
Date of approval:	10.05.2023
Date of defense:	16.11.2023

Acting director:	Prof. Dr. Jürgen Köhler
------------------	-------------------------

Doctoral committee:	Prof. Dr. Thomas Scheibel	(reviewer)
	Prof. Dr. Holger Kress	(reviewer)
	Prof. Dr. Stefan Geimer	(chairman)
	Prof. Dr. Andreas Möglich	

In nature, nothing is perfect and everything is perfect.

- Alice Walker -

TABLE OF CONTENTS

LIST OF FIGURES	I
LIST OF TABLES	II
LIST OF SYMBOLS AND ABBREVIATIONS	III
SUMMARY	1
ZUSAMMENFASSUNG	3
1 INTRODUCTION	7
1.1 NATURE AS A BLUEPRINT: MIMICKING NATURAL STRUCTURES TO DESIGN BIOINSPIRED MATERIALS	7
1.2 SILK.....	9
1.3 SPIDER SILK.....	11
1.4 HIERARCHICAL STRUCTURE OF MAJOR AMPULLATE SILK FIBERS.....	14
1.5 NATURAL MAJOR AMPULLATE SILK PROTEINS	17
1.5.1 REPETITIVE CORE DOMAIN.....	19
1.5.2 NON-REPETITIVE TERMINAL DOMAINS.....	22
1.6 NATURAL SILK SPINNING PROCESS.....	23
1.7 SEQUENCE-STRUCTURE-FUNCTION RELATIONSHIP	25
1.8 ENGINEERING AND ASSEMBLY OF SPIDER SILK FOR MATERIAL APPLICATIONS ..	27
1.8.1 RECOMBINANT SPIDER SILK PROTEINS.....	30
1.8.2 SELF-ASSEMBLY PROPERTIES OF ENGINEERED ADF3 AND ADF4	32
1.8.3 ARTIFICIAL SPIDER SILK FIBER SPINNING	34
2 AIM OF THE WORK	41
3 SYNOPSIS	43
3.1 PRODUCTION OF NATURE-LIKE RECOMBINANT SPIDER SILK PROTEINS	45
3.2 STRUCTURAL AND FUNCTIONAL CHARACTERIZATION OF SPIDROIN INTERPLAY AND ASSEMBLY IN A MULTI-COMPONENT APPROACH.....	48
3.3 TWO-IN-ONE SPIDER SILK WITH MULTIFUNCTIONAL PROPERTIES	53

3.4 STRUCTURAL CHARACTERIZATION OF HIGHLY-CONCENTRATED AQUEOUS SPINNING DOPES AND FIBERS	55
4 REFERENCES	59
5 PUBLICATION LIST	77
6 INDIVIDUAL CONTRIBUTION TO PUBLICATIONS	78
PUBLICATIONS	81
Publication I Engineering of silk proteins for materials applications	81
Publication II Interplay of Different Major Ampullate Spidroins during Assembly and Implications for Fiber Mechanics	91
Publication III Two-In-One Spider Silk Protein with Combined Mechanical Features in All- Aqueous Spun Fibers	113
Publication IV Tyrosine’s Unique Role in the Hierarchical Assembly of Recombinant Spider Silk Proteins: From Spinning Dope to Fibers	127
DANKSAGUNG	149
EIDESSTATTLICHE VERSICHERUNGEN UND ERKLÄRUNGEN	151

LIST OF FIGURES

FIGURE 1. CYCLES OF INNOVATIONS AND ENTREPRENEURSHIP ACROSS 250 YEAR.....	7
FIGURE 2. SCHEMATIC CLASSIFICATION OF DIFFERENT SILK TYPES PRODUCED BY FEMALE ORB-WEAVING SPIDERS FOR SEVERAL USES	12
FIGURE 3. HIERARCHICAL STRUCTURE OF THE SPIDERS' DRAGLINE SILK AND ITS' MECHANICAL PROPERTIES	15
FIGURE 4. SETUP OF SPIDER SILK PROTEINS AND COMMON STRUCTURAL MOTIFS.....	18
FIGURE 5. SCHEMATIC REPRESENTATION OF THE NATURAL SPINNING PROCESS OF SPIDER DRAGLINE SILK.....	24
FIGURE 6. CHARACTERISTIC TENSILE PROPERTIES OF SPIDER SILK FIBER	26
FIGURE 7. SELECTED APPROACHES OF MOLECULAR ENGINEERING TO COMBINE FUNCTIONAL MOTIFS INTO RECOMBINANT SILK PROTEINS	29
FIGURE 8. SCHEMATIC ILLUSTRATION OF THE BIOTECHNOLOGICAL PRODUCTION AND PROCESSING OF RECOMBINANT SPIDER SILK	31
FIGURE 9. PRODUCTION STRATEGY OF AQUEOUS SPINNING DOPES MADE OF RECOMBINANT SPIDROINS COMPRISING TERMINAL DOMAINS.	36
FIGURE 10. OVERVIEW OF THE THESIS TOPICS UNRAVELING THE NATIVE SPIDER SILK SPINNING PROCESS USING DIFFERENT RECOMBINANT SILK PROTEIN VARIANTS.	43
FIGURE 11. OVERVIEW OF THE RECOMBINANT SPIDROINS DERIVED FROM THE MASP2 ANALOGS.....	47
FIGURE 12. PRODUCTION AND SELF-ASSEMBLY OF RECOMBINANT FULL-LENGTH SILK PROTEINS.....	49
FIGURE 13. BIOINSPIRED FIBER PRODUCTION STRATEGY USING A MICROFLUIDIC SETUP TO MIMIC THE KEY FACTORS OF SPIDERS' NATURAL SPINNING PROCESS.....	51
FIGURE 14. REAL STRESS-STRAIN CURVES OF ARTIFICIAL AND NATURAL SPIDER SILK FIBERS.....	52
FIGURE 15. SELF-ASSEMBLY OF DIFFERENT SPIDROIN VARIANTS	54
FIGURE 16. DLS OF BSD (A) AND CSD (B).....	56
FIGURE 17. LIGHT MICROSCOPY IMAGES OF BSD (TOP, I–III) AND CSD (BOTTOM, IV–VI), BOTH AT A CONCENTRATION OF 100 MG/ML.....	57

LIST OF TABLES

TABLE 1. TENSILE MECHANICAL PROPERTIES OF (A) NATURAL IN COMPARISON TO (B) SYNTHETIC MATERIALS.	10
TABLE 2. COMPARISON OF MECHANICAL PROPERTIES OF SELECTED SPIDER SILK TYPES FROM DIFFERENT SPIDER SPECIES	13
TABLE 3. EXAMPLES FOR STRUCTURAL MOTIFS OF CORE DOMAINS FROM VARIOUS MAJOR AMPULLATE SPIDROINS (MASp) AND DIFFERENT SPIDER SPECIES.	21
TABLE 4. COMPARISON OF THE CHARACTERISTICS OF MAN-MADE FIBERS FROM VARIOUS SPIDER SILK PROTEINS (WITH OR WITHOUT TDS) SPUN BY WET-SPINNING (W) OR MICROFLUIDICS (M).	37

LIST OF SYMBOLS AND ABBREVIATIONS

ADF	<i>Araneus diadematus</i> Fibroin
AFM	Atomic force microscopy
β -ME	β -Mercaptoethanol
BSD	Biomimetic spinning dope
CD	Circular dichroism
CSD	Classical spinning dope
CTD	Carboxyl-terminal domain
Da	Dalton
DLS	Dynamic light scattering
eADF	Engineered ADF
<i>E. coli</i>	<i>Escherichia coli</i>
EtOH	Ethanol
FTIR	Fourier-transform infrared spectroscopy
FSD	Fourier self-deconvolution
HFIP	1,1,1,3,3,3-Hexafluoropropan-2-ol
IEC	Ion exchange chromatography
IMAC	Immobilized metal ion affinity chromatography
IPA	Isopropyl alcohol
KP	Potassium phosphate
M	Molar
MA	Major Ampullate
MaSp	Major ampullate spidroin
MeOH	Methanol
MW	Molecular weight
n. a.	Not available
NMR	Nuclear magnetic resonance
NTD	Amino-terminal domain
PAGE	Polyacrylamide gel electrophoresis
PEG	Polyethylene glycol
RH	Relative humidity
rpm	Revolutions per minute
rt	Room temperature
sc	supercontracted
SEM	Scanning electron microscopy
TEM	Transmission electron microscopy
ThT	Thioflavin T
TIO	Two-in-one
Tris	Tris(hydroxymethyl)aminomethane
UV	Ultraviolet
w/v	Weight per volume
Θ	Ellipticity

SUMMARY

Stronger than steel, tougher than Kevlar – native spider silk fibers exhibit outstanding mechanical properties unmatched by most other known natural or synthetic fibrous materials. Combined with lightweight, biocompatibility, and biodegradability, spider silk represents an unprecedented material with potential for a multitude of applications in emerging technical and biomedical fields.

Among all spider silk types, dragline silk, also known as major ampullate (MA) silk, is the most extensively studied and contains at least two proteins, so-called major ampullate spidroins (MaSps). MaSps comprise a tripartite structure of a large repetitive core domain, flanked by small non-repetitive amino- and carboxyl-terminal domains (NTD and CTD). While the core domain determines the mechanical properties of the final fiber, the terminal domains (TDs) play an essential role during the spinning process. Most prominent spidroins are MaSp1 and MaSp2, which differ mainly in their proline content (MaSp1 < 0.4%, MaSp2 > 10%). As a unique attribute of all known orb-weaver spiders, the dragline silk of *Araneus diadematus* contains two MaSp2 variants, named *A. diadematus* fibroin (ADF) 3 and 4, exhibiting significant differences regarding solubility and self-assembly. So far, processing approaches have predominantly used one variant of engineered ADFs, either eADF3 or eADF4.

This work aimed to further unravel the natural spinning process, providing insights into the hierarchical self-assembly and interaction of MaSps in terms of sequence-structure-function relations. Ultimately, the objective was to open new routes for designing biomimetic materials with nature-like properties.

A significant part of this work deals with the study of MaSp interplay with implications for fiber mechanics. Cloning of DNA constructs, production, and purification of different MaSp variants with NTD and CTD was developed and optimized. Mixtures of both spidroins were prepared either by co-production in bacteria (*in vivo*) or by refolding during dialysis (*in vitro*), yielding eADF3 and eADF4 homo- and heterodimers through the dimerization of their CTDs. Structural characterization and self-assembly of protein mixtures and individual one-protein variants were carried out, indicating that TDs control the alignment and molecular interplay into higher-order structures. Aqueous spinning dopes were prepared, and a microfluidic wet-spinning approach was developed mimicking the natural spinning process as close as possible. Fibers were

post-stretched and further studied using tensile tests and microscopy. *In vivo* co-produced mixtures of homo- and heterodimers yielded hierarchically structured nature-like performing fibers. Tensile tests revealed a strength (834 ± 34 MPa), elasticity (32 ± 1 %), Young's modulus (5 ± 0.4 GPa) as well as toughness (143 ± 6 MJm⁻³), representing the best fiber performance from artificially spun spider silk fibers out of all-aqueous spinning systems to date. The heterodimers substantially contributed to the superior fiber mechanics, and their assignments were at least twofold. On the one hand, the heterodimers acted as cross-linkers to mediate between homodimers, on the other hand, they also actively participated in fibril assembly.

The next step was to study hybrid spidroins combining biophysical and biochemical characteristics of eADF3 and eADF4 in one protein. A novel two-in-one (TIO) spidroin in the presence of TDs was engineered, resembling amino acid motifs from both eADF variants. The TIO spidroins were conveniently produced and purified with 25 times higher yields compared to the heterodimers, which were isolated from a mixture of homo- and heterodimers using a two-step chromatographic separation strategy. Detailed analyzes by CD-, fluorescence, and UV/Vis spectroscopy revealed similar structural characteristics in both hybrid variants. In phosphate- and shear-induced assembly experiments the hierarchical self-assembly into β -sheet-rich superstructures was demonstrated. Fibers spun from TIO spidroins using the previously established biomimetic wet-spinning process obtained mechanical properties at least twice as high as fibers spun from individual spidroins or blend.

Another part of the thesis provides investigations of the structural self-assembly of MaSps from highly concentrated aqueous spinning dopes to fibers spun thereof. Spectroscopic and microscopic analyzes of eADF3-CTD spinning dopes revealed that spidroins in biomimetic phosphate-containing dopes transitioned from monomer/dimer equilibrium to micelle-like assemblies gradually over time and ultimately achieved liquid-liquid phase separation. The combination of solution and solid-state NMR analysis of ¹³C/¹⁵N isotopically enriched eADF3-CTD dopes and fibers implicated Tyrosine's importance in the assembly process, in particularly Tyrosine ring packing in non- β -sheet, disordered helical domains.

Overall, this work gives structural insights into the hierarchical self-assembly of MaSps, emphasizing the importance of protein interplay for functional complexity. These findings enabled the production of biomimetic fibers with spider silk-like mechanical properties and paved the way for the development of new silk alternatives, applicable in various high-tech fields.

ZUSAMMENFASSUNG

Stärker als Stahl, zäher als Kevlar - natürliche Spinnenseidenfasern verfügen über einzigartige mechanische Eigenschaften, welche kein anderes natürliches oder synthetisches Fasermaterial erreicht. In Kombination mit geringem Gewicht, Biokompatibilität und biologischer Abbaubarkeit ist Spinnenseide ein beispielloses Material mit großem Potenzial für vielfältige Anwendungen in modernen technischen und biomedizinischen Bereichen.

Von allen Spinnenseidenarten ist die *Dragline* Seide, auch *Major Ampullate* (MA) Seide genannt, am besten untersucht und setzt sich aus mindestens zwei Proteinen zusammen, den so genannten *Major Ampullate* Spidroinen (MaSps). MaSps sind strukturell dreiteilig aufgebaut, bestehend aus einer großen repetitiven Kerndomäne, welche von kleineren nicht repetitiven amino- und carboxy-terminalen Domänen (NTD und CTD) flankiert wird. Während die Kerndomäne die mechanischen Eigenschaften der Faser bestimmt, spielen terminale Domänen (TDs) eine wesentliche Rolle im Verlauf des Spinnprozesses. Die am häufigsten vorkommenden Spidroine MaSp1 und MaSp2, unterscheiden sich hauptsächlich im Prolingehalt (MaSp1 < 0,4 %, MaSp2 > 10 %). Unter allen Radnetzspinnen, besitzt *Araneus diadematus* als einzigartiges Attribut zwei MaSp2-Varianten, die als *A. diadematus* Fibroin (ADF) 3 und 4 bezeichnet werden und sich hinsichtlich Löslichkeit sowie Selbstorganisation maßgeblich voneinander unterscheiden. Bislang wurden in Untersuchungen zur Verarbeitung und Anwendung keine Proteinmischungen, sondern nur einzelne Proteinvarianten, eADF3 oder eADF4 verwendet.

Ziel dieser Arbeit war es, den natürlichen Spinnprozess weiter zu entschlüsseln und Einblicke in die hierarchische Selbstorganisation und Interaktion von MaSps in Abhängigkeit ihrer Sequenz, Struktur und Funktionsbeziehung zu gewinnen. Darauf aufbauend sollten innovative biomimetische Materialien mit naturähnlichen Eigenschaften entwickelt werden.

Ein wesentlicher Teil dieser Arbeit befasst sich mit dem Zusammenspiel unterschiedlicher MaSps und daraus resultierenden Einflüssen auf die Fasermechanik. Der Arbeitsprozess begann mit der Klonierung von DNA-Konstrukten kodierend für unterschiedliche MaSp-Varianten sowie der Entwicklung und Optimierung biotechnologischer Produktions-/Reinigungsstrategien. Im Anschluss wurden Gemische aus eADF3- und eADF4-Varianten entweder durch die Co-Produktion in Bakterien (*in vivo*) oder durch Rückfaltung in der Dialyse (*in vitro*) hergestellt. Die Proteingemische enthielten Homo- und Heterodimere aus eADF3 und eADF4, initiiert durch

dimerisierte CTDs. Des Weiteren wurden die Spidroingemische strukturell charakterisiert und die Selbstassemblierung im Vergleich zu einzelnen Proteinvarianten untersucht, wobei TDs die Ausrichtung und das molekulare Zusammenspiel zu Strukturen höherer Ordnung maßgeblich kontrollierten. Es wurden wässrige Spinnlösungen hergestellt und zu Fasern versponnen, wofür ein mikrofluidisches Nassspinnverfahren etabliert wurde, welches den natürlichen Spinnprozess nachahmt. Die nachgestreckten Fasern wurden mikroskopisch und des Weiteren in Zugversuchen mechanisch untersucht. MaSp Mischungen von *in vivo* produzierten Homo- und Heterodimeren erzielten hierarchisch strukturierte Fasern, die den natürlichen Spinnenseidenfasern entsprachen. Es wurden mechanische Eigenschaften erreicht, welche im Hinblick auf Zugfestigkeit (834 ± 34 MPa), Elastizität (32 ± 1 %), Elastizitätsmodul ($5 \pm 0,4$ GPa) sowie Zähigkeit (143 ± 6 MJm⁻³) die bisher besten Werte von allen künstlich gesponnenen Spinnenseidenfasern aus wässrigen Spinnssystemen. Hierbei war die Rolle der Heterodimere essenziell, da sie zum einen als Vernetzer zwischen den einzelnen Homodimeren agierten, zum anderen aktiv am Fibrillen- und Faseraufbau beteiligt waren.

Im nächsten Schritt wurden hybride Spidroinvarianten untersucht, welche die biophysikalischen und biochemischen Eigenschaften von eADF3 und eADF4 vereinten. Es wurde ein neues Zwei-in-Eins (*two-in-one*, TIO) Spidroin mit TDs entwickelt, zusammengesetzt aus den Aminosäuremotiven beider eADF Varianten. Die Produktion und Reinigung der TIO-Spidroine ergab eine 25-fach höhere Ausbeute im Vergleich zu Heterodimeren, welche aus einem Gemisch von Homo- und Heterodimeren mittels eines zweistufigen chromatographischen Trennverfahrens isoliert wurden. Eingehende Analysen mittels CD-, Fluoreszenz- und UV/Vis-Spektroskopie ergaben ähnliche strukturelle Merkmale in beiden Hybridvarianten. In Phosphat- und Scherinduzierten Assemblierungsexperimenten wurde die hierarchische Selbstassemblierung zu β -Faltblatt-reichen Strukturelementen nachgewiesen. Fasern, die im zuvor etablierten biomimetischen Nassspinnverfahren aus TIO-Spidroinen gesponnen wurden, wiesen im Vergleich zu Fasern aus einzelnen Spidroinvarianten oder einer Spidroin-Mischung mindestens zweifach höhere mechanische Eigenschaften auf.

Ein weiterer Teil der Arbeit befasst sich mit der Untersuchung der strukturellen Selbstassemblierung von MaSps, von hochkonzentrierten wässrigen Spinnlösungen bis hin zu daraus gesponnenen Fasern. Spektroskopische und mikroskopische Untersuchungen von eADF3-CTD Spinnlösungen ergaben, dass Spidroine in biomimetischen phosphathaltigen Spinnlösungen

im Verlauf der Zeit aus einem Monomer/Dimer-Gleichgewicht heraus zu Mizellen-artigen Assemblaten und schließlich in eine Flüssig-Flüssig-Phasentrennung übergingen. Kombinierte Flüssig- und Festkörper-NMR Experimente von $^{13}\text{C}/^{15}\text{N}$ isotopenmarkierten eADF3-CTD Spinnlösungen und Fasern implizierte die besondere Rolle von Tyrosinen im Assemblierungsprozess, speziell die Tyrosin-Ringpackung in ungeordneten helikalen Domänen.

Diese Dissertation liefert Einblicke in die strukturelle und hierarchische Selbstorganisation von MaSps und verdeutlicht die Bedeutung des Zusammenspiels von Proteinen für die funktionelle Komplexität. Die Herstellung biomimetischer Spinnlösungen und Fasern mit spinnenseidenähnlichen und anpassungsfähigen mechanischen Eigenschaften ebnet den Weg für die Entwicklung von seidenbasierten Materialien, die in verschiedenen High-Tech-Bereichen eingesetzt werden können.

1 INTRODUCTION

1.1 NATURE AS A BLUEPRINT: MIMICKING NATURAL STRUCTURES TO DESIGN BIOINSPIRED MATERIALS

Natural materials have been used by humans since early ages to ensure survival. As history progressed, technological development advanced, and interest in synthetic alternatives was awakened. Innovation cycles impacted urban demographics and trade, from the Industrial Revolution in the 18th century until today, whereby cycle longevity shortened with each wave (**Figure 1**).¹ In the meantime, society is transitioning between the fifth and sixth wave, and clean technologies have come to the forefront since climate change and the limited availability of raw materials, promoting a reorientation in materials research to develop environmentally-friendly and sustainable polymers.²

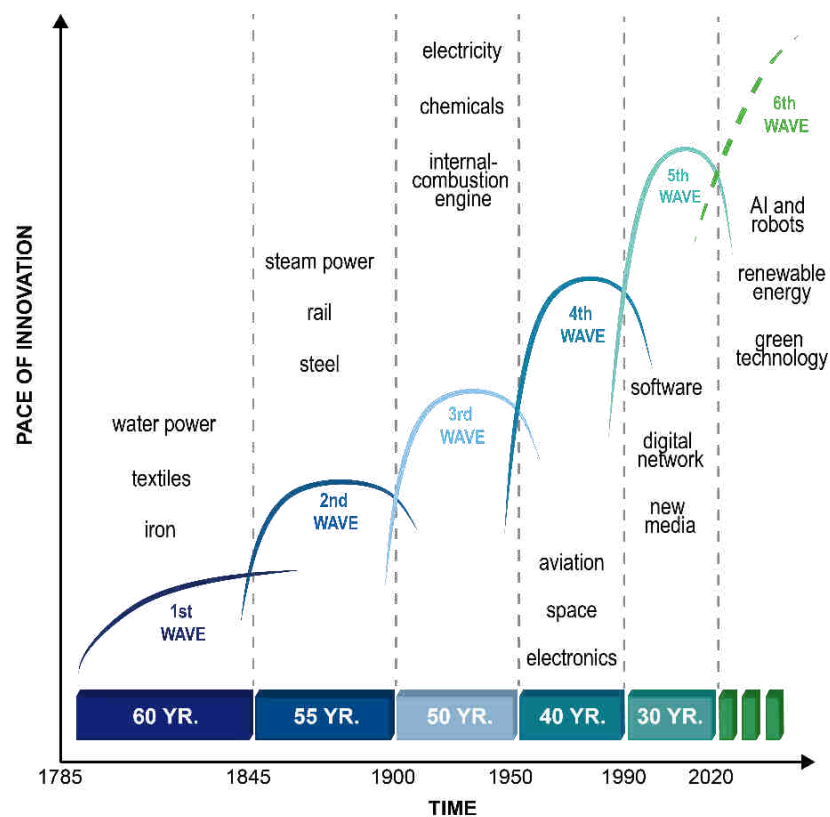


Figure 1. Cycles of innovations and entrepreneurship across 250 years. The economist Joseph Schumpeter developed the theory of innovations, linking technological innovations with economic growth. Today, renewable energies and green technologies open new routes to meet growing human needs in harmony with nature. The figure is inspired by Palousis *et al.*¹ and The Natural Edge Project.³

Nowadays, materials are indispensable in all technological aspects, and scientists continue to be fascinated and inspired by the complexity of natural structures.⁴ Over billions of years of evolution, nature perfected a plethora of materials built up by a limited selection of polymeric and ceramic components or building blocks.^{4,5} Materials often share common design motifs (layered, columnar, or fibrous), enabling the combination of unique features such as lightweight, exceptional mechanical properties, self-healing, and multi-functionality. One of the essential inherent properties is the hierarchical arrangement of the components from nano- to macroscopic length scales.² A complex hierarchy of self-organized structures achieves maximal performance in adapting to environmental changes.^{6,7} Natural materials often combine remarkable strength and toughness, exceeding their individual building blocks.⁶ A well-known example is silk, as it combines stiff and soft components, namely highly ordered β -sheet crystals within a semi-amorphous matrix, enabling extraordinary toughness unmatched by most other known natural or man-made fibrous materials.^{4,8} Besides mechanical properties, nature's hierarchical design provides a diversity of other interesting characteristics, i.e., superior wettability, structural color, antireflective properties, reversible adhesion, or anti-fouling features. For example, the special surface topography of lotus leaves exhibits excellent water repellency, attained by papillae that act as rough microstructures with a superimposed dense wax layer as hydrophobic protection.^{6,9} Gecko's footpads are composed of keratinous hairs, which are subdivided into nanostructures enabling reversible adhesive forces during locomotion.¹⁰⁻¹² The transparent hollow structured hairs of polar bears offer diverse advantages such as lightweight, thermal insulating, and guidance of light transmission to trap ultraviolet radiation.^{13,14} Also, the wings of *Morpho* butterflies consist of a translucent membrane covered by a layer of periodically nano-structured scales. The multi-colored iridescence of the wings relies on the combined effects of light interference and light diffraction.^{7,15}

These, as well as many other fascinating models, encourage scientists to learn from nature. However, the design and fabrication of synthetic materials mimicking the hierarchical architecture is not a trivial undertaking. Since applications have emerged in different fields like medicine, electronics, optics, fabrics, buildings, transportation, etc., requirements for new high-performance materials are diverse in terms of mechanical properties, sustainability, durability, or biocompatibility.² To accomplish this, understanding the structure-function relationship in natural materials can be an inspiration to engineer synthetic structures and hence promote innovations and breakthroughs for modern materials.^{8,13,16,17}

1.2 SILK

Silk has fascinated mankind over millennia as a renewable raw material with characteristics such as lightweight, shiny appearance, and outstanding mechanics.¹⁸ The simplest form of exploiting silk is known among the Australian Aborigines, who used spider silks as fishing lines, and the New Guinean natives' development of fishing nets and bags.¹⁹ Civilizations as early as ancient Romans and Greeks have been inspired by the biological diversity of silk to adapt spider silk as dressings and sutures for wound treatments.^{19,20} Historically, the trade along the prominent Silk Road of silk textiles and other goods produced by cocoon silk of the domestic silk moth *Bombyx mori* was an important episode in promoting culture, politics, economics, and technology in Asian and European continents.^{21,22}

The term “silk” is defined as a protein-based fiber produced by animals that belong to the phylum of *Arthropoda*, including the classes of *Myriapoda*, *Insecta*, and *Arachnida* on land, water, and air.^{23,24} Among them, spiders and silkworms are the most popular silk-secreting ones, using the fibers for similar purposes, such as prey capture, survival, reproduction, and offspring protection.^{21,23} In total, there are probably more than 200 000 different silks with either major or minor differences in the amino acid sequence.²⁵ Although a wide diversity has evolved within hundreds of million years, silks contain common elements from a molecular point of view.²³ With few exceptions, large proteins are secreted in specialized glands and stored in highly concentrated aqueous solutions, also known as spinning dopes. Silk proteins reveal long stretches of highly repetitive amino acid residues involving glycine, serine, and alanine.^{18,21} The unique primary structure of silk proteins encodes α -helices and β -sheets predominantly, resulting in a composite material of amorphous and crystalline domains.^{23,26} Despite the evolutionary distance, insects, and spiders share hierarchical regularities which allow proteins to pack efficiently and form strong networks of hydrogen bonds within or between proteins, which contributes to the mechanical strength and stability of silk.²⁶ In addition, silk spinning among different animals involves a phase transition upon shearing from a liquid solution to a water-insoluble solid fiber.^{23,25,27} One fiber can have diameters ranging from a few nanometers to a few microns and lengths varying from a few millimeters to over 1000 meters.²⁸ Depending on the respective use, silks differ significantly in terms of their mechanical properties (**Table 1**). Comparing the mechanics of various natural as well as synthetic materials, spider silk belongs to one of the most impressive materials as it

combines properties such as strength and toughness, which seem mutually exclusive.^{4,13,29} Although high-tech fibers comprise higher strength and stiffness, spider silk fibers demonstrate substantially higher toughness according to their greater extensibility.³⁰ In comparison to Kevlar, the strongest synthetic polymer fiber material to date, spider silk can absorb three times more energy before it breaks and can be designated as nature's high-performance fiber.

Table 1. Tensile mechanical properties of (a) natural in comparison to (b) synthetic materials.

a. Natural materials					
Material	Strength [MPa]	Extensibility [%]	Toughness [MJm ⁻³]	Young's Modulus [GPa]	Source
Spider silk <i>Araneus diadematus</i>	1180	24	167	8	31
Silkworm silk <i>Bombyx mori</i>	600	18	70	7	32
Mussel silk <i>Mytilus galloprovincialis</i>	200	50	82	2	33
Honey bee silk <i>Apis mellifera</i>	130	204	-	-	34
Lacewing egg stalk silk <i>Chrysoperla carnea</i> (70 % RH)	155	210	87	3	35
Collagen	100	13	6	1	36
Elastin	2	150	2	0.001	32,37
Chitin	80	1	n. a.	3	38
Bone	160	3	4	20	32
Bamboo	700	5	n. a.	46	39,40
Cork	1	7	n. a.	0.03	41
b. Synthetic materials					
Material	Strength [MPa]	Extensibility [%]	Toughness [MJm ⁻³]	Young's Modulus [GPa]	Source
Kevlar 49	2300	4	41	162	42
Carbon	4000	1	25	300	32
Enamel	60	5	4	37	43,44
Nylon	950	18	80	5	32
Steel	1500	1	6	200	32

Note: The values are based on individual publications and have been rounded to indicate the order of magnitude rather than exact values.

1.3 SPIDER SILK

"What's miraculous about a spider's web?" said Mrs. Arable. "I don't see why you say a web is a miracle - it's just a web."

"Ever try to spin one?" asked Dr. Dorian."

In 1952, the American author E. B. White captured the complexity of spider web constructions in his novel "Charlotte's Web" narratively well. All spiders (*Arachnida*) produce more than one type of silk, which was the fundament for their evolutionary success, reflected in the diversity with more than 48 000 spider species as one of the largest animal groups in the world.⁴⁵

Orb-weaving spiders (*Araneidae*) can build up to seven mechanically distinct silk fibers using separate glands, ducts, and spigots, located on the posterior end of the spider's abdomen.^{28,46,47} The construction of a web requires the combination of these different silk types, which is the final level of hierarchical organization.⁴⁸ Over millions of years, orb-webs have been adapted to withstand the kinetic impact of the spider's prey, leading to the evolution of five different silk types to generate the web, besides one special silk for egg sac cases and one that serves as glue silk (**Figure 2**).⁴⁹ Depending on the tailored uses of each silk type, the mechanical properties differ substantially from one another and span a wide range (**Table 2**), based on differences in biochemical composition.^{46,47,50-52} Each silk type is composed of specific silk proteins (spidroins), which are selectively produced by specialized epithelial cells in morphologically divergent silk glands,⁵² descended from one common origin.^{53,54} However, each gland-spinneret may also synthesize small amounts of spidroins that are predominantly produced in other silk glands.^{55,56}

Each spider silk type and its underlying spidroins are named after the corresponding glands in which they are produced.⁴⁹ Major ampullate (MA) silk constitutes the frame and radii of the orb-web and the dragline, the lifeline to escape from enemies.^{47,57} Unlike other spider silk types, MA silk, is the most studied one as it reveals a remarkable combination of strength and extensibility, which ultimately results in high toughness, and further dragline fibers are easily accessible by silking spiders.^{30,58} However, MA silks offer interesting phenomena, such as humidity-driven supercontraction, which causes shrinking of the thread length up to half its dry state and swelling in the diameter.⁵⁹ Silk's molecular structure is reorganized due to the dissociation of hydrogen bonds with drastic changes in mechanical and physical properties.⁶⁰⁻⁶³

The background of the supercontraction is at least twofold. On the one hand, it may prevent sagging in of the webs at high humidity, on the other hand, it allows the spiders to adapt silk properties for various ecological functions.⁶⁴ The supercontraction effect is fully reversible and also documented among other silk types but is most pronounced in MA silk.⁶⁵⁻⁶⁷ Another interesting feature of MA silk represents its shape memory effect, which provides shape and stability to the web.³⁰ Dragline silks comprise a torsional dampening behavior, helping the spider to drag down without twisting and swinging.^{49,68} Upon external twisting of a dragline thread, it can reversibly and totally recover its initial form.⁶⁸

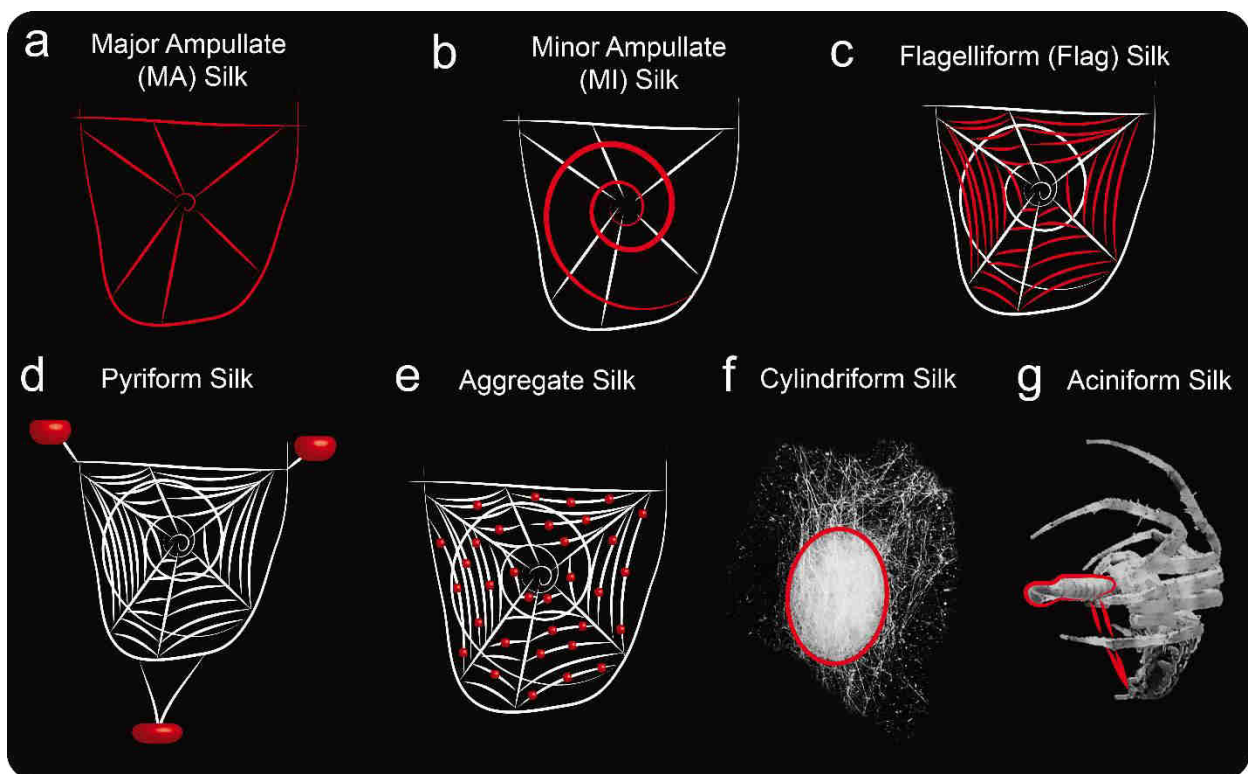


Figure 2. Schematic classification of different silk types produced by female orb-weaving spiders for several uses. Each specific silk type is highlighted in red. **(a)** Major Ampullate (MA) silk: structural elements frame and radii, dragline, **(b)** Minor Ampullate (MI) silk: auxiliary spiral and web reinforcement, **(c)** Flagelliform (Flag) silk: capture, **(d)** Pyriform silk: attachment to substances, **(e)** Aggregate silk: aqueous sticky coating and capture signal, **(f)** Cylindriform silk: egg sac case, **(g)** Aciniform silk: prey wrapping and egg case packing.

For scaffolding and structural reinforcement of the web, minor ampullate (MI) silk is used in auxiliary spirals.⁶⁹ Although MA and MI silk proteins share similarities in amino acid sequence and secondary structure, their threads display distinctions in mechanical characteristics.⁷⁰

Hypotheses imply differences in protein assembly during the spinning or post-stretching process.⁷¹ MI silk mechanics particularly vary to a greater extent among species than the properties of MA silks, allowing more diverse applications of MI silk that would not be feasible for draglines.^{50,72} Further, MI fibers comprise different physical properties regarding hydrophilicity as they show low sensibility to water, hence, comprise no supercontraction effect when wet.⁷¹

Table 2. Comparison of mechanical properties of selected spider silk types from different spider species. Indicated are relative value ranges rather than exact values to give a comprehensible order of magnitude. Mechanical data of silks are subjected to high variability, depending among others on the experimental setup as well as spider age and fitness.

Spider silk type (different spider species)	Strength [MPa]	Extensibility [%]	Young's Modulus [GPa]	Source
Major Ampullate	1000 - 1600	20 - 35	7 - 14	52,73-75
Minor Ampullate	400 - 1200	5 - 25	4 - 10	52,73,76
Flagelliform	500 - 1400	100 - 270	0.001 - 0.003	32,73,77
Cylindriform	400 - 2300	20 - 40	8 - 12	52,78,79
Aciniform	700 - 1000	40 - 80	9 - 10	73,80,81

Among the silk types produced by orb-weaving spiders, flagelliform (Flag) silk is characterized by its extreme elasticity and high hysteresis.^{32,82} Even at low forces, Flag silk extends more than ten times as much as MA silk, a feature that has been preserved for over 100 million years.^{54,83} Flag silk is the major component of the sticky capture spiral and is coated with an aqueous glue made of aggregate silk.⁸⁴ Aggregate glands produce sticky droplets that act as glues to detain and aid prey capture.^{85,86} The stickiness can be attributed to abundant glycoproteins with high extensibility and elasticity.⁸⁷⁻⁸⁹ Further, a high percentage of charged amino acid residues within the aggregate proteins contribute to water retention. The orb-web droplets are distributed non-homogenously among the Flag fibers and behave as viscoelastic solids.^{88,89} If, for example, a flying insect is caught in the orb-web at high speed, the aggregate droplets are stretched quickly, and the liquid-like behavior of the droplets is to the fore. High viscous resistance provides a large adhesive force and detains the prey in the web. In the course of escape attempts, the solid-like

behavior of the droplet is advantageous. At low extension rates, the droplets act like a rubber band, from which the prey cannot free itself while expending its energy.⁸⁶

In ancient spiders, the primary purpose of silk was for reproduction either by producing egg sacs in females or constructing a silken platform to deposit sperm in males.^{53,54} Today, only female spiders produce a unique cylindrical silk, also known as tubuliform silk, in the reproductive season for creating egg cases and cocoons.⁹⁰ After males charge their palps with sperm and transfer it via sperm webs into the female epigynum, they die soon after mating, whereas females store the sperm until egg-laying.⁹¹⁻⁹³ It was shown that tubuliform glands are subjected to structural and morphological changes just before egg-laying to accommodate the volume of protein secretion.^{94,95} Tubuliform silk has a relatively high tensile strength and stiffness, which provides the required structural stability to protect the offspring from attackers and parasites until hatching.^{55,83} Compared to other silks, tubuliform fibers appear to be more irregular with small knobs and grooves on their surface to increase flexural stiffness.⁹⁶ Aciniform silks are used by araneoid spiders to encase their eggs, build sperm webs for mating or build webs for prey wrapping. This type of silk exhibits the highest toughness out of all silks due to its unique extensibility.⁸⁰

The mechanical performance combined with high biocompatibility designated spider silk fibers, particularly MA silks, a rich source of inspiration for biomedical and technical applications. In the last decades, research interest has grown in the hope of replicating its remarkable characteristics in the course of modern biotechnology.

1.4 HIERARCHICAL STRUCTURE OF MAJOR AMPULLATE SILK FIBERS

The unsurpassed mechanical properties of MA silk are based equally on both the inherently hierarchical nature and the molecular components, directly correlated in a structure-function relationship (**Figure 3**).^{81,97,98} The composition of MA silk can vary substantially between spider species and even between fibers of one spider. Further, the spider's nutritional conditions impact fiber formation.⁹⁹⁻¹⁰¹ In a top-down perspective, the hierarchy includes five levels, a nanofibrillary network, crystal networks, β -crystallites, secondary structures, and amino acid sequences, respectively.¹⁰² The thread is made up of a core-shell structure and can be divided into five layers, including a lipid coat, a glyco coat, a skin, an outer, and an inner core.^{81,103,104} The outermost lipid

layer protects the silk filament against external environmental influences and degradation of microorganisms and may serve for communication via species- and sex-specific pheromones.¹⁰⁵ The lipid coat is loosely connected to the inner layers and does not substantially contribute to the mechanical performance. In contrast, the glyco layer appears to be tighter attached. It functions as the interface to its environment, regulating the water balance and thereby indirectly impacting the supercontraction and mechanical strength.⁸¹ The skin consists of MI-like spidroins, impart plasticity to the fiber, and provides mechanical support by enclosing the core material. In the case of MA silk, the core contains at least two MA spidroins, with different biochemical and physicochemical compositions.^{103,106}

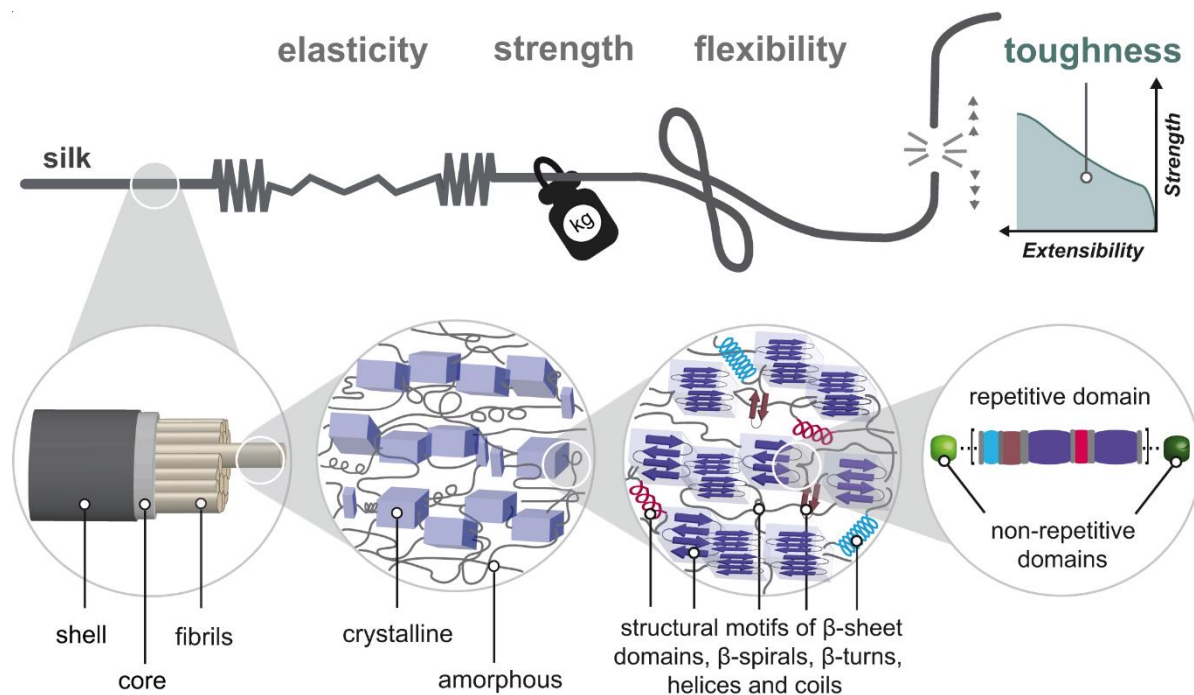


Figure 3. Hierarchical structure of the spiders' dragline silk and its' mechanical properties. A thread is modeled as an ensemble of numerous fibrils with nanometer-sized crystallites embedded in an amorphous matrix along the fiber axis. Each crystal consists of highly ordered and densely packed β -sheets, defining the mechanical strength of the silk. Further, the amorphous matrix comprises secondary structures such as β -spirals, β -turns, helices, and random coils, influencing properties such as elasticity and flexibility. Distribution, arrangement, and the relative ratio of amino acid sequence elements impart the structural motifs and hence the overall mechanical properties. Reprinted with kind permission of the publisher Elsevier from Saric, M., & Scheibel, T., Engineering of silk proteins for materials applications. *Current opinion in biotechnology*, 2019, 60, 213-220.¹⁰⁷

The hierarchical complexity of silk at a large span in length scales imposes a combination of requirements and structural patterns. On the microscale, the core of the silk is built by a bundle of twisted nanofibrils that assemble in parallel along the fiber axis into large structures.¹⁰⁸ The geometric confinement of fibrils combined into a fiber enables a uniform flaw-tolerant state, resulting in synergistic resilience to deformation and failure.¹⁰⁹ The fibrils contain a nanometer-sized crystalline network embedded in an amorphous matrix, enabling the silk's fascinating behaviors.^{102,110} The disordered amorphous phase is built by β -spirals, β -turns, helical structures, and random coils, which together endow the fiber its flexibility and elasticity. The tensile strength and toughness of the threads are obtained through stiff crystals, which are tightly packed in anti-parallel β -sheet stretches with high orientation. The interplay of crystalline and amorphous phases ensures the complementary features of strength and toughness.¹¹¹⁻¹¹³ The fiber processing conditions (e. g., spinning speed) determine the density of β -crystallites and the extent of ordered and disordered regions the proteins adopt, which is directly related to the mechanical performance.¹¹⁴ On a molecular level, design motifs are determined by the highly repetitive spidroin sequence that facilitates the potential for a high density of hydrogen bonds between β -sheets and a variety of secondary structures.^{112,114} Hydrogen bonds enable the ability to self-heal, as they can be easily restored after breaking, resulting in another highly useful property, toughness, to prevent brittle failure.¹¹⁵

1.5 NATURAL MAJOR AMPULLATE SILK PROTEINS

Despite the diversity in spider species, the major constituents of MA silk are structural proteins, known as major ampullate spidroins (MaSps), exhibiting a preserved three-partite composition (**Figure 4**).^{116,117} The schematic structure of soluble spidroins is composed of a large (<350 kDa) unfolded central domain with highly repetitive modules, enclosed by small (<15 kDa) globularly folded non-repetitive terminal domains (TDs).^{97,116,118,119} At a soluble state, the core domains lack tertiary structures and remain intrinsically unstructured, which is an important functional feature representing high conformational flexibility.¹²⁰ The non-repetitive amino- and carboxyl-terminal domains (NTD, CTD) play a crucial role in the storage of soluble MaSps as well as promoting their self-assembly into insoluble fibers.^{121,122} Dragline threads consist of several MaSps with differences in terms of amino acid composition, module repetitions, sequence variation, and molecular weight, which significantly determine the functional and mechanical properties.^{116,123,124} In principle, four main amino acid motifs are identified in the core domain such as poly-alanine (A)_n repeats, glycine-alanine (GA)_n repeats, glycine-rich sequences with (GGX)_n or (GPGXX)_n repeats, where X is typically leucine, tyrosine, or glutamine (**Figure 4, Table 3**).^{76,125} Each motif can be repeated up to 100 times and can constitute 40 to 200 amino acids.^{46,80,110,118} The potential secondary structures of the individual amino acid motifs and their impact on MA silks' mechanical features have been intensively studied within the last decades (see 1.5.1). Further, spider silk is not only composed of MaSps but also of non-spidroin proteins, so-called spider silk-constituting elements (SpiCEs), of various sizes with low molecular weight and yet unknown functions.¹²⁶⁻¹²⁹

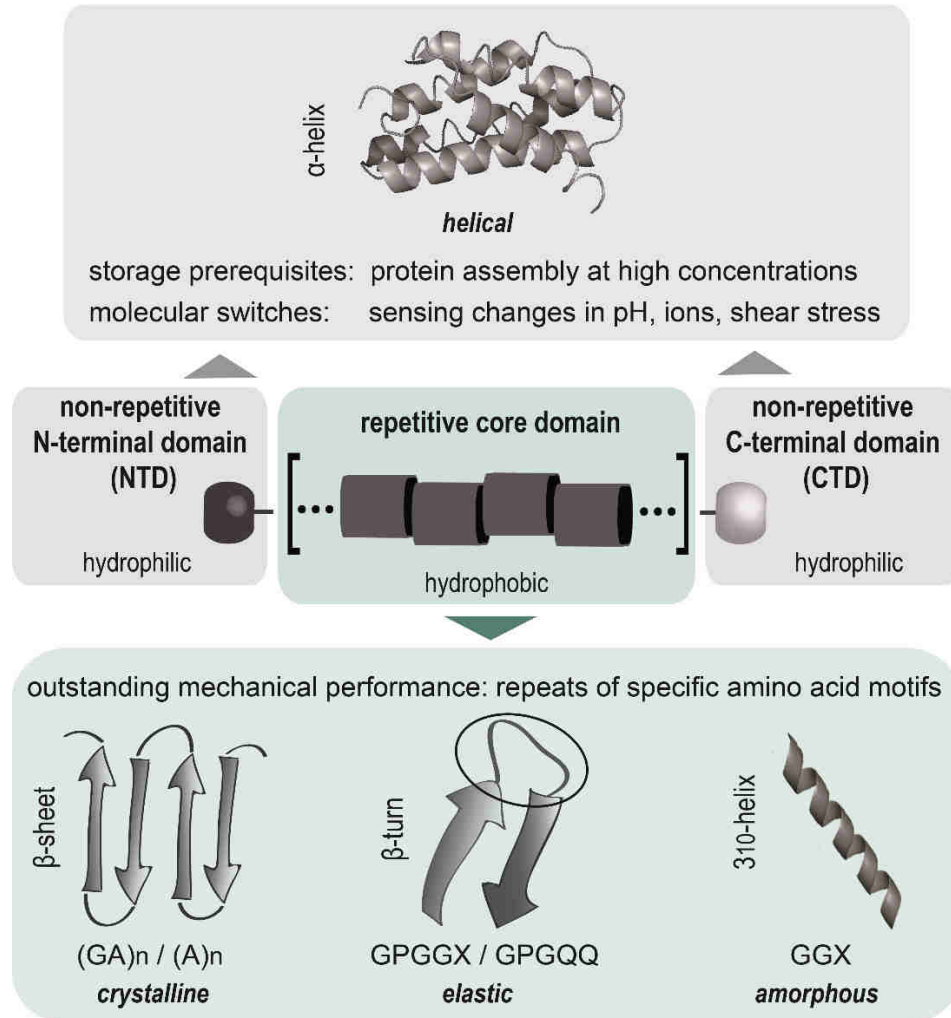


Figure 4. Setup of spider silk proteins and common structural motifs. The highly repetitive core domain of spidroins is intrinsically unstructured, comprising modules with a distinct subset of amino acid motifs with alternating glycine-rich and polyalanine regions. The large repetitive section contributes to the mechanical properties of the final fiber. In contrast, the non-repetitive amino- and carboxyl-terminal domains show a globular fold, acting as molecular switches upon environmental changes and control units in self-assembly. X: predominantly alanine, glycine, serine, tyrosine, glutamine, and leucine

1.5.1 REPETITIVE CORE DOMAIN

Recently, genomic and transcriptome analysis revealed that MaSp1s are encoded by at least five gene families (**Table 3**).¹³⁰ The exact MaSp1 composition varies between spider species.^{16,101,117,131,132} Most prominent dragline spidroins are MaSp1 and MaSp2, which mainly differ according to their proline content. MaSp1 represents a proline-poor variant (<0.4 %), whereas MaSp2 is rich in proline (>10 %).⁴⁶ MaSp1 and MaSp2 have been well investigated for decades in various spiders, while other MaSp families (MaSp3, MaSp4, and MaSp5) were recently discovered and are so far only found in a few spiders.^{124,130,133,134}

A module of MaSp1 displays conserved blocks of poly-Ala, poly-Gly-Ala, and several GGX repeats.^{82,125,135,136} Poly-Ala and poly-Gly-Ala stretches form tightly packed anti-parallel β -sheets, which constitute defined nanosized crystals. The poly-Ala sequences are arranged alternately on the sides of the backbone, interlocking with an adjacent chain by hydrophobic interactions.^{137,138} Connected β -sheets blocks contribute to fibers' tensile strength.^{113,139,140} The higher the level of β -sheet interactions, the higher the binding energy and strength in the final fiber. Poly-Ala-Gly regions show less hydrophobic interactions compared to poly-alanine ones since the glycine residues are not able to provide the same hydrophobic intercalations.¹²⁵ Iterations of GGX motifs fold predominantly into 3_{10} -helical structures providing an amorphous matrix for the β -sheet nanocrystals.^{81,119,141} Interstrand hydrogen bonds are present in 3_{10} -helices, which comprise different geometries than that of rarely found 3_1 -helices.¹⁴²⁻¹⁴⁴ Further, GGX motifs can induce folding into β -turns and coil structures.^{139,140,143} The reversibility of the folded structures contributes to extensibility and provides mobility to the crystalline network.^{125,145}

MaSp2 comprises penta-peptide GPGXX motifs, which usually can be further subdivided into GPGQQ and GPGGX (X typically is A, G, S, Y, Q, or L), yielding elasticity upon the formation of β -turns and spiral structures.¹²⁵ The presence of prolines involves intrinsic disorder due to the pyrrolidine ring in the chain backbone, lacking amide groups for potential hydrogen bonds.^{146,147} Therefore, proline-containing motifs favor the formation of β -turns which is fundamental for the elastomeric properties of silk fibers.^{125,148} Further, the degree of proline content is linked to the fiber's supercontraction and its mechanical properties, as mentioned before (see 1.3).^{64,149,150}

A closer examination of the MA silk of *A. diadematus* revealed a higher proline content of 16 %, compared to other species (1 to 11 %).^{46,151,152} Interestingly, the dragline silk of *A. diadematus* contains two MaSp2 proteins, namely *A. diadematus* fibroin (ADF) 3 and 4, as a

unique feature among all known orb-weaving spider species.⁴⁶ Both ADF proteins are secreted in the same compartment of the spinning gland, leading to the suggestion that they could interact shortly after translation, for example, along the secretory pathway.^{52,118,153} ADF3 encodes for polyalanine blocks, GGX motifs as well as GPGQQ motifs, whereas ADF4 comprises polyalanine and motifs of GPGGX.^{46,57} Both MaSp2 derivatives exhibit distinct differences in assembly and solubility properties. While ADF3 is known to be hydrophilic and remains soluble even at high concentrations, ADF4 is in comparison less soluble at high concentrations, resulting in self-assembly into filamentous morphologies.^{154,155}

In addition to MaSp1 and MaSp2, a novel short form of MaSp1, so-called MaSp1s, was identified in *Cyrtophora moluccensis* in 2013.¹²³ MaSp1s was determined as a small protein with a molecular weight of approximately 40 kDa. It exhibits conserved TDs and typical MaSp1 motifs in the core domain, although it was not characterized by a repetitive structure since motifs were irregularly distributed and significantly shorter compared to common MaSps.¹²³

Although the specific purpose of MaSp3/4/5 in dragline silks remains unclear, it is believed that they may contribute to silk's toughness.¹³⁰ MaSp3 families contain an XGGRGY motif, in which X is either aspartic acid or serine.^{124,130,133,156} Compared to MaSp1 or MaSp2 of *L. hesperus*, MaSp3 has much more polar (35 % vs. 16 %) and acidic residues (6 % vs. 1 %).¹²⁴ MaSp4 of *C. darwini* comprises an alternative poly-X tail, a VSVVSTTVS sequence, composed of neutral amino acid residues other than typical polyalanine. The GPGPQ sequence is a unique attribute only seen in MaSp4 so far,¹⁵⁷ contributing to flexibility by β -turn packing. Together with GPGG motifs seen in *C. darwini*, both building blocks also might enhance silk toughness.^{130,134} Phylogenetic studies revealed that MaSp4 belongs to the same clade as MaSp2, hence, constituting a lineage and a new subfamily of MaSp2.^{130,134} In contrast, MaSp5 seems to represent a new family of MaSp since no clustering into other clades of MaSp families is possible. Also, MaSp5 displays no polyalanine sequence but tandemly ordered GGLGGSG or GSGGR repetitive motifs providing elasticity to the fiber.

Table 3. Examples of structural motifs of core domains from various major ampullate spidroins (MaSp) and different spider species. The G represents glycine, P proline, and X varying amino acid residues, which are predominantly alanine, glycine, serine, tyrosine, glutamine, and leucine. ADF stands for *A. diadematus* fibroin. The column “individual MaSp motifs” contains motifs that could not yet be correlated to specific secondary structures.

Spider	Spidroin	individual MaSp motif	Structure			Source
			<i>elastic</i>	<i>crystalline</i>	<i>amorphous</i>	
			β -turn spiral	β -sheet	3_{10} -helix	
<i>Trichonephila clavipes</i>	MaSp1	GGYGGL GGYGGRF GGYGGL	XQQ GPGXX	(A) _n AS	GGX	129,134,137, 138
<i>Cyrtophora moluccensis</i>	short MaSp1			(A) _n	GGX	123
<i>Trichonephila clavipes</i>	MaSp2		GPGGX GPGQQ	(A) _n		97,137
<i>Araneus diadematus</i>	MaSp2: ADF3		GPGQQ	(A) _n	GGX	46,57
<i>Araneus diadematus</i>	MaSp2: ADF4		GPGGX	(A) _n		46,57
<i>Latrodectus hesperus</i>	MaSp3	DGGRGGY		(A) _n	GGX	124,129,133
<i>Caerostris darwini</i>	MaSp3	SGGRGGY		(A) _n	GGX	130
<i>Trichonephila clavipes</i>	MaSp3	DGGR GGYGGL		(A) _n	GGX	129,158
<i>Caerostris darwini</i>	MaSp4		GPGPQ GPGG	VSVVSTTVS		130,134,159
<i>Araneus ventricosus</i>	MaSp4		GPGPQ			157
<i>Caerostris darwini</i>	MaSp5	GGLGGSG GSGGR				130,134

1.5.2 NON-REPETITIVE TERMINAL DOMAINS

Storage and assembly of MaSps are predominantly controlled by their non-repetitive amino-terminal (NTD) and carboxyl-terminal domains (CTD). Unlike the repetitive central domains with varying sequences, TDs are evolutionary highly conserved among MaSp, but also spider species and some silk types.¹⁶⁰⁻¹⁶² The high conservation underlines the importance of TDs regarding spidroin folding and functionality. TDs contain 100 to 150 amino acid residues and fold into α -helical secondary structures organized in a five-helix bundle.^{110,122,163} Spidroins are stored at high concentrations in spinning dopes and presumably form micellar-like assemblies, whereby the hydrophilic TDs shield the hydrophobic stretches of the core domain from the solvent.^{52,141,164-166} Both TDs act as molecular switches to guide the self-assembly of MaSps into a highly ordered fibrillar network triggered by ion exchange, acidification, and mechanical stress.^{122,166,167} Hereby, TDs guide the transition from liquid spinning dope to solid fiber and prevent protein aggregation in the spiders spinning gland.^{168,169}

In NTD, conserved charged amino acid residues (Asp, Glu, Arg, Lys) are exposed on the spidroin surface and organized in clusters.^{121,170} At neutral pH, NTDs remain monomeric in the presence of chaotropic salts (NaCl).¹²¹ Upon acidification and a decreasing chaotropic salt concentration, the monomeric five-helix bundle, undergoes structural changes into a more tightly packed conformation. Additionally, a stable anti-parallel dimer can be formed within a few milliseconds upon the protonation of the clustered acidic residues.^{121,171-175} In contrast, the conserved charged amino acids of CTDs are stabilized by intramolecular salt bridges (Arg-Asp, Arg-Glu) located within the domain and proven to be essential for CTD's structural integrity.¹²² CTD are stabilized by a permanent disulfide cross-linked parallel-oriented dimer due to one conserved cysteine residue in each monomer.^{46,122,176,177} Further, the CTD dimer is locked via non-covalent interactions between two helices of the bundle structure, which are fixed in a clamp-like manner.¹²² During spinning, hydrophobic patches on the surfaces of CTDs are exposed, serving as anchor points for the correct spidroin alignment along with fiber assembly.¹²² Multivalent linking of anti-parallel NTD dimers and parallel-oriented CTD dimers yields an apparently endless and highly stable fiber network.^{139,170,178,179} In studies with recombinant NTD and CTD, no molecular interactions between them were identified at solvent conditions similar to the ones during spinning.¹⁶⁶ Folding of individual TDs was not affected by the opposing domain, while NTDs adapt their structure depending on the ionic environment, CTDs respond to shearing stress,

implicating a double-safety mechanism. Hereby, a stepwise response to external stimuli, separately controlled by TDs, prevents premature aggregation and controls timing of spidroins assembly from a soluble, intrinsically unfolded state into β -sheet-rich fibers.

1.6 NATURAL SILK SPINNING PROCESS

While biological materials are usually grown structures, silks are actively spun in a highly complex process involving sequential changes of spidroin conformation.^{114,180} The spider's spinning apparatus is located in its abdomen and can be divided into four sections, as exemplarily illustrated in **Figure 5** for MA silk. In the first part, a long coiled tail, spidroins are produced and secreted from epithelial cells into the lumen of the gland.^{52,181} Here, dimerization of CTDs oriented in parallel takes place at neutral pH by a covalent disulfide bond and electrostatic forces, whereas the NTDs remain monomeric.¹²² In the ampulla, which represents the second part, the spidroins are stored at concentrations up to 50 % w/v, yielding a spinning dope.¹⁴¹ To avoid unspecific aggregation, amphiphilic spidroins are stored in the presence of sodium and chloride ions by forming supramolecular, micelle-like assemblies in a process of microphase separation.^{141,155,164,165,169,171} The hydrophilic folded TDs are located on the surface of micelles, shielding the hydrophobic unstructured domains from the surrounding aqueous environment.^{155,167} The highly concentrated spinning dope shows characteristics of a liquid crystalline phase, which enables the MaSps to flow in a pre-aligned manner along the axis through the spinning gland, representing part three of the spinning apparatus, an S-shaped narrowing duct.^{49,182} The spinning dope is exposed to constant elongational flow, resulting in the rearrangement of the spidroin domains in parallel to the long axis. Further, β -sheet crystalline alignments trigger the formation of nanofibers.^{49,139,144,183} The duct is lined with a cuticle that enables rapid exchange of ions and dehydration to aid the processing of the silk precursor.¹⁸² As the spinning dope travels down the duct, chaotropic sodium and chloride ions are replaced by kosmotropic potassium and phosphate ions, with the CTDs acting as a trigger for controlled salting-out of the MaSps.^{122,171,184} Phosphate is known to increase the surface tension of water, initiating hydrophobic interactions.^{185,186} The MaSps conformational reorganization is further promoted by carbonic anhydrases that lower the pH from 7.2 to at least 5.7.^{52,172,187,188} Upon acidification, the negatively charged carboxylate groups of NTDs conserved acidic amino acids are neutralized, leading to changes of the tertiary

and quaternary structure. The NTDs dimerize in an antiparallel manner.^{175,179,189} In the last section of the spinning apparatus, excess water is resorbed, and the spinning dope viscosity increases. The dehydration mechanism serves as the last control level to “lock-in” any fibrillization during spinning to be quasi-irreversible.¹⁹⁰ Further, shear stress increases due to the draw-down tapering of the spinning duct and an active pulling out of the spigot.^{52,171,191}

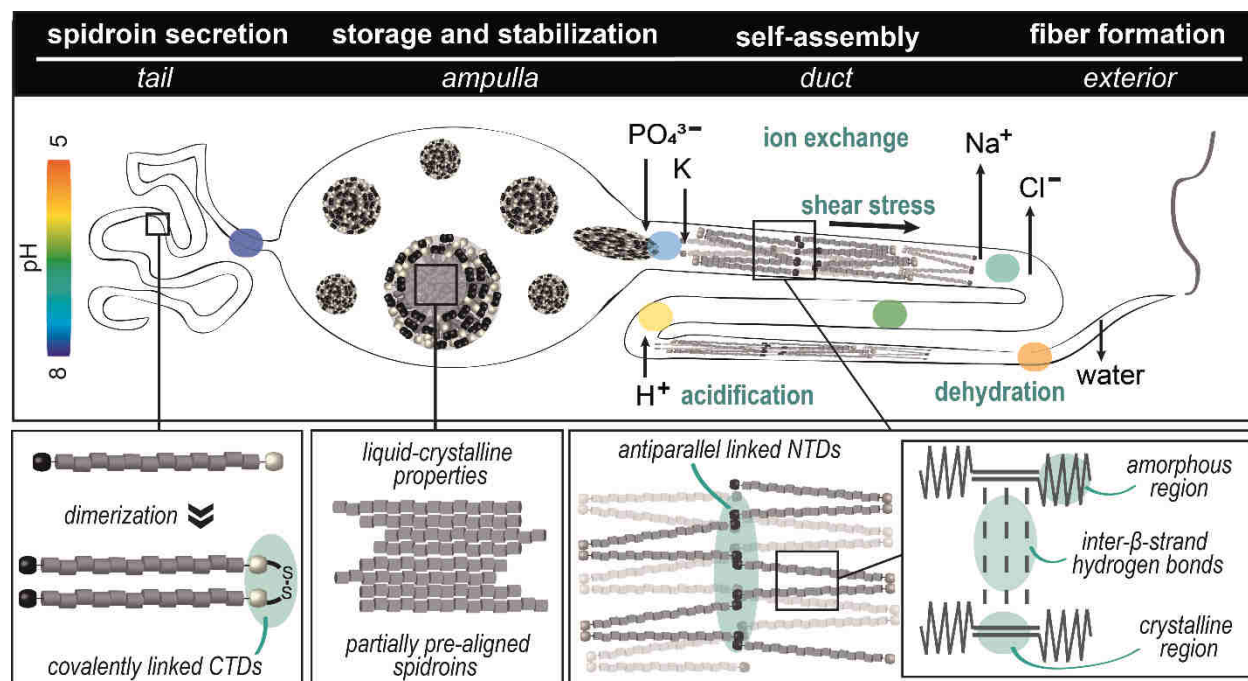


Figure 5. Schematic representation of the natural spinning process of spider dragline silk. The spinning gland is divided into four sections in which the MaSps undergo the conversion from a soluble to an insoluble state. Once MaSps are secreted, the non-repetitive carboxyl-terminal region builds a permanent parallel-oriented dimer, covalently linked by a disulfide bond. The MaSps are assumed to be stored in micelle-like structures at concentrations up to 50 % (w/v), whereby the polyalanine blocks of the repetitive domain pre-align in a liquid crystalline phase. In the course of spinning, chemical and mechanical triggers, such as shear forces, acidification, salting out, and dehydration, induce the assembly of MaSps. Hereby, the liquid crystalline phase further aligns along the elongational flow axis to the formation of β -sheet crystals. At lower pH values, antiparallel linked dimers are formed by the non-repetitive amino-terminal domain, building a potentially endless and highly stable network. As soon as the solid fiber emerges, the spider pulls and stretches the fiber, which leads to further alignment of the molecules. Modified with kind permission of the publisher John Wiley & Sons from Saric, M., Eisoldt, L., Döring, V., & Scheibel, T., *Advanced Materials*, 2021, 33(9), 2006499.¹⁹²

During the drawing process, the dragline obtains its typical core-skin structure upon homogenous coating of the assembled spidroin core region with glycoproteins.^{52,81,182} All external spinning triggers act synergistically, inducing phase separation between spidroins and aqueous solution and, thereby, converting the liquid dope to a solid fiber within milliseconds.^{106,193,194} Before the silk thread exits the spigot, it passes a muscle-associated valve, which on the one hand acts as a brake and, on the other hand, assists in restarting spinning after internal rupture.¹⁸² On a macroscopic level, the spider pulls and stretches the solid fiber from the spinneret into the air with controlled reeling speed using its hind legs or body weight.^{195,196} The microstructure and mechanical properties of fibers are highly dependent on spinning conditions, in particular reeling speed, as they affect the arrangement of β -sheet crystals within the amorphous matrix.^{197,198} Further, dragline silk properties are subjected to a variety of parameters, depending among others on spider age, fitness, nutritional fitness, and climatic conditions.¹⁹⁹⁻²⁰¹

1.7 SEQUENCE-STRUCTURE-FUNCTION RELATIONSHIP

Considerable research has been devoted to understanding the relationship between sequence, structure, and function of spidroins. Experimental as well as computational studies have been carried out to determine the role of β -crystallization and amorphous regions on the mechanical properties of MA silks.⁹⁸ The predominant nano-crystalline components are built by anti-parallel β -strands interconnected by hydrogen bonds providing high tensile strength. The stacked β -sheet crystals exhibit sizes of approximately 2 nm x 5 nm x 7 nm, whereby the size and volume fraction of the crystalline phase significantly affect the fiber mechanics.^{195,202-204} In computational studies, increasing crystal sizes obtained decreasing strength as crack-like flaws appeared by the gradual failure of hydrogen bonds under tension.¹¹² Larger crystals are deformed by bending, whereas smaller crystals are deformed by higher rupture forces dominated by shear.^{98,205} Dynamic simulations of β -sheet crystals with a varying number of alanines revealed an optimum of 8 alanine residues for each strand, which fits the observation of native spider silk comprising β -strands of typically 8-10 residues.^{32,206} To ensure ideal packing geometry, the maximum number of alanines is restricted to 12 residues. Among the natural amino acids, alanine has the highest helix-formation potential, hence, if less than 6 alanines are present, hardly any β -sheets are formed.²⁰⁶⁻²⁰⁹

The amorphous region consisting of a mixture of coils, β -turns, and 3_{10} -helices also influences spider silk mechanics. Since the amorphous chains are partially pre-stressed, the supercontraction of fibers upon wetting is facilitated.²¹⁰⁻²¹² In the dry fiber core, the pre-stress induces a non-equilibrium which is compensated by surrounding structures and hydrogen bonds.²¹⁰ When the fiber is subjected to lateral load, the energy is transferred through the crystals into the amorphous spidroin chains interlinking nanocrystals.^{184,211} However, the mechanical performance of fibers is not solely based on primary and secondary structures but also intra- and intermolecular interactions of tertiary and quaternary structures during the spinning process.

The mechanical properties of spider silk fibers can be analyzed by stress-strain tests, demonstrating the relationship between a force applied to the silk fiber and the elongational deformation. Generally, the characteristic tensile properties of spider silk fibers exhibit a non-linear behavior in a multi-level regime, each with its features (**Figure 6**).^{113,213} In principle, the nanoconfinement of β -crystals plays a crucial role in the mechanical performance of fibers, especially the control over structural arrangement.²¹⁴

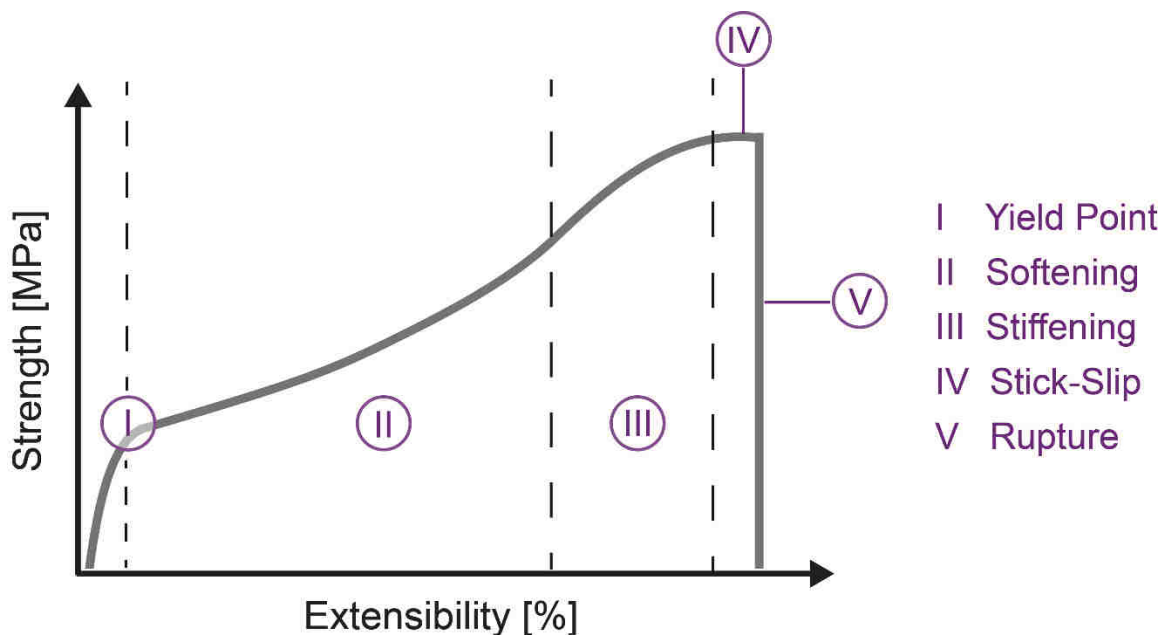


Figure 6. Characteristic tensile properties of spider silk fibers. (I) The Yield Point displays the onset of plastic deformation at low stresses. (II) The softening phase indicates entropic unfolding and stretching of the amorphous strands along the fiber axis. (III) The stiffening phase is observed after the full extension of amorphous chains. Hydrogen bonds break in the crystalline phase at high stresses. (IV) The stick-slip motions suggest the final unfolding of β -sheet crystals until (V) fiber rupture.

In phase one, silk fibers are homogeneously stretched at low stresses, which leads to the breaking of hydrogen bonds of the β -turns, β -spirals, and 3_{10} -helices in the amorphous matrix. The initial phase culminates in a yield point, constituting the initial stiff behavior.^{111,213,215} The second phase is characterized by a softening phase that is accompanied by the unfolding of the protein chains in the amorphous region along the load direction.¹¹³ This behavior appears to be gradual as the secondary structures unwind relatively to their hidden length after hydrogen bond breaking.¹¹¹ At the same time, new hydrogen bonds are formed, building β -sheet nanocrystals in the amorphous phases.²¹⁵ Once the amorphous regions are fully elongated and stretched, the load is transferred to the crystalline regions in a so-called stiffening phase. At higher stresses, the β -sheet crystals have to sustain higher strains.^{111,113} It was hypothesized that the deformation of crystallites causes stick-slip motions as ruptured strands reform short-term hydrogen bonds.^{98,214,216,217} As hydrogen bonds in the crystalline phase further break, and crystal sizes decrease upon pulling, the strain distribution is more uniform, causing a significant increase in the mechanical performance.⁹⁸ In the last phase, β -sheets are completely unfolded, and the silk's maximum tensile strength is reached until the fiber ruptures.²¹⁸

1.8 ENGINEERING AND ASSEMBLY OF SPIDER SILK FOR MATERIAL APPLICATIONS

Based on the highly adaptive structure-function relations, spider silk combines superb mechanical performance with biodegradability and biocompatibility when brought in contact with the human body.^{58,219-221} Consequently, spider silk represents an exciting biopolymer for engineering green, stimuli-responsive, or multifunctional (bio)materials to address biomedical and technical challenges. For both, industry and commerce, the sustainability of materials and production processes is becoming increasingly important.^{114,222} Since territorial, sexual, or hunger-dependent cannibalism is well-known among spiders, industrial farming of spiders is not feasible.²²³⁻²²⁵ Moreover, spiders held in captivity generate less silk with lower quality, and thus lower mechanical properties, as this strongly relies on climate, spider's health, and nutritional status.¹⁹⁹⁻²⁰¹ Forced silking of spiders only obtains low yields per session and appears to depend on reeling speed, besides other known parameters.^{197,226} In the last decades, biotechnological production routes in amenable hosts have been developed to yield spidroins with consistent

quality.^{227,228} In addition, recombinant production enables the functionalization by molecular engineering to empower silk with new properties.¹⁰⁷

Two different approaches are pursued to produce spidroins recombinantly. One possibility is the heterologous production of native (partial) silk gene sequences, mostly truncated cDNA, in different prokaryotic and eukaryotic expression hosts, such as bacteria,^{229,230} yeast,²³¹ plants,^{232,233} insect cells,^{234,235} mammalian cells,²³⁶ and even transgenic animals.²³⁷⁻²⁴⁰ However, this approach showed only limited success due to high costs and low yields, which can be explained by differences in the codon usage of spiders compared to most hosts.²⁴¹ The abundant amino acid residues glycine and alanine are encoded only by a few codons, resulting in inefficient translation events. Moreover, the highly repetitive nature of spider silk genes hinders their manipulation by polymerase chain reaction.^{30,57,110} To circumvent these difficulties, the second and more common approach was established using synthetic genes. Therefore, relevant amino acid motifs of the natural spidroins were identified and subsequently translated back into synthetic DNA sequences comprising repetitive blocks, considering the codon usage of the host organism.²⁴² Most commonly used for recombinant production is *Escherichia coli* (*E. coli*) due to the broad knowledge about its high-density cultivation, production scalability, short doubling times, low costs, and simple to obtain genetic modifications.^{110,243,244} Although significant progress has been made toward spidroin yields and qualities, some challenges need to be overcome in the near future. The production of highly repetitive proteins with a molecular weight comparable to that of natural spidroins entails difficulties, i. e. inefficient transcription, discontinuous translation, gene instability, or truncations due to the bacterial ribosomal machinery.²⁴⁵⁻²⁴⁷ Usually, the produced spidroins have much lower molecular weights than those of natural ones. However, strategies have been explored to produce native-sized recombinant spidroins, for example, by engineering the metabolic pathways of *E. coli*²⁴⁸ or using split intein-mediated ligation of spidroins.²⁴⁹

Driven by ingenuity and the need for innovation, spider silk engineering at the molecular level (**Figure 7**) enables the design of customized functional materials with novel functions for defined applications.^{107,250,251} Even minor manipulations of the sequence by replacing one single amino acid residue (**Figure 7 a**) impact the hydrophobicity of the spidroins and the materials made thereof, suitable e. g. for tissue engineering.^{179,252-254} Functional peptides can be either fused to the proteins' termini or incorporated within the amino acid sequence (**Figure 7 b**). The integration of

functional peptides can implement a cleavable sequence as well as binding motifs or domains, valuable for tissue engineering,²⁵⁵ such as nerve and bone regeneration,^{256,257} implant coating,²⁵⁸ or cancer targeting²⁵⁹ among other applications. Further, fusions of spidroins with functional molecules (**Figure 7 c**), i. e. DNA,^{260,261} glycopolymers,²⁶² or organic ligands,²⁶³ impart controllable superstructures or empower spidroins with novel functions. Inspired by the silk architecture, amphiphilic block co-polymers open new routes to design smart materials.^{264,265} Functionalization of silk materials can also be achieved by blending or doping silk solutions with functional additives. Multilevel modifications require knowledge about the hierarchical set-up of silk to exploit its physical properties.^{251,266} Computational investigations can contribute to the design, prediction, and understanding of silk proteins and materials.^{98,111,267,268}

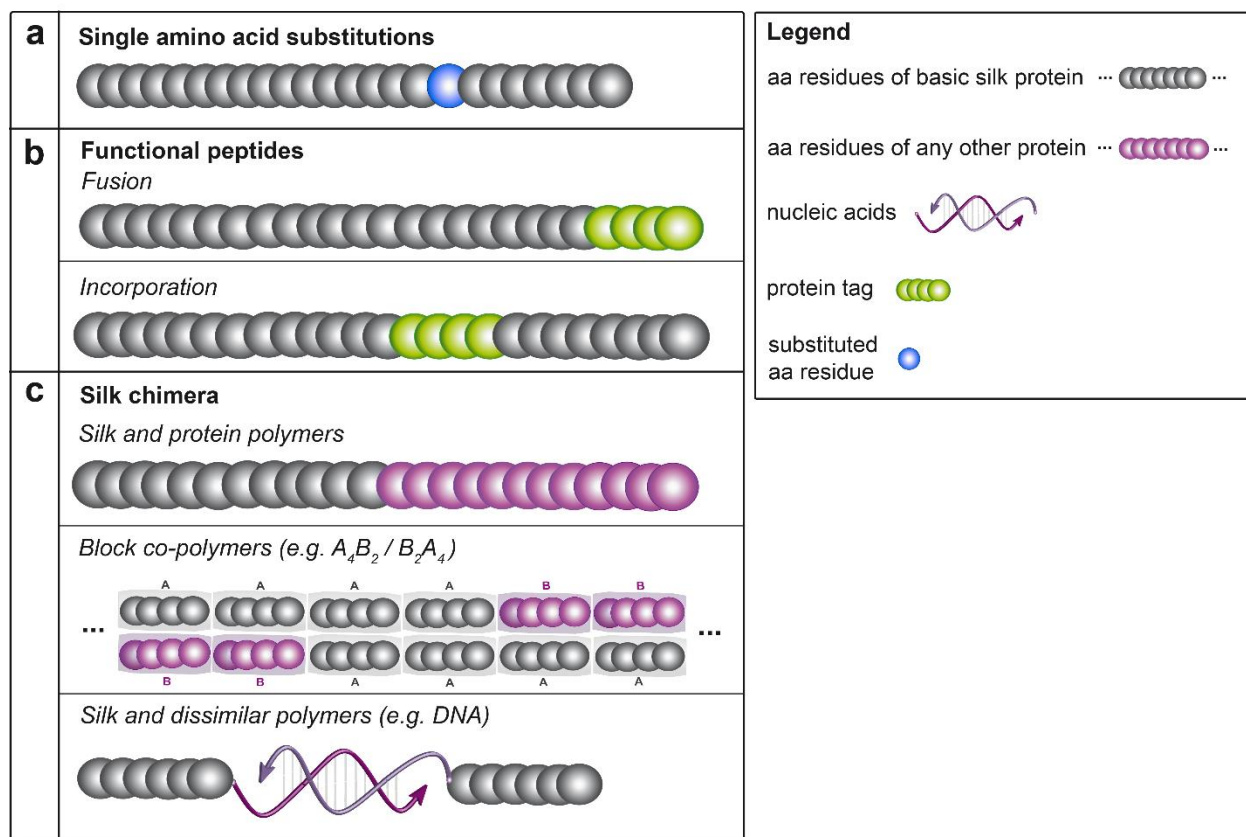


Figure 7. Selected approaches of molecular engineering to combine functional motifs into recombinant silk proteins. **(a)** single amino acid (aa) substitutions, **(b)** fusion or modification with functional peptides, **(c)** silk chimeras comprising multiple components of proteins or dissimilar polymers. The spheres represent amino acid residues, and colorations highlight the engineered area in the respective silk constructs. Modified from Saric, M., & Scheibel, T., Engineering of silk proteins for materials applications. Current opinion in biotechnology, 2019, 60, 213-220, with kind permission of the publisher Elsevier.¹⁰⁷

1.8.1 RECOMBINANT SPIDER SILK PROTEINS

The recombinant engineered spidroins used in this work are based on the two MaSp2-variants ADF3 (NCBI GenBank code: AAC47010) and ADF4 (NCBI GenBank code: AAC47011) of the European garden spider *A. diadematus*, called eADF3 and eADF4, respectively. A schematic illustration of the biotechnological process flow is shown in **Figure 8**. After DNA extraction from the spider's MA silk gland, genetic information was decoded in ADF3 and ADF4, and highly repetitive conserved amino acid blocks could be identified (**Figure 8 a**). Next, corresponding consensus motifs were engineered, which can be combined modularly using a custom-designed cloning system for seamless multimerization (**Figure 8 b**).^{154,242} The synthetic gene sequences were adapted regarding size and bacterial codon usage. Generally, the repetitive core domain of eADF4 is composed of a consensus module termed C (carboxyl-group of glutamic acid), whereas eADF3 is built up of alternating consensus modules A (alanine-(A)-rich) and Q (glutamine-(Q)-rich).²⁴² The exact amino acid composition of a single module is given in Figure 8 b. While the C module of eADF4 contains GPGGX or polyalanine (A)_n motifs, modules A and Q of eADF3 comprise polyalanine (A)_n as well as GGX repeats, and GPGQQ motifs, respectively (see **Table 3**).⁵⁷ In addition, non-repetitive TDs from the native genes can optionally be linked to the synthetic genes (**Figure 8 c**). Up to now, several variants have been designed with varying compositions and a number of core domains in the presence and absence of TDs. In this study, the CTDs of *A. diadematus* (NR3 of ADF3, NR4 of ADF4) and *L. hesperus* (NRC1 of MaSp1) were used. Since the NTDs of *A. diadematus* are unresolved, but NTDs are highly conserved throughout MaSps and spider species,^{121,160} the established NTD (NRN1 of MaSp1) of *L. hesperus* was included. In the natural NTD, a linker region of one subunit was detected in a crevice and assumed to connect the NTD to the repetitive core domain to further lock the chain alignment.¹²¹ Therefore, a native linker region was fused to the NTD (NRN1L) to mimic the natural model. Usually, the spidroins are modified with tags, either to increase production and purification efficiency or for detection using Western blot analysis. The engineered synthetic gene sequences are cloned into expression vectors which are transformed into *E. coli* and expressed (**Figure 8 d**). The recombinant spidroin variants can be purified after bacterial lysis, using either a column-based or column-free method.¹⁵⁴ The purified spidroins can be freeze-dried for long-term storage and resolubilized if required.

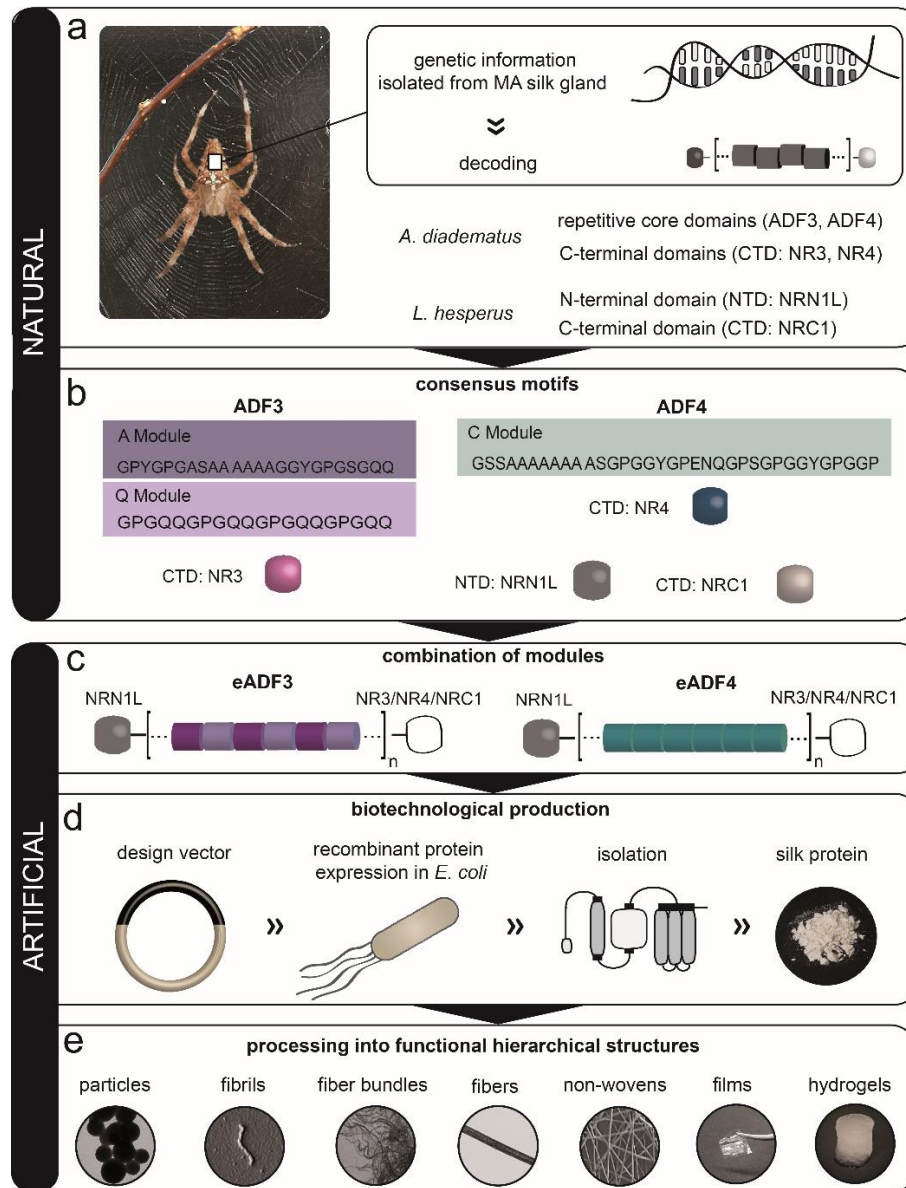


Figure 8. Schematic illustration of the biotechnological production and processing of recombinant spider silk. **(a)** After DNA extraction from spiders' MA silk glands, genetic information was decoded, and amino acid motifs could be identified. The amino acid sequences were back-translated into DNA sequences considering efficient bacterial codon usage. **(b)** Sequence motifs of modules A, Q, and C are derived from the two MaSp2 analogs ADF3 and ADF4 from *Araneus diadematus*. As published before,¹⁵⁴ modules could be multimerized in an arbitrary seamless manner. Contrary to the repetitive core domains, which display diverse sequences, the TDs of MaSps are evolutionarily highly conserved. Since no NTDs of ADF3 or ADF4 are identified so far, the well-studied NTD of *L. hesperus* was used instead. In addition, CTDs from both spider species could be used. **(c)** Scheme of engineered spidroin variants eADF3 and eADF4. **(d)** For biotechnological production in *Escherichia coli*, gene sequences encoding for spidroins can be cloned into expression vectors. Spidroins can be purified in column as well as non-column approaches and freeze-dried for long-term storage. **(e)** Processing into different hierarchically structured morphologies for various applications.

1.8.2 SELF-ASSEMBLY PROPERTIES OF ENGINEERED ADF3 AND ADF4

Recombinant spidroins can self-assemble and be processed into a myriad of hierarchically structured morphologies, namely particles, nano- and microfibers, hydrogels, nonwoven meshes, and films, among others, tailored for different applications (**Figure 8 e**). In the following, these morphologies are presented below in more detail for *A. diadematus* MaSp2 derivatives eADF3 and eADF4.

For recombinant eADF4, it was demonstrated that at least two C-modules are required for self-assembly. With increasing C-module numbers, the assembly kinetics were accelerated, however, the assembled structures appeared visually the same in the final result.²⁶⁹ The majority of studies utilize an eADF4 variant with 16 consecutive C modules (eADF4(C₁₆)), comprising a molecular mass of 50 kDa. So far, a variant with a CTD (eADF4(C₁₆NR4)) has been cloned and investigated in very few studies,^{154,270,271} but no derivative with a NTD has been developed yet. For recombinant eADF3, predominantly variants of either 12 or 24 consecutive (AQ) modules (eADF3((AQ)₁₂ / eADF3((AQ)₂₄) were consolidated over time, comprising molecular weights of 48 kDa or 95 kDa, respectively.¹⁵⁴ In the past, eADF3 variants equipped with CTD as well as NTD were studied.^{31,122,154,167,179,272} The solubility of eADF3 and eADF4 core domains differs considerably, which was investigated in experimental and computational analysis.^{154,273} It has been shown that the solubility of eADF3 is about four times higher than eADF4, as the interaction with the surrounding aqueous solutions is preferred over the interaction with hydrophobic polypeptide chains.^{154,236} These differences in the solubility behavior play a decisive role in the stimuli-responsive assembly performance, valuable for materials with wide applications.

Previous studies investigated the impact of conditions involved in the mediation of native fibers regarding biochemical properties, self-assembly, and aggregation. The physico-chemical parameters as they occur in the spinning process of spiders can initiate self-assembly of recombinant spidroins. One possibility is the ionic stimulation upon the addition of phosphate ions. Since phosphate increases the surface tension of water, hydrophobic interactions between polyalanine motifs cause the assembly of spidroins. At phosphate concentrations below 300 mM, eADF4 self-assembled into β -sheet rich nanofibrils approximately 2-10 nm in diameter,^{274,275} similar to those fibrils detected in the natural counterpart.²⁷⁶ For the nanofibril assembly of eADF4, a two-phase model was suggested.²⁶⁹ The first part involves a nucleation phase, in which

intrinsically unstructured silk monomers transiently fold into anti-parallel β -sheets via interlinked poly-alanine stretches in adjacent C-modules. In the second part, the elongation phase, another soluble monomer docks to the exposed fibril end, inducing a structural change in the monomer and facilitating a new nucleation docking site. Based on the nanofibrillization behavior, eADF4 variants facilitate the fabrication of physically cross-linked hydrogels at concentrations above 2 % w/v and aqueous conditions.²⁷⁷ Hydrogels made of recombinant silk proteins, for example, can be used in biomedical applications for biofabrication and 3D printing of cell-loaded bioinks^{278,279} or the administration of water-soluble and water-insoluble drug depots.²⁸⁰ Recently, nanohydrogels were utilized for bioselective binding of proteins in an immobilized setup.²⁸¹

For eADF3, it was demonstrated that the addition of phosphate at low concentrations induced the aggregation into higher supramolecular structures without nanofibrillar characteristics due to its solubility described above.¹⁶⁷ At high phosphate concentrations (> 400 mM), eADF4 and eADF3 formed spherical particles based on a liquid-liquid phase separation involving a protein-rich and a solvent-rich phase.^{274,282} Sphere sizes depended on the protein concentration, mixing conditions, and final salting-out concentration, yielding particles with diameters in the range of approximately 250 nm to 3 μ m.²⁸²⁻²⁸⁴ Microspheres made of recombinant spidroins constitute a class of biomimetic materials that can be obtained in a simple all-aqueous process and facilitate delivery of sensitive drugs or genes.^{252,284,285} Several eADF4 variants were identified to be promising candidates for either targeted drug delivery with controllable drug release upon changes in the pH or redox state,^{286,287} or drug-releasing composite materials with long-lasting anti-microbial features.²⁸⁸

During the passage along the spinning duct, MaSps are exposed to mechanical shear forces, which can also be mimicked *in vitro*. Investigations of eADF3 under shear stress revealed strong assembly behavior, enhanced in the presence of TDs, independent of salt concentration,^{122,167,179,282} whereas eADF4 did not assemble in response to elongation flow.²⁸² eADF3 without TD yielded ill-defined β -sheet-rich aggregates upon shearing. At the same time, TD-comprising eADF3 formed aligned fibrillary aggregates, similar to fiber-bundles, with dimensions of microns to millimeters after shearing for several hours. While eADF3 variants are ideally suitable for producing single fibers by wet-spinning from aqueous dope systems,^{31,289} eADF4 fibers from organic dopes have been wet-spun, applicable for regenerative medicine²⁹⁰ or commercial uses, e.g., cosmetics and textile fabrication (BIOSTEEL® by company AMSilk).^{107,291} In a proof of

concept study by Rammensee *et al.*,²⁸² the assembly of an eADF3/eADF4 mixture (without TDs) was tested regarding fiber-forming parameters in a microfluidic approach. Although the introduction of shearing, salting out, and pH changes led to the formation of a few microfibers, these could not be extracted and investigated using tensile tests. The next chapter (see 1.8.3) will discuss the broad topic of wet-spinning and microfluidics of recombinant spidroins in more detail. In addition, sub-micrometer and nanometer fibers of eADF4 were obtained by electrospinning using organic^{219,292-295} or aqueous solvents,²⁹⁶ yielding nonwoven fiber mats, which were either utilized as cell culture substrates^{292,297} or filtration applications.²⁹³⁻²⁹⁵

Water-insoluble films represent a further versatile morphology, made of eADF4 variants, comprising thicknesses from nano- to micrometer range depending on conditions such as solvent, post-treatment, or substrate surface on which the films self-assemble.^{271,298-300} Films were utilized as suitable substrate or scaffold for coating implants^{220,301} as well as catheters³⁰² to minimize thrombotic fouling or negative side effects of the foreign body reaction, enhance cell activities (adhesion, migration, differentiation, and proliferation),^{254,292,303,304} provide a new energy technology for light-induced hydrogen production,³⁰⁵ or prevent anti-microbial infestation on biomedical or technical materials.³⁰⁶⁻³⁰⁸

1.8.3 ARTIFICIAL SPIDER SILK FIBER SPINNING

Over the last few years, the demand for fiber-based materials has increased, as they offer a wide range of applications, both in commercial and research areas. Great efforts have been made to obtain high quality and quantity of fibers. In principle, modern artificial fiber spinning technologies are based either on polymer melts or polymer solutions which can be utilized in different processes like melt spinning, dry-spinning, electrospinning, or wet-spinning.^{29,309,310} In the most basic setup of melt spinning, highly viscous melts are usually produced by heating thermoplastic polymers, which are subsequently spun into fibers by extrusion and rapid cooling.^{311,312} On the contrary, in solution spinning approaches, polymers are dissolved in organic or inorganic solvents, and fibers are spun either by polymer precipitation in coagulation baths (wet spinning) or removing the solvent by evaporation (dry and electrospinning).^{309,313} Depending on the employed spinning method, fibers vary in their parameters, i. e. surface morphology, diameter, appearance, and mechanical properties. In this section, the focus lies on the wet-spinning and

microfluidic spinning of recombinant spidroins as they mimic the native spider silk spinning system best.

In wet-spinning processes, a highly concentrated dope is extruded through a nozzle or spinneret into a coagulation bath, filled with a liquid in which the spidroins precipitate, and a fiber only a few microns in diameter is solidified. In spider silk, spidroins constitute the structural components of the spinning dope, and water is the solvent. In artificial approaches, highly concentrated spinning dopes (10-50 % w/v) usually are produced by dissolving recombinant spidroins using strong denaturants^{248,314-316} (e. g. HFIP, formic acid, LiBr) or aqueous buffer,^{31,236,317-320} to yield the concentrations of natural spinning dopes (50 % w/v).¹⁴¹ Another approach to producing spinning dopes involves regenerated/reconstituted native spider silk fibers dissolved in organic solvents.³²¹⁻³²⁴ Since access to natural spider silk is limited, and fibers spun from reconstituted dopes did not yield the desired mechanical properties, the focus of current silk fiber research is on utilizing recombinant spidroins. Organic solvents, in particular, offer the opportunity to dissolve spidroins even with high molecular weights quickly at high concentrations.²⁴⁸ However, there are significant disadvantages in using organic solvents, especially for industry, namely high costs, challenging disposal regulations, and difficulties in the removal of the solvent from the fiber, which is indispensable for biomedical applications.³²² In addition, the strong interactions between protein and solvent, on the one hand, enable high spidroins solubility, but on the other hand, may hinder the subsequent assembly during the spinning process. For this reason, the production of spinning dope solutions in an aqueous system seems favorable, achieving concentrations of up to 50 % w/v in the past.^{236,319,325,326} Aqueous spinning dopes can be obtained either by concentrating low-concentrated solutions,^{31,318-320,326} dissolving directly at high concentration,^{325,327} or by utilizing the self-assembly behavior of spidroins.^{31,155,169} The preparation of highly concentrated spinning dopes may become difficult as spidroins tend to aggregate, which is why the biophysical properties of the individual recombinant spidroins are essential to consider.

Heidebrecht *et al.*³¹ established two routes for the preparation of aqueous spinning dopes (**Figure 9**) from recombinant eADF3 spidroins of different sizes and in the presence of TDs. First, a start solution was prepared by dissolving the proteins in guanidinium thiocyanate, which was subsequently removed stepwise by dialysis against a stabilizing saline Tris-buffer, yielding a concentration of 2-3 % w/v. Subsequently, one possibility was to dialyze the solution against polyethylene glycol (PEG) to remove water and obtain a highly concentrated dope (10-17 % w/v),

which was called classical spinning dope (CSD). Alternatively, spidroins comprising CTDs were dialyzed against a phosphate-containing buffer, initiating a phase separation into a low concentrated phase (not suitable for spinning) and a highly concentrated phase (9-15 % w/v), the latter was named biomimetic spinning dope (BSD).^{31,155} It is assumed that the presence of phosphate ions initiates the formation of micellar-like assemblies, as supposed in former studies.^{164,167,169} Fibers spun from BSD showed superior mechanical properties compared to those from CSD, which was attributed to the higher alignment of β -sheet nanocrystals in the BSD fibers.²⁸⁹

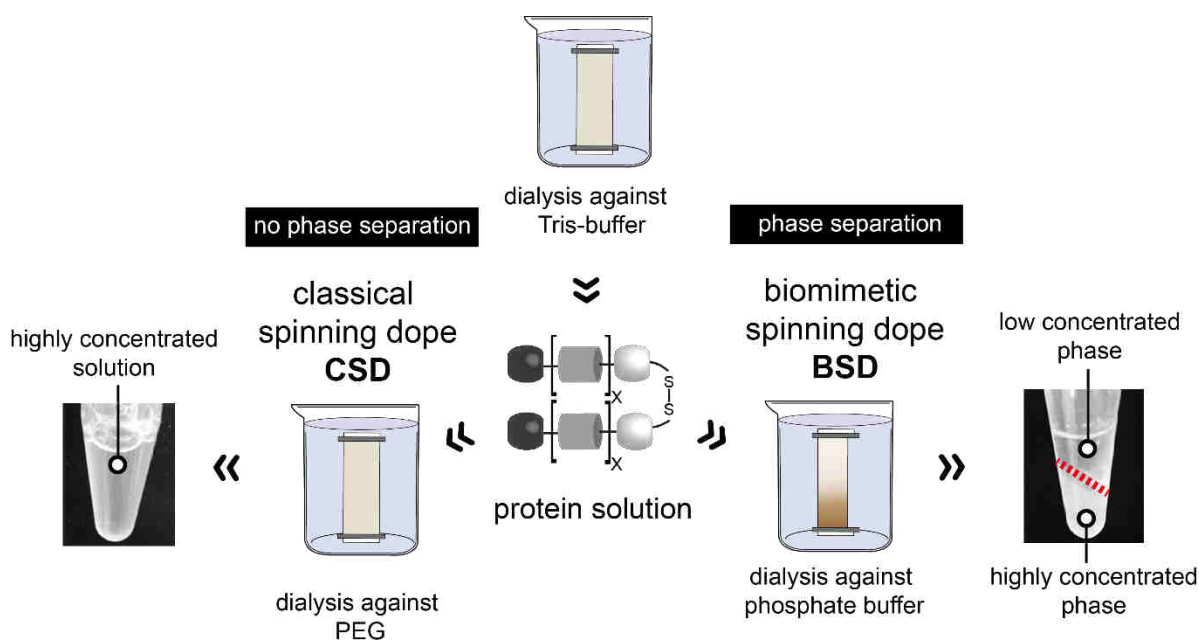


Figure 9. Production strategy of aqueous spinning dopes made of recombinant spidroins comprising terminal domains. Classical spinning dopes (CSD) were obtained by dialyzing a spidroin solution against polyethylene glycol (PEG) to remove water, obtaining a highly concentrated solution. Biomimetic spinning dopes (BSD) were prepared using dialysis against a phosphate-containing buffer, and a phase-separated solution was obtained.

Table 4. Comparison of the characteristics of man-made fibers from various spider silk proteins (with or without TDs) spun by wet-spinning (W) or microfluidics (M).

Origin spider / spidroin	Recombinant spidroin	TDs	Molecular mass [kDa]	Solvent / coagulation bath	Spinning method	Fiber diameter [μm]	Strength [MPa]	Extensibility [%]	Toughness [MJm ⁻³]	Young's Modulus [GPa]	Source
<i>L. mactans</i> / TuSp1	eTuSp1	✓	16	HFIP / IPA + MeOH	M	45	78 ± 4	17 ± 1	11 ± 0.8	2 ± 0.4	315
<i>A. aurantia</i> / MaSp2	2Ex12	✗	71	HFIP / IPA	W	74 ± 33	49 ± 7	3 ± 2	n. a.	0.04 ± 0.03	314
<i>N. clavipes</i> / MaSp1	96-mer	✗	284	HFIP / MeOH	W	25	508 ± 108	15 ± 5	n. a.	21 ± 4	248
<i>N. clavipes</i> / MaSp1	WS-PSD-3x	✗	47	Water / EtOH	M	18	286 ± 137	18 ± 12	37 ± 28	8 ± 4	317
<i>N. antipodiana</i> / TuSp1, MiSp1	11RPC	✓	378	HFIP / Water	W	14	308 ± 57	10	n. a.	9 ± 3	316
<i>A. diadematus</i> / MaSp2 (ADF3)	eADF3	✓	152	Water / IPA	W	27 ± 10	370 ± 59	110 ± 25	189 ± 33	4 ± 1	31
<i>A. diadematus</i> / MaSp2 (ADF3)	ADF3	✓	120	Water / MeOH + Water	W	20	219	59	103	4.9	236
<i>T. clavipes</i> / MaSp1	N16C	✓	144	Water / Water	M	34 ± 0.7	288 ± 20	47 ± 3	100 ± 13	3 ± 0.7	320
<i>E. australis</i> / MaSp1, <i>A. ventricosus</i> / MiSp	NT2RepCT	✓	100	Water / Water	W	12 ± 2	162 ± 8	37 ± 5	45 ± 7	6 ± 0.8	318
<i>A. diadematus</i> forcibly silked	-	✓	-	-	-	4 ± 0.4	1183 ± 334	24 ± 8	167 ± 65	8 ± 2	31
<i>A. diadematus</i> supercontracted	-	✓	-	-	-	5 ± 0.1	795 ± 42	39 ± 1	129 ± 6	4 ± 0.2	192

EtOH: Ethanol, IPA: Isopropyl alcohol, HFIP: 1,1,1,3,3,3-Hexafluoropropan-2-ol, MaSp: Major Ampullate Spidroin, MeOH: Methanol, n. a.: not available, TDs: terminal domains

The continuous extrusion of spinning dopes usually is carried out into coagulation baths containing monohydric alcohols or mixtures of alcohol and water, resulting in the dehydration of the fibers.³²⁸ Generally speaking, wet-spinning is a rather slow method compared to other spinning techniques, resulting in a higher degree of spidroin alignment and improved mechanical performance.³²⁸ A washing step follows to remove the residues of the coagulation bath and the spinning dope solvent.³²⁹ Afterwards, the fibers are post-stretched, as it is also done by spiders, in order to align the β -sheet crystals along the fiber axis.^{330,331} Here, the composition of the post-stretching bath has a substantial influence on the fiber. While primary alcohols (methanol, ethanol, etc.) impart higher stiffness and strength to the fibers, secondary alcohols (e. g., isopropyl alcohol) increase extensibility.³³⁰

Microfluidic wet-spinning is a modern technique that deals with processing small volumes of fluids, usually in a mild environment, within miniaturized channels of engineered configurations.³³²⁻³³⁵ Due to its capacity to mimic aspects of the native spider silk spinning system through precise and systematic control over individual fluids, microfluidics has emerged as a remarkable approach for the production of microfibers.³³⁶ The spinning dope and a sheath fluid flow through channels into a microfluidic device and merge at a junction (see **3.2, Figure 13**). On the microscale, these flows are laminar, and solidification of the fluids occurs by slow diffusion at the interface. The spinning dope is hydrodynamically focused by the sheath fluid, inducing spidroin assembly and solidification into fibers extruded through an outlet.³³⁶ To date, few studies have been conducted in which recombinant spidroins have been investigated concerning their self-assembly behavior utilizing microfluidics.^{282,315,317,320,337}

Due to numerous parameters, fiber spinning appears to be highly complex, hence, the ideal combination of spinning dope, coagulation, and post-stretching bath have to be established and optimized for each spidroin individually. Fibers spun artificially display far different mechanical properties compared to natural ones (**Table 4**). In general, the mechanical performance of the fibers improves with a low diameter and higher molecular weight of the recombinant spidroins. Native-sized spidroins yielded fibers (spun from organic dopes) with a Young's Modulus of 21 GPa, at least twice that of natural dragline silk, and respectable strength of 508 MPa.²⁴⁸ The best fiber mechanics to date spun from an aqueous system were achieved with biomimetic dopes containing recombinant spidroins with TDs, displaying nature-like toughness of 189 MJ/m³ due to the

significantly higher elasticity of 110 % despite lower strength of 370 MPa in comparison to the natural dragline silk.³¹

Artificially spun fibers are commonly compared to native fibers. Since the mechanical properties of collected natural dragline silks are subjected to very high variability (see 1.6),¹⁹⁴ controlled supercontraction of forcibly silked fibers is nowadays a widely used method to yield consistent data with representative real tensile properties of naturally spun fibers (**Table 4**).³³⁸⁻³⁴⁰

2 AIM OF THE WORK

Natural spider silk fibers exhibit mechanical and biological properties unmatched by most other known natural or man-made fibrous materials, designating spider silk as a rich source of inspiration for a plethora of applications in technical and biomedical fields. Even though spider silks have been in the focus of scientific research for decades, it was yet not possible to fabricate synthetic fibers mimicking the outstanding properties of their native counterparts due to their complex hierarchical architectures from a molecular to the macroscopic level.

The aim of this work was to examine individual intrinsic and extrinsic aspects of the natural spider silk spinning process in more detail and further unravel the hierarchical self-assembly of MaSps regarding structure-function relations to create biomimetic materials. Therefore, various recombinant MaSps based on the ones found in the MA silk of the European garden spider *A. diadematus*, namely ADF3 and ADF4, were used, and the following research objectives for the thesis were defined:

Objective (1) is to study the so far unknown interplay of MaSps with implications for self-assembly and fiber mechanics. Although almost all natural MA silk fibers are built from at least two or more spidroins, yet artificial approaches have predominantly used only one class of recombinant spidroins. In this work, it was sought to produce MaSp mixtures of eADF3 and eADF4 variants and investigate intermolecular interactions regarding solubility and self-assembly into higher-order structures. Although the tripartite structure of MaSps is well-known, including highly repetitive core and non-repetitive domains, the function of the terminal domains as molecular features was barely investigated in full-length spidroins. Therefore, recombinant variants in the presence and absence of terminal domains were used to study their impact on the self-assembly process upon external stimuli. Ultimately, it was aimed to develop a fully aqueous, biomimetic spinning process to yield artificial high-performance fibers that imitate the mechanical properties of native spider silk fibers as closely as possible.

Objective (2) is to engineer bioinspired hybrid spidroin with multifunctional properties. Instead of using MaSp mixtures, a simplified two-in-one (TIO) approach should be developed to exploit the potential of combining individual characteristics of eADF3 and eADF4. The hybrid variant should be obtained either by a covalent bond (TIO spidroin) or solely by dimerization of

the carboxyl-terminal domain (heterodimer). Further, the spidroins were to be investigated in structural and functional aspects and processed into fibers.

Objective (3) is to develop a molecular understanding of MaSps pre-assembly in spinning dopes and their structural state in fibers spun thereof. The natural spinning process is highly controlled and involves sequential conformational changes of the MaSps. Still, the current gap in knowledge revolves around the importance of the constitution of spinning dopes as pre-requisites for fibers with outstanding mechanical properties. Here, it was aimed to provide a detailed and holistic view regarding the hierarchical assembly process across length scales from soluble spidroins in spinning dopes through the spun fiber state. Therefore, eADF3-CTD was utilized as a simplified representative spidroin model, unlabeled as well as $^{13}\text{C}/^{15}\text{N}$ labeled. The combination of biophysical methods allowed to track the spidroin assembly and structural characteristics.

3 SYNOPSIS

In the course of this dissertation, it was aimed to understand and mimic the natural spinning process in all important respects. Structural insights into the self-assembly of spidroins helped to unravel how nature-like performing fibers are created and how synthetic silk alternatives can be designed for versatile applications in high-tech fields. A schematic overview of the thesis projects is shown in **Figure 10**.

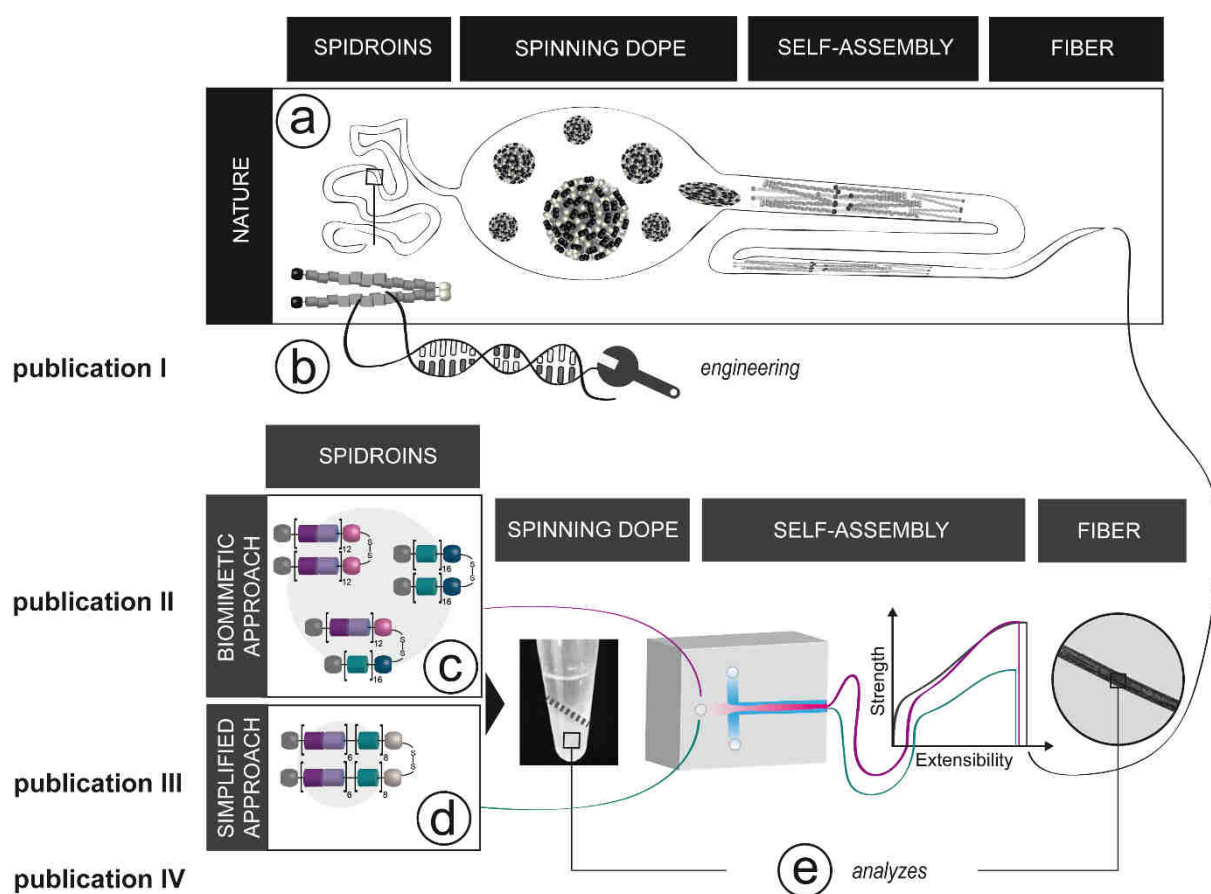


Figure 10. Overview of the thesis topics unraveling the native spider silk spinning process using different recombinant silk protein variants. **(a)** Illustration of a natural spinning process is divided into four sections: spidroin production, storage in highly concentrated spinning dopes, self-assembly, and fiber formation. **(b)** A part of the work provides an overview of how silk proteins can be engineered at the molecular level, enabling tailored functionalization for manifold technical and medical applications. **(c)** For the first time, recombinant spidroins comprising terminal domains were co-produced, yielding a mixture of homo- and heterodimers, which could be spun in nature-like performing fibers upon biomimetic spinning. Particularly, the heterodimers played an essential role in mediating self-assembly within the mixture. **(d)** In a simplified approach, two-in-one spidroins were studied in structural and functional aspects, showing multifunctional characteristics of both underlying eADF variants as well as excellent processability into green high-performance fibers. **(e)** A combination of biophysical methods allowed to track the assembly from the formation of the dope to the final spun fiber.

Initially, an overview of recent advances in the functionalization of silk proteins on a molecular level is provided (**publication I**). With this, genetic engineering approaches enabling tailored modifications towards optimized or novel functions in silk materials were reviewed, considering current challenges in the biotechnological production of functionalized silk proteins. Insights into the fabrication of engineered silk proteins are shown and how self-assembly into higher-order structures is utilized for technical and medical materials.

The second part of the thesis constitutes the thematic focus, dealing with the development of an aqueous fiber production approach mimicking the natural spinning process as close as possible (**publication II**). Mixtures comprising eADF3 and eADF4 variants were prepared either by co-production in bacteria (*in vivo*) or by refolding (*in vitro*). Cloning of DNA, production, and purification of different MaSp variants was developed and optimized. Structural characterization and self-assembly of protein mixtures and individual one-protein variants were carried out to investigate the impact of MaSp interplay and the influence of terminal domains. Aqueous spinning dopes were prepared, and a microfluidic wet-spinning approach was developed and optimized. Fibers were post-stretched and further studied using tensile tests and microscopy.

The third part of the thesis provides investigations of hybrid spidroin variants combining characteristics of eADF3 and eADF4 (**publication III**). The heterodimer was isolated from a mixture of homo- and heterodimers using a two-step column purification strategy. Next, a convenient approach was established by combining mechanical and chemical characteristics of eADF3 and eADF4. A two-in-one spidroin in the presence of TDs was cloned, produced, and purified. Both hybrid variants were structurally characterized and self-assembled upon shearing or the addition of phosphate ions to test the potential for fiber assembly. Highly concentrated aqueous spinning dopes could be prepared from the TIO spidroin and fibers were spun in a biomimetic, aqueous wet-spinning process, post-stretched, and analyzed using tensile tests and microscopy.

In the fourth part of the thesis, new findings of MaSps structural self-assembly were gained from studies of highly concentrated aqueous spinning dopes and fibers spun thereof (**publication IV**). The recombinant spidroin eADF3-CTD was produced both unlabeled and isotope (^{13}C , ^{15}N) labeled. The production route of isotopically enriched spidroins was newly

developed in this work. Highly concentrated, aqueous spinning dopes were prepared and analyzed by combining biophysical techniques to track the spidroin assembly and understand atomic level structural states at different buffer conditions. Several solid-state NMR experiments were performed to investigate secondary structures in fibers spun from different spinning dopes.

3.1 PRODUCTION OF NATURE-LIKE RECOMBINANT SPIDER SILK PROTEINS

The focus of this work was primarily on terminal domains-comprising recombinant spider silk proteins derived from the two MaSp2 proteins ADF3 and ADF4 of the European garden spider *Araneus diadematus*. Corresponding consensus modules termed C (carboxyl-group of glutamic acid), A (alanine-rich), and Q (glutamine-rich) were multimerized to obtain the repetitive proteins, details on the individual engineered eADF variants are given in 1.8.1 and 1.8.2. In contrast to the repetitive core domains with varying sequences, the TDs of MaSps are evolutionary highly conserved between different species (publication II, Figure S1),^{160,161} which is why TDs of *A. diadematus* and *L. hesperus* were used in this study. For the expression of synthetic spider silk genes, the host organism *E. coli* was used, as it is a convenient and widely utilized system.^{110,243} Since the production of recombinant MaSps with molecular weights comparable to that of native-sized spidroins (200-330 kDa)^{118,341} entails difficulties such as low yields, variants with lower molecular weights (46-150 kDa) were designed (**Figure 11**). Spidroins with CTDs formed parallel-oriented dimers covalently bonded by an intermolecular disulfide bridge.^{122,176,177} Since the standard redox potential of the CTDs is lower (-300 to -320 mV)³⁴² compared to the redox potential within the cytosol of *E. coli* (-260 to -280 mV),^{343,344} the oxidation of the cysteine's thiol groups can already take place in the bacterial cytosol.

The engineered MaSps NTD-eADF4-CTD, as well as all hybrid eADF constructs such as the heterodimer, and two-in-one (TIO) spidroin, were newly designed in the course of this work. In contrast, other employed reference spidroins such as eADF3, eADF3-CTD, NTD-eADF3-CTD, eADF4, and eADF4-CTD were already studied previously.^{31,154,270} For the sake of clarity, only the trivial names of the individual spidroin variants are used in the text, but the systematic description can be taken from **Figure 11**, a more detailed overview is given in publication II (Figure S2). Cloning, production, and purification for new spidroin variants were developed and optimized.

Spidroins were examined individually and in mixtures to study the impact and interplay of eADF3 and eADF4 on hierarchical self-assembly (publication II).¹⁹² Since native ADF3 and ADF4 are secreted in the same compartment of the spinning gland,⁵² a new co-production route for the recombinant variants was established in publication II. Herefore, genes encoding NTD-eADF3-CTD and NTD-eADF4-CTD were cloned into an expression vector (pRSFDuet-1) bearing two multiple cloning sites under the control of two separate T7-promoters.

The co-production *in vivo* in *E. coli* yielded a mixture comprising homodimers and heterodimers in a stoichiometric ratio, further purification and processing of the mixture were also established in this work. The spidroin mixture comprised a molecular content of 450 kDa, which is significantly higher compared to recombinant spidroins from other studies (284 kDa²⁴⁸ or 378 kDa³¹⁶), representing the largest ones published so far. Since it is impossible to produce heterodimers individually based on the dimerization of the CTDs of monomers, they were isolated from the dimeric mixture in a developed on-column strategy in publication III, utilizing immobilized metal ion chromatography (IMAC) and ion-exchange chromatography (IEC).

For the covalent TIO spidroin, the core domain was engineered modularly using 6 eADF3(AQ) modules and 8 eADF4(C) modules, as well as TDs, were added to the core domain (publication III). The yielded molecular weight was comparable to the individual reference spidroins NTD-eADF3-CTD and NTD-eADF4-CTD, described above in 1.8.2. Gene expression and protein purification of TIO were carried out in a column-free approach similar to the previously published strategy.¹⁵⁴

For solution and solid NMR experiments (publication IV), isotopically (¹³C/¹⁵N) enriched eADF3-CTD spidroins were needed to optimize NMR assignment and structure determination.^{345,346} To obtain high amounts of isotope labeled spidroins for spinning dope and fiber processing, a production route was developed in which *E. coli* first grow in complex medium until high density was reached and then resuspended in minimal medium supplemented with ¹³C-glucose and ¹⁵N ammonia sulfate to produce eADF3-CTD.


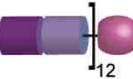
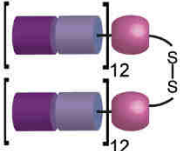
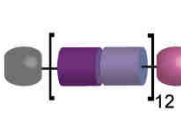
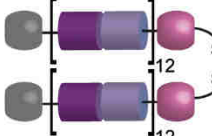
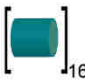
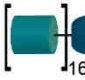
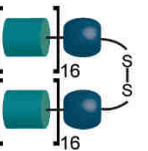
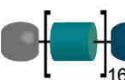
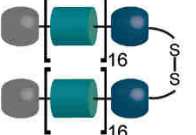
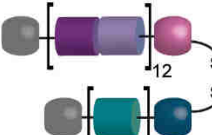
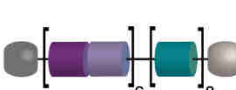
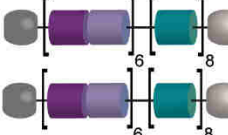






Protein	Monomer	Dimer
eADF3 (AQ) ₁₂	 48 kDa	—
eADF3-CTD (AQ) ₁₂ NR3	 60 kDa	 120 kDa
NTD-eADF3-CTD NRN1L(AQ) ₁₂ NR3	 76 kDa	 152 kDa
eADF4 C ₁₆	 47 kDa	—
eADF4-CTD C ₁₆ NR4	 58 kDa	 116 kDa
NTD-eADF4-CTD* NRN1LC ₁₆ NR4	 74 kDa	 148 kDa
heterodimer* NRN1L(AQ) ₁₂ NR3/NRN1LC ₁₆ NR4	—	 150 kDa
two-in-one (TIO)* NRN1L(AQ) ₆ C ₈ NRC1	 75 kDa	 150 kDa
Legend		
<p>Terminal domains</p> <p>NTD of <i>L. hesperus</i>  NRN1L CTD of <i>A. diadematus</i>  NR3  NR4</p> <hr/> <p>Recombinant core domains of <i>A. diadematus</i></p> <p> module A  module Q  module C</p>		
* : new variant developed in this work		

Figure 11. Overview of the recombinant spidroins derived from the MaSp2 analogs ADF3 (NCBI GenBank code: AAC47010) and ADF4 (NCBI GenBank code: AAC47011), terminal domains originated from either *A. diadematus* or *L. hesperus*. If the spidroins comprise CTDs, dimers are obtained. The trivial names (bold), which are further used in the text for simplicity and the systematic names, are given. The theoretical molecular weight of the monomeric or dimeric variants was determined using the online tool ProtParam (<https://web.expasy.org/protparam/>). New variants that have been designed within the thesis are highlighted with an asterisk.

3.2 STRUCTURAL AND FUNCTIONAL CHARACTERIZATION OF SPIDROIN INTERPLAY AND ASSEMBLY IN A MULTI-COMPONENT APPROACH

Natural MA silk fibers are composed of several MaSps,^{16,129} and the MA silk of *A. diadematus* contains two MaSp2 proteins (ADF3 and ADF4), which is known to be a unique attribute among all so far known orb-weaver spiders.⁴⁶ Since both ADF spidroins are secreted in the same compartment of the spinning gland,⁵² publication II examined the interaction of engineered spidroins and unraveled how this interplay contributes interdependently to assembly and fiber mechanics. Therefore, eADF variants comprising all domains (NTD-eADF3-CTD, NTD-eADF4-CTD) were co-produced in *E. coli* (*in vivo* approach). After purification, the purity for all spidroins was determined by UV/Vis, fluorescence spectroscopy, and SDS-PAGE (publication II Figure S3, S4, and Table S1). Mixtures comprising three dimeric species were identified in SDS-PAGE representing homo- and heterodimers, which provided evidence of the interaction between different MaSps already at a molecular level (**Figure 12**). In addition, heterodimerization was also obtained *in vitro* by refolding during dialysis. Western blot analyses revealed that the heterodimers occurred in a nearly stoichiometric distribution of 1:1:1 compared to each homodimer. In collaboration with Dr. Lukas Eisoldt and Volker Döring (Chair of Biomaterials, University of Bayreuth), similar observations were made with eADFs only comprising CTDs (publication II Figure 1). Regarding secondary structure content and thermal unfolding, far-UV CD revealed in the isolated heterodimers hybrid characteristics of both individual eADF3 and eADF4 homodimer variants (publication II, Figure 2).

The hierarchical self-assembly of recombinant MaSps was investigated, using a matrix of eADF variants in the presence and absence of TDs. Spidroin samples were dialyzed against Tris-buffer at concentrations of 20 μ M, and assembly was triggered upon adding potassium phosphate (50-150 mM) under naturally occurring conditions. Using microscopic (AFM, TEM) and spectroscopic (UV/vis, fluorescence) methods, it was shown that eADF3 assembled substantially differently compared to eADF4 according to their physicochemical characteristics¹⁵⁴ (**Figure 12**; publication II Figure 2 and Figure S5).

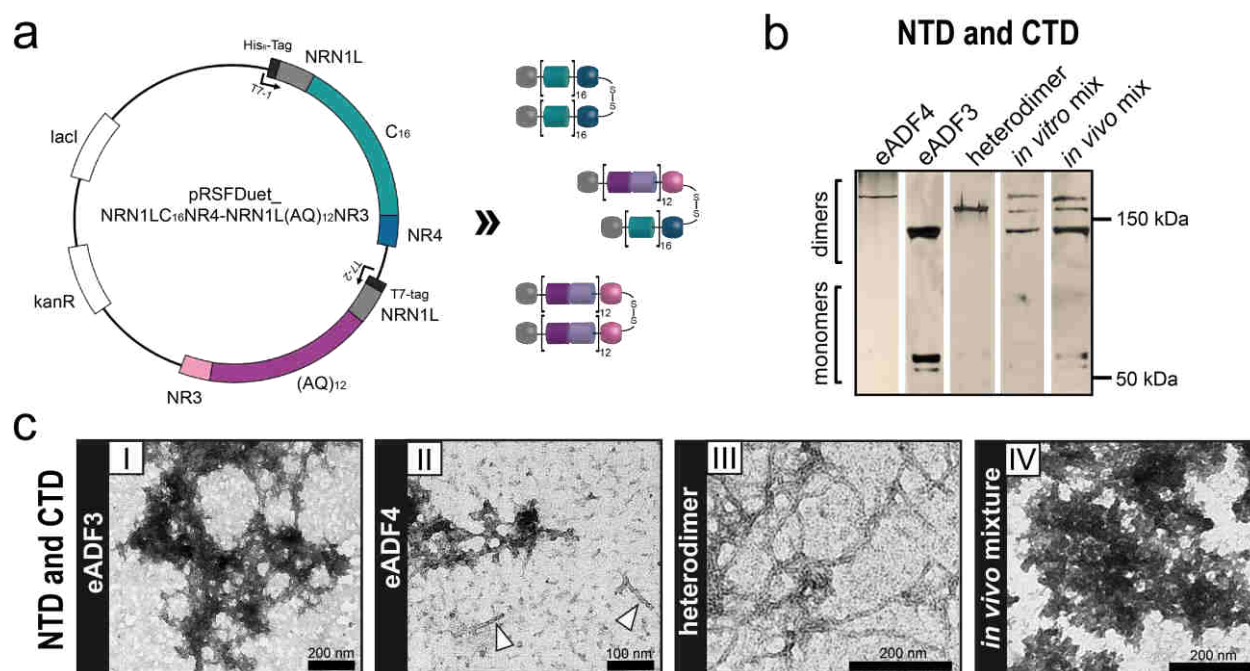


Figure 12. Production and self-assembly of recombinant full-length silk proteins. **(a)** Illustration of the vector used for co-expression of engineered genes *eADF3* and *eADF4*. **(b)** Analyzes of dimer formation of different ADF variants produced *in vitro* and *in vivo* using silver-stained SDS-PAGE. **(c)** Self-assembly of all-domains-containing recombinant MaSp2 variants in the presence of kosmotropic phosphate ions was analyzed using TEM. Spidroin variants were analyzed in the presence of both amino- and carboxyl-terminal domains. **(I)** NTD-eADF3-CTD, **(II)** NTD-eADF4-CTD, arrows highlight fibrillar structures, **(III)** purified heterodimers (without homodimers present), **(IV)** *in vivo* mixtures of NTD-eADF3-CTD/NTD-eADF4-CTD homo- and heterodimers. All protein samples were assembled at 20 μ M in 10 mM Tris-buffer, pH 8, and 50 – 150 mM phosphate buffer. The assays were performed for 1 day at room temperature. Modified from publication II with kind permission of the publisher John Wiley & Sons from Saric, M., Eisoldt, L., Döring, V., & Scheibel, T., *Advanced Materials*, 2021, 33(9), 2006499.¹⁹²

While in the case of eADF3, only amorphous aggregates were displayed, whether TDs were available or not, eADF4 showed different fibrillary morphologies depending on the presence of TDs. Particularly, it could be demonstrated that the fibril formation of eADF4 is highly affected by TDs as they increase solubility^{121,122} and control assembly to prevent premature aggregation. Interestingly, Thioflavin T (cross- β -sheet sensitive dye) assays demonstrated that the heterodimers self-assembled into a network of branched cross- β -sheet rich nanofibrils, which were strongly interconnected and distinctive in form and shape compared to that assembled by the one-protein variants. However, mixtures with all dimer species (*in vivo* and *in vitro*) showed large assemblies.

An all-aqueous biomimetic setup was established (**Figure 13**) to investigate the influence of heterodimerization and spidroins interplay on fiber assembly as well as fiber mechanics, recapitulating all key factors of the spider's natural spinning process. Aqueous, highly concentrated (10-13% w/v) spinning solutions of BSD or CSD were produced (see Figure 9) using MaSps comprising NTDs and CTDs. The spidroins were exposed to shear forces on their way from the syringe to the microfluidic chip and further pre-assembled upon the addition of phosphate at a low concentration of 30 mM and in a neutral environment of pH 8. As soon as the spidroin solution was extruded into the coagulation bath, containing a phosphate concentration of 0.5 - 1.0 M at pH 6, microfibers were formed, which were manually post-stretched to maximum and post-treated. The mimicry of the natural system in terms of full-length spidroins exposed to ionic and mechanical stimuli in a complete aqueous spinning setup was specifically designed in this work, which has to my knowledge not been done in any other study so far.

Tensile tests of post-stretched fibers spun from BSD displayed substantially improved mechanical properties compared to CSD ones (**Figure 14**, publication II Table 1), confirmed in previous studies analyzing fibers spun from eADF3 variants.³¹ Employing X-ray scattering, BSD fibers made of NTD-eADF3-CTD exhibited a higher molecular order due to the increased alignment of nanocrystals and amorphous structures.²⁸⁹ Biomimetic fibers spun from the *in vivo* mixture of homo- and heterodimers yielded nature-like performing fibers concerning all mechanical properties such as tensile strength (834 ± 34 MPa), elasticity (32 ± 1 %), Young's modulus (5 ± 0.4 GPa) as well as toughness (143 ± 6 MJm⁻³). Especially the strength values of the *in vivo* BSD fibers are the highest ever reported for an aqueous spinning setup (see **Table 4**). Stress-strain curves displayed that *in vivo* fibers combine features of individual components with NTD-eADF3-CTD contributing to extensibility, while NTD-eADF4-CTD impart high strength. The heterodimeric variant's importance became particularly clear compared to fibers spun from homodimer blends lacking the heterodimer, showing significantly lower mechanical properties (**Figure 14**, publication II Table 1).

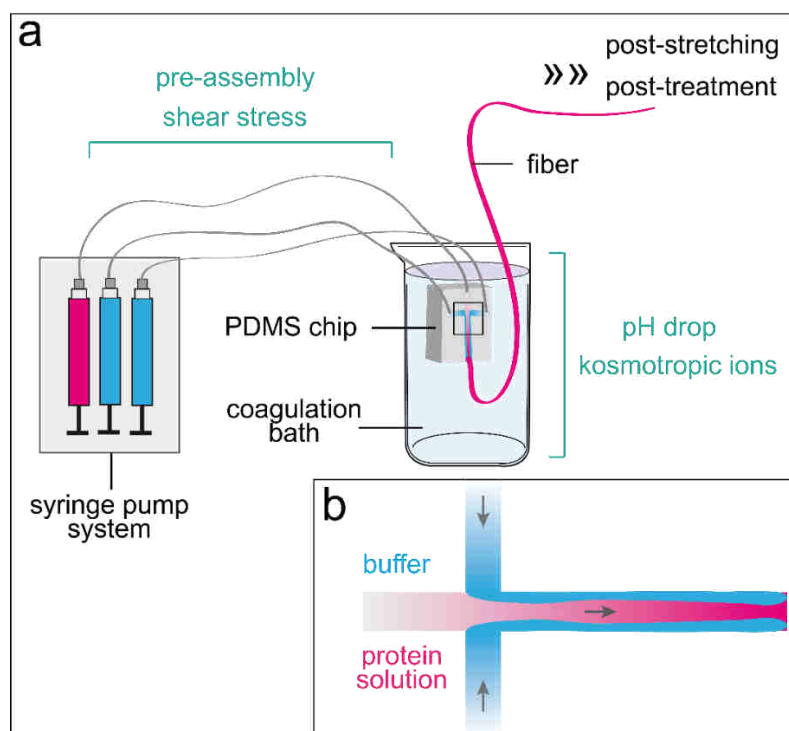


Figure 13. Bioinspired fiber production strategy using a microfluidic setup to mimic the key factors of spiders' natural spinning process. A microfluidic chip is connected to three simultaneously pumped syringes containing the spidroin dope and the phosphate buffer solutions. **(a)** An aqueous, highly concentrated spinning dope made of recombinant spidroins with terminal domains is exposed to shear forces on its way from the syringe to the microfluidic chip and further pre-assemble upon the addition of phosphate buffer at low concentration. A fiber is formed as soon as the dope solution is extruded into the coagulation bath containing high phosphate concentration at low pH. **(b)** Zoom-in of the microchip inlet showing a flow-focusing channel for spidroin assembly. Reprinted and adapted from publication III with permission from Saric, M. & Scheibel, T. Two-In-One Spider Silk Protein with Combined Mechanical Features in All-Aqueous Spun Fibers. *Biomacromolecules*, 24(4), 1744-1750. Copyright 2023, American Chemical Society.

Consequently, the heterodimers acted not only as cross-linkers, mediating different responses to phosphate between each homodimer, but also actively participated in fibril assembly (publication II Figure S5). The mechanical properties of *in vitro* fibers outperformed those of one-protein fibers. Still, they were lower compared to *in vivo* ones, which were assigned to different concepts of spidroin folding. During *in vivo* co-production in *E. coli*, the cellular chaperon machinery ensures efficient “native-like” spidroin conformations. In the course of producing *in vitro* mixtures, refolding and dimerization took place in step-wise dialysis, whereby some proteins may partially fold into intermediate states.³⁴⁷ Fibers spun from *in vitro* mixtures were less stretchable (350 %) than *in vivo* ones (400 %) since spidroin

assembly might be impeded by premature misfolded proteins in the *in vitro* dopes, causing more molecule entanglements within the fibers which further leads to lower mechanics.

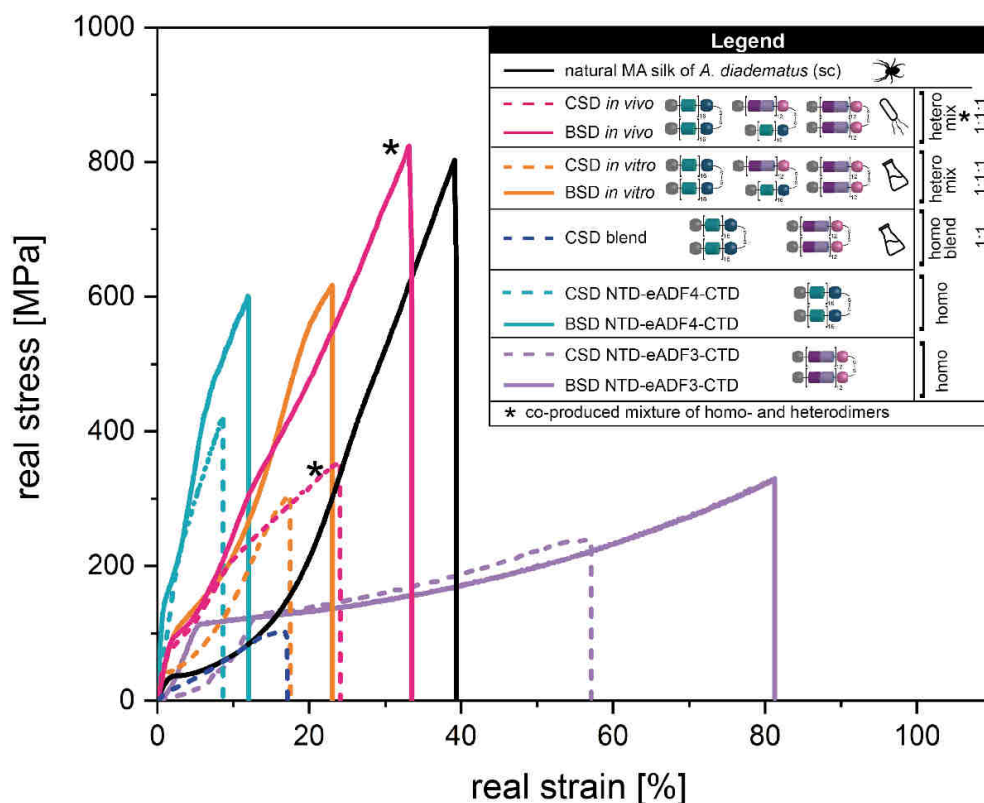


Figure 14. Real stress-strain curves of artificial and natural spider silk fibers. Tensile tests of post-stretched fibers of recombinant full-length eADF3 and eADF4 spun from classical (CSD, colored dashed lines) as well as biomimetic (BSD, colored solid lines) spinning dopes were made in comparison to those of supercontracted (sc) natural *A. diadematus* MaSp fibers (black). Mechanical properties of fibers are displayed spun of eADF3/eADF4 homo- and heterodimers mixtures from *in vivo* production in *E. coli* (pink) and *in vitro* production (orange), blend only containing eADF3 or eADF4 homodimers (blue), as well as one-protein fibers composed of NTD-eADF4-CTD (cyan) or NTD-eADF3-CTD (purple). Modified from publication II with kind permission of the publisher John Wiley & Sons from Saric, M., Eisoldt, L., Döring, V., & Scheibel, T., *Advanced Materials*, 2021, 33(9), 2006499.¹⁹²

Overall, to fully replicate the mechanical properties of natural silk, it is essential to mimic the natural spinning process as close as possible. It is known that the MaSps size strongly correlates with tensile strength due to an increased density of interchain interactions.^{248,249} Spidroin mixtures used in this study contained mainly dimeric spidroins, contributing to a high molecular weight content (450 kDa). In addition, our findings emphasize the importance of spidroins' intermolecular interactions to be essential in controlling hierarchical alignment at the

supramolecular level. Each spidroin serves a specific purpose, is indispensable in the spinning process, and contributes to functional complexity. In former studies, missing TDs led to inferior mechanical performance compared to spidroins comprising NTD and CTD.³¹ In this work, further evidence was provided that TDs acted as essential molecular switches by sensing changes in pH, ions, and shearing forces during spinning to support the transition from liquid dopes to solid fibers. The last important step in the process involved the post-stretching of fibers in achieving the alignment of molecules inside the fiber, which was also mimicked from the native system.

3.3 TWO-IN-ONE SPIDER SILK WITH MULTIFUNCTIONAL PROPERTIES

Based on the previous findings emphasizing the importance of the heterodimer in a multi-component approach (publication II),¹⁹² a simplified concept was developed in publication III by engineering a novel two-in-one (TIO) spidroin. By combining the individual physico-chemical features of eADF3 and eADF4, a multifunctional spidroin was designed. The presence of functional TDs enabled handling and application in aqueous systems similar to the heterodimer.

The heterodimer was isolated from an *in vivo* mixture of homo- and heterodimers using a two-step purification strategy, including IMAC and IEC. The TIO spidroin was purified in a column-free approach, similar to previously reported protocols,¹⁵⁴ yielding 25 times higher protein amounts compared to the heterodimer.

Both heterodimer and TIO were structurally characterized by far-UV CD spectroscopy revealing a similar secondary structure content. The random coil spectrum originated from the unfolded repetitive core domain,¹⁵⁴ whereas the α -helical signals arose from the TDs comprising five helix bundles.^{122,163} Concerning the structural analysis of both TD-containing spidroins, far-UV CD indicated acidification-induced conformational changes in the NTD due to its' dimerization, as observed previously.^{121,170,175} Studies of thermal and chemical stability demonstrated significantly higher stabilities at pH 6 compared to pH 8 for both dimeric hybrid proteins. A comparison of the heterodimers and TIO spidroins theoretical biochemical properties, such as molecular weight, pI, number of charged amino acid residues, and mean hydrophobicity, display high similarities, which is reflected in the analog structural integrity.

Overall, the TIO variant represented a simplified substitute for the heterodimer to enable the production of synthetic morphologies that require high spidroin amounts.

In the natural system, spidroins are stored in the presence of sodium chloride ions, which are exchanged for potassium phosphate ions, and spidroins are subjected to shear forces along the spinning duct. Phosphate-induced self-assembly analyses of heterodimer and TIO displayed similar kinetics in time-dependent turbidity assays (**Figure 15 a**). Nanofibrillization behavior upon the addition of phosphate was facilitated by the eADF4-content.^{269,274,275} TEM images of the assembled structures showed branched nanofibrils comprising a high content of cross- β -sheets, detectable by ThT staining and subsequent fluorescence spectrometry. The ability of TIO to form nanofibrils opens the possibility for self-assembly into hierarchically structured morphologies. When mechanical stimuli were applied, both hybrid variants formed fiber-bundles, which were several millimeters in length, cross- β -sheet-rich, and highly ordered (**Figure 15 b**). The impact of eADF3 contributed to a strong assembly behavior upon shearing.^{122,167,179,282} A similar assembly behavior of the heterodimer and the TIO was assumed based on the structural and functional characterization.

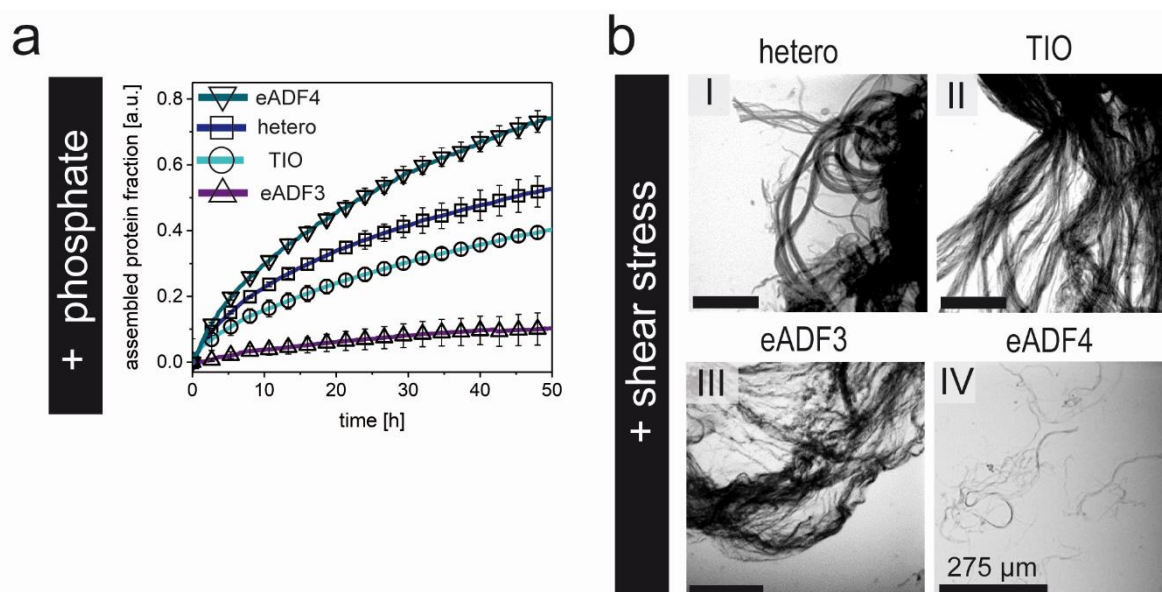


Figure 15. Self-assembly of different spidroin variants. **(a)** Phosphate-induced fibril assembly kinetics by measuring turbidity at 340 nm. **(b)** Microscopy images (I-IV) of macroscopic fibers formed by rotation. Scale bars represent 275 μm . Reprinted and adapted from publication III with permission from Saric, M. & Scheibel, T. Two-In-One Spider Silk Protein with Combined Mechanical Features in All-Aqueous Spun Fibers. *Biomacromolecules*, 24(4), 1744-1750. Copyright 2023, American Chemical Society.

Subsequently, the self-assembly of TIO into fibers was investigated. Fibers were spun from all-aqueous spinning dopes using the bioinspired microfluidic spinning system (**Figure 13**) as previously established in publication II.¹⁹² Tensile tests of post-stretched biomimetic fibers spun from TIO exhibited strength, extensibility, toughness, and Young's Modulus of 419 MPa, 24 %, 61 MJm⁻³, 4 GPa, respectively, twice that of eADF3/eADF4 blends or individual spidroins.¹⁹² The biophysical and biochemical properties of the two underlying spidroins, eADF3 and eADF4, were combined in the TIO variant, which had an impact on the processed fibers. While eADF4 contributed to fiber strength, toughness, and extensibility were provided by eADF3.

3.4 STRUCTURAL CHARACTERIZATION OF HIGHLY-CONCENTRATED AQUEOUS SPINNING DOPES AND FIBERS

Spider silk fibers self-assemble rapidly from soluble spidroins stored in highly concentrated spinning dopes, which are exposed to sequential conformational changes upon chemical and physical stimuli. Both, publications II and III, and previous work,³¹ have demonstrated that fibers spun from biomimetic phosphate-containing spinning dopes (BSD) had substantially superior mechanical properties compared to those spun from spinning dopes lacking the kosmotropic impact of phosphate (CSD). Previously, vibrational spectroscopy and wide and small X-ray scattering (WAXS and SAXS) revealed a higher molecular order in biomimetic fibers made from eADF3-CTD,²⁸⁹ which is presumably dictated by the spinning dope. A considerable number of questions remain unsolved regarding the structural arrangement of MaSps since, with few exceptions,^{169,320} studies of highly concentrated biomimetic spinning dopes are rare.

Publication IV lays the foundation to study atomic and mesoscale interactions in recombinant spinning dopes and fibers spun thereof. Highly concentrated aqueous spinning dopes were prepared from eADF3-CTD according to the protocol illustrated in **Figure 9**. For time-dependent analyses, BSD and CSD samples were taken after 0, 2, 4, and 6 h during dope preparation. Size and population distributions of eADF3-CTD were monitored by dynamic light scattering (DLS) (**Figure 16**). In both, CSD and BSD, monomeric and dimeric spidroins, as

well as larger hierarchical assemblies were present, but different assembly processes were observed driven by the buffer conditions.

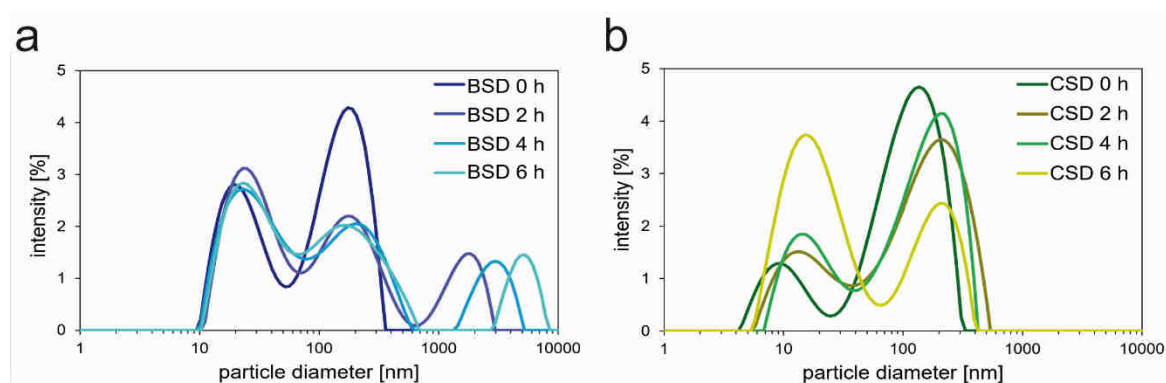


Figure 16. DLS of BSD (a) and CSD (b). Samples were taken after 0, 2, 4, and 6 h to follow the assembly process of the spinning solutions. After this, no further changes were observed, and the dope production was completed. During the assembly, the concentrations gradually increased. For the BSD, concentrations at 0, 2, 4, and 6 h were 27, 63, 96, and 177 mg/mL, respectively. For the CSD, concentrations at 0, 2, 4, and 6 h were 25, 41, 106, and 197 mg/mL, respectively. Details on spidroin diameters are given in publication IV, Supporting Information Table S1. Reprinted from publication IV with permission from Stengel, D., Saric, M., Johnson, H. R., Schiller, T., Diehl, J., Chalek, K., Onofrei, D., Scheibel, T. & Holland, G. P. (2023). Tyrosine’s Unique Role in the Hierarchical Assembly of Recombinant Spider Silk Proteins: From Spinning Dope to Fibers. *Biomacromolecules*, 24(3), 1463-1474. Copyright 2023, American Chemical Society.

Only in BSD, the spidroins gradually evolved from monomers/dimers to pre-assemblies, probably micelles, and ultimately micron scale assemblies (~3000 nm) due to the presence of phosphate. Micellar-like structures were already assumed in previous studies of eADF3-CTD (publication II Figure 2).^{155,164,168,192} Light microscopy images of final BSD displayed protein droplets arose from liquid-liquid phase separation (**Figure 17**, I-III). Previous studies of native and recombinant MaSp2 systems have demonstrated similar phase separation with phosphate.¹⁶⁹ In BSD, kosmotropic phosphate ions increased the surface tension of water^{185,186} and promoted hydrophobic interactions between poly(Ala) motifs of spidroins, forming large hierarchical assemblies. In contrast, CSD seems to be composed of a single coherent phase (**Figure 17**, IV-VI) since the presence of chaotropic ions promoted high interactions between protein and solvent. The foundation for a high molecular structural order is already set in the dope preparation as kosmotropic phosphate ions pre-order recombinant spidroins in BSD leading to liquid-liquid phase separation and representing an important prerequisite prior to spinning.

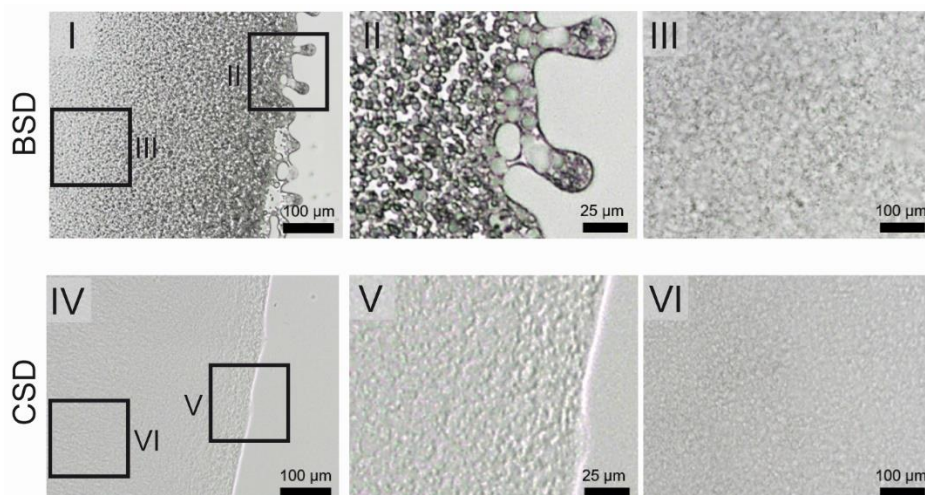


Figure 17. Light microscopy images of BSD (top, I–III) and CSD (bottom, IV–VI), both at a concentration of 100 mg/mL. Regions from (II, III, V, VI) are enlarged to see the differences between the systems, where the BSD contains large droplets indicative of liquid-liquid phase separation. Reprinted from publication IV with permission from Stengel, D., Saric, M., Johnson, H. R., Schiller, T., Diehl, J., Chalek, K., Onofrei, D., Scheibel, T. & Holland, G. P. (2023). Tyrosine’s Unique Role in the Hierarchical Assembly of Recombinant Spider Silk Proteins: From Spinning Dope to Fibers. *Biomacromolecules*, 24(3), 1463-1474. Copyright 2023, American Chemical Society.

In solution nuclear magnetic resonance (NMR) experiments isotopically ($^{13}\text{C}/^{15}\text{N}$) enriched eADF3-CTD dopes were studied to understand the atomic-level interactions. The primary amino acid sequence of eADF3-CTD was used as guidance (publication IV Figure 1). In 3D HNCACB and CBCAcoNH experiments, several di- and some tri-peptide motifs were assigned in the ^1H – ^{15}N heteronuclear single quantum correlation (HSQC) spectrum of BSD, showing similarity to natural MA silk dopes as investigated previously.^{348,349} Comparing ^1H – ^{15}N HSQC spectra of BSD and CSD, the overall structural state of recombinant eADF3-CTD was random coil in both cases, but assignments in ^{13}C direct detect spectra on 3D and ^1H – ^{13}C HSQC NMR experiments provided valuable differences between the two dopes. BSD displayed sharper resonance lines when compared to CSD for several environments, indicating a pre-ordering of spidroins in the BSD. Also, small chemical shift perturbations in the Tyr aromatic ring environment were seen as it was significantly more ordered for BSD likely due to hydrogen-bonding differences resulting in varying Tyr ring packing. Studies of other protein systems that undergo liquid-liquid phase separation have previously implicated Tyr ring and hydrogen-bonding interaction as driving force.³⁵⁰⁻³⁵³

Next, eADF3-CTD fibers were spun from CSD and BSD in an all-aqueous biomimetic spinning system established before (**Figure 13**).¹⁹² Solid-state NMR (SSNMR) helped to explore the significantly improved mechanical properties of BSD fibers compared to CSD ones. Using ¹³C SSNMR, the secondary structural state of eADF3-CTD in CSD and BSD fibers was investigated. For example, in 2D ¹³C–¹³C dipolar assisted rotational resonance (DARR) experiments, CSD and BSD fibers were compared to natural dragline silks, demonstrating high structural similarities based on nearly identical ¹³C chemical shifts. Comparing ¹H–¹³C cross-polarization magic-angle-spinning (CP-MAS) SSNMR spectra of CSD and BSD fibers, no structural differences for the poly(Ala) stretches were seen. Most if not all the Ala present in the repetitive core domain converted from random coil (before fiber spinning) to β -sheet structure (77%) (spun fibers). But, significant differences in the Tyr aromatic ring environment in the non- β -sheet, disordered helical domain were observed in 2D ¹H–¹³C (heteronuclear correlation) HETCOR SSNMR spectra of BSD. The large downfield chemical shift for the aromatic ¹H resonances in BSD fibers suggested that the Tyr rings are located in a more polar environment. A recurring result since differences in Tyr packing could be traced from biomimetic dope to final spun BSD fibers, highlighting the importance of Tyr in spider silk assembly.

4 REFERENCES

- 1 Palousis, N., Hargroves, K., Paten, C. & Smith, M. in *Proceedings of the 4th ASEE/AaeE Global Colloquium on Engineering Education*. 1-14 (School of Engineering, The University of Queensland).
- 2 Peter Fratzl, K. J., Martin Möller, Thomas Scheibel, Karin Sternberg. *Materials Research: Inspired by Nature – Innovation Potential of Biologically Inspired Materials*. *acatech DISCUSSION Munich* (2020).
- 3 Hargroves, K., Smith, M. & Lovins, H. *Prospering in a Carbon Constrained World: Profitable Opportunities for Greenhouse Gas Emmissions Reduction*. *Chicago and European Climate Exchange (CCX/EUX). Opportunities Executive Report*. Colorado/Nathan, Queensland: *The Natural Edge Project* (2005).
- 4 Wegst, U. G., Bai, H., Saiz, E., Tomsia, A. P. & Ritchie, R. O. Bioinspired structural materials. *Nature materials* **14**, 23-36 (2015).
- 5 Ashby, M. F., Gibson, L., Wegst, U. & Olive, R. The mechanical properties of natural materials. I. Material property charts. *Proceedings of the Royal Society of London. Series A: Mathematical and Physical Sciences* **450**, 123-140 (1995).
- 6 Zhang, C., Mcadams, D. A. & Grunlan, J. C. Nano/Micro-Manufacturing of Bioinspired Materials: a Review of Methods to Mimic Natural Structures. *Advanced Materials* **28**, 6292-6321 (2016).
- 7 Meyers, M. A., Chen, P.-Y., Lin, A. Y.-M. & Seki, Y. Biological materials: structure and mechanical properties. *Progress in materials science* **53**, 1-206 (2008).
- 8 Wang, Y., Naleway, S. E. & Wang, B. Biological and bioinspired materials: Structure leading to functional and mechanical performance. *Bioactive Materials* **5**, 745-757 (2020).
- 9 Samaha, M. A., Tafreshi, H. V. & Gad-el-Hak, M. Superhydrophobic surfaces: From the lotus leaf to the submarine. *Comptes Rendus Mecanique* **340**, 18-34 (2012).
- 10 Ruibal, R. & Ernst, V. The structure of the digital setae of lizards. *Journal of Morphology* **117**, 271-293 (1965).
- 11 Autumn, K., Liang, Y. A., Hsieh, S. T., Zesch, W., Chan, W. P., Kenny, T. W., Fearing, R. & Full, R. J. Adhesive force of a single gecko foot-hair. *Nature* **405**, 681-685 (2000).
- 12 Pacheco-Torgal, F. & Labrincha, J. Biotechnologies and bioinspired materials for the construction industry: an overview. *International Journal of Sustainable Engineering* **7**, 235-244 (2014).
- 13 Zhao, N., Wang, Z., Cai, C., Shen, H., Liang, F., Wang, D., Wang, C., Zhu, T., Guo, J. & Wang, Y. Bioinspired materials: from low to high dimensional structure. *Advanced Materials* **26**, 6994-7017 (2014).
- 14 Bahnert, T., Schlosser, U., Gutmann, R. & Schollmeyer, E. Textile solar light collectors based on models for polar bear hair. *Solar energy materials and solar cells* **92**, 1661-1667 (2008).
- 15 Xu, D., Yu, H., Xu, Q., Xu, G. & Wang, K. Thermoresponsive photonic crystal: synergistic effect of poly (N-isopropylacrylamide)-co-acrylic acid and morpho butterfly wing. *ACS applied materials & interfaces* **7**, 8750-8756 (2015).
- 16 Malay, A. D., Craig, H. C., Chen, J., Oktaviani, N. A. & Numata, K. Complexity of spider dragline silk. *Biomacromolecules* **23**, 1827-1840 (2022).
- 17 Bittencourt, D. M. d. C., Oliveira, P., Michalczechen-Lacerda, V. A., Rosinha, G. M. S., Jones, J. & Rech Filho, E. L. Bioengineering of spider silks for the production of biomedical materials. *Frontiers in Bioengineering and Biotechnology*, 1405 (2022).
- 18 Herold, H. M. & Scheibel, T. Applicability of biotechnologically produced insect silks. *Zeitschrift für Naturforschung C* **72**, 365-385 (2017).
- 19 Holland, C., Numata, K., Rnjak-Kovacina, J. & Seib, F. P. The biomedical use of silk: past, present, future. *Advanced healthcare materials* **8**, 1800465 (2019).
- 20 Wright, C. S. Rome and the Road to the Distant East. *Available at SSRN 3943069* (2021).

- 21 Scheibel, T., Zahn, H. & Krasowski, A. Silk. *Ullmann's Encyclopedia of Industrial Chemistry*, 1-15 (2016).
- 22 Xiang, H., Liu, X., Li, M., Zhu, Y. n., Wang, L., Cui, Y., Liu, L., Fang, G., Qian, H. & Xu, A. The evolutionary road from wild moth to domestic silkworm. *Nature Ecology & Evolution* **2**, 1268-1279 (2018).
- 23 Craig, C. L. Evolution of arthropod silks. *Annual review of entomology* **42**, 231-267 (1997).
- 24 Reddy, N. *Silk: Materials, Processes, and Applications*. (Woodhead Publishing, 2019).
- 25 Porter, D. & Vollrath, F. Silk as a biomimetic ideal for structural polymers. *Advanced Materials* **21**, 487-492 (2009).
- 26 Sutherland, T. D., Young, J. H., Weisman, S., Hayashi, C. Y. & Merritt, D. J. Insect silk: one name, many materials. *Annual review of entomology* **55**, 171-188 (2010).
- 27 Greving, I., Cai, M., Vollrath, F. & Schniepp, H. C. Shear-induced self-assembly of native silk proteins into fibrils studied by atomic force microscopy. *Biomacromolecules* **13**, 676-682 (2012).
- 28 Vollrath, F., Porter, D. & Dicko, C. in *Handbook of Textile Fibre Structure* 146-198 (Elsevier, 2009).
- 29 Xu, Z., Wu, M., Ye, Q., Chen, D., Liu, K. & Bai, H. Spinning from nature: Engineered preparation and application of high-performance bio-based fibers. *Engineering* (2022).
- 30 Heim, M., Keerl, D. & Scheibel, T. Spider silk: from soluble protein to extraordinary fiber. *Angewandte Chemie International Edition* **48**, 3584-3596 (2009).
- 31 Heidebrecht, A., Eisoldt, L., Diehl, J., Schmidt, A., Geffers, M., Lang, G. & Scheibel, T. Biomimetic fibers made of recombinant spidroins with the same toughness as natural spider silk. *Advanced materials* **27**, 2189-2194 (2015).
- 32 Gosline, J., Guerette, P., Ortlepp, C. & Savage, K. The mechanical design of spider silks: from fibroin sequence to mechanical function. *Journal of Experimental Biology* **202**, 3295-3303 (1999).
- 33 Hagenau, A., Suhre, M. H. & Scheibel, T. R. Nature as a blueprint for polymer material concepts: Protein fiber-reinforced composites as holdfasts of mussels. *Progress in polymer science* **39**, 1564-1583 (2014).
- 34 Hepburn, H. R., Chandler, H. D. & Davidoff, M. Extensometric properties of insect fibroins: The green lacewing cross- β , honeybee α -helical and greater waxmoth parallel- β conformations. *Insect Biochemistry* **9**, 69-77 (1979).
- 35 Bauer, F. & Scheibel, T. Artificial egg stalks made of a recombinantly produced lacewing silk protein. *Angewandte Chemie International Edition* **51**, 6521-6524 (2012).
- 36 Gosline, J., Lillie, M., Carrington, E., Guerette, P., Ortlepp, C. & Savage, K. Elastic proteins: biological roles and mechanical properties. *Philosophical Transactions of the Royal Society of London. Series B: Biological Sciences* **357**, 121-132 (2002).
- 37 Aaron, B. & Gosline, J. Elastin as a random-network elastomer: A mechanical and optical analysis of single elastin fibers. *Biopolymers: Original Research on Biomolecules* **20**, 1247-1260 (1981).
- 38 Gadgey, K. K. & Bahekar, A. Studies on extraction methods of chitin from crab shell and investigation of its mechanical properties. *Int. J. Mech. Eng. Technol* **8**, 220-231 (2017).
- 39 Amada, S. & Untao, S. Fracture properties of bamboo. *Composites Part B: Engineering* **32**, 451-459 (2001).
- 40 Yu, Y., Wang, H., Lu, F., Tian, G. & Lin, J. Bamboo fibers for composite applications: a mechanical and morphological investigation. *Journal of materials science* **49**, 2559-2566 (2014).
- 41 Anjos, O., Pereira, H. & Rosa, M. E. Tensile properties of cork in the tangential direction: Variation with quality, porosity, density and radial position in the cork plank. *Materials & Design* **31**, 2085-2090, doi:10.1016/j.matdes.2009.10.048 (2010).
- 42 Zhu, D., Mobasher, B. & Rajan, S. D. Dynamic tensile testing of Kevlar 49 fabrics. *Journal of materials in civil engineering* **23**, 230-239 (2011).
- 43 Chun, K., Choi, H. & Lee, J. Comparison of mechanical property and role between enamel and dentin in the human teeth. *Journal of dental biomechanics* **5** (2014).

- 44 Stanford, J. W., Paffenbarger, G., Kumpula, J. W. & Sweeney, W. Determination of some compressive properties of human enamel and dentin. *The Journal of the American Dental Association* **57**, 487-495 (1958).
- 45 Bargel, H., Hopfe, C. & Scheibel, T. Proteinfasern als Hochleistungsmaterial: Evolution, Eigenschaften und Anwendungen von Spinnenseide. *Biologie in unserer Zeit* **50**, 434-443 (2020).
- 46 Guerette, P. A., Ginzinger, D. G., Weber, B. H. & Gosline, J. M. Silk properties determined by gland-specific expression of a spider fibroin gene family. *Science* **272**, 112-115 (1996).
- 47 Gosline, J. M., DeMont, M. E. & Denny, M. W. The structure and properties of spider silk. *Endeavour* **10**, 37-43 (1986).
- 48 Heim, M., Römer, L. & Scheibel, T. Hierarchical structures made of proteins. The complex architecture of spider webs and their constituent silk proteins. *Chemical Society Reviews* **39**, 156-164 (2010).
- 49 Eisoldt, L., Smith, A. & Scheibel, T. Decoding the secrets of spider silk. *Materials Today* **14**, 80-86 (2011).
- 50 Stauffer, S. L., Coguill, S. L. & Lewis, R. V. Comparison of physical properties of three silks from *Nephila clavipes* and *Araneus gemmoides*. *Journal of Arachnology*, 5-11 (1994).
- 51 Vollrath, F. Spider webs and silks. *Scientific American* **266**, 70-77 (1992).
- 52 Vollrath, F. & Knight, D. P. Liquid crystalline spinning of spider silk. *Nature* **410**, 541-548 (2001).
- 53 Shultz, J. W. The origin of the spinning apparatus in spiders. *Biological Reviews* **62**, 89-113 (1987).
- 54 Shear, W. A., Palmer, J. M., Coddington, J. A. & Bonamo, P. M. A Devonian spinneret: early evidence of spiders and silk use. *Science* **246**, 479-481 (1989).
- 55 Garb, J. E. & Hayashi, C. Y. Modular evolution of egg case silk genes across orb-weaving spider superfamilies. *Proceedings of the National Academy of Sciences* **102**, 11379-11384 (2005).
- 56 Babb, P. L., Lahens, N. F., Correa-Garhwal, S. M., Nicholson, D. N., Kim, E. J., Hogenesch, J. B., Kuntner, M., Higgins, L., Hayashi, C. Y. & Agnarsson, I. The *Nephila clavipes* genome highlights the diversity of spider silk genes and their complex expression. *Nature Genetics* **49**, 895-903 (2017).
- 57 Scheibel, T. Spider silks: recombinant synthesis, assembly, spinning, and engineering of synthetic proteins. *Microbial cell factories* **3**, 1-10 (2004).
- 58 Vollrath, F. Strength and structure of spiders' silks. *Reviews in Molecular Biotechnology* **74**, 67-83 (2000).
- 59 Work, R. W. & Morosoff, N. A physico-chemical study of the supercontraction of spider major ampullate silk fibers. *Textile research journal* **52**, 349-356 (1982).
- 60 Giesa, T., Schuetz, R., Fratzl, P., Buehler, M. J. & Masic, A. Unraveling the molecular requirements for macroscopic silk supercontraction. *ACS nano* **11**, 9750-9758 (2017).
- 61 Blackledge, T. A., Boutry, C., Wong, S.-C., Baji, A., Dhinojwala, A., Sahni, V. & Agnarsson, I. How super is supercontraction? Persistent versus cyclic responses to humidity in spider dragline silk. *Journal of Experimental Biology* **212**, 1981-1989 (2009).
- 62 Holland, G. P., Lewis, R. V. & Yarger, J. L. WISE NMR characterization of nanoscale heterogeneity and mobility in supercontracted *Nephila clavipes* spider dragline silk. *Journal of the American Chemical Society* **126**, 5867-5872 (2004).
- 63 Yang, Z., Liivak, O., Seidel, A., LaVerde, G., Zax, D. B. & Jelinski, L. W. Supercontraction and backbone dynamics in spider silk: ¹³C and ²H NMR studies. *Journal of the American Chemical Society* **122**, 9019-9025 (2000).
- 64 Boutry, C. & Blackledge, T. A. Evolution of supercontraction in spider silk: structure–function relationship from tarantulas to orb-weavers. *Journal of Experimental Biology* **213**, 3505-3514 (2010).
- 65 Gosline, J., Pollak, C., Guerette, P., Cheng, A., DeMont, M. & Denny, M. in *ACS Symposium Series*. 328-341 (Washington, DC: American Chemical Society, [1974]-).
- 66 Boutry, C. & Blackledge, T. A. Wet webs work better: humidity, supercontraction and the performance of spider orb webs. *Journal of Experimental Biology* **216**, 3606-3610 (2013).

- 67 Cohen, N., Levin, M. & Eisenbach, C. D. On the Origin of Supercontraction in Spider Silk. *Biomacromolecules* **22**, 993-1000 (2021).
- 68 Emile, O., Le Floch, A. & Vollrath, F. Shape memory in spider draglines. *Nature* **440**, 621-621 (2006).
- 69 Vienneau-Hathaway, J. M., Brassfield, E. R., Lane, A. K., Collin, M. A., Correa-Garhwal, S. M., Clarke, T. H., Schwager, E. E., Garb, J. E., Hayashi, C. Y. & Ayoub, N. A. Duplication and concerted evolution of MiSp-encoding genes underlie the material properties of minor ampullate silks of cobweb weaving spiders. *BMC evolutionary biology* **17**, 1-18 (2017).
- 70 Nakamura, H., Kono, N., Mori, M., Masunaga, H., Numata, K. & Arakawa, K. Composition of minor ampullate silk makes its properties different from those of major ampullate silk. *bioRxiv*, 2022.2012.2012.520175 (2022).
- 71 Guinea, G., Elices, M., Plaza, G., Perea, G., Daza, R., Riekkel, C., Agulló-Rueda, F., Hayashi, C., Zhao, Y. & Pérez-Rigueiro, J. Minor ampullate silks from Nephila and Argiope spiders: tensile properties and microstructural characterization. *Biomacromolecules* **13**, 2087-2098 (2012).
- 72 Papadopoulos, P., Ene, R., Weidner, I. & Kremer, F. Similarities in the structural organization of major and minor ampullate spider silk. *Macromolecular rapid communications* **30**, 851-857 (2009).
- 73 Lewis, R. V. Spider silk: ancient ideas for new biomaterials. *Chemical reviews* **106**, 3762-3774 (2006).
- 74 Blackledge, T., Kuntner, M. & Agnarsson, I. Bioprospecting finds the toughest biological material: extraordinary silk from a giant riverine orb spider. *Plos one* **5**, 1 (2010).
- 75 Swanson, B. O., Blackledge, T. A., Beltrán, J. & Hayashi, C. Y. Variation in the material properties of spider dragline silk across species. *Applied Physics A* **82**, 213-218 (2006).
- 76 Rising, A., Nimmervoll, H., Grip, S., Fernandez-Arias, A., Storckenfeldt, E., Knight, D. P., Vollrath, F. & Engström, W. Spider silk proteins—mechanical property and gene sequence. *Zoological science* **22**, 273-281 (2005).
- 77 Hayashi, C. Y. & Lewis, R. V. Spider flagelliform silk: lessons in protein design, gene structure, and molecular evolution. *Bioessays* **23**, 750-756 (2001).
- 78 Candelas, G. C., Ortiz, A. & Molina, C. The cylindrical or tubiliform glands of *Nephila clavipes*. *Journal of Experimental Zoology* **237**, 281-285 (1986).
- 79 Van Nimmen, E., Gellynck, K., Gheysens, T., Van Langenhove, L. & Mertens, J. Modeling of the stress-strain behavior of egg sac silk of the spider *Araneus diadematus*. *The Journal of Arachnology* **33**, 629-639 (2005).
- 80 Hayashi, C. Y., Blackledge, T. A. & Lewis, R. V. Molecular and mechanical characterization of aciniform silk: uniformity of iterated sequence modules in a novel member of the spider silk fibroin gene family. *Molecular biology and evolution* **21**, 1950-1959 (2004).
- 81 Sponner, A., Vater, W., Monajembashi, S., Unger, E., Grosse, F. & Weisshart, K. Composition and hierarchical organisation of a spider silk. *PloS one* **2**, e998 (2007).
- 82 Hayashi, C. Y. & Lewis, R. V. Evidence from flagelliform silk cDNA for the structural basis of elasticity and modular nature of spider silks. *Journal of molecular biology* **275**, 773-784 (1998).
- 83 Tokareva, O., Jacobsen, M., Buehler, M., Wong, J. & Kaplan, D. L. Structure–function–property–design interplay in biopolymers: Spider silk. *Acta biomaterialia* **10**, 1612-1626 (2014).
- 84 Blackledge, T. A., Summers, A. P. & Hayashi, C. Y. Gumfooted lines in black widow cobwebs and the mechanical properties of spider capture silk. *Zoology* **108**, 41-46 (2005).
- 85 Coddington, J. A. Spinneret silk spigot morphology: evidence for the monophyly of orbweaving spiders, Cyrtophorinae (Araneidae), and the group Theridiidae plus Nesticidae. *Journal of Arachnology*, 71-95 (1989).
- 86 Townley, M. A. & Tillinghast, E. K. in *Spider ecophysiology* 283-302 (Springer, 2013).
- 87 Tillinghast, E. K., Townley, M. A., Wight, T. N., Uhlenbruck, G. & Janssen, E. The adhesive glycoprotein of the orb web of *Argiope aurantia* (Araneae, Araneidae). *MRS Online Proceedings Library (OPL)* **292** (1992).

- 88 Sahni, V., Blackledge, T. A. & Dhinojwala, A. Viscoelastic solids explain spider web stickiness. *Nature Communications* **1**, 1-4 (2010).
- 89 Sahni, V., Blackledge, T. A. & Dhinojwala, A. A review on spider silk adhesion. *The Journal of Adhesion* **87**, 595-614 (2011).
- 90 Tian, M. & Lewis, R. V. Molecular characterization and evolutionary study of spider tubuliform (eggcase) silk protein. *Biochemistry* **44**, 8006-8012 (2005).
- 91 Christenson, T. E. Alternative reproductive tactics in spiders. *American Zoologist* **24**, 321-332 (1984).
- 92 Foelix, R. *Biology of spiders*. (OUP USA, 2011).
- 93 Wherry, T. & Elwood, R. Relocation, reproduction and remaining alive in the orb-web spider. *Journal of Zoology* **279**, 57-63 (2009).
- 94 Moon, M. J. Fine structural analysis of the cocoon silk production in the garden spider, *Argiope aurantia*. *Korean Journal of Biological Sciences* **7**, 35-41 (2003).
- 95 Herrera, E., Nguyen, L. T., Escobar, E., Ouriel, W. & Casem, M. L. Alteration of tubuliform silk gland cytoarchitecture with the reproductive cycle of the Western black widow spider, *Latrodectus hesperus*. *Invertebrate Biology* **134**, 332-340 (2015).
- 96 Blackledge, T. A. & Hayashi, C. Y. Silken toolkits: biomechanics of silk fibers spun by the orb web spider *Argiope argentata* (Fabricius 1775). *Journal of experimental biology* **209**, 2452-2461 (2006).
- 97 Hinman, M. B. & Lewis, R. V. Isolation of a clone encoding a second dragline silk fibroin. *Nephila clavipes* dragline silk is a two-protein fiber. *Journal of Biological Chemistry* **267**, 19320-19324 (1992).
- 98 Yarger, J. L., Cherry, B. R. & Van Der Vaart, A. Uncovering the structure–function relationship in spider silk. *Nature Reviews Materials* **3**, 1-11 (2018).
- 99 Crews, S. C. & Opell, B. D. The features of capture threads and orb-webs produced by unfed *Cyclosa turbinata* (Araneae: Araneidae). *The Journal of Arachnology* **34**, 427-434 (2006).
- 100 Tillinghast, E. K. & Townley, M. A. Silk glands of araneid spiders: selected morphological and physiological aspects. (1994).
- 101 Guehrs, K. H., Schlott, B., Grosse, F. & Weisshart, K. Environmental conditions impinge on dragline silk protein composition. *Insect molecular biology* **17**, 553-564 (2008).
- 102 Qiu, W., Patil, A., Hu, F. & Liu, X. Y. Hierarchical structure of silk materials versus mechanical performance and mesoscopic engineering principles. *Small* **15**, 1903948 (2019).
- 103 Li, S., McGhie, A. & Tang, S. New internal structure of spider dragline silk revealed by atomic force microscopy. *Biophysical journal* **66**, 1209-1212 (1994).
- 104 Vollrath, F., Holtet, T., Thøgersen, H. C. & Frische, S. Structural organization of spider silk. *Proceedings of the Royal Society of London. Series B: Biological Sciences* **263**, 147-151 (1996).
- 105 Schulz, S. Composition of the silk lipids of the spider *Nephila clavipes*. *Lipids* **36**, 637-647 (2001).
- 106 Knight, D., Knight, M. & Vollrath, F. Beta transition and stress-induced phase separation in the spinning of spider dragline silk. *International journal of biological macromolecules* **27**, 205-210 (2000).
- 107 Saric, M. & Scheibel, T. Engineering of silk proteins for materials applications. *Current opinion in biotechnology* **60**, 213-220 (2019).
- 108 Xu, G., Gong, L., Yang, Z. & Liu, X. What makes spider silk fibers so strong? From molecular-crystallite network to hierarchical network structures. *Soft Matter* **10**, 2116-2123 (2014).
- 109 Giesa, T., Arslan, M., Pugno, N. M. & Buehler, M. J. Flaw-tolerance in silk fibrils explains strength, extensibility and toughness of spider silk. (2011).
- 110 Heidebrecht, A. & Scheibel, T. Recombinant production of spider silk proteins. *Advances in applied microbiology* **82**, 115-153 (2013).
- 111 Nova, A., Ketten, S., Pugno, N. M., Redaelli, A. & Buehler, M. J. Molecular and nanostructural mechanisms of deformation, strength and toughness of spider silk fibrils. *Nano letters* **10**, 2626-2634 (2010).
- 112 Ketten, S., Xu, Z., Ihle, B. & Buehler, M. J. Nanoconfinement controls stiffness, strength and mechanical toughness of β -sheet crystals in silk. *Nature materials* **9**, 359-367 (2010).

- 113 Keten, S. & Buehler, M. J. Nanostructure and molecular mechanics of spider dragline silk protein assemblies. *Journal of the Royal Society Interface* **7**, 1709-1721 (2010).
- 114 Vollrath, F., Porter, D. & Holland, C. The science of silks. *MRS bulletin* **38**, 73-80 (2013).
- 115 Buehler, M. J. Tuning weakness to strength. *Nano Today* **5**, 379-383 (2010).
- 116 Xu, M. & Lewis, R. V. Structure of a protein superfiber: spider dragline silk. *Proceedings of the National Academy of Sciences* **87**, 7120-7124 (1990).
- 117 Blamires, S. J., Wu, C.-L. & Tso, I.-M. Variation in protein intake induces variation in spider silk expression. *PLoS One* **7**, e31626 (2012).
- 118 Ayoub, N. A., Garb, J. E., Tinghitella, R. M., Collin, M. A. & Hayashi, C. Y. Blueprint for a high-performance biomaterial: full-length spider dragline silk genes. *PLoS one* **2**, e514 (2007).
- 119 Spöner, A., Schlott, B., Vollrath, F., Unger, E., Grosse, F. & Weisshart, K. Characterization of the protein components of *Nephila clavipes* dragline silk. *Biochemistry* **44**, 4727-4736 (2005).
- 120 Lefèvre, T., Boudreault, S., Cloutier, C. & Pézolet, M. Diversity of molecular transformations involved in the formation of spider silks. *Journal of molecular biology* **405**, 238-253 (2011).
- 121 Askarieh, G., Hedhammar, M., Nordling, K., Saenz, A., Casals, C., Rising, A., Johansson, J. & Knight, S. D. Self-assembly of spider silk proteins is controlled by a pH-sensitive relay. *Nature* **465**, 236-238 (2010).
- 122 Hagn, F., Eisoldt, L., Hardy, J. G., Vendrely, C., Coles, M., Scheibel, T. & Kessler, H. A conserved spider silk domain acts as a molecular switch that controls fibre assembly. *Nature* **465**, 239-242 (2010).
- 123 Han, L., Zhang, L., Zhao, T., Wang, Y. & Nakagaki, M. Analysis of a new type of major ampullate spider silk gene, MaSp1s. *International journal of biological macromolecules* **56**, 156-161 (2013).
- 124 Collin, M. A., Clarke III, T. H., Ayoub, N. A. & Hayashi, C. Y. Genomic perspectives of spider silk genes through target capture sequencing: Conservation of stabilization mechanisms and homology-based structural models of spidroin terminal regions. *International journal of biological macromolecules* **113**, 829-840 (2018).
- 125 Hayashi, C. Y., Shipley, N. H. & Lewis, R. V. Hypotheses that correlate the sequence, structure, and mechanical properties of spider silk proteins. *International journal of biological macromolecules* **24**, 271-275 (1999).
- 126 Pham, T., Chuang, T., Lin, A., Joo, H., Tsai, J., Crawford, T., Zhao, L., Williams, C., Hsia, Y. & Vierra, C. Dragline silk: A fiber assembled with low-molecular-weight cysteine-rich proteins. *Biomacromolecules* **15**, 4073-4081 (2014).
- 127 Chaw, R. C., Correa-Garhwal, S. M., Clarke, T. H., Ayoub, N. A. & Hayashi, C. Y. Proteomic evidence for components of spider silk synthesis from black widow silk glands and fibers. *Journal of proteome research* **14**, 4223-4231 (2015).
- 128 Larracas, C., Hekman, R., Dyrness, S., Arata, A., Williams, C., Crawford, T. & Vierra, C. A. Comprehensive proteomic analysis of spider dragline silk from black widows: a recipe to build synthetic silk fibers. *International journal of molecular sciences* **17**, 1537 (2016).
- 129 Kono, N., Nakamura, H., Mori, M., Yoshida, Y., Ohtoshi, R., Malay, A. D., Moran, D. A. P., Tomita, M., Numata, K. & Arakawa, K. Multicomponent nature underlies the extraordinary mechanical properties of spider dragline silk. *bioRxiv* (2021).
- 130 Kono, N., Ohtoshi, R., Malay, A. D., Mori, M., Masunaga, H., Yoshida, Y., Nakamura, H., Numata, K. & Arakawa, K. Darwin's bark spider shares a spidroin repertoire with *Caerostris extrusa* but achieves extraordinary silk toughness through gene expression. *Open Biology* **11**, 210242 (2021).
- 131 Zax, D. B., Armanios, D. E., Horak, S., Malowniak, C. & Yang, Z. Variation of mechanical properties with amino acid content in the silk of *Nephila clavipes*. *Biomacromolecules* **5**, 732-738 (2004).
- 132 Arakawa, K., Kono, N., Malay, A. D., Tateishi, A., Ifuku, N., Masunaga, H., Sato, R., Tsuchiya, K., Ohtoshi, R. & Pedrazzoli, D. 1000 spider silkomes: Linking sequences to silk physical properties. *Science Advances* **8**, eabo6043 (2022).

- 133 Kono, N., Nakamura, H., Ohtoshi, R., Moran, D. A. P., Shinohara, A., Yoshida, Y., Fujiwara, M., Mori, M., Tomita, M. & Arakawa, K. Orb-weaving spider *Araneus ventricosus* genome elucidates the spidroin gene catalogue. *Scientific reports* **9**, 1-13 (2019).
- 134 Garb, J. E., Haney, R. A., Schwager, E. E., Gregorič, M., Kuntner, M., Agnarsson, I. & Blackledge, T. A. The transcriptome of Darwin's bark spider silk glands predicts proteins contributing to dragline silk toughness. *Communications biology* **2**, 1-8 (2019).
- 135 Urry, D. W., Luan, C.-H. & Peng, S. Q. Molecular biophysics of elastin structure, function and pathology. *The molecular biology and pathology of elastic tissues* **117**, 4-30 (1995).
- 136 Keten, S. & Buehler, M. J. Atomistic model of the spider silk nanostructure. *Applied physics letters* **96**, 153701 (2010).
- 137 Winkler, S. & Kaplan, D. L. Molecular biology of spider silk. *Reviews in Molecular Biotechnology* **74**, 85-93 (2000).
- 138 Thiel, B. & Viney, C. β sheets and spider silk. *Science* **273**, 1480-1481 (1996).
- 139 Van Beek, J. D., Hess, S., Vollrath, F. & Meier, B. The molecular structure of spider dragline silk: folding and orientation of the protein backbone. *Proceedings of the National Academy of Sciences* **99**, 10266-10271 (2002).
- 140 Lefèvre, T., Rousseau, M.-E. & Pézolet, M. Protein secondary structure and orientation in silk as revealed by Raman spectromicroscopy. *Biophysical journal* **92**, 2885-2895 (2007).
- 141 Hijirida, D. H., Do, K. G., Michal, C., Wong, S., Zax, D. & Jelinski, L. W. ¹³C NMR of *Nephila clavipes* major ampullate silk gland. *Biophysical journal* **71**, 3442-3447 (1996).
- 142 Barlow, D. & Thornton, J. Helix geometry in proteins. *Journal of molecular biology* **201**, 601-619 (1988).
- 143 Gray, G. M., Van der Vaart, A., Guo, C., Jones, J., Onofrei, D., Cherry, B. R., Lewis, R. V., Yarger, J. L. & Holland, G. P. Secondary structure adopted by the gly-gly-x repetitive regions of dragline spider silk. *International journal of molecular sciences* **17**, 2023 (2016).
- 144 Giesa, T., Perry, C. C. & Buehler, M. J. Secondary structure transition and critical stress for a model of spider silk assembly. *Biomacromolecules* **17**, 427-436 (2016).
- 145 Kümmerlen, J., Van Beek, J., Vollrath, F. & Meier, B. Local structure in spider dragline silk investigated by two-dimensional spin-diffusion nuclear magnetic resonance. *Macromolecules* **29**, 2920-2928 (1996).
- 146 Vollrath, F. & Porter, D. Spider silk as archetypal protein elastomer. *Soft Matter* **2**, 377-385 (2006).
- 147 Hurley, J. H., Mason, D. A. & Matthews, B. W. Flexible-geometry conformational energy maps for the amino acid residue preceding a proline. *Biopolymers: Original Research on Biomolecules* **32**, 1443-1446 (1992).
- 148 Rauscher, S., Baud, S., Miao, M., Keeley, F. W. & Pomes, R. Proline and glycine control protein self-organization into elastomeric or amyloid fibrils. *Structure* **14**, 1667-1676 (2006).
- 149 Savage, K. N. & Gosline, J. M. The effect of proline on the network structure of major ampullate silks as inferred from their mechanical and optical properties. *Journal of Experimental Biology* **211**, 1937-1947 (2008).
- 150 Liu, Y., Shao, Z. & Vollrath, F. Elasticity of spider silks. *Biomacromolecules* **9**, 1782-1786 (2008).
- 151 Marhabaie, M., Leeper, T. C. & Blackledge, T. A. Protein composition correlates with the mechanical properties of spider (*Argiope trifasciata*) dragline silk. *Biomacromolecules* **15**, 20-29 (2014).
- 152 Liu, Y., Spöner, A., Porter, D. & Vollrath, F. Proline and processing of spider silks. *Biomacromolecules* **9**, 116-121 (2008).
- 153 Gaines IV, W. A. & Marcotte Jr, W. R. Identification and characterization of multiple Spidroin 1 genes encoding major ampullate silk proteins in *Nephila clavipes*. *Insect molecular biology* **17**, 465-474 (2008).
- 154 Huemmerich, D., Helsen, C. W., Quedzuweit, S., Oschmann, J., Rudolph, R. & Scheibel, T. Primary structure elements of spider dragline silks and their contribution to protein solubility. *Biochemistry* **43**, 13604-13612 (2004).

- 155 Exler, J. H., Hümmerich, D. & Scheibel, T. The amphiphilic properties of spider silks are important for spinning. *Angewandte Chemie International Edition* **46**, 3559-3562 (2007).
- 156 Ramezaniaghdam, M., Nahdi, N. D. & Reski, R. Recombinant spider silk: promises and bottlenecks. *Frontiers in Bioengineering and Biotechnology* **10** (2022).
- 157 Wen, R., Wang, S., Wang, K., Yang, D., Zan, X. & Meng, Q. Complete gene sequence and mechanical property of the fourth type of major ampullate silk protein. *Acta Biomaterialia* **155**, 282-291 (2023).
- 158 Bergmann, F., Stadlmayr, S., Millesi, F., Zeitlinger, M., Naghilou, A. & Radtke, C. The properties of native Trichonephila dragline silk and its biomedical applications. *Biomaterials Advances*, 213089 (2022).
- 159 Babb, P. L., Gregorič, M., Lahens, N. F., Nicholson, D. N., Hayashi, C. Y., Higgins, L., Kuntner, M., Agnarsson, I. & Voight, B. F. Characterization of the genome and silk-gland transcriptomes of Darwin's bark spider (*Caerostris darwini*). *Plos one* **17**, e0268660 (2022).
- 160 Garb, J. E., Ayoub, N. A. & Hayashi, C. Y. Untangling spider silk evolution with spidroin terminal domains. *BMC evolutionary biology* **10**, 1-16 (2010).
- 161 Challis, R., Goodacre, S. & Hewitt, G. Evolution of spider silks: conservation and diversification of the C-terminus. *Insect molecular biology* **15**, 45-56 (2006).
- 162 Beckwith, R. & Arcidiacono, S. Sequence conservation in the C-terminal region of spider silk proteins (Spidroin) from *Nephila clavipes* (Tetragnathidae) and *Araneus bicentenarios* (Araneidae). *Journal of Biological Chemistry* **269**, 6661-6663 (1994).
- 163 Rising, A., Hjälm, G., Engström, W. & Johansson, J. N-terminal nonrepetitive domain common to dragline, flagelliform, and cylindrical spider silk proteins. *Biomacromolecules* **7**, 3120-3124 (2006).
- 164 Parent, L. R., Onofrei, D., Xu, D., Stengel, D., Roehling, J. D., Addison, J. B., Forman, C., Amin, S. A., Cherry, B. R. & Yarger, J. L. Hierarchical spidroin micellar nanoparticles as the fundamental precursors of spider silks. *Proceedings of the National Academy of Sciences* **115**, 11507-11512 (2018).
- 165 Jin, H.-J. & Kaplan, D. L. Mechanism of silk processing in insects and spiders. *Nature* **424**, 1057-1061 (2003).
- 166 Bauer, J. & Scheibel, T. Conformational stability and interplay of helical N- and C-terminal domains with implications on major ampullate spidroin assembly. *Biomacromolecules* **18**, 835-845 (2017).
- 167 Eisoldt, L., Hardy, J. G., Heim, M. & Scheibel, T. R. The role of salt and shear on the storage and assembly of spider silk proteins. *Journal of structural biology* **170**, 413-419 (2010).
- 168 Lin, T.-Y., Masunaga, H., Sato, R., Malay, A. D., Toyooka, K., Hikima, T. & Numata, K. Liquid crystalline granules align in a hierarchical structure to produce spider dragline microfibrils. *Biomacromolecules* **18**, 1350-1355 (2017).
- 169 Malay, A. D., Suzuki, T., Katashima, T., Kono, N., Arakawa, K. & Numata, K. Spider silk self-assembly via modular liquid-liquid phase separation and nanofibrillation. *Science advances* **6**, eabb6030 (2020).
- 170 Hagn, F., Thamm, C., Scheibel, T. & Kessler, H. pH-Dependent Dimerization and Salt-Dependent Stabilization of the N-terminal Domain of Spider Dragline Silk—Implications for Fiber Formation. *Angewandte Chemie International Edition* **50**, 310-313 (2011).
- 171 Knight, D. P. & Vollrath, F. Changes in element composition along the spinning duct in a *Nephila* spider. *Naturwissenschaften* **88**, 179-182 (2001).
- 172 Andersson, M., Chen, G., Otikovs, M., Landreh, M., Nordling, K., Kronqvist, N., Westermark, P., Jörnvall, H., Knight, S. & Ridderstråle, Y. Carbonic anhydrase generates CO₂ and H⁺ that drive spider silk formation via opposite effects on the terminal domains. *PLoS biology* **12**, e1001921 (2014).
- 173 Vollrath, F., Knight, D. & Hu, X. Silk production in a spider involves acid bath treatment. *Proceedings of the Royal Society of London. Series B: Biological Sciences* **265**, 817-820 (1998).
- 174 Ries, J., Schwarze, S., Johnson, C. M. & Neuweiler, H. Microsecond folding and domain motions of a spider silk protein structural switch. *Journal of the American Chemical Society* **136**, 17136-17144 (2014).

- 175 Bauer, J., Schaal, D., Eisoldt, L., Schweimer, K., Schwarzinger, S. & Scheibel, T. Acidic residues control the dimerization of the N-terminal domain of black widow spiders' major ampullate spidroin 1. *Scientific reports* **6**, 1-9 (2016).
- 176 Spohner, A., Unger, E., Grosse, F. & Weisshart, K. Conserved C-termini of spidroins are secreted by the major ampullate glands and retained in the silk thread. *Biomacromolecules* **5**, 840-845 (2004).
- 177 Ittah, S., Michaeli, A., Goldblum, A. & Gat, U. A model for the structure of the C-terminal domain of dragline spider silk and the role of its conserved cysteine. *Biomacromolecules* **8**, 2768-2773 (2007).
- 178 Kronqvist, N., Otikovs, M., Chmyrov, V., Chen, G., Andersson, M., Nordling, K., Landreh, M., Sarr, M., Jörnvall, H. & Wennmalm, S. Sequential pH-driven dimerization and stabilization of the N-terminal domain enables rapid spider silk formation. *Nature communications* **5**, 1-11 (2014).
- 179 Bauer, J. & Scheibel, T. Dimerization of the conserved N-terminal domain of a spider silk protein controls the self-assembly of the repetitive core domain. *Biomacromolecules* **18**, 2521-2528 (2017).
- 180 Greving, I., Terry, A. E., Holland, C., Boulet-Audet, M., Grillo, I., Vollrath, F. & Dicko, C. Structural Diversity of Native Major Ampullate, Minor Ampullate, Cylindriform, and Flagelliform Silk Proteins in Solution. *Biomacromolecules* **21**, 3387-3393 (2020).
- 181 Moon, M. J. & Tillinghast, E. K. Silk production after mechanical pulling stimulation in the ampullate silk glands of the barn spider, *Araneus cavaticus*. *Entomological Research* **34**, 123-130 (2004).
- 182 Vollrath, F. & Knight, D. Structure and function of the silk production pathway in the spider *Nephila edulis*. *International Journal of Biological Macromolecules* **24**, 243-249 (1999).
- 183 Knight, D. & Vollrath, F. Liquid crystals and flow elongation in a spider's silk production line. *Proceedings of the Royal Society of London. Series B: Biological Sciences* **266**, 519-523 (1999).
- 184 Papadopoulos, P., Sölter, J. & Kremer, F. Structure-property relationships in major ampullate spider silk as deduced from polarized FTIR spectroscopy. *The European Physical Journal E* **24**, 193-199 (2007).
- 185 Arakawa, T. & Timasheff, S. N. Theory of protein solubility. *Methods in enzymology* **114**, 49-77 (1985).
- 186 Zhang, Y. & Cremer, P. S. Interactions between macromolecules and ions: the Hofmeister series. *Current opinion in chemical biology* **10**, 658-663 (2006).
- 187 Dicko, C., Kenney, J. M., Knight, D. & Vollrath, F. Transition to a β -sheet-rich structure in spidroin in vitro: the effects of pH and cations. *Biochemistry* **43**, 14080-14087 (2004).
- 188 Dicko, C., Vollrath, F. & Kenney, J. M. Spider silk protein refolding is controlled by changing pH. *Biomacromolecules* **5**, 704-710 (2004).
- 189 Foo, C. W. P., Bini, E., Hensman, J., Knight, D., Lewis, R. & Kaplan, D. Role of pH and charge on silk protein assembly in insects and spiders. *Applied Physics A* **82**, 223-233 (2006).
- 190 Porter, D. & Vollrath, F. The role of kinetics of water and amide bonding in protein stability. *Soft Matter* **4**, 328-336 (2008).
- 191 Tillinghast, E. K., Chase, S. & Townley, M. A. Water extraction by the major ampullate duct during silk formation in the spider, *Argiope aurantia* Lucas. *Journal of insect physiology* **30**, 591-596 (1984).
- 192 Saric, M., Eisoldt, L., Döring, V. & Scheibel, T. Interplay of Different Major Ampullate Spidroins during Assembly and Implications for Fiber Mechanics. *Advanced Materials* **33**, 2006499 (2021).
- 193 Chen, X., Knight, D. P. & Vollrath, F. Rheological characterization of *Nephila* spidroin solution. *Biomacromolecules* **3**, 644-648 (2002).
- 194 Ortlepp, C. S. & Gosline, J. M. Consequences of forced silking. *Biomacromolecules* **5**, 727-731 (2004).
- 195 Du, N., Liu, X. Y., Narayanan, J., Li, L., Lim, M. L. M. & Li, D. Design of superior spider silk: from nanostructure to mechanical properties. *Biophysical journal* **91**, 4528-4535 (2006).

- 196 Vollrath, F., Madsen, B. & Shao, Z. The effect of spinning conditions on the mechanics of a spider's dragline silk. *Proceedings of the Royal Society of London. Series B: Biological Sciences* **268**, 2339-2346 (2001).
- 197 Young, R. J., Holland, C., Shao, Z. & Vollrath, F. Spinning conditions affect structure and properties of Nephila spider silk. *MRS Bulletin*, 1-10 (2021).
- 198 Riekel, C., Madsen, B., Knight, D. & Vollrath, F. X-ray diffraction on spider silk during controlled extrusion under a synchrotron radiation X-ray beam. *Biomacromolecules* **1**, 622-626 (2000).
- 199 Madsen, B., Shao, Z. Z. & Vollrath, F. Variability in the mechanical properties of spider silks on three levels: interspecific, intraspecific and intraindividual. *International journal of biological macromolecules* **24**, 301-306 (1999).
- 200 Yang, Y., Chen, X., Shao, Z., Zhou, P., Porter, D., Knight, D. P. & Vollrath, F. Toughness of spider silk at high and low temperatures. *Advanced Materials* **17**, 84-88 (2005).
- 201 Anotaux, M., Toscani, C., Leborgne, R., Châline, N. & Pasquet, A. Aging and foraging efficiency in an orb-web spider. *Journal of ethology* **32**, 155-163 (2014).
- 202 Grubb, D. T. & Jelinski, L. W. Fiber morphology of spider silk: the effects of tensile deformation. *Macromolecules* **30**, 2860-2867 (1997).
- 203 Riekel, C., Bränden, C., Craig, C., Ferrero, C., Heidelbach, F. & Müller, M. Aspects of X-ray diffraction on single spider fibers. *International Journal of Biological Macromolecules* **24**, 179-186 (1999).
- 204 Glišović, A., Vehoff, T., Davies, R. J. & Salditt, T. Strain dependent structural changes of spider dragline silk. *Macromolecules* **41**, 390-398 (2008).
- 205 Su, I. & Buehler, M. J. Nanomechanics of silk: the fundamentals of a strong, tough and versatile material. *Nanotechnology* **27**, 302001 (2016).
- 206 Xiao, S., Stacklies, W., Debes, C. & Gräter, F. Force distribution determines optimal length of β -sheet crystals for mechanical robustness. *Soft Matter* **7**, 1308-1311 (2011).
- 207 Cetinkaya, M., Xiao, S. & Gräter, F. Effects of crystalline subunit size on silk fiber mechanics. *Soft Matter* **7**, 8142-8148 (2011).
- 208 Bratzel, G. & Buehler, M. J. Sequence-structure correlations in silk: Poly-Ala repeat of N. clavipes MaSp1 is naturally optimized at a critical length scale. *Journal of the mechanical behavior of biomedical materials* **7**, 30-40 (2012).
- 209 Spek, E. J., Wu, H.-C. & Kallenbach, N. R. The role of alanine sequences in forming β -sheets of spider dragline silk. *Journal of the American chemical Society* **119**, 5053-5054 (1997).
- 210 Papadopoulos, P., Sölter, J. & Kremer, F. Hierarchies in the structural organization of spider silk—a quantitative model. *Colloid and Polymer Science* **287**, 231-236 (2009).
- 211 Ene, R., Papadopoulos, P. & Kremer, F. Quantitative analysis of infrared absorption coefficient of spider silk fibers. *Vibrational Spectroscopy* **57**, 207-212 (2011).
- 212 Ene, R., Papadopoulos, P. & Kremer, F. Partial deuteration probing structural changes in supercontracted spider silk. *Polymer* **51**, 4784-4789 (2010).
- 213 Cranford, S. W., Tarakanova, A., Pugno, N. M. & Buehler, M. J. Nonlinear material behaviour of spider silk yields robust webs. *Nature* **482**, 72-76 (2012).
- 214 Giesa, T., Arslan, M., Pugno, N. M. & Buehler, M. J. Nanoconfinement of spider silk fibrils begets superior strength, extensibility, and toughness. *Nano letters* **11**, 5038-5046 (2011).
- 215 Qin, Z. & Buehler, M. J. Cooperativity governs the size and structure of biological interfaces. *Journal of biomechanics* **45**, 2778-2783 (2012).
- 216 Colomban, P. & Dinh, H. M. Origin of the variability of the mechanical properties of silk fibres: 2 The nanomechanics of single silkworm and spider fibres. *Journal of Raman Spectroscopy* **43**, 1035-1041 (2012).
- 217 Colomban, P., Dinh, H. M., Bunsell, A. & Mauchamp, B. Origin of the variability of the mechanical properties of silk fibres: 1-The relationship between disorder, hydration and stress/strain behaviour. *Journal of Raman Spectroscopy* **43**, 425-432 (2012).
- 218 Alam, P. Protein unfolding versus β -sheet separation in spider silk nanocrystals. *Advances in Natural Sciences: Nanoscience and Nanotechnology* **5**, 015015 (2014).

- 219 Müller-Herrmann, S. & Scheibel, T. Enzymatic degradation of films, particles, and nonwoven meshes made of a recombinant spider silk protein. *ACS Biomaterials Science & Engineering* **1**, 247-259 (2015).
- 220 Zeplin, P. H., Maksimovikj, N. C., Jordan, M. C., Nickel, J., Lang, G., Leimer, A. H., Römer, L. & Scheibel, T. Spider silk coatings as a bioshield to reduce periprosthetic fibrous capsule formation. *Advanced Functional Materials* **24**, 2658-2666 (2014).
- 221 Tachibana, Y., Darbe, S., Hayashi, S., Kudasheva, A., Misawa, H., Shibata, Y. & Kasuya, K.-i. Environmental biodegradability of recombinant structural protein. *Scientific Reports* **11**, 1-10 (2021).
- 222 Tao, H., Kaplan, D. L. & Omenetto, F. G. Silk materials—a road to sustainable high technology. *Advanced materials* **24**, 2824-2837 (2012).
- 223 Fox, L. R. Cannibalism in natural populations. *Annual review of ecology and systematics* **6**, 87-106 (1975).
- 224 Wise, D. H. Cannibalism, food limitation, intraspecific competition, and the regulation of spider populations. *Annu. Rev. Entomol.* **51**, 441-465 (2006).
- 225 Pompozzi, G. & Simó, M. Hunger and territorial-dependent cannibalism in females of a South American species of wolf spider (Araneae: Lycosidae). *Studies on Neotropical Fauna and Environment* **55**, 242-246 (2020).
- 226 Craig, C. L., Riekel, C., Herberstein, M. E., Weber, R. S., Kaplan, D. & Pierce, N. E. Evidence for diet effects on the composition of silk proteins produced by spiders. *Molecular Biology and Evolution* **17**, 1904-1913 (2000).
- 227 Whittall, D. R., Baker, K. V., Breitling, R. & Takano, E. Host systems for the production of recombinant spider silk. *Trends in Biotechnology* **39**, 560-573 (2021).
- 228 Lang, G., Herold, H. & Scheibel, T. Properties of engineered and fabricated silks. *Fibrous proteins: Structures and mechanisms*, 527-573 (2017).
- 229 Arcidiacono, S., Mello, C., Kaplan, D., Cheley, S. & Bayley, H. Purification and characterization of recombinant spider silk expressed in *Escherichia coli*. *Applied microbiology and biotechnology* **49**, 31-38 (1998).
- 230 Huang, W., Lin, Z., Sin, Y., Li, D., Gong, Z. & Yang, D. Characterization and expression of a cDNA encoding a tubuliform silk protein of the golden web spider *Nephila antipodiana*. *Biochimie* **88**, 849-858 (2006).
- 231 Teulé, F., Aubé, C., Ellison, M. & Abbott, A. Biomimetic manufacturing of customised novel fibre proteins for specialised applications. *AUTEX Res J* **3**, 160-165 (2003).
- 232 Hauptmann, V., Weichert, N., Menzel, M., Knoch, D., Paege, N., Scheller, J., Spohn, U., Conrad, U. & Gils, M. Native-sized spider silk proteins synthesized in planta via intein-based multimerization. *Transgenic research* **22**, 369-377 (2013).
- 233 Menassa, R., Zhu, H., Karatzas, C. N., Lazaris, A., Richman, A. & Brandle, J. Spider dragline silk proteins in transgenic tobacco leaves: accumulation and field production. *Plant Biotechnology Journal* **2**, 431-438 (2004).
- 234 Huebnerich, D., Scheibel, T., Vollrath, F., Cohen, S., Gat, U. & Ittah, S. Novel assembly properties of recombinant spider dragline silk proteins. *Current Biology* **14**, 2070-2074 (2004).
- 235 Miao, Y., Zhang, Y., Nakagaki, K., Zhao, T., Zhao, A., Meng, Y., Nakagaki, M., Park, E. Y. & Maenaka, K. Expression of spider flagelliform silk protein in *Bombyx mori* cell line by a novel Bac-to-Bac/BmNPV baculovirus expression system. *Applied microbiology and biotechnology* **71**, 192-199 (2006).
- 236 Lazaris, A., Arcidiacono, S., Huang, Y., Zhou, J.-F., Duguay, F., Chretien, N., Welsh, E. A., Soares, J. W. & Karatzas, C. N. Spider silk fibers spun from soluble recombinant silk produced in mammalian cells. *science* **295**, 472-476 (2002).
- 237 Xu, H.-T., Fan, B.-L., Yu, S.-Y., Huang, Y.-H., Zhao, Z.-H., Lian, Z.-X., Dai, Y.-P., Wang, L.-L., Liu, Z.-L. & Fei, J. Construct synthetic gene encoding artificial spider dragline silk protein and its expression in milk of transgenic mice. *Animal Biotechnology* **18**, 1-12 (2007).
- 238 Wen, H., Lan, X., Zhang, Y., Zhao, T., Wang, Y., Kajiura, Z. & Nakagaki, M. Transgenic silkworms (*Bombyx mori*) produce recombinant spider dragline silk in cocoons. *Molecular biology reports* **37**, 1815-1821 (2010).

- 239 Xu, J., Dong, Q., Yu, Y., Niu, B., Ji, D., Li, M., Huang, Y., Chen, X. & Tan, A. Mass spider silk production through targeted gene replacement in *Bombyx mori*. *Proceedings of the National Academy of Sciences* **115**, 8757-8762 (2018).
- 240 Copeland, C. G., Bell, B. E., Christensen, C. D. & Lewis, R. V. Development of a process for the spinning of synthetic spider silk. *ACS biomaterials science & engineering* **1**, 577-584 (2015).
- 241 Tokareva, O., Michalczechen-Lacerda, V. A., Rech, E. L. & Kaplan, D. L. Recombinant DNA production of spider silk proteins. *Microbial biotechnology* **6**, 651-663 (2013).
- 242 Vendrely, C. & Scheibel, T. Biotechnological production of spider-silk proteins enables new applications. *Macromolecular bioscience* **7**, 401-409 (2007).
- 243 Edlund, A. M., Jones, J., Lewis, R. & Quinn, J. C. Economic feasibility and environmental impact of synthetic spider silk production from *Escherichia coli*. *New biotechnology* **42**, 12-18 (2018).
- 244 Venkatesan, H., Chen, J. & Hu, J. Fibers made of recombinant spidroins—a brief review. *AATCC Journal of Research* **6**, 37-40 (2019).
- 245 Dinjaski, N. & Kaplan, D. L. Recombinant protein blends: silk beyond natural design. *Current opinion in biotechnology* **39**, 1-7 (2016).
- 246 Fahnstock, S. & Irwin, S. Synthetic spider dragline silk proteins and their production in *Escherichia coli*. *Applied microbiology and biotechnology* **47**, 23-32 (1997).
- 247 Rising, A., Widhe, M., Johansson, J. & Hedhammar, M. Spider silk proteins: recent advances in recombinant production, structure–function relationships and biomedical applications. *Cellular and Molecular Life Sciences* **68**, 169-184 (2011).
- 248 Xia, X.-X., Qian, Z.-G., Ki, C. S., Park, Y. H., Kaplan, D. L. & Lee, S. Y. Native-sized recombinant spider silk protein produced in metabolically engineered *Escherichia coli* results in a strong fiber. *Proceedings of the National Academy of Sciences* **107**, 14059-14063 (2010).
- 249 Bowen, C. H., Dai, B., Sargent, C. J., Bai, W., Ladiwala, P., Feng, H., Huang, W., Kaplan, D. L., Galazka, J. M. & Zhang, F. Recombinant spidroins fully replicate primary mechanical properties of natural spider silk. *Biomacromolecules* **19**, 3853-3860 (2018).
- 250 Deptuch, T. & Dams-Kozłowska, H. Silk materials functionalized via genetic engineering for biomedical applications. *Materials* **10**, 1417 (2017).
- 251 Sutherland, T. D., Huson, M. G. & Rapson, T. D. Rational design of new materials using recombinant structural proteins: Current state and future challenges. *Journal of structural biology* **201**, 76-83 (2018).
- 252 Doblhofer, E. & Scheibel, T. Engineering of recombinant spider silk proteins allows defined uptake and release of substances. *Journal of pharmaceutical sciences* **104**, 988-994 (2015).
- 253 Elsner, M. B., Herold, H. M., Müller-Herrmann, S., Bargel, H. & Scheibel, T. Enhanced cellular uptake of engineered spider silk particles. *Biomaterials science* **3**, 543-551 (2015).
- 254 Petzold, J., Aigner, T. B., Touska, F., Zimmermann, K., Scheibel, T. & Engel, F. B. Surface features of recombinant spider silk protein eADF4 ($\kappa 16$)-made materials are well-suited for cardiac tissue engineering. *Advanced Functional Materials* **27**, 1701427 (2017).
- 255 Steiner, D., Winkler, S., Heltmann-Meyer, S., Trossmann, V. T., Fey, T., Scheibel, T., Horch, R. E. & Arkudas, A. Enhanced vascularization and de novo tissue formation in hydrogels made of engineered RGD-tagged spider silk proteins in the arteriovenous loop model. *Biofabrication* **13**, 045003 (2021).
- 256 An, B., Tang-Schomer, M. D., Huang, W., He, J., Jones, J. A., Lewis, R. V. & Kaplan, D. L. Physical and biological regulation of neuron regenerative growth and network formation on recombinant dragline silks. *Biomaterials* **48**, 137-146 (2015).
- 257 Dinjaski, N., Plowright, R., Zhou, S., Belton, D. J., Perry, C. C. & Kaplan, D. L. Osteoinductive recombinant silk fusion proteins for bone regeneration. *Acta biomaterialia* **49**, 127-139 (2017).
- 258 Nilebäck, L., Hedin, J., Widhe, M., Floderus, L. S., Krona, A., Bysell, H. & Hedhammar, M. Self-assembly of recombinant silk as a strategy for chemical-free formation of bioactive coatings: A real-time study. *Biomacromolecules* **18**, 846-854 (2017).

- 259 Florczak, A., Jastrzebska, K., Mackiewicz, A. & Dams-Kozłowska, H. Blending two bioengineered spider silks to develop cancer targeting spheres. *Journal of Materials Chemistry B* **5**, 3000-3011 (2017).
- 260 Humenik, M., Drechsler, M. & Scheibel, T. Controlled hierarchical assembly of spider silk-DNA chimeras into ribbons and raft-like morphologies. *Nano letters* **14**, 3999-4004 (2014).
- 261 Molina, A., Scheibel, T. & Humenik, M. Nanoscale patterning of surfaces via DNA directed spider silk assembly. *Biomacromolecules* **20**, 347-352 (2018).
- 262 Hardy, J. G., Pfaff, A., Leal-Egaña, A., Müller, A. H. & Scheibel, T. R. Glycopolymer functionalization of engineered spider silk protein-based materials for improved cell adhesion. *Macromolecular bioscience* **14**, 936-942 (2014).
- 263 Harvey, D., Bardelang, P., Goodacre, S. L., Cockayne, A. & Thomas, N. R. Antibiotic Spider Silk: Site-Specific Functionalization of Recombinant Spider Silk Using “Click” Chemistry. *Advanced Materials* **29**, 1604245 (2017).
- 264 Huang, W., Krishnaji, S., Tokareva, O. R., Kaplan, D. & Cebe, P. Tunable crystallization, degradation, and self-assembly of recombinant protein block copolymers. *Polymer* **117**, 107-116 (2017).
- 265 Liu, B., Wang, T., Xiao, L., Zhang, G., Li, G., Luo, J. & Liu, X. A directed self-assembly quasi-spider silk protein expressed in *Pichia pastoris*. *Biotechnology & Biotechnological Equipment* **32**, 451-461 (2018).
- 266 Zhou, Z., Zhang, S., Cao, Y., Marelli, B., Xia, X. & Tao, T. H. Engineering the future of silk materials through advanced manufacturing. *Advanced Materials* **30**, 1706983 (2018).
- 267 Patil, S., Markert, B. & Gräter, F. in *Proceedings of the 3rd GAMM Seminar on Continuum Biomechanics II–21*. 75-87.
- 268 Krishnaji, S. T., Bratzel, G., Kinahan, M. E., Kluge, J. A., Staii, C., Wong, J. Y., Buehler, M. J. & Kaplan, D. L. Sequence–structure–property relationships of recombinant spider silk proteins: integration of biopolymer design, processing, and modeling. *Advanced functional materials* **23**, 241-253 (2013).
- 269 Humenik, M., Magdeburg, M. & Scheibel, T. Influence of repeat numbers on self-assembly rates of repetitive recombinant spider silk proteins. *Journal of structural biology* **186**, 431-437 (2014).
- 270 Eisoldt, L. *Funktion und Einfluss der nicht-repetitiven, terminalen Domänen auf Speicherung und Assemblierung von Spinnenseidenproteinen*, (2013).
- 271 Slotta, U., Tammer, M., Kremer, F., Koelsch, P. & Scheibel, T. Structural analysis of spider silk films. *Supramolecular Chemistry* **18**, 465-471 (2006).
- 272 Thamm, C. & Scheibel, T. Recombinant production, characterization, and fiber spinning of an engineered short major ampullate spidroin (MaSp1s). *Biomacromolecules* **18**, 1365-1372 (2017).
- 273 Zbilut, J. P., Scheibel, T., Hümmerich, D., Webber Jr, C. L., Colafranceschi, M. & Giuliani, A. Statistical approaches for investigating silk properties. *Applied Physics A* **82**, 243-251 (2006).
- 274 Slotta, U. K., Rammensee, S., Gorb, S. & Scheibel, T. An engineered spider silk protein forms microspheres. *Angewandte Chemie International Edition* **47**, 4592-4594 (2008).
- 275 Slotta, U., Hess, S., Spieß, K., Stromer, T., Serpell, L. & Scheibel, T. Spider silk and amyloid fibrils: a structural comparison. *Macromolecular bioscience* **7**, 183-188 (2007).
- 276 Kenney, J. M., Knight, D., Wise, M. J. & Vollrath, F. Amyloidogenic nature of spider silk. *European journal of biochemistry* **269**, 4159-4163 (2002).
- 277 Schacht, K. & Scheibel, T. Controlled hydrogel formation of a recombinant spider silk protein. *Biomacromolecules* **12**, 2488-2495 (2011).
- 278 Lechner, A., Trossmann, V. T. & Scheibel, T. Impact of Cell Loading of Recombinant Spider Silk Based Bioinks on Gelation and Printability. *Macromolecular Bioscience*, 2100390 (2021).
- 279 DeSimone, E., Schacht, K., Pellert, A. & Scheibel, T. Recombinant spider silk-based bioinks. *Biofabrication* **9**, 044104 (2017).
- 280 Neubauer, V. J., Trossmann, V. T., Jacobi, S., Döbl, A. & Scheibel, T. Recombinant Spider Silk Gels Derived from Aqueous–Organic Solvents as Depots for Drugs. *Angewandte Chemie International Edition* **60**, 11847-11851 (2021).

- 281 Humenik, M., Preiß, T., Gödrich, S., Papastavrou, G. & Scheibel, T. Functionalized DNA-spider silk nanohydrogels for controlled protein binding and release. *Materials Today Bio* **6**, 100045 (2020).
- 282 Rammensee, S., Slotta, U., Scheibel, T. & Bausch, A. R. Assembly mechanism of recombinant spider silk proteins. *Proceedings of the National Academy of Sciences* **105**, 6590-6595 (2008).
- 283 Lammel, A., Schwab, M., Slotta, U., Winter, G. & Scheibel, T. Processing conditions for the formation of spider silk microspheres. *ChemSusChem: Chemistry & Sustainability Energy & Materials* **1**, 413-416 (2008).
- 284 Spiess, K., Lammel, A. & Scheibel, T. Recombinant spider silk proteins for applications in biomaterials. *Macromolecular bioscience* **10**, 998-1007 (2010).
- 285 Lucke, M., Mottas, I., Herbst, T., Hotz, C., Römer, L., Schierling, M., Herold, H. M., Slotta, U., Spinetti, T. & Scheibel, T. Engineered hybrid spider silk particles as delivery system for peptide vaccines. *Biomaterials* **172**, 105-115 (2018).
- 286 Lammel, A. S., Hu, X., Park, S.-H., Kaplan, D. L. & Scheibel, T. R. Controlling silk fibroin particle features for drug delivery. *Biomaterials* **31**, 4583-4591 (2010).
- 287 Herold, H. M., Döbl, A., Wohlrab, S., Humenik, M. & Scheibel, T. Designed Spider Silk-Based Drug Carrier for Redox-or pH-Triggered Drug Release. *Biomacromolecules* **21**, 4904-4912 (2020).
- 288 Kumari, S., Bargel, H. & Scheibel, T. Recombinant spider silk-silica hybrid scaffolds with drug-releasing properties for tissue engineering applications. *Macromolecular rapid communications* **41**, 1900426 (2020).
- 289 Anton, A. M., Heidebrecht, A., Mahmood, N., Beiner, M., Scheibel, T. & Kremer, F. Foundation of the outstanding toughness in biomimetic and natural spider silk. *Biomacromolecules* **18**, 3954-3962 (2017).
- 290 Steiner, D., Lang, G., Fischer, L., Winkler, S., Fey, T., Greil, P., Scheibel, T., Horch, R. E. & Arkudas, A. Intrinsic vascularization of recombinant eADF4 (C16) spider silk matrices in the arteriovenous loop model. *Tissue Engineering Part A* **25**, 1504-1513 (2019).
- 291 Salehi, S. & Scheibel, T. Biomimetic spider silk fibres: From vision to reality. *The Biochemist* **40**, 4-7 (2018).
- 292 Leal-Egaña, A., Lang, G., Mauerer, C., Wickinghoff, J., Weber, M., Geimer, S. & Scheibel, T. Interactions of fibroblasts with different morphologies made of an engineered spider silk protein. *Advanced Engineering Materials* **14**, B67-B75 (2012).
- 293 Müller, F., Zainuddin, S. & Scheibel, T. Roll-to-Roll Production of Spider Silk Nanofiber Nonwoven Meshes Using Centrifugal Electrospinning for Filtration Applications. *Molecules* **25**, 5540 (2020).
- 294 Jokisch, S., Neuenfeldt, M. & Scheibel, T. Silk-based fine dust filters for air filtration. *Advanced Sustainable Systems* **1**, 1700079 (2017).
- 295 Müller, F., Jokisch, S., Bargel, H. & Scheibel, T. Centrifugal electrospinning enables the production of meshes of ultrathin polymer fibers. *ACS Applied Polymer Materials* **2**, 4360-4367 (2020).
- 296 DeSimone, E., Aigner, T. B., Humenik, M., Lang, G. & Scheibel, T. Aqueous electrospinning of recombinant spider silk proteins. *Materials Science and Engineering: C* **106**, 110145 (2020).
- 297 Aigner, T., Haynl, C., Salehi, S., O'Connor, A. & Scheibel, T. Nerve guidance conduit design based on self-rolling tubes. *Materials Today Bio* **5**, 100042 (2020).
- 298 Borkner, C. B., Lentz, S., Müller, M., Fery, A. & Scheibel, T. Ultrathin spider silk films: Insights into spider silk assembly on surfaces. *ACS Applied Polymer Materials* **1**, 3366-3374 (2019).
- 299 Wohlrab, S., Spieß, K. & Scheibel, T. Varying surface hydrophobicities of coatings made of recombinant spider silk proteins. *Journal of Materials Chemistry* **22**, 22050-22054 (2012).
- 300 Hofmaier, M., Urban, B., Lentz, S., Borkner, C. B., Scheibel, T., Fery, A. & Müller, M. Dichroic Fourier Transform Infrared Spectroscopy Characterization of the β -Sheet Orientation in Spider Silk Films on Silicon Substrates. *The Journal of Physical Chemistry B* **125**, 1061-1071 (2021).
- 301 Zeplin, P., Berninger, A., Maksimovikj, N., Van Gelder, P., Scheibel, T. & Walles, H. Improving the biocompatibility of silicone implants using spider silk coatings: immunohistochemical analysis of capsule formation. *Handchirurgie, Mikrochirurgie,*

- Plastische Chirurgie: Organ der Deutschsprachigen Arbeitsgemeinschaft für Handchirurgie: Organ der Deutschsprachigen Arbeitsgemeinschaft für Mikrochirurgie der Peripheren Nerven und Gefäße: Organ der V.* **46**, 336-341 (2014).
- 302 Borkner, C. B., Wohlrab, S., Möller, E., Lang, G. & Scheibel, T. Surface modification of polymeric biomaterials using recombinant spider silk proteins. *ACS Biomaterials Science & Engineering* **3**, 767-775 (2017).
- 303 Salehi, S., Koeck, K. & Scheibel, T. Spider silk for tissue engineering applications. *Molecules* **25**, 737 (2020).
- 304 Esser, T. U., Troßmann, V. T., Lentz, S., Engel, F. B. & Scheibel, T. Designing of spider silk proteins for human induced pluripotent stem cell-based cardiac tissue engineering. *Materials Today Bio* **11**, 100114 (2021).
- 305 Herold, H. M., Aigner, T. B., Grill, C. E., Krüger, S., Taubert, A. & Scheibel, T. SpiderMAEn: recombinant spider silk-based hybrid materials for advanced energy technology. *Bioinspired, Biomimetic and Nanobiomaterials* **8**, 99-108 (2019).
- 306 Kumari, S., Lang, G., DeSimone, E., Spengler, C., Trossmann, V. T., Lückner, S., Hudel, M., Jacobs, K., Krämer, N. & Scheibel, T. Engineered spider silk-based 2D and 3D materials prevent microbial infestation. *Materials Today* **41**, 21-33 (2020).
- 307 Huang, T., Kumari, S., Herold, H., Bargel, H., Aigner, T. B., Heath, D. E., O'Brien-Simpson, N. M., O'Connor, A. J. & Scheibel, T. Enhanced antibacterial activity of Se nanoparticles upon coating with recombinant spider silk protein eADF4 (κ 16). *International Journal of Nanomedicine* **15**, 4275 (2020).
- 308 Sommer, C., Bargel, H., Raßmann, N. & Scheibel, T. Microbial repellence properties of engineered spider silk coatings prevent biofilm formation of opportunistic bacterial strains. *MRS Communications*, 1-7 (2021).
- 309 Nakajima, T., Kajiwara, K. & McIntyre, J. E. *Advanced fiber spinning technology*. (Woodhead Publishing, 1994).
- 310 Greiner, A. & Wendorff, J. H. Electrospinning: a fascinating method for the preparation of ultrathin fibers. *Angewandte Chemie International Edition* **46**, 5670-5703 (2007).
- 311 Katayama, K., Nakamura, K. & Amano, T. Structural formation during melt spinning process. *Kolloid-Zeitschrift und Zeitschrift für Polymere* **226**, 125-134 (1968).
- 312 Raghavan, B., Soto, H. & Lozano, K. Fabrication of melt spun polypropylene nanofibers by forspinning. *Journal of Engineered Fibers and Fabrics* **8**, 155892501300800106 (2013).
- 313 Jelinski, L. W., Blye, A., Liivak, O., Michal, C., LaVerde, G., Seidel, A., Shah, N. & Yang, Z. Orientation, structure, wet-spinning, and molecular basis for supercontraction of spider dragline silk. *International journal of biological macromolecules* **24**, 197-201 (1999).
- 314 Brooks, A. E., Stricker, S. M., Joshi, S. B., Kamerzell, T. J., Middaugh, C. R. & Lewis, R. V. Properties of synthetic spider silk fibers based on *Argiope aurantia* MaSp2. *Biomacromolecules* **9**, 1506-1510 (2008).
- 315 Chen, J., Hu, J., Sasaki, S. & Naka, K. Modular assembly of a conserved repetitive sequence in the spider eggcase silk: from gene to fiber. *ACS Biomaterials Science & Engineering* **4**, 2748-2757 (2018).
- 316 Lin, Z., Deng, Q., Liu, X. Y. & Yang, D. Engineered large spider eggcase silk protein for strong artificial fibers. *Advanced materials* **25**, 1216-1220 (2013).
- 317 Peng, Q., Zhang, Y., Lu, L., Shao, H., Qin, K., Hu, X. & Xia, X. Recombinant spider silk from aqueous solutions via a bio-inspired microfluidic chip. *Scientific reports* **6**, 1-12 (2016).
- 318 Andersson, M., Jia, Q., Abella, A., Lee, X.-Y., Landreh, M., Purhonen, P., Hebert, H., Tenje, M., Robinson, C. V. & Meng, Q. Biomimetic spinning of artificial spider silk from a chimeric minispidroin. *Nature chemical biology* **13**, 262-264 (2017).
- 319 Arndt, T., Laity, P. R., Johansson, J., Holland, C. & Rising, A. Native-like Flow Properties of an Artificial Spider Silk Dope. *ACS Biomaterials Science & Engineering* **7**, 462-471 (2021).
- 320 Hu, C.-F., Qian, Z.-G., Peng, Q., Zhang, Y. & Xia, X.-X. Unconventional Spidroin Assemblies in Aqueous Dope for Spinning into Tough Synthetic Fibers. *ACS Biomaterials Science & Engineering* **7**, 3608-3617 (2021).

- 321 Shao, Z., Vollrath, F., Yang, Y. & Thøgersen, H. C. Structure and behavior of regenerated spider silk. *Macromolecules* **36**, 1157-1161 (2003).
- 322 Seidel, A., Liivak, O. & Jelinski, L. W. Artificial spinning of spider silk. *Macromolecules* **31**, 6733-6736 (1998).
- 323 Seidel, A., Liivak, O., Calve, S., Adaska, J., Ji, G., Yang, Z., Grubb, D., Zax, D. B. & Jelinski, L. W. Regenerated spider silk: Processing, properties, and structure. *Macromolecules* **33**, 775-780 (2000).
- 324 Wu, R., Bae, J., Jeon, H. & Kim, T. Spider-inspired regenerated silk fibroin fiber actuator via microfluidic spinning. *Chemical Engineering Journal* **444**, 136556 (2022).
- 325 Jones, J. A., Harris, T. I., Tucker, C. L., Berg, K. R., Christy, S. Y., Day, B. A., Gaztambide, D. A., Needham, N. J., Ruben, A. L. & Oliveira, P. F. More than just fibers: an aqueous method for the production of innovative recombinant spider silk protein materials. *Biomacromolecules* **16**, 1418-1425 (2015).
- 326 Arcidiacono, S., Mello, C. M., Butler, M., Welsh, E., Soares, J. W., Allen, A., Ziegler, D., Laue, T. & Chase, S. Aqueous processing and fiber spinning of recombinant spider silks. *Macromolecules* **35**, 1262-1266 (2002).
- 327 Jones, J. A., Harris, T. I., Oliveira, P. F., Bell, B. E., Alhabib, A. & Lewis, R. V. Importance of heat and pressure for solubilization of recombinant spider silk proteins in aqueous solution. *International journal of molecular sciences* **17**, 1955 (2016).
- 328 Doblhofer, E., Heidebrecht, A. & Scheibel, T. To spin or not to spin: spider silk fibers and more. *Applied microbiology and biotechnology* **99**, 9361-9380 (2015).
- 329 Jestin, S. & Poulin, P. in *Nanotube superfiber materials* 167-209 (Elsevier, 2014).
- 330 Albertson, A. E., Teulé, F., Weber, W., Yarger, J. L. & Lewis, R. V. Effects of different post-spin stretching conditions on the mechanical properties of synthetic spider silk fibers. *Journal of the mechanical behavior of biomedical materials* **29**, 225-234 (2014).
- 331 An, B., Hinman, M. B., Holland, G. P., Yarger, J. L. & Lewis, R. V. Inducing β -sheets formation in synthetic spider silk fibers by aqueous post-spin stretching. *Biomacromolecules* **12**, 2375-2381 (2011).
- 332 Nge, P. N., Rogers, C. I. & Woolley, A. T. Advances in microfluidic materials, functions, integration, and applications. *Chemical reviews* **113**, 2550-2583 (2013).
- 333 Konwarh, R., Gupta, P. & Mandal, B. B. Silk-microfluidics for advanced biotechnological applications: A progressive review. *Biotechnology advances* **34**, 845-858 (2016).
- 334 Sun, J., Chen, J., Liu, K. & Zeng, H. Mechanically strong proteinaceous fibers: Engineered fabrication by microfluidics. *Engineering* (2021).
- 335 Zhang, M., Peng, X., Fan, P., Zhou, Y. & Xiao, P. Recent Progress in Preparation and Application of Fibers Using Microfluidic Spinning Technology. *Macromolecular Chemistry and Physics* **223**, 2100451 (2022).
- 336 Shang, L., Yu, Y., Liu, Y., Chen, Z., Kong, T. & Zhao, Y. Spinning and applications of bioinspired fiber systems. *ACS nano* **13**, 2749-2772 (2019).
- 337 Renberg, B., Andersson-Svahn, H. & Hedhammar, M. Mimicking silk spinning in a microchip. *Sensors and Actuators B: Chemical* **195**, 404-408 (2014).
- 338 Garrote, J., Ruiz, V., Troncoso, O. P., Torres, F. G., Arnedo, M., Elices, M., Guinea, G. V. & Pérez-Rigueiro, J. Application of the Spider Silk Standardization Initiative (S3I) methodology to the characterization of major ampullate gland silk fibers spun by spiders from Pantanos de Villa wetlands (Lima, Peru). *Journal of the mechanical behavior of biomedical materials* **111**, 104023 (2020).
- 339 Pérez-Rigueiro, J., Elices, M. & Guinea, G. Controlled supercontraction tailors the tensile behaviour of spider silk. *Polymer* **44**, 3733-3736 (2003).
- 340 Elices, M., Plaza, G. R., Arnedo, M. A., Pérez-Rigueiro, J., Torres, F. G. & Guinea, G. V. Mechanical behavior of silk during the evolution of orb-web spinning spiders. *Biomacromolecules* **10**, 1904-1910 (2009).
- 341 Jackson, C. & O'Brien, J. P. Molecular weight distribution of *Nephila clavipes* dragline silk. *Macromolecules* **28**, 5975-5977 (1995).

- 342 Hümmerich, D. *Design, Synthese und Analyse von Spinnenseidenproteinen*, Technische Universität München, (2005).
- 343 Hwang, C., Sinskey, A. J. & Lodish, H. F. Oxidized redox state of glutathione in the endoplasmic reticulum. *Science* **257**, 1496-1502 (1992).
- 344 Gilbert, H. F. & McLean, V. Molecular and cellular aspects of thiol-disulfide exchange. *Advances in enzymology and related areas of molecular biology* **63**, 69-69 (1993).
- 345 Marley, J., Lu, M. & Bracken, C. A method for efficient isotopic labeling of recombinant proteins. *Journal of biomolecular NMR* **20** (2001).
- 346 Sattler, M., Schleucher, J. & Griesinger, C. Heteronuclear multidimensional NMR experiments for the structure determination of proteins in solution. *Progress in nuclear magnetic resonance spectroscopy* **34**, 93-158 (1999).
- 347 Yamaguchi, H. & Miyazaki, M. Refolding techniques for recovering biologically active recombinant proteins from inclusion bodies. *Biomolecules* **4**, 235-251 (2014).
- 348 Xu, D., Yarger, J. L. & Holland, G. P. Exploring the backbone dynamics of native spider silk proteins in Black Widow silk glands with solution-state NMR spectroscopy. *Polymer* **55**, 3879-3885 (2014).
- 349 Onofrei, D., Stengel, D., Jia, D., Johnson, H. R., Trescott, S., Soni, A., Addison, B., Muthukumar, M. & Holland, G. P. Investigating the atomic and mesoscale interactions that facilitate spider silk protein pre-assembly. *Biomacromolecules* **22**, 3377-3385 (2021).
- 350 Murthy, A. C., Dignon, G. L., Kan, Y., Zerze, G. H., Parekh, S. H., Mittal, J. & Fawzi, N. L. Molecular interactions underlying liquid–liquid phase separation of the FUS low-complexity domain. *Nature structural & molecular biology* **26**, 637-648 (2019).
- 351 Lin, Y., Currie, S. L. & Rosen, M. K. Intrinsically disordered sequences enable modulation of protein phase separation through distributed tyrosine motifs. *Journal of Biological Chemistry* **292**, 19110-19120 (2017).
- 352 Gabryelczyk, B., Cai, H., Shi, X., Sun, Y., Swinkels, P. J., Salentinig, S., Pervushin, K. & Miserez, A. Hydrogen bond guidance and aromatic stacking drive liquid-liquid phase separation of intrinsically disordered histidine-rich peptides. *Nature communications* **10**, 5465 (2019).
- 353 Lim, J., Kumar, A., Low, K., Verma, C. S., Mu, Y., Miserez, A. & Pervushin, K. Liquid–liquid phase separation of short histidine-and tyrosine-rich peptides: Sequence specificity and molecular topology. *The Journal of Physical Chemistry B* **125**, 6776-6790 (2021).

5 PUBLICATION LIST

- I. **Saric, M.**, & Scheibel, T. (2019). Engineering of silk proteins for materials applications. *Current opinion in biotechnology*, 60, 213-220.
<https://doi.org/10.1016/j.copbio.2019.05.005>

- II. **Saric, M.**, Eisoldt, L., Döring, V., & Scheibel, T. (2021). Interplay of Different Major Ampullate Spidroins during Assembly and Implications for Fiber Mechanics. *Advanced Materials*, 33(9), 2006499.
<https://doi.org/10.1002/adma.202006499>

- III. **Saric, M.**, & Scheibel, T. (2023). Two-In-One Spider Silk Protein with Combined Mechanical Features in All-Aqueous Spun Fibers. *Biomacromolecules*, 24(4), 1744-1750. Copyright 2023, American Chemical Society.
<https://doi.org/10.1021/acs.biomac.2c01500>

- IV. Stengel, D., **Saric, M.**, Johnson, H. R., Schiller, T., Diehl, J., Chalek, K., Onofrei, D., Scheibel, T., & Holland, G. P. (2023). Tyrosine's Unique Role in the Hierarchical Assembly of Recombinant Spider Silk Proteins: From Spinning Dope to Fibers. *Biomacromolecules*, 24(3), 1463-1474.
<https://doi.org/10.1021/acs.biomac.2c01467>

6 INDIVIDUAL CONTRIBUTION TO PUBLICATIONS

Publication I

Saric, M., & Scheibel, T. (2019). Engineering of silk proteins for materials applications. *Current opinion in biotechnology*, 60, 213-220.

The concept of this review article was prepared by Thomas Scheibel and myself. I wrote the manuscript including text and figures, Thomas Scheibel contributed to the scientific discussions and the completion of the manuscript.

Publication II

Saric, M., Eisoldt, L., Döring, V., & Scheibel, T. (2021). Interplay of Different Major Ampullate Spidroins during Assembly and Implications for Fiber Mechanics. *Advanced Materials*, 33(9), 2006499.

The conceptualization and experimental design were done by L. Eisoldt, T. Scheibel, and me. Cloning work, protein production, and establishment of purification of the protein variants only containing carboxyl-terminal domains were done by L. Eisoldt, V. Döring, and me. Cloning, protein production and purification of the full-length protein variants were done by me. Structural characterization and assembly experiments were done by L. Eisoldt, V. Döring, and me. The development of a biomimetic microfiber process using microfluidics was done by me. Spinning dope preparation, microfluidics wet-spinning, and post-stretching experiments were done by me. Characterization of the fibers using an optical microscope and tensile tests, as well as statistical analysis were done by me. The manuscript was written by T. Scheibel, L. Eisoldt and me. The figures were prepared by myself, results were scientifically discussed by all authors, and T. Scheibel supervised the project and engaged in finalizing the manuscript.

Publication III

Saric, M., & Scheibel, T. (2023). Two-In-One Spider Silk Protein with Combined Mechanical Features in All-Aqueous Spun Fibers. *Biomacromolecules*.

The conceptualization of this publication was done by T. Scheibel and me. The manuscript including experiments, text and figures was prepared by myself, T. Scheibel participated in scientific discussions and contributed to the completion of this manuscript.

Publication IV

Stengel, D., **Saric, M.**, Johnson, H. R., Schiller, T., Diehl, J., Chalek, K., Onofrei D., Scheibel, T., & Holland, G. P. (2023). Tyrosine's Unique Role in the Hierarchical Assembly of Recombinant Spider Silk Proteins: From Spinning Dope to Fibers. *Biomacromolecules*, 24(3), 1463-1474.

The conceptualization and experimental design were done by D. Stengel, D. Onofrei, G. P. Holland, T. Scheibel, and me. Protein production, isotope labeling, and purification of proteins were performed by J. Diehl, T. Schiller, and me. Spinning dope preparation and fiber production, as well as characterization of dopes using DLS and light microscopy, were done by me. Spinning dope preparation, solution NMR, as well as solid-state NMR of fibers, were done by D. Stengel, D. Onofrei, K. Chalek, and H. R. Johnson. All authors contributed to analyzing the results. D. Stengel and I were the primary authors, G. P. Holland finalized the manuscript. All authors commented and edited the final version of the manuscript.

PUBLICATIONS

Publication I

Engineering of silk proteins for materials applications

Saric, M. and Scheibel, T.

Published in *Current opinion in biotechnology*, 60, 213-220.

2019

Reprinted with kind permission from the publisher Elsevier Ltd.



Engineering of silk proteins for materials applications

Merisa Saric¹ and Thomas Scheibel^{1,2,3,4,5,6}



Silk combines biological properties, such as non-toxicity and biodegradability, with physico-chemical ones, for example, mechanical strength. Based on molecular engineering, nowadays also new non-silk functions can be implemented in silk materials. Driven by rational design and ingenuity, innovative recombinant silk proteins can be designed with a plethora of functions to address biomedical and technological challenges. Herein, we review advances in engineering silk proteins for tailored functions at the molecular level. Insights are provided in genetically engineered silk fusions with functional or other structural proteins and in hybrids with DNA. In such novel materials, self-assembly features of silk are combined and utilized with expedient properties of the additional components. The availability of functionalized silk materials is opening routes toward a whole set of novel applications not achievable with natural silk or other polymers.

Addresses

¹ Lehrstuhl Biomaterialien, Universität Bayreuth, Universitätsstraße 30, D-95440 Bayreuth, Germany

² Forschungszentrum für Bio-Makromoleküle (BIOmac), Universität Bayreuth, Universitätsstraße 30, D-95440 Bayreuth, Germany

³ Bayreuther Zentrum für Kolloide und Grenzflächen (BZKG), Universität Bayreuth, Universitätsstraße 30, D-95440 Bayreuth, Germany

⁴ Bayreuther Materialzentrum (BayMat), Universität Bayreuth, Universitätsstraße 30, D-95440 Bayreuth, Germany

⁵ Bayreuther Zentrum für Molekulare Biowissenschaften (BZMB), Universität Bayreuth, Universitätsstraße 30, D-95440 Bayreuth, Germany

⁶ Bayerisches Polymerinstitut (BPI), Universität Bayreuth, Universitätsstraße 30, D-95440 Bayreuth, Germany

Corresponding author:

*Scheibel, Thomas (thomas.scheibel@bm.uni-bayreuth.de)

Current Opinion in Biotechnology 2019, 60:213–220

This review comes from a themed issue on **Chemical biotechnology**

Edited by **Thomas Ward** and **Sven Panke**

<https://doi.org/10.1016/j.copbio.2019.05.005>

0958-1669/© 2019 Elsevier Ltd. All rights reserved.

Introduction

Silk is defined as a class of fibrous proteins, which is extracorporally applied by animals of the phylum of arthropods, including the classes of Insecta, Arachnida, and Myriapoda [1,2]. Among them, silkworms and spiders are the most prominent silk producers. Since

millions of years, silk fibers have evolved diversely to be used as protective shelter, dispersal, prey capture, cocoons and for reproduction [1]. Also, humans have utilized silk since thousands of years for several applications highlighting its importance in culture, economy, and science [3]. The cocoon silk of the domesticated silk moth *Bombyx mori* (mulberry silk) is most commonly used for textile applications [2,3], while silks from spiders have been often applied for medical purposes such as wound dressings and sutures [4]. These examples already show a broad usability for many applications, since silks often reveal excellent mechanical properties such as high strength and extensibility resulting in a great toughness (Figure 1) in combination with good biocompatibility, biodegradability, non-toxicity, and low immunogenicity when brought in contact with the human body [5–7]. So far, no other natural or synthetic fibrous material can accomplish these remarkable mechanical characteristics, which are based on the hierarchical setup of silk proteins and the strict control of structural arrangements during fiber assembly [8]. Despite the diversity of silks and their sequences from different organisms, common structural patterns can be seen. Generally, the proteinaceous silk core is composed of fibrils, which are oriented along the fiber axis and contain nanometer-sized crystallites embedded in an amorphous matrix [3]. These crystals comprise tightly stacked anti-parallel β -sheet stretches, which contribute to the silk's tensile strength and high toughness [8]. Additionally, β -spirals, β -turns, random coils, and helices form an amorphous region and provide flexibility and elasticity to the fiber [1,8]. Besides the relative ratio and distribution of crystalline and amorphous parts, the nanoconfinement of β -sheet crystals is a key factor in obtaining good mechanical properties [9]. It was detected that nanometer-sized crystals reveal higher toughness than larger β -sheet crystals [9]. At molecular level, structural motifs are given by the protein's sequence, showing a highly repetitive core domain flanked by highly conserved non-repetitive terminal domains. The core domain contains alternating crystalline domains and amorphous regions and is responsible for the mechanical properties of the final fiber [10], while the non-repetitive termini are essential for storage of silk proteins at high concentrations and are playing an important role for fiber assembly by acting as molecular switches sensing pH-changes, mechano-changes, and changes in ionic strength and composition [11].

Utilization of natural animal-based materials such as silk in applications often entails several drawbacks, for example, impurities, batch-to-batch fluctuations in quality and quantity, or difficulties in domesticating the animals (e.g.

Figure 1

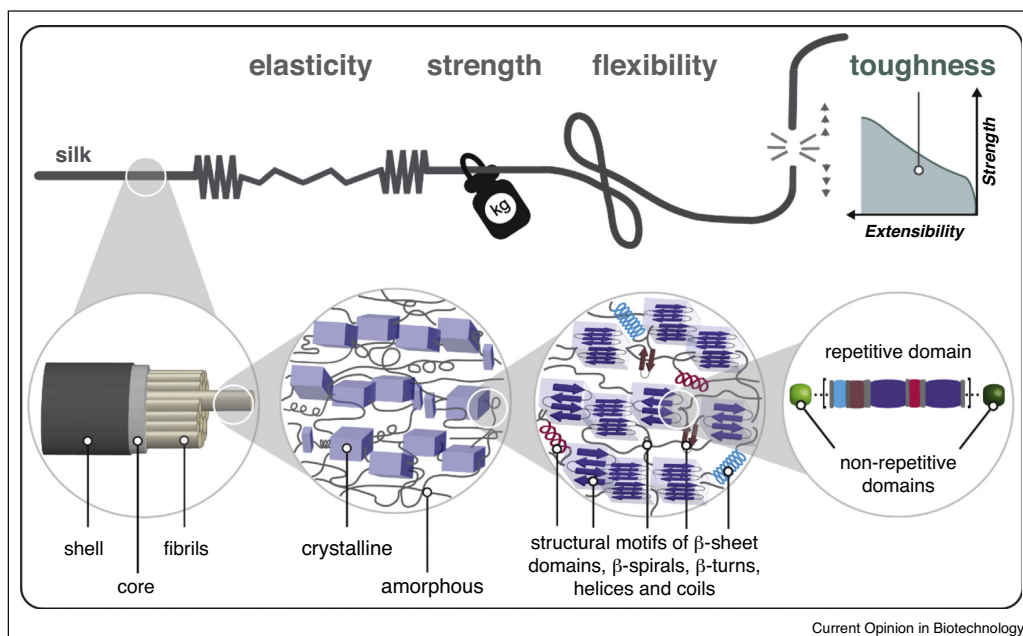


Illustration of the hierarchical spider silk structure and its mechanical properties yielding an outstanding toughness. One spider silk thread is composed of numerous fibrils containing nanometer-sized crystallites embedded in an amorphous matrix. These nanocrystals comprise highly ordered and tightly packed β -sheets, whereas the amorphous matrix exhibits secondary structures such as β -spirals, β -turns, random coils, and helices. The structural motifs are defined by the silk sequences. Distribution, order and relative ratio of amino acid sequence elements significantly influence the mechanical properties, such as elasticity and flexibility (amorphous matrix) or strength (crystallites). Stress strain analysis provides information about the toughness, which is seen by the area underneath a stress-strain curve.

in case of spiders) [8,12**]. In recent years, several biotechnological production routes have been developed to establish an alternative source of silk on an industrial scale, ensuring constant quality and biological safety [8,12**]. Genetic engineering of silk proteins allows to design a multitude of future-oriented ecological materials with tunable features for defined applications and best possible performance [13–15]. Knowledge concerning the sequence-structure-function relationship of the proteins is essential for the engineering process in order to avoid a negative impact on the physical properties [14,16*]. Great progress has been made concerning the modification of proteins by changing the amino acid composition or utilizing the ability to generate fusion constructs with other materials (mainly peptides and proteins) with synergistic properties [14]. Such functionalization of the underlying silk proteins enables the development of customized functional materials.

Living in an increasingly resource-constrained world, the development of bio-based materials with low environmental footprint is indispensable. Bioinspired silk materials can replace traditional synthetic polymers, especially when they are functionalized for explicit applications, and

consequently contribute to green fabrication and to circular economy in terms of sustainability and performance [17]. Innovative solutions have been developed by interdisciplinary research teams to recombinantly produce functionalized silk proteins at large scale and in high quality. Thereby, several commercial applications have emerged over time in several market segments, such as cosmetics, regenerative medicine, or textile fabrication (Table 1).

Here, we review recent advances in engineering of recombinant silk proteins at the molecular level to achieve novel functions. Accordingly, we pay special attention to genetic modifications to establish new characteristics of the silk proteins. Moreover, we highlight current limitations and present approaches to overcome some of these challenges in the near future.

Functionalization of silk proteins using molecular engineering

Functionalized recombinant silk proteins are currently investigated concerning their application as green biopolymers by researchers within different disciplines. Molecular engineering techniques are applied to design

Table 1

Selection of industrially applied spider silk constructs					
Company/country	Origin	Proteins ^a	Expression host	Product/brand	Application
AMSilk/Germany	Spider <i>Araneus diadematus</i>	ADF-3, ADF-4	<i>E. coli</i>	BIOSTEEL [®]	Running shoes, airplane wings, watchbands
				Silkgel, silkbeads BioShield-S1 Microsilk [™]	Cosmetics Medical implants Ties, caps, knives
Bolt Threads/USA	Spider <i>Argiope bruennichi</i>	MaSp2	Yeast		
Kraig Biocraft Laboratories/USA	Silkworm <i>Bombyx mori</i> ;	MaSp, MiSp, Flag, fhc	Silkworm	Dragon Silk [™] Monster Silk [®]	Potential body armor
	Spiders <i>Nephila clavipes</i> , <i>Lactrodectus geometricus</i> , <i>Argiope trifasciata</i>				
Spiber/Japan	Different spider species (company's secret)	MaSp, Flag	Microorganisms	QMONOS [™]	Outdoor jacket

^a No details on recombinant proteins and their individual modifications available.

bio-based silk proteins with tunable features (Table 2). While the present review covers molecular engineering of recombinant silk proteins, silk materials also can be functionalized at the macroscopic level resulting in composite materials. Briefly, this can be accomplished by mixing the silk solution with other biopolymers (gelatin, collagen etc.) to impart adjustable mechanical features or by doping with functional components for example, magnetic nanoparticles. Recent innovations in these multilevel modifications are reviewed in detail elsewhere [18].

Silk proteins can be modified via manipulation of the amino acid sequence by adding functional sequence tags or even entire proteins [14]. Figure 2 outlines some functionalization strategies. Replacing individual amino acids within the core sequence of a silk protein (Figure 2a) using site-directed mutagenesis [19] has already been shown to influence the properties of materials made thereof. For example, aside from changes in hydrophobicity [20], structural changes can be induced [21].

Modification with functional peptides in selected locations at the silk sequence further empower new protein properties. The peptide sequences can be either fused by molecular means at the silk's termini or incorporated within its core sequence (Figure 2b) [16*]. First-mentioned approach is the most common one, since it is less affecting the general protein properties that is, the physicochemical ones, and it is easier to implement. At molecular level, vectors comprising the silk gene can be modified with gene cassettes encoding functional motifs by consecutive digestion and ligations steps. Modifications with functional peptides can be further tuned by integrating a cleavable peptide linker sequence, offering many advantages as, for example, releasing the functional domains *in vivo* [22*].

Silk proteins can also be hybridized with other (bio) polymers to provide new properties and new functional complexity. Numerous silk-based chimeric proteins have been analyzed to involve one or more additional functional components together with silk, whereby other proteins or even dissimilar polymers can be fused to the silk motifs. Several known strategies for the rational design of silk-based hybrid materials have evolved using recombinant DNA technology, such as concatemerization and recursive ligation providing the production of a variety of genes with different sizes [23*,24]. Combinatorial approaches using PCR or RCA-based amplification strategies such as OEPCR (Overlap Extension Polymerase Chain Reaction) or OERCA (Overlap Extension Rolling Circle Amplification) are less time-consuming strategies, focusing on designing DNA-libraries with various features [24].

Fusion of functional molecules with recombinant silk proteins can also be achieved by chemical conjugation utilizing highly efficient site-specific click chemistry [25,26]. In versatile approaches, chemical agents react with accessible amine or thiol reactive groups of amino acid residues such as lysine or cysteine. Such modifications of silk proteins enable for example, the linkage with DNA via azide groups (Figure 2c) to achieve controllable microarchitectures [27], functionalization with glycopolymers [28], or conjugation with different organic ligands conferring either antibiotic or fluorescent properties with silk [29]. Chimeric silk proteins can also be produced with intein *trans*-splicing allowing directional ligation of the repetitive silk modules [30].

One possibility for creating artificial proteins mimicking the properties of natural silk ones is the design of protein-based amphiphilic block co-polymers (ABCs), based on hydrophobic sequences forming β -sheet crystalline regions

Table 2

Functionalization of silk proteins by molecular engineering

Origin/recombinant silk protein	Functionalization	Gained function/proposed application	Reference
<i>E. australis</i> /MaSp1 4RepCT	RGD motifs 1: CTGRGDSPAC 2: STGRGDSPAS	Cell adhesion/tissue engineering	[21]
	Antimicrobial motif GIGKFLHSAGKFGKAFVGEIMKS	Antimicrobial activity/implant coating	[51]
	Xylanase (XynA) enzyme from <i>B. subtilis</i>	Polysaccharide degradation/diagnostics, biosensor	[56]
	Mucin binding domains 1: Six lysine residues 2: Human galectin-3 carbohydrate	1: Nonspecific mucin adhesion 2: Specific mucin binding/mucosal wound dressing	[50]
<i>N. clavipes</i> /MaSp1/MaSp2	i.e. R5 domain (SSKKSGSYSGSKGSKRRIL)	Silica binding/bone regeneration, osteogenesis	[35,36,55]
	Hydroxyapatite binding domain (VTKHLNQLSQSY)	Biomaterialization/bone regeneration	[47]
	Block co-polymers: HBA ₆ , HBA ₃ , HBA ₂ , HBA, HAB ₂ , and HAB ₃ ; A-block: hydrophobic poly-alanine rich B-block: hydrophilic glycine rich H: histidine-tag	Amphiphilic block co polymers/design of smart materials, drug delivery	[31]
	NCAM binding domain (GRGGLAAAGRGLAAAGRGLGY)	Cell adhesion/nerve regeneration	[46]
	Poly-lysine domain	Therapeutic nucleic acid carrier/cancer treatment	[52]
	Her2 binding peptides 1: MYWGDHSHWLQYWY 2: LTVSPWY	Drug delivery/cancer targeting	[53]
	Single aa substitution (Glu to Lys)	Cell adhesion/enhanced cellular uptake/ cardiac tissue engineering	[20,43,48]
<i>A. diadematus</i> /MaSp2 ADF4	5' – 5' DNA (antiparallel) 5' – 3' DNA (parallel) TWJ (three-way junction)	Controlled formation of superstructures/ technological applications	[27]
	Antigenic peptide from ovalbumin	Cytotoxic T-cell priming/delivery of protein-based vaccination	[22*]
	CPP motifs R ₆ G (RRRRRRRRG) Tat (RKKRRQRRR) RGD (GGSGGRGDSPG)	Cell adhesion/enhanced cellular uptake	[43,44]
	1: 4 silk units, 7 elastin units 2: 4 silk units, 15 elastin units	Simulate hepatic vascular system/cancer-therapeutic treatment	[34]
<i>B. mori</i> silk fibroin and mammalian elastin/ 1: SELP-47K 2: SELP-815K			
<i>B. mori</i> /(L)-chain or (H)-chain of silk fibroin	Laminin B1 chain: TS(CDPGYIGSRAS) ₈ Fibronectin: (TGRGDSPAS) ₈	Cell adhesion/vascularization, vascular grafts	[45]

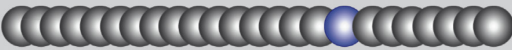


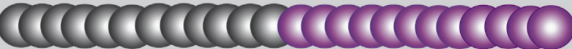
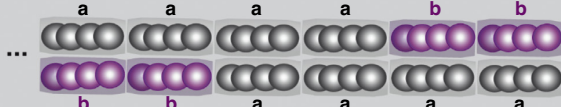






ADF, *Araneus diadematus* Fibroin; CPP, Cell Penetrating Peptide; MaSp, Major Ampullate Spidroin; NCAM, neural cell adhesion molecule; SELP, silk-elastin-like polymer with silk-like units (GAGAGS)_x and elastin-like units (GVGVP)_y; R5 domain derived from a silaffin protein; Tat protein: *trans*-activator of transcription protein.

and hydrophilic sequences forming disordered non-crystalline regions [31]. By changing the hydrophobic/hydrophilic ratio of different silk-like block co-polymers, thermo-physical properties of the polymers can be altered [31]. Inspired by the silk architecture, protein-based or protein-like amphiphilic block co-polymers open up myriads of possibilities of applications originating from the natural mechanism of silk self-assembly and crystallization to gain silk-based properties [31,32].

Silk-elastin-like polymers (SELPs), for example, are composed of tandemly repeated crystalline silk blocks and

elastomeric elastin domains [33**]. By strategic placement of charged amino acids or variation of silk and elastin-like blocks in each repeated unit, their properties can be precisely controlled in genetically engineered SELP co-polymers [34]. In one example of organic-inorganic hybrid materials, silk-silica binding peptide chimeras biologically mediate mineralization by sequence control [35,36]. For instance, silica-promoting peptide domains derived from silaffin can be genetically fused with the silk protein sequence, and the biosilicification process is induced and regulated by addition of silica precursors, which lead to silica deposition [37].

Figure 2

Molecular engineering of silk proteins		Reference
(a)	Single amino acid substitutions 	[48]
(b)	Functional peptides <i>Fusion</i> 	[22 [*]]
	<i>Incorporation</i> 	[21]
(c)	Silk chimera <i>Silk and protein polymers</i> 	[34]
	<i>Block co-polymers (e.g. a₄b₂ / b₂a₄)</i> 	[31]
	<i>Silk and dissimilar polymers (e.g. DNA)</i> 	[27]
Legend aa residues of basic silk protein ...  ... aa residues of any other protein ...  ... nucleic acids  protein tag  substituted aa residue 		
Current Opinion in Biotechnology		

Molecular engineering of recombinant silk proteins.

Selected strategies display (a) single amino acid (aa) substitutions, (b) fusion or modification with functional peptides, (c) silk chimeras comprising multiple components of proteins or dissimilar polymers. Spheres illustrate amino acid residues, and coloration highlights the engineered area in the respective silk constructs.

Current limitations in recombinant production of engineered silk proteins

So far, great progress has been made in the development of engineering approaches for silk proteins, but several limitations still exist concerning their production. The extent of modifications such as the incorporation of functional tags in a silk protein domain is limited. Structural properties of silk regarding self-assembly into higher ordered structures need to be maintained to guarantee the functional properties within the final material [16^{*}].

Computational simulations would provide knowledge on the correlation between structure and function and would allow to optimize new potentials of materials based on recombinant silk proteins [38,39^{**}]. However, these tools are still at their infancy, and further research is necessary in order to expand the impact of computational tools on silk material development.

Many challenges in engineered silk production are linked to the expression hosts. *Escherichia coli* is the most often

used host organism due to the possibility of simple genetic modification, short doubling times, and fast adjustments if necessary [8]. Although progress toward decent yields and qualities during recombinant protein production has been made, several steps of biotechnological production require improvement. In the upstream process, slight modifications can strongly influence the highly complex molecular silk interactions [38]. Moreover, expression of highly repetitive genes and production of proteins with a molecular weight comparable to that of natural silk proteins entail additional difficulties in *E. coli*. Gene instability, truncations, inefficient transcription, discontinuous translation, and low expression levels are substantial restrictions caused by the bacterial ribosomal machinery and must be overcome [33**]. Engineering the metabolic pathways of the expression host provides an opportunity to produce native-sized silk proteins [40] and further increases protein yields as well as quality [33**]. Recently, high molecular weight silk proteins were achieved by split intein-mediated ligation, which can be obtained using hosts like *E. coli* [30,41**] or plants [42].

Applications of functionalized recombinant silk proteins

Functionalization of silk proteins enables the development of a multitude of materials with unprecedented versatilities for example for medical applications including diagnostics, biosensing, or regeneration of soft and hard tissues (Table 2). New functionalized materials combining physical silk properties and biologically active peptides comprising for example, specific cell binding motifs achieved proper cell attachment and proliferation suitable for tissue engineering [12**]. Incorporation of a cell binding motif, for example, the tri-peptide RGD (Arg-Gly-Asp), into silk demonstrated increased cell attachment, cellular uptake, spreading, stress fiber formation and focal adhesion [21,43,44]. Since the outer surface of most mammalian cells is negatively charged, polycationic materials surfaces are preferred [43]. In case of recombinant spider silk proteins based on the MaSp2 derivative ADF4 of the European garden cross spider the substitution of all glutamic acid residues with lysine ones in the silk sequence changed the polyanionic character into a polycationic one, which significantly increased cell attachment [20,44], but also the implementation of peptide tags showed this improvement (Table 2) [43,44].

Further approaches were realized regarding vascularization and development of vascular graft materials using fibronectin-based or laminin-based peptide sequences [45], and neural tissue engineering toward nerve regeneration utilizing a NCAM (neural cell adhesion molecule) binding domain [46] (Table 2). Steady advances have also been made in bone regeneration using hydroxyapatite binding domains coupled to silk to induce biomineralization and to control osteogenesis [47]. Among the development of putative cardiovascular repair materials, cell adhesive silk

materials support proliferation of cardiomyocytes and their proper cell-to-cell interactions [48].

The morphological diversity of silk provides a powerful tool to meet the requirements of various applications [49]. The use of silk coatings has been reported to be suitable for mucosal wound dressings utilizing mucin binding domains for specific and non-specific interactions [50]. Aside from the promotion of cell adhesion, sequences can be fused to silk proteins introducing antimicrobial properties to suppress bacterial growth on silk-coated medical implants [51]. Such functionalization reduces local infections after implantation.

In a different type of application, the increasing demand for drug delivery systems is pushing the development of innovative silk particles or spheres, acting as functionalized drug carriers (Table 2). The cellular uptake efficiency of such carriers can be significantly enhanced as well as the specificity of therapeutics for a target tissue, when specific targeting tags are implemented [12**]. In general, drugs are encapsulated in carriers in order to protect the therapeutic from degradation, to prevent the organism from undesirable interactions and to reduce toxicity. For instance, fusion of silk proteins with a nucleic acid binding domain triggers the encapsulation of RNA-based therapeutics and leads to immune cell internalization [52]. Silk particles made of a spider silk protein fusion with an antigenic peptide from ovalbumin successfully activated cytotoxic T-cells and initiated an immune response demonstrating the potential of a new protein-based vaccination strategy [22*]. In this context, significant efforts have been made not only in protein-based vaccination [22*], but also in highly promising cancer treatments by improving immunotherapeutic effects *in vivo* [52,53]. In the course of potential chemoembolization agents, SELP (silk-elastin-like polymer) constructs with varying lengths of silk-like units (GAGAGS)_x and elastin-like blocks (GVGVP)_x, were analyzed *in vitro* in microfluidic channels to simulate the hepatic vascular system [34]. Afterwards, *in vivo* tests were performed, where the SELPs gelled at the site of interest, resulting in significant tumor shrinkage [34]. This approach has taken advantage of SELPs to be part of stimulus or multi-stimuli responsive systems, which can be controlled by a broad variety of environmental triggers including temperature, pH, ionic strength, enzymatic stimuli, and electric fields [54*].

Silk-based biomaterials for bone-repair use silk-silica chimeras to biologically mediate mineralization [35]. Silica-binding peptides (SiBPs), such as the R5 domain as a silica promoting silaffin protein component (Table 2), can play an important role in bone-regeneration applications, and it was shown that they enable the deposition of biosilica on silk hybrids [55]. A further promising application is in the field of disease diagnostics and

biosensing. Herein, silk can be used for immobilization of enzymes on solid supports [56] or for site-specific capture of target molecules such as antibodies in functional coatings [57].

Outlook

Great progress has been made in the development of engineered silk materials for a variety of applications. Understanding structure-function relations of silk proteins using computational simulations will very likely guide engineering of artificial silk in the future. Utilizing technologies such as intein splicing can overcome protein size limitations within biotechnological production, and further enable the fabrication of new recombinant silk proteins with additional properties, even in combination with non-silk polymers. Especially combined approaches regarding functionalization at the molecular level, but also modification of silk materials at the macroscopic level open up new routes toward the ecological green fabrication of high-performance polymers for a myriad of technical and medical applications.

Conflict of interest statement

T.S. is co-founder of the company AMSilk GmbH.

Acknowledgement

Financial support is provided by the Collaborative Research Center TRR 225 TP C01.

References and recommended reading

Papers of particular interest, published within the period of review, have been highlighted as:

- of special interest
- of outstanding interest

1. Craig CL: **Evolution of arthropod silks**. *Annu Rev Entomol* 1997, **42**:231-267.
2. Sutherland TD, Young JH, Weisman S, Hayashi CY, Merritt DJ: **Insect silk: one name, many materials**. *Annu Rev Entomol* 2010, **55**:171-188.
3. Scheibel T, Zahn H, Krasowski A: **Silk**. *Ullmann's Encyclopedia of Industrial Chemistry*. 6th ed.. 2016:1-15.
4. Newman J, Newman C: **Oh what a tangled web: the medicinal uses of spider silk**. *Int J Dermatol* 1995, **34**:290-292.
5. Vollrath F: **Strength and structure of spiders' silks**. *Rev Mol Biotechnol* 2000, **74**:67-83.
6. Zeplin PH, Maksimovikj NC, Jordan MC, Nickel J, Lang G, Leimer AH, Römer L, Scheibel T: **Spider silk coatings as a bioshield to reduce periprosthetic fibrous capsule formation**. *Adv Funct Mater* 2014, **24**:2658-2666.
7. Müller-Herrmann S, Scheibel T: **Enzymatic degradation of films, particles, and nonwoven meshes made of a recombinant spider silk protein**. *ACS Biomater Sci Eng* 2015, **1**:247-259.
8. Heidebrecht A, Scheibel T: **Recombinant production of spider silk proteins**. *Adv Appl Microbiol* 2013, **82**:115-153.
9. Keten S, Xu Z, Ihle B, Buehler MJ: **Nanoconfinement controls stiffness, strength and mechanical toughness of β -sheet crystals in silk**. *Nat Mater* 2010, **9**:359.
10. Muiznieks LD, Keeley FW: **Biomechanical design of elastic protein biomaterials: a balance of protein structure and conformational disorder**. *ACS Biomater Sci Eng* 2016, **3**:661-679.
11. Bauer J, Scheibel T: **Conformational stability and interplay of helical N- and C-terminal domains with implications on major ampullate spidroin assembly**. *Biomacromolecules* 2017, **18**:835-845.
12. Aigner TB, DeSimone E, Scheibel T: **Biomedical applications of recombinant silk-based materials**. *Adv Mater* 2018, **30**:1704636. The review gives a critical overview of various utilized recombinant silk proteins for applications in biomedical engineering, focusing on the most beneficial characteristics and advantages of artificial silk compared to other biomaterials.
13. Jiang J, Zhang S, Qian Z, Qin N, Song W, Sun L, Zhou Z, Shi Z, Chen L, Li X: **Protein bricks: 2D and 3D bio-nanostructures with shape and function on demand**. *Adv Mater* 2018, **30**:1705919.
14. Deptuch T, Dams-Kozłowska H: **Silk materials functionalized via genetic engineering for biomedical applications**. *Materials* 2017, **10**:1417.
15. Ling S, Chen W, Fan Y, Ke Z, Jin K, Haipeng Y, Buehler MJ, Kaplan DL: **Biopolymer nanofibrils: structure, modeling, preparation, and applications**. *Prog Polym Sci* 2018, **85**:1-56.
16. Sutherland TD, Huson MG, Rapson TD: **Rational design of new materials using recombinant structural proteins: current state and future challenges**. *J Struct Biol* 2018, **201**:76-83. The authors analyze advantages and limitations of recombinant structural proteins as sequence-defined polymers for templates in rational design approaches of new materials.
17. Tao H, Kaplan DL, Omenetto FG: **Silk materials—a road to sustainable high technology**. *Adv Mater* 2012, **24**:2824-2837.
18. Zhou Z, Zhang S, Cao Y, Marelli B, Xia X, Tao TH: **Engineering the future of silk materials through advanced manufacturing**. *Adv Mater* 2018, **30**:1706983.
19. Bauer J, Scheibel T: **Dimerization of the conserved N-terminal domain of a spider silk protein controls the self-assembly of the repetitive core domain**. *Biomacromolecules* 2017, **18**:2521-2528.
20. Doblhofer E, Scheibel T: **Engineering of recombinant spider silk proteins allows defined uptake and release of substances**. *J Pharm Sci* 2015, **104**:988-994.
21. Widhe M, Shalaly ND, Hedhammar M: **A fibronectin mimetic motif improves integrin mediated cell binding to recombinant spider silk matrices**. *Biomaterials* 2016, **74**:256-266.
22. Lucke M, Mottas I, Herbst T, Hotz C, Römer L, Schierling M, Herold HM, Slotta U, Spinetti T, Scheibel T: **Engineered hybrid spider silk particles as delivery system for peptide vaccines**. *Biomaterials* 2018, **172**:105-115. This work demonstrates a novel vaccine strategy using a protein-based vaccination system, utilizing engineered silk particles as carrier of incorporated peptide antigens, highlighting the powerful tool of functionalization.
23. Yigit S, Dinjaski N, Kaplan DL: **Fibrous proteins: at the crossroads of genetic engineering and biotechnological applications**. *Biotechnol Bioeng* 2016, **113**:913-929. The authors outline roadmaps of recent cloning strategies of different fibrous proteins to overcome challenges in biotechnological production for a broad range of applications.
24. Huber MC, Schreiber A, Wild W, Benz K, Schiller SM: **Introducing a combinatorial DNA-toolbox platform constituting defined protein-based biohybrid-materials**. *Biomaterials* 2014, **35**:8767-8779.
25. Kundu B, Kurland NE, Bano S, Patra C, Engel FB, Yadavalli VK, Kundu SC: **Silk proteins for biomedical applications: bioengineering perspectives**. *Progr Polym Sci* 2014, **39**:251-267.
26. Thirumurugan P, Matosiuk D, Jozwiak K: **Click chemistry for drug development and diverse chemical-biology applications**. *Chem Rev* 2013, **113**:4905-4979.
27. Humenik M, Drechsler M, Scheibel T: **Controlled hierarchical assembly of spider silk-DNA chimeras into ribbons and raft-like morphologies**. *Nano Lett* 2014, **14**:3999-4004.

220 Chemical biotechnology

28. Hardy JG, Pfaff A, Leal-Egaña A, Müller AH, Scheibel TR: **Glycopolymer functionalization of engineered spider silk protein-based materials for improved cell adhesion.** *Macromol Biosci* 2014, **14**:936-942.
29. Harvey D, Bardelang P, Goodacre SL, Cockayne A, Thomas NR: **Antibiotic spider silk: site-specific functionalization of recombinant spider silk using "click" chemistry.** *Adv Mater* 2017, **29**:1604245.
30. Lin S, Chen G, Liu X, Meng Q: **Chimeric spider silk proteins mediated by intein result in artificial hybrid silks.** *Biopolymers* 2016, **105**:385-392.
31. Huang W, Krishnaji S, Tokareva OR, Kaplan D, Cebe P: **Tunable crystallization, degradation, and self-assembly of recombinant protein block copolymers.** *Polymer* 2017, **117**:107-116.
32. Liu B, Wang T, Xiao L, Zhang G, Li G, Luo J, Liu X: **A directed self-assembly quasi-spider silk protein expressed in *Pichia pastoris*.** *Biotechnol Bioengin Equip* 2018, **32**:451-461.
33. Dinjaski N, Kaplan DL: **Recombinant protein blends: silk beyond natural design.** *Curr Opin Biotechnol* 2016, **39**:1-7.
- The authors review on the manipulation of several natural biopolymers in hybrids, recombinant protein blends or 'recombinamers' utilizing bioengineering.
34. Poursaid A, Price R, Tiede A, Olson E, Huo E, McGill L, Ghandehari H, Cappello J: **In situ gelling silk-elastinlike protein polymer for transarterial chemoembolization.** *Biomaterials* 2015, **57**:142-152.
35. Martín-Moldes Z, Ebrahimi D, Plowright R, Dinjaski N, Perry CC, Buehler MJ, Kaplan DL: **Intracellular pathways involved in bone regeneration triggered by recombinant silk-silica chimeras.** *Adv Funct Mater* 2018, **28**:1702570.
36. Plowright R, Dinjaski N, Zhou S, Belton DJ, Kaplan DL, Perry CC: **Influence of silk-silica fusion protein design on silica condensation in vitro and cellular calcification.** *RSC Adv* 2016, **6**:21776-21788.
37. Foo CWP, Patwardhan SV, Belton DJ, Kitchel B, Anastasiades D, Huang J, Naik RR, Perry CC, Kaplan DL: **Novel nanocomposites from spider silk-silica fusion (chimeric) proteins.** *Proc Natl Acad Sci U S A* 2006, **103**:9428-9433.
38. Jang Y, Champion JA: **Self-assembled materials made from functional recombinant proteins.** *Acc Chem Res* 2016, **49**:2188-2198.
39. Yarger JL, Cherry BR, Van Der Vaart A: **Uncovering the structure-function relationship in spider silk.** *Nat Rev Mater* 2018, **3**:18008.
- Here the authors highlight experimental and computational studies, which give insights into structure-function relationships that can guide engineering of recombinant silk proteins for superior material production.
40. Xia XX, Qian Z-G, Ki CS, Park YH, Kaplan DL, Lee SY: **Native-sized recombinant spider silk protein produced in metabolically engineered *Escherichia coli* results in a strong fiber.** *Proc Natl Acad Sci U S A* 2010, **107**:14059-14063.
41. Bowen CH, Dai B, Sargent CJ, Bai W, Ladiwala P, Feng H, Huang W, Kaplan DL, Galazka JM, Zhang F: **Recombinant spidroins fully replicate primary mechanical properties of natural spider silk.** *Biomacromolecules* 2018, **19**:3853-3860.
- This paper presents a combinatorial approach of synthetic and chemical biology tools to tackle long-standing problems in recombinant production of repetitive silk proteins comprising high molecular weights.
42. Weichert N, Hauptmann V, Helmold C, Conrad U: **Seed-specific expression of spider silk protein multimers causes long-term stability.** *Front Plant Sci* 2016, **7**:6.
43. Elsner MB, Herold HM, Müller-Herrmann S, Bargel H, Scheibel T: **Enhanced cellular uptake of engineered spider silk particles.** *Biomater Sci* 2015, **3**:543-551.
44. Schierling MB, Doblhofer E, Scheibel T: **Cellular uptake of drug loaded spider silk particles.** *Biomater Sci* 2016, **4**:1515-1523.
45. Asakura T, Isozaki M, Saotome T, Tatematsu K-i, Sezutsu H, Kuwabara N, Nakazawa Y: **Recombinant silk fibroin incorporated cell-adhesive sequences produced by transgenic silkworm as a possible candidate for use in vascular graft.** *J Mater Chem B* 2014, **2**:7375-7383.
46. An B, Tang-Schomer MD, Huang W, He J, Jones JA, Lewis RV, Kaplan DL: **Physical and biological regulation of neuron regenerative growth and network formation on recombinant dragline silks.** *Biomaterials* 2015, **48**:137-146.
47. Dinjaski N, Plowright R, Zhou S, Belton DJ, Perry CC, Kaplan DL: **Osteoinductive recombinant silk fusion proteins for bone regeneration.** *Acta Biomater* 2017, **49**:127-139.
48. Petzold J, Aigner TB, Touska F, Zimmermann K, Scheibel T, Engel FB: **Surface features of recombinant spider silk protein eADF4 (κ 16)-made materials are well-suited for cardiac tissue engineering.** *Adv Funct Mater* 2017, **27**:1701427.
49. Borkner CB, Elsner MB, Scheibel T: **Coatings and films made of silk proteins.** *ACS Appl Mater Interfaces* 2014, **6**:15611-15625.
50. Petrou G, Jansson R, Höggqvist M, Erlandsson J, Wågberg L, Hedhammar M, Cruzier T: **Genetically engineered mucoadhesive spider silk.** *Biomacromolecules* 2018, **19**:3268-3279.
51. Nilebäck L, Hedin J, Widhe M, Floderus LS, Krona A, Bysell H, Hedhammar M: **Self-assembly of recombinant silk as a strategy for chemical-free formation of bioactive coatings: a real-time study.** *Biomacromolecules* 2017, **18**:846-854.
52. Kozłowska AK, Florczak A, Smialek M, Dondajewska E, Mackiewicz A, Kortylewski M, Dams-Kozłowska H: **Functionalized bioengineered spider silk spheres improve nuclease resistance and activity of oligonucleotide therapeutics providing a strategy for cancer treatment.** *Acta Biomater* 2017, **59**:221-233.
53. Florczak A, Jastrzebska K, Mackiewicz A, Dams-Kozłowska H: **Blending two bioengineered spider silks to develop cancer targeting spheres.** *J Mater Chem B* 2017, **5**:3000-3011.
54. Huang W, Rollett A, Kaplan DL: **Silk-elastin-like protein biomaterials for the controlled delivery of therapeutics.** *Expert Opin Drug Deliv* 2015, **12**:779-791.
- SELP hybrid biomaterials demonstrate great potential for versatile biomedical applications, facilitated by simple genetical engineering and controllable stimuli.
55. Zhou S, Huang W, Belton DJ, Simmons LO, Perry CC, Wang X, Kaplan DL: **Control of silicification by genetically engineered fusion proteins: silk-silica binding peptides.** *Acta Biomater* 2015, **15**:173-180.
56. Jansson R, Courtin CM, Sandgren M, Hedhammar M: **Rational design of spider silk materials genetically fused with an enzyme.** *Adv Funct Mater* 2015, **25**:5343-5352.
57. Horak J, Jansson R, Dev A, Nilebäck L, Behnam K, Linnros J, Hedhammar M, Karlström AE: **Recombinant spider silk as mediator for one-step, chemical-free surface biofunctionalization.** *Adv Funct Mater* 2018, **28**:1800206.

Publication II

Interplay of Different Major Ampullate Spidroins during Assembly and Implications for Fiber Mechanics

Saric, M., Eisoldt, L., Döring, V., and Scheibel, T.

Advanced Materials, 33(9), 2006499.

2021

Reprinted with kind permission from the publisher John Wiley & Sons.

Interplay of Different Major Ampullate Spidroins during Assembly and Implications for Fiber Mechanics

Merisa Saric, Lukas Eisoldt, Volker Döring, and Thomas Scheibel*

Major ampullate (MA) spider silk has fascinating mechanical properties combining strength and elasticity. All known natural MA silks contain at least two or more different spidroins; however, it is unknown why and if there is any interplay in the spinning dope. Here, two different spidroins from *Araneus diadematus* are co-produced in *Escherichia coli* to study the possible dimerization and effects thereof on the mechanical properties of fibers. During the production of the two spidroins, a mixture of homo- and heterodimers is formed triggered by the carboxyl-terminal domains. Interestingly, homodimeric species of the individual spidroins self-assemble differently in comparison to heterodimers, and stoichiometric mixtures of homo- and heterodimers yield spidroin networks upon assembly with huge impact on fiber mechanics upon spinning. The obtained results provide the basis for man-made tuning of spinning dopes to yield high-performance fibers.


Spider silk fibers are the toughest known biopolymeric materials in nature combining strength and elasticity.^[1] Among all spider silk types, major ampullate (MA) silk, also known as dragline silk, is most intensely studied due to its accessibility through the possibility of silking spiders, which is not as easily possible for other silk types.^[2] MA silk threads comprise several proteins, known as major ampullate spidroins (MaSps), which differ among spiders concerning molecular weight, amino acid composition and functional (i.e., mechanical) impact on mechanical properties.^[3–6] Most prominent spidroins are MaSp1 and MaSp2, which mainly exhibit differences in their proline content (MaSp 1 < 0.4%, MaSp2 > 10%).^[7] In some spiders also short variants of MaSp1 (i.e., MaSp1s) and other MaSp variants such as MaSp3 and MaSp4 have been identified with unknown impact on fiber performance.^[4,8–10] Among MA silk that of *Araneus diadematus* has a surprisingly high proline content based on the unusual presence of two MaSp2 variants, named *A. diadematus* fibroin (ADF) 3 and 4,

which is a unique attribute among the known orb-weaver spiders.^[7] Both ADF proteins are secreted in the same compartment of the spinning gland.^[11] Genome analysis suggests that different MaSps are produced within the same cell as opposed to separated cells, which led to the assumption that they might already interact within the cell shortly after translation (e.g., along the secretory pathway).^[12,13]

Most MA spidroins comprise a large repetitive core domain, flanked by small non-repetitive terminal domains (TDs) (Figure 1a),^[3] and the exact composition of MaSps in spider silk fibers depends on the spider species.^[14–16] Individual repeats consist of 30–60 amino acid residues with specific amino acid motifs. The most prominent motif in MaSp is a polyalanine stretch of 5–14 residues depending on the spider species.^[17] In the final fiber, the polyalanine stretches form tightly packed β -sheet crystallites responsible for its mechanical strength.^[18–21] Other common amino acid motifs are GGX or GPGXX, which form loosely structured regions that may contribute to the flexibility of the fiber.^[18,22,23] While GGX is found predominantly in MaSp1, GPGXX stretches are mostly found in MaSp2.^[7,13] MaSp3 lacks typical poly-alanine or GPG motifs, but exhibits explicitly more polar and acidic residues in comparison to MaSp1 and MaSp2.^[4] The silk gene transcript of MaSp4, highly expressed in *Caerostris darwini* spinning glands, contains a unique GPGPQ amino acid motif and might be a quite special variant found in this explicit species.^[10]

However, spidroin sequence composition is only one factor important for fiber performance, and other factors, such as environmental, nutrition or stress levels, also play a crucial role.^[14–16] Assembly of MaSps is mainly coordinated through their TDs. In contrast to the repetitive core domains with varying sequences, the TDs of MaSps are evolutionary highly conserved.^[24,25] Amino-(NTD) and carboxyl-terminal domains (CTD) play a significant role in preventing protein aggregation within the spiders' gland as well as in vitro and control self-assembly of spidroins into highly ordered fibrils and fibers upon external triggers such as ion exchange, acidification and shear force.^[26] In general, it could be shown that TDs play a significant role in the formation of supra-molecular, micellar-like assemblies important for storage of the spidroins at high concentrations in the spinning dope, as well as in alignment of recombinant MaSps during fiber assembly.^[27–34] The conversion of the liquid spinning dope into a solid fiber is enabled within the spinning duct. Amino-terminal MaSp domains remain monomeric at neutral pH and form antiparallel dimers upon acidification.^[27,35–37] CTDs of ADF3 and ADF4 comprise five-helix bundles and form disulfide-linked permanent parallel dimers

M. Saric, Dr. L. Eisoldt, V. Döring, Prof. T. Scheibel
Lehrstuhl Biomaterialien
Universität Bayreuth
Prof-Rüdiger-Bormann-Str. 1, Bayreuth 95447, Germany
E-mail: thomas.scheibel@bm.uni-bayreuth.de

 The ORCID identification number(s) for the author(s) of this article can be found under <https://doi.org/10.1002/adma.202006499>.

© 2021 The Authors. Advanced Materials published by Wiley-VCH GmbH. This is an open access article under the terms of the Creative Commons Attribution-NonCommercial-NoDerivs License, which permits use and distribution in any medium, provided the original work is properly cited, the use is non-commercial and no modifications or adaptations are made.

DOI: 10.1002/adma.202006499

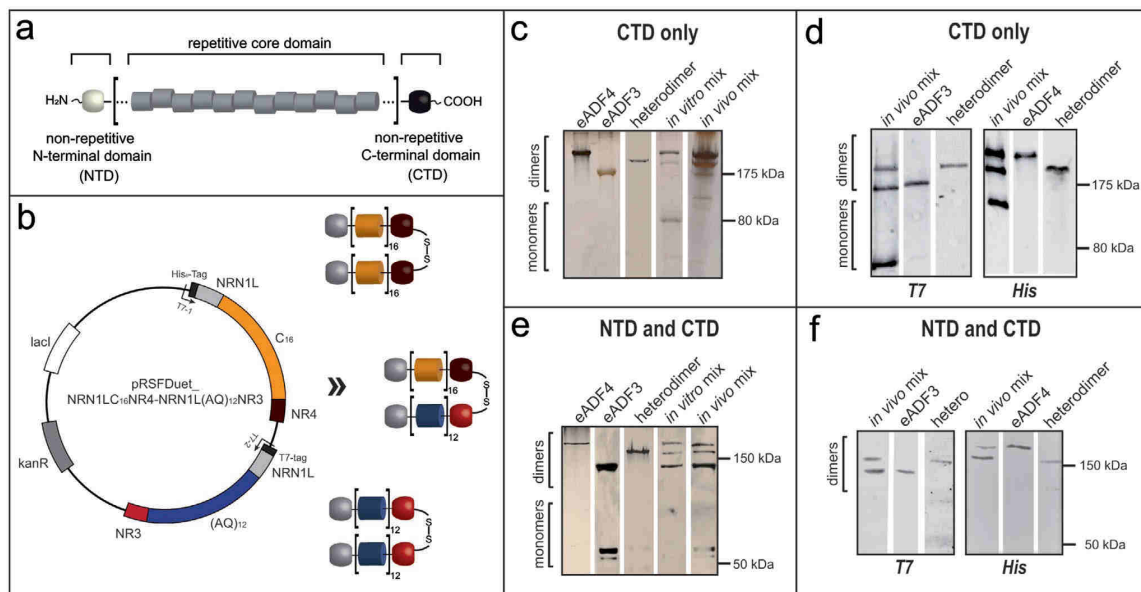


Figure 1. Scheme of used recombinant spider silk proteins and their dimerization state. a) The primary structure of spidroins comprises a highly repetitive core domain flanked by NTDs and CTDs.^[31] b) Illustration of the plasmid used for co-expression of engineered genes. An overview of all investigated recombinant proteins derived from ADF3 and ADF4 is given in Figure S2 in the Supporting Information. Details on protein purities are shown in Figures S3 and S4 and Table S1 in the Supporting Information. c–f) Analyses of dimer formation of different ADF variants produced in vitro and in vivo using silver-stained SDS-PAGE (c,e) and western blots (d,f) of purified eADF3-CTD/eADF4-CTD homo- and heterodimers (c,d) and NTD-eADF3-CTD/NTD-eADF4-CTD homo- and heterodimers (e,f). In vivo and in vitro mix samples both contained the mixture of eADF3 (T7-tagged) and eADF4 (His-tagged) variants.

(Figure S1a,b, Supporting Information).^[27] Intramolecular salt bridges, based on charged acidic residues and a single arginine, have been shown to be essential for the structural integrity of the tightly folded CTDs.^[26] Upon spinning, the CTDs are destabilized by acidification-induced protonation of the acidic side chains. In addition, salting-out and shear forces expose hydrophobic patches on the surfaces of the CTDs, which are anchor points for guiding the correct spidroin alignment along fiber formation.^[27]

ADF3 and ADF4 are both MaSp2-type proteins but they exhibit differences in hydrophobicity,^[38] which has raised the question why *A. diadematus* has two MaSp2 derivatives. Although the molecular nature of individual MaSps is well described, not much is known about the interplay of MaSps and concerning its impact on mechanical properties of spider silk fibers. In this study, we investigated how spidroins of *A. diadematus* interact through their CTDs and how this interaction contributes to self-assembly and fiber mechanics. The amino-terminal domains of *A. diadematus* spidroins have not been identified so far, but NTDs are well conserved throughout MaSps in different spider species as described in detail elsewhere.^[25,35] Therefore, the established MaSp1 NTD domain of *Latrodectus hesperus* (Figure S1c,d, Supporting Information) was used to engineer all-domains-containing recombinant proteins.^[39,40] Upon co-production in bacteria (in vivo) or refolding (in vitro), the impact of MaSp interplay was investigated on self-assembly in the spinning dope as well as on fiber mechanics upon spinning.

Although ADF3 and ADF4 are both MaSp2-like proteins based on their proline content, they differ significantly in the further sequence of their repetitive core domains yielding quite

different hydrophobicity/hydrophilicity.^[38] Based on consensus sequences, engineered variants have been designed, produced and purified, varying in the presence/absence of TDs (Figures S2–S4 and Table S1, Supporting Information). Previously, we identified that due to the redox potential of the individual cysteine residues in the CTDs, disulfide-linked dimers were formed even in the cytoplasm of *Escherichia coli*.^[27] Since both CTDs of ADF3 and ADF4 show a sequence identity of 58% and a similarity of 73%,^[38] we investigated their ability to heterodimerize when incorporated in respective engineered variants (eADF3/4). To analyze effects upon co-expression, eADF3 and eADF4 were both cloned into one plasmid under the control of two separate T7-promoters (Figure 1b). To distinguish between both proteins, eADF3 was tagged with an amino-terminal T7 sequence, whereas eADF4 was fused with a hexahistidine (His₆)-tag. eADF3 and eADF4 disulfide-linked dimers were identified upon production in *E. coli* as expected and identified using non-reducing SDS-PAGE followed by western blot analysis, which also showed the presence of heterodimers (Figure 1c–f).

Heterodimerization was also investigated in vitro. Tris(2-carboxyethyl) phosphine was added as a reducing agent to a 1:1 mixture of purified and chemically denatured (with guanidinium thiocyanate) eADF3 and eADF4, followed by refolding in Tris-buffer. Again, SDS-PAGE and western blot analysis revealed the presence of the heterodimer. Interestingly, dimerization took place in a nearly statistical distribution of 1:1:1 of the three dimeric species, two homo- and one heterodimer (Figure 1d,f).

It has been previously shown that the CTDs play an important role in solubilizing spidroins, but also in triggering fiber assembly.^[27] TDs respond individually to external stimuli and independently control the core domains' self-assembly process. At physiological pH, the conformational state of dimerized CTDs (with parallel orientation) prevents fiber formation. Upon acidification they switch their conformational state to transform from the soluble into an aligned state which is a prerequisite for fiber assembly.^[27] NTDs are monomeric at neutral pH and function as further solubility-enhancing components for the assembly-prone core domain. Upon acidification, NTDs dimerize in an anti-parallel fashion.^[35] In order to investigate the impact of C-terminal heterodimerization on self-assembly as a first step, a simplified experimental approach with non-dynamic conditions was needed, and, therefore, only eADFs comprising CTDs were analyzed to begin with. First, isolated heterodimers were compared to each respective eADF3-CTD and eADF4-CTD homodimer, exhibiting hybrid characteristics of both MaSp2 species at the molecular level. Concerning secondary structure content, far-UV-CD indicated no significant differences between the individual protein species (Figure 2a). The broad minimum at 205 nm and a plateau at 219 nm indicated a mainly random-coil/PPII dominated structure with α -helical portions. The random coil signals arise from the intrinsically unfolded repetitive core domain in solution,^[38] whereas the α -helical contributions derive from the nonrepetitive CTDs NR3 and NR4 comprising five helix-bundles.^[27,38] Thermal unfolding experiments showed a melting point of 66 °C for the heterodimer, which is 2 °C above that of the eADF3-CTD homodimer and 1.5 °C below that of the eADF4-CTD dimer (Figure 2b). Upon cooling, the heterodimer refolded to the same state as both homodimers, indicating that the process was fully reversible.^[38]

Next, self-assembly kinetics of the three dimeric species was analyzed in the presence of phosphate ions (Figure 2c). As shown previously, eADF3 and eADF4 proteins have different assembly and solubility properties, based on the sequence differences of their core domains, when exposed to naturally occurring assembly triggers like phosphate ions or elongational forces.^[38,41] eADF4 is known to be more hydrophobic, favorably interacting with other protein molecules and thus aggregating at high concentrations. In contrast, eADF3 appears to be more hydrophilic, as it bonds water molecules and remains fully soluble and conformationally extended at many conditions. These findings could be confirmed, as eADF3-CTD showed the slowest and eADF4-CTD the fastest assembly kinetics under identical conditions. Interestingly, the kinetics of heterodimers was only slightly slower than that of eADF4-CTD homodimers, indicating a strong influence of eADF4 on heterodimer assembly. Since eADF4 has already been shown to self-assemble into cross- β -sheet rich fibrils,^[42] all three spidroin variants were assembled in the presence of the β -sheet sensitive dye Thioflavin T (ThT) in order to indicate the formation of cross- β -sheet structures (Figure 2d). Throughout the experiment, eADF3 showed significantly (5–10 times) less ThT specific fluorescence than the other two dimeric species, thereby supporting the kinetics results. The self-assembled spidroin variants formed disordered aggregates without any defined structures in case of eADF3-CTD using atomic force microscopy (AFM), eADF4-CTD

samples, on the other hand, were clustered, unbranched nanofibrils with varying sizes (Figure 2e,f,h,i). Interestingly, the heterodimers formed also nanofibrils, which were clearly distinctive in form and shape from the respective homodimeric assemblies, revealing a network of short, often branched fibrils sometimes covered by larger filaments (Figure 2g,i). Overall, the heterodimers demonstrated physico-chemical properties derived from both individual proteins.

The AFM results could be confirmed using transmission electron microscopy (TEM) (Figure S5, Supporting Information). TEM was further used to demonstrate how recombinant eADF spidroins assemble in presence or absence of TDs. In case of eADF3, only amorphous aggregates rather than distinct fibrils could be detected, no matter whether terminal domains were present or not (Figure S5a–c, Supporting Information). eADF4 without terminal domains self-assembled into β -sheet-rich nanofibrils as published previously (Figure S5f, Supporting Information).^[42] In comparison, eADF4-CTD showed various morphologies of nanofibril-like structures assembled in bundles as well as small aggregates (Figure S5e, Supporting Information), whereas NTD-eADF4-CTD displayed often rather short agglutinated fibril fragments (Figure S5d, Supporting Information). The results indicate that TDs significantly affected the self-assembly process (Figure S5d–f, Supporting Information). Individual heterodimers with CTD or with both NTD and CTD assembled into fibrillary network structures (Figure S5g,h, Supporting Information). Constructs containing mixtures of eADF3 and eADF4 (comprising only CTDs or both TDs) resulted in aggregated assemblies without any fibrillary morphologies (Figure S5i–l, Supporting Information). These results supported the hypothesis that TDs are significantly involved in the control of solubility as well as self-assembly of the spidroin core domains by stabilizing the soluble state of spidroins.^[27]

To investigate the influence of heterodimerization on fiber assembly and fiber mechanics, all-domain NTD-eADF3-CTD and NTD-eADF4-CTD were dimerized upon co-production in *E. coli* or upon refolding in vitro yielding the same stoichiometric ratio of homo- and heterodimers. Aqueous, highly concentrated spinning dopes of the mixtures were prepared akin to a previously published protocol by Heidebrecht et al.^[43] Classical spinning dopes (CSD) were achieved using dialysis against poly(ethylene glycol) (PEG) in order to remove water and to obtain high protein concentrations. In contrast, biomimetic spinning dopes (BSD) were processed using dialysis against a phosphate buffer initiating self-assembly of the spidroins yielding a high-density phase.^[31] Protein concentrations typically ranged from 10 to 15% w/v. Microfibers were produced using a microfluidic multichannel device^[44] to facilitate processing (Figure S6, Supporting Information). Phosphate-containing spinning buffers (30×10^{-3} M potassium phosphate, pH 8) and coagulation baths (0.5–1 M potassium phosphate, pH 6) were employed mimicking the natural spinning environment. Overall, the here presented approach is mimicking parts of the natural assembly process. Based on aqueous highly concentrated spinning dopes, the spidroins were exposed to shear forces on their way from the syringe to the microfluidic chip and further pre-assembled upon addition of low concentrations of phosphate. As soon as the spidroins were extruded into the coagulation bath containing high phosphate concentration at

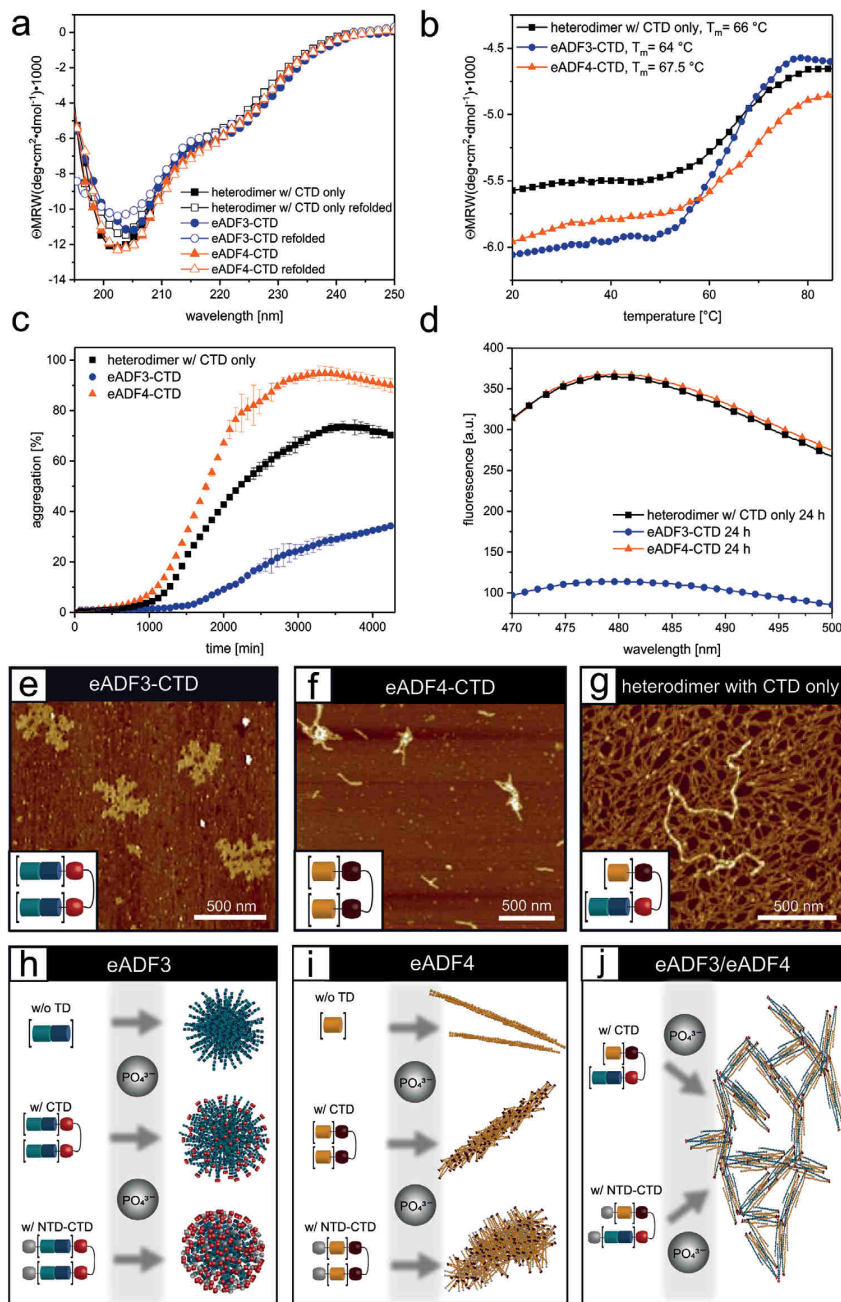


Figure 2. Structural characterization and fibril assembly of individual homo- and heterodimeric spidroins comprising ADF3/4 CTD. a) Far UV circular dichroism spectra of dimeric eADF3-CTD (blue), eADF4-CTD (orange), and the heterodimer consisting of both proteins (black) in Tris-buffer (pH 8). b) Melting points of all three dimer species as determined using far-UV spectroscopy. c) Fibril assembly kinetics of the three dimer species in presence of phosphate buffer (pH 8) by measuring turbidity at 340 nm. d) Thioflavin T binding to fibers made of the dimer species depicted the presence of cross β -sheet-rich structures in the eADF4-containing samples. e–g) Morphologies of assemblies of the dimer species: e) eADF3-CTD, f) eADF4-CTD, and g) eADF3/eADF4-CTD heterodimer in presence of phosphate buffer, investigated using AFM. h–j) Model of self-assembly of the two known MaSp2 variants of *A. diadematus* individually and in a mixture. h) eADF3 preferentially forms large globular-shaped assemblies with little distinct secondary structural elements,^[31] whether TDs are present or not. i) eADF4 forms β -sheet-rich nanofibrils,^[42] and TDs severely influence nanofibril formation. j) Upon heterodimerization of eADF3-CTD/eADF4-CTD or NTD-eADF4-CTD/NTD-eADF4-CTD, fibrillary network structures could be detected. TD: terminal domain.

Table 1. Comparison of mechanical properties of man-made and natural spider silk fibers. Fibers made of different variants comprising terminal domains were spun in a biomimetic set-up using: a) “classical” spinning dopes 10–13% w/v or b) “biomimetic” self-assembled spinning dopes 15% w/v, poststretched and post-treated. Tensile testing was performed at 30% rH.

a. Classical spinning dope (CSD)					
Protein	NTD-eADF3-CTD ^{a)}	NTD-eADF4-CTD	In vitro mixture with NTD and CTD	In vivo mixture with NTD and CTD	Homodimer blend with NTD and CTD ^{a)}
Stretching [%]	600	300	350	400	300
Diameter [μm]	31 ± 0.5	29 ± 0.2	36 ± 0.5	29 ± 0.8	32 ± 3
Extensibility [%]	59 ± 1	8 ± 0.2	17 ± 0.9	25 ± 1	17 ± 5
Strength [MPa]	239 ± 12	417 ± 15	308 ± 13	353 ± 14	103 ± 21
Toughness [MJ m ⁻³]	71 ± 3	17 ± 1	26 ± 1	47 ± 2	11 ± 4
Young's Modulus [GPa]	1 ± 0.1	4 ± 0.4	2 ± 0.1	3 ± 0.2	1 ± 0.6
Number of samples	n = 6	n = 7	n = 7	n = 9	9
b. Biomimetic spinning dope (BSD)					
Protein	NTD-eADF3-CTD ^{a)}	NTD-eADF4-CTD	In vitro mixture with NTD and CTD	In vivo mixture with NTD and CTD	Supercontracted natural MA silk <i>A. diadematus</i>
Stretching [%]	600	300	350	400	/
Diameter [μm]	23 ± 1	33 ± 0.3	37 ± 0.4	27 ± 1	5 ± 0.1
Extensibility [%]	80 ± 1	10 ± 0.2	22 ± 0.5	32 ± 1	39 ± 1
Strength [MPa]	329 ± 11	602 ± 26	614 ± 29	834 ± 34	795 ± 42
Toughness [MJ m ⁻³]	137 ± 6	32 ± 2	70 ± 6	143 ± 6	129 ± 6
Young's Modulus [GPa]	3 ± 0.3	6 ± 0.5	4 ± 0.2	5 ± 0.4	4 ± 0.2
Number of samples	n = 7	n = 7	n = 7	n = 7	n = 9

^{a)}Fibers produced in a coagulation bath comprising 80% isopropyl alcohol.

low pH, a fiber was formed. In this experimental setup, fibers made from BSD were more homogenous in comparison to those from CSD. Phosphate-induced self-assembly of recombinant spidroins in BSDs obtained fibers with mechanical properties equaling that of a natural fiber (Table 1, Figure 3). Light microscopy and scanning electron microscopy (SEM) images of all fibers produced demonstrated similar morphological features (Figures S7a–c, S8a–c, BSD, Supporting Information) in case of CSD fibers, only NTD-eADF4-CTD encountered few interior defects (Figures S7a, S8a, CSD, Supporting Information). Tensile properties of all artificially spun fibers were compared to supercontracted (sc) natural MA silk of *A. diadematus*. Supercontracted fibers were used, as natural dragline silks are subjected to a high variability depending on for example spider age and fitness, the temperature and the silking conditions.^[45] Supercontraction of forcibly silked fibers is a widely used method, as it yields consistent data and is representative of the real mechanical properties of naturally spun fibers.^[46] No solid NTD-eADF3-CTD fibers could be obtained using the microfluidics set-up. Intermolecular interactions of the hydrophilic eADF3 core domain likely impeded proper self-assembly in presence of phosphate and induced rather unspecific agglomeration than fiber assembly. Therefore, NTD-eADF3-CTD fibers were produced in a coagulation bath filled with 80% isopropyl alcohol as described previously.^[43] Mechanical properties of fibers derived from BSD comprising the in vivo mixture were comparable to those of natural MA silk concerning all mechanical aspects, such as strength (834 ± 34 MPa), toughness (143 ± 6 MJ m⁻³) and extensibility (32 ± 1%). As expected, tensile

tests of all BSD variants demonstrated considerably improved mechanical properties compared to the corresponding CSD variants. Although not comparable to the in vivo mixture, the mechanical characteristics of in vitro BSD fibers outperformed those from one-protein fibers, being twice as extensible (22 ± 0.5%) compared to NTD-eADF4-CTD and twice as strong (614 ± 29 MPa) compared to NTD-eADF3-CTD fibers (Table 1b, Figure 3). Fibers spun from NTD-eADF4-CTD (BSD and CSD) could be poststretched only up to 300% and displayed lower values for tensile strength, toughness, and extensibility compared to the other variants, but the highest Young's Modulus (6 ± 0.5 MPa) of all tested artificial fiber samples. The mechanical differences between in vitro and in vivo fibers might be due to spidroin folding. During in vivo co-production in *E. coli*, the cellular chaperon machinery ensures efficient protein folding. Molecular chaperones interact co-translationally with the nascent polypeptide chain emerging from ribosomes, minimizing the probability of premature misfolding.^[47,48] The in vivo protein mixture was purified to yield properly folded proteins with “native-like” conformations. In the course of producing in vitro mixtures, individual homodimers had to be chemically denatured and reduced first, before refolding and dimerization took place in step-wise dialysis by gradually removing the denaturant from the proteins. During this procedure, spidroins may have partially folded into intermediate or misfolded states.^[49] The fact that poststretching of in vitro fibers was possible up to 350% of the initial length without breaking compared to in vivo ones (poststretching up to 400%) underlines that spidroin assembly probably was impeded by present misfolded proteins

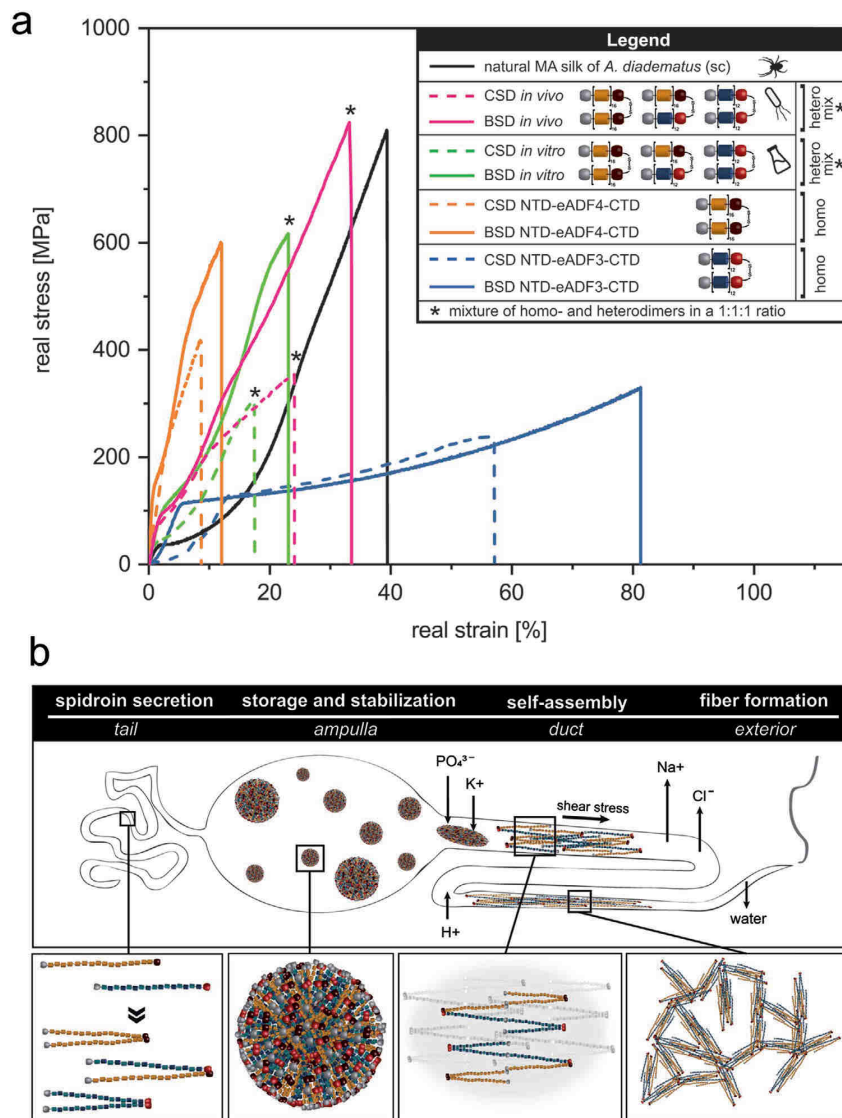


Figure 3. Real stress–strain curves of recombinant and natural spider silk fibers. a) Tensile tests of poststretched fibers of eADF3 and eADF4 spun from classical (CSD, colored dashed lines) as well as biomimetic (BSD, colored solid lines) spinning dopes were made in comparison to those of sc natural *A. diadematus* major ampullate spidroin fibers (black). Mechanical properties of fibers are displayed spun of eADF3/eADF4 homo- and heterodimers mixtures from *in vivo* production in *E. coli* (pink) and *in vitro* production (green), as well as one-protein fibers composed of NTD-eADF4-CTD (orange) or NTD-eADF3-CTD (blue). b) Upon co-production, spidroins form both homo- and heterodimers. In the course of assembly, micellar-like structures have been identified which formed by microphase separation.^[31,33,34,36] In the spinning duct, factors such as ion exchange, acidification and shear stress initiate fiber assembly of the spinning dope.^[32] A mixture of homo- and heterodimers of eADF3 and eADF4 yield highly interconnected networks of the differently structured proteins, which allow the production of fibers with significantly improved mechanical properties due to a better load dissipation based on the combination of crystallinity (eADF4) and elasticity (eADF3).

in the *in vitro* dopes, causing slightly less structural alignment of the molecules within the fiber yielding lower mechanical properties (Table 1b, Figure 3).

Additionally, blends containing the two homodimers (NTD-eADF3-CTD and NTD-eADF4-CTD) were tested (Table 1; Figure S9, Supporting Information). Interestingly, no BSD

could be obtained with this mixture due to aggregation during phosphate dialysis. Since eADF3 and eADF4 exhibit different assembly behaviors, the behaviors of the respective homodimers probably interfered during assembly. Although CSDs could be obtained, fibers could only be produced in an isopropyl alcohol coagulation setup similar to NTD-eADF3-CTD fibers.

The overall mechanical properties of homodimer blend fibers were much lower (Table 1) than that of CSD and BSD fibers spun from mixtures additionally containing the heterodimer. Consequently, the presence of the heterodimer and assemblies made thereof likely serves as a mediator between individual eADF3 assemblies and eADF4 assemblies within the dope and during fiber formation. It is supposed that the assemblies of the respective homodimers are integrated in an interpenetrating network derived from the heterodimers, significantly enhancing the mechanical characteristics of fibers. Therefore, fibers spun from *in vivo* mixtures combined mechanical features of each component with NTD-eADF4-CTD contributing to strength and NTD-eADF3-CTD to extensibility of the fibers.

Mimicking natural spider silk fibers has been a challenging task, as despite decades of research it has not yet been possible to imitate its' hierarchical structure and its mechanical properties. Especially it is of particular importance to stay as close to the natural process as possible (i.e., being biomimetic) to obtain hierarchically structured fibers with mechanical properties equaling that of natural ones. Inspired by the complex natural spinning process from the molecular to the macroscopic level, our approach sheds light on the underlying molecular mechanisms important for proper assembly. The two known MaSp2 derivatives of *A. diadematus*, ADF3 and ADF4, exhibit different physicochemical characteristics. While the recombinant variant eADF3 assembles without significant β -sheet content and the assemblies show micellar-like appearance (Figure 2h),^[31] recombinant eADF4 can assemble into nano-sized cross- β -fibrils (Figure 2i).^[42] Intriguingly, heterodimerization initiated by the CTDs of these spidroins gained fibrillary network structures upon assembly (Figure 2j). Utilizing these molecular features in combination with biomimetic spinning yielded mechanically nature-like performing fibers. Our findings support the hypothesis that intermolecular interactions of TDs in the spinning dope control structural alignment as well as formation of higher-order protein structures (Figure 3b).^[36,50] Ultimately, this work underlines the importance of MaSp interaction at a (supra)molecular level and the contribution of this interplay to control solubility as well as self-assembly with significant impact on the mechanical performance of fibers.

In a biological context, spiders can regulate the expression of spider silk genes and subsequently control protein content with obvious implications on assembly properties. This comes in line with the finding that spiders tune or adapt their fiber mechanics, which is an important attribute when spiders are exposed to fluctuating environmental conditions.^[51] Our findings will allow to develop man-made high-performance bioinspired fibers, in which the combination of proteins will utilize functional complexity and opens up new expedient properties useful for a whole set of novel applications.

Experimental Section

Protein Production: The individually produced proteins eADF3-CTD ((AQ)₁₂NR3), NTD-eADF3-CTD (NRN1L(AQ)₁₂NR3), eADF4-CTD (C₁₆NR4) and NTD-eADF4-CTD (NRN1LC₁₆NR4) bearing N-terminal T7-tags were produced and purified as described previously.^[38,41] For co-expression, genes encoding eADF3-CTD/NTD-eADF3-CTD (T7-Tag) and eADF4-CTD/NTD-eADF4-CTD (His-Tag) were cloned into

a pRSFDuet-1 expression vector bearing two multiple cloning sites. Gene expression and protein purification was carried out similar to the previously published procedure.^[38] The CTD heterodimer was purified using an immobilized metal ion affinity chromatography (HisTrap HP, GE Healthcare), followed by an anion exchange column (Q Sepharose FF, GE Healthcare).

Protein Preparation and Analysis: Lyophilized proteins were dissolved in 6 M guanidinium thiocyanate and dialyzed three times against 50×10^{-3} M Tris/HCl pH 8, 150×10^{-3} M NaCl at room temperature (RT). Protein aggregates were separated upon centrifugation at $130\,000 \times g$ for 20 min at RT. Protein samples were investigated using 8%, 10%, or 12% SDS-PAGE (2.5 μ g protein). Gels were either silver stained or used for western blot (WB) analysis. WBs were analyzed using His-Tag or T7-Tag antibody HRP conjugates (Novagen) and ECL plus (GE Healthcare) according to the manufacturers' recommendations. For circular dichroism spectroscopy measurements, proteins were dialyzed against 10×10^{-3} M Tris-buffer buffer (pH 8), centrifuged at $180\,000 \times g$ for 1 h at 4 °C and diluted to 3.4×10^{-6} M. Far-UV circular dichroism spectra were recorded (Jasco J-715) in triplicates using cuvettes with 0.1 cm path lengths and spectra were subsequently smoothed by applying a Savitzky–Golay filter. Thermal transitions were determined recording changes at 220 nm with heating/cooling rates of 1 °C min⁻¹.

Self-Assembly Analyzes: Fibril formation of the different protein variants was triggered at similar conditions as described previously.^[52] Proteins were dialyzed against 10×10^{-3} M Tris/HCl, pH 8 and ultracentrifuged at $180\,000 \times g$ for 1 h at 4 °C. Assembly was started upon addition of sodium phosphate or potassium phosphate (pH 8) at a final concentration of 50 – 100×10^{-3} M at 20 °C. Turbidity assays were recorded at 340 nm in triplicates using UV/vis spectrometry. For assembly kinetics, 10×10^{-6} M ThT was added to proteins dissolved in phosphate buffer and transferred to Quartz UV-microcuvettes. The fluorescence was monitored at an excitation wavelength of 440 nm after 24 h of incubation at 25 °C. Assembly morphologies were analyzed using TEM or AFM. A transmission electron microscope (JEOL JEM-2100) was used, and images were taken using a device camera (UltraScan 4000, Gatan Inc.) with Gatan Digital Micrograph software. AFM scanning (Dimension ICON, NanoScope V controller, Bruker) was performed in TappingMode using Si cantilevers (OTESPA-R3, f_0 300 kHz, k : 26 N m⁻¹, Bruker). Data processing was done using NanoScope Analysis software 1.5 (Bruker).

Production and Analyzes of Fibers: Spinning dopes were prepared as previously described.^[43] Lyophilized proteins were dissolved in 6 M guanidinium thiocyanate and dialyzed against 50×10^{-3} M Tris/HCl, pH 8.0, 150×10^{-3} M NaCl. CSD were prepared upon dialysis against a 20% w/v PEG (35 kDa) solution, and BSD were obtained by dialysis against 30×10^{-3} M potassium phosphate buffer (pH 8). For fiber production, spinning dopes were extruded at flow rates of 50 – 150μ L h⁻¹ through a microfluidic chip into a coagulation bath filled with 0.5–1 M potassium phosphate buffer (pH 6). 30×10^{-3} M potassium phosphate buffer (pH 8) was used as sheath flows at 600 – 800μ L h⁻¹. Only fibers spun from NTD-eADF3-CTD were produced using a different coagulation bath comprising 80% isopropyl alcohol as described previously.^[43] All fibers were manually poststretched to maximum in 80% isopropyl alcohol, post-treated in 70% ethanol, and analyzed using an optical microscope (Leica DM13000B, software Leica V4.3). Fiber diameters were monitored with 20 \times , 40 \times , and 100 \times object lenses. From each fiber sample, several representative images were analyzed at different sites ($n \geq 10$) to measure the quadratic mean of the fiber diameter and its standard deviation. For SEM, fiber samples were sputter-coated with 1.3 nm platinum (EM ACE600 sputter coater, Leica) and imaged (Apreo VS, Thermo Fisher Scientific). For tensile testing, fiber sections ($n \geq 7$) were placed on plastic sample holders with a 2 mm gap using superglue (UHU GmbH Co. KG). Female, adult *A. diadematus* spiders were fed with fruit flies; fibers were collected by forcibly silking at 12 cm s⁻¹, and submerged into distilled water for supercontraction. Tensile testing (BOSE Electroforce 3220) was performed using a 0.49 N load cell at a pulling rate of 0.005 mm s⁻¹ at 30% relative humidity. Mechanical properties were quantitatively evaluated using Microsoft Excel 2016

(Microsoft Corporation, Redmond, WA, USA) or Origin 9.4 (OriginLab Corporation, Northampton, MA, USA) considering real stress and real strain data.

Supporting Information

Supporting Information is available from the Wiley Online Library or from the author.

Acknowledgements

The authors thank Anika Winkler for TEM imaging, and Claudia Stemmann as well as Dr. Hendrik Bargel for SEM measurements. Further, the authors would like to thank Svenja Schiemann for kinetic assembly measurements, and Yeldem Koc for assistance in cloning of spidroin variants. The authors thank Dr. Elise Liensdorf and Dr. Stephen Strassburg for proof reading. Financial support was provided by the Deutsche Forschungsgemeinschaft SFB 840 TP A08.

Open access funding enabled and organized by Projekt DEAL.

Conflict of Interest

T.S. is co-founder and shareholder of the company AMSilk GmbH.

Data Availability Statement

Research data are not shared.

Keywords

bioinspired fibers, heterodimers, protein interplay, self-assembly, spider silk

Received: September 23, 2020

Revised: December 17, 2020

Published online:

- [1] F. Vollrath, *Rev. Mol. Biotechnol.* **2000**, *74*, 67.
- [2] M. Heim, D. Keerl, T. Scheibel, *Angew. Chem., Int. Ed.* **2009**, *48*, 3584.
- [3] M. Xu, R. V. Lewis, *Proc. Natl. Acad. Sci. USA* **1990**, *87*, 7120.
- [4] M. A. Collin, T. H. Clarke III, N. A. Ayoub, C. Y. Hayashi, *Int. J. Biol. Macromol.* **2018**, *113*, 829.
- [5] L. Han, L. Zhang, T. Zhao, Y. Wang, M. Nakagaki, *Int. J. Biol. Macromol.* **2013**, *56*, 156.
- [6] S. M. Correa-Garhwal, T. H. Clarke, M. Janssen, L. Crevecoeur, B. N. McQuillan, A. H. Simpson, C. J. Vink, C. Y. Hayashi, *Sci. Rep.* **2019**, *9*, 13656.
- [7] P. A. Guerette, D. G. Ginzinger, B. H. Weber, J. M. Gosline, *Science* **1996**, *272*, 112.
- [8] N. Kono, H. Nakamura, R. Ohtoshi, D. A. P. Moran, A. Shinohara, Y. Yoshida, M. Fujiwara, M. Mori, M. Tomita, K. Arakawa, *Sci. Rep.* **2019**, *9*, 8380.
- [9] C. Thamm, T. Scheibel, *Biomacromolecules* **2017**, *18*, 1365.
- [10] J. E. Garb, R. A. Haney, E. E. Schwager, M. Gregorič, M. Kuntner, I. Agnarsson, T. A. Blackledge, *Commun. Biol.* **2019**, *2*, 275.
- [11] F. Vollrath, D. P. Knight, *Nature* **2001**, *410*, 541.
- [12] W. A. Gaines IV, W. R. Marcotte Jr., *Insect Mol. Biol.* **2008**, *17*, 465.
- [13] N. A. Ayoub, J. E. Garb, R. M. Tinghitella, M. A. Collin, C. Y. Hayashi, *PLoS One* **2007**, *2*, e514.
- [14] S. J. Blamires, C.-L. Wu, I.-M. Tso, *PLoS One* **2012**, *7*, e31626.
- [15] K. H. Guehrs, B. Schlott, F. Grosse, K. Weisshart, *Insect Mol. Biol.* **2008**, *17*, 553.
- [16] D. B. Zax, D. E. Armanios, S. Horak, C. Malowniak, Z. Yang, *Biomacromolecules* **2004**, *5*, 732.
- [17] X. Hu, K. Vasanthavada, K. Kohler, S. McNary, A. Moore, C. Vierra, *Cell. Mol. Life Sci.* **1986**, *63*, 2006.
- [18] J. D. Van Beek, S. Hess, F. Vollrath, B. Meier, *Proc. Natl. Acad. Sci. USA* **2002**, *99*, 10266.
- [19] A. D. Parkhe, S. K. Seeley, K. Gardner, L. Thompson, R. V. Lewis, *J. Mol. Recognit.* **1997**, *10*, 1.
- [20] D. H. Hijirida, K. G. Do, C. Michal, S. Wong, D. Zax, L. W. Jelinski, *Biophys. J.* **1996**, *71*, 3442.
- [21] A. Simmons, E. Ray, L. W. Jelinski, *Macromolecules* **1994**, *27*, 5235.
- [22] T. Lefevre, J. Leclerc, J.-F. Rioux-Dubé, T. Buffeteau, M.-C. Paquin, M.-E. Rousseau, I. Cloutier, M. Auger, S. M. Gagné, S. Boudreault, *Biomacromolecules* **2007**, *8*, 2342.
- [23] A. H. Simmons, C. A. Michal, L. W. Jelinski, *Science* **1996**, *271*, 84.
- [24] R. Challis, S. Goodacre, G. Hewitt, *Insect Mol. Biol.* **2006**, *15*, 45.
- [25] J. E. Garb, N. A. Ayoub, C. Y. Hayashi, *BMC Evol. Biol.* **2010**, *10*, 243.
- [26] J. Bauer, T. Scheibel, *Biomacromolecules* **2017**, *18*, 835.
- [27] F. Hagn, L. Eisdoldt, J. G. Hardy, C. Vendrely, M. Coles, T. Scheibel, H. Kessler, *Nature* **2010**, *465*, 239.
- [28] L. Eisdoldt, J. G. Hardy, M. Heim, T. R. Scheibel, *J. Struct. Biol.* **2010**, *170*, 413.
- [29] M. Stark, S. Grip, A. Rising, M. Hedhammar, W. Engström, G. Hjälml, J. Johansson, *Biomacromolecules* **2007**, *8*, 1695.
- [30] A. Spöner, W. Vater, W. Rommerskirch, F. Vollrath, E. Unger, F. Grosse, K. Weisshart, *Biochem. Biophys. Res. Commun.* **2005**, *338*, 897.
- [31] J. H. Exler, D. Hümmerich, T. Scheibel, *Angew. Chem., Int. Ed.* **2007**, *46*, 3559.
- [32] L. Eisdoldt, T. Scheibel, A. Smith, *Mater. Today* **2011**, *14*, 80.
- [33] T.-Y. Lin, H. Masunaga, R. Sato, A. D. Malay, K. Toyooka, T. Hikima, K. Numata, *Biomacromolecules* **2017**, *18*, 1350.
- [34] A. D. Malay, T. Suzuki, T. Katashima, N. Kono, K. Arakawa, K. Numata, *Sci. Adv.* **2020**, *6*, eabb6030.
- [35] G. Askarieh, M. Hedhammar, K. Nordling, A. Saenz, C. Casals, A. Rising, J. Johansson, S. D. Knight, *Nature* **2010**, *465*, 236.
- [36] L. R. Parent, D. Onofrei, D. Xu, D. Stengel, J. D. Roehling, J. B. Addison, C. Forman, S. A. Amin, B. R. Cherry, J. L. Yarger, N. C. Gianneschi, G. P. Holland, *Proc. Natl. Acad. Sci. USA* **2018**, *115*, 11507.
- [37] Z. Lin, W. Huang, J. Zhang, J. S. Fan, D. Yang, *Proc. Natl. Acad. Sci. USA* **2009**, *106*, 8906.
- [38] D. Huemmerich, C. W. Helsen, S. Quedzuweit, J. Oschmann, R. Rudolph, T. Scheibel, *Biochemistry* **2004**, *43*, 13604.
- [39] J. Bauer, D. Schaal, L. Eisdoldt, K. Schweimer, S. Schwarzinger, T. Scheibel, *Sci. Rep.* **2016**, *6*, 34442.
- [40] J. Bauer, T. Scheibel, *Biomacromolecules* **2017**, *18*, 2521.
- [41] S. Rammensee, U. Slotta, T. Scheibel, A. Bausch, *Proc. Natl. Acad. Sci. USA* **2008**, *105*, 6590.
- [42] U. Slotta, S. Hess, K. Spieß, T. Stromer, L. Serpell, T. Scheibel, *Macromol. Biosci.* **2007**, *7*, 183.
- [43] A. Heidebrecht, L. Eisdoldt, J. Diehl, A. Schmidt, M. Geffers, G. Lang, T. Scheibel, *Adv. Mater.* **2015**, *27*, 2189.
- [44] M. E. Kinahan, E. Filippidi, S. Köster, X. Hu, H. M. Evans, T. Pfohl, D. L. Kaplan, J. Wong, *Biomacromolecules* **2011**, *12*, 1504.
- [45] B. Madsen, Z. Z. Shao, F. Vollrath, *Int. J. Biol. Macromol.* **1999**, *24*, 301.
- [46] J. Garrote, V. Ruiz, O. P. Troncoso, F. G. Torres, M. Arnedo, M. Elices, G. V. Guinea, J. Pérez-Rigueiro, *J. Mech. Behav. Biomed. Mater.* **2020**, *111*, 104023.
- [47] A. A. Komar, *Trends Biochem. Sci.* **2009**, *34*, 16.
- [48] F. U. Hartl, M. Hayer-Hartl, *Nat. Struct. Mol. Biol.* **2009**, *16*, 574.
- [49] H. Yamaguchi, M. Miyazaki, *Biomolecules* **2014**, *4*, 235.
- [50] D. P. Knight, F. Vollrath, *Naturwissenschaften* **2001**, *88*, 179.
- [51] Y. Aoyanagi, K. Okumura, *Phys. Rev. Lett.* **2010**, *104*, 038102.
- [52] U. K. Slotta, S. Rammensee, S. Gorb, T. Scheibel, *Angew. Chem., Int. Ed.* **2008**, *47*, 4592.

Copyright WILEY-VCH Verlag GmbH & Co. KGaA, 69469 Weinheim, Germany, 2018.

Supporting Information

Interplay of different major ampullate spidroins during assembly and implications for fiber mechanics

*Merisa Saric, Lukas Eisoldt, Volker Döring, Thomas Scheibel**

Extended experimental section

Protein production:

eADF3-CTD ((AQ)₁₂NR3), NTD-eADF3-CTD (NRN1L(AQ)₁₂NR3) and eADF4-CTD (C₁₆NR4) bearing N-terminal T7-tags were produced and purified as described previously.^{[38,}

^{41]} The gene for NTD-eADF4-CTD (NRN1LC₁₆NR4) was inserted into a pET29 vector (Novagen, Merck) encoding an N-terminal T7-tag and expressed in *E. coli* BL21-Gold (DE3) (Agilent Technologies) upon induction with 1 mM IPTG (at OD₆₀₀ of 30) for 2.5 h at 25 °C. For co-expression, genes encoding NTD-eADF3-CTD (T7-Tag) and NTD-eADF4-CTD (His-Tag) were cloned into a pRSFDuet-1 expression vector (Novagen, Merck) bearing two multiple cloning sites. Gene expression was induced in *E. coli* strain BL21-Gold (DE3) using 1 mM IPTG (at OD₆₀₀ of 30) for 3 h at 25 °C. Protein purification was carried out similarly to the previously published procedure.^[38] Briefly, *E. coli* cells were mechanically cracked using a high-pressure homogenizer, cell remnants were removed using centrifugation, and the supernatant was heated for 30 min to 65 °C and again centrifuged. Next, 400-500 mM ammonia sulfate was added to the supernatant and incubated over night at 4 °C. After centrifugation, the protein pellet was solved in 6 M guanidinium thiocyanate and dialyzed three times against 5 L of 10 mM ammonia bicarbonate at room temperature (RT) using dialysis membranes with a molecular weight cut-off of 12–14 kDa (Servapor, Serva). The heterodimer eADF3/eADF4-CTD was purified using a two-step column procedure, and as a first step immobilized metal ion

affinity chromatography (HisTrap HP, GE Healthcare) was used to isolate eADF4 proteins comprising a histidine tag. In the second step, an anion exchange column (Q Sepharose FF, GE Healthcare) was used to isolate eADF3/eADF4-CTD heterodimers with a linear gradient from 0-500 mM sodium chloride over 20 column volumes. For long-term storage, the proteins were freeze-dried at -20 °C. Nucleic acids contaminants were determined using UV/Vis spectroscopy, and contaminations with *E. coli* proteins using fluorescence spectroscopy as described previously.^[38] UV/Vis absorbance was measured using a UV/Vis spectrophotometer (NanoDrop ND-1000), fluorescence spectra were recorded using cuvettes with 1 cm path length and a fluorescence spectrometer (Jasco FP6500) at protein concentrations of 0.5 mg/mL in 10 mM Tris/HCl (pH 8) at room temperature. Excitation wavelengths were selected at 278 nm (tyrosine) and 295 nm (tryptophane) and emission wavelengths in a range of 300-350 nm. Spectra analysis was done using SpectraManager 1.08.02 (Jasco).

Microscopic analyzes of self-assembled morphologies:

For transmission electron microscopy (TEM), 10 µL of the pre-assembled protein suspension was spotted on supports (Pioloform 100 mesh copper grids (Plano GmbH)), washed with 10 µL of ddH₂O (Millipore) and negatively stained upon incubation with 5 µL of 2 % w/v uranyl acetate solution for 2 min. A transmission electron microscope (JEOL JEM-2100) was used at 80 kV, and images were taken using a 4000 × 4000 charge-coupled device camera (UltraScan 4000, Gatan Inc.) with Gatan Digital Micrograph software. Atomic force microscopy (AFM) samples were prepared by pipetting 10 µL of self-assembled protein samples onto mica plates (L 10 mm, V1 grade, Plano GmbH). After incubation for 10 min, the samples were washed four times with 20 µL of ddH₂O (Millipore) and dried before imaging for at least 24 h at room temperature. AFM scanning (DimensionTM ICON, NanoScope V controller, Bruker) was performed in TappingModeTM using Si cantilevers (OTESPA-R3, f₀ 300 kHz, k: 26 N/m, Bruker). Data processing was done using NanoScope Analysis software 1.5 (Bruker).

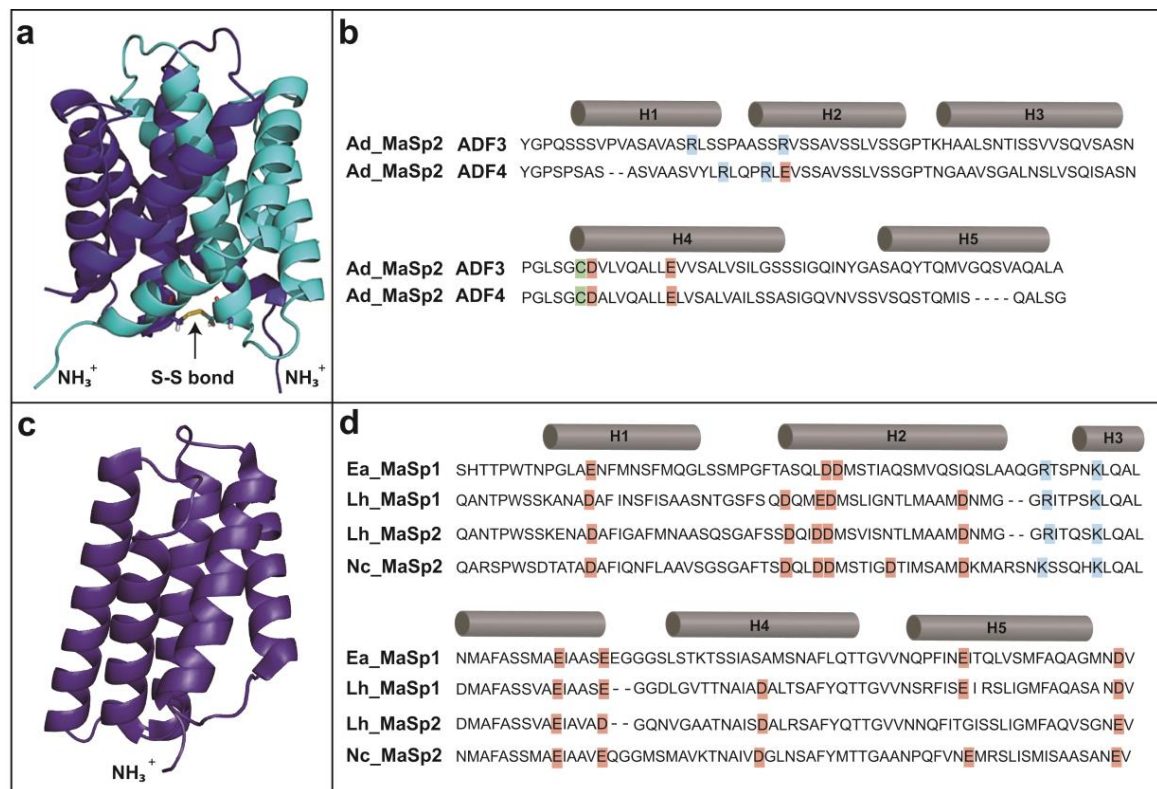
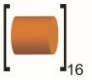
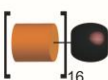
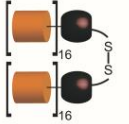
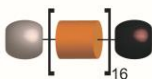
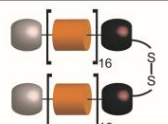
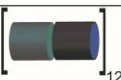
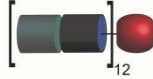
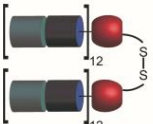
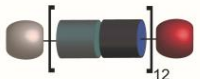
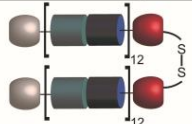
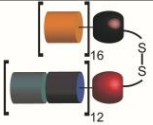
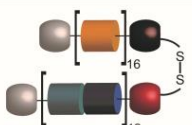


Figure S1. Comparison of sequence homologies from non-repetitive terminal domains. **(a)** Structure of the parallel dimer of the non-repetitive CTD (PDB: 2KHM) from *A. diadematus* (Ad_MaSp2). Each monomer, depicted in blue and cyan, comprises a five-helix bundle with one conserved cysteine in helix 4 forming a disulfide bond covalently linking the two monomers.^[27] **(b)** Alignment of the CTDs from ADF3 (Uniprot: Q16987) and ADF4 (Uniprot: Q16988), named NR3 and NR4 (sequence identity: 58 %, sequence similarity: 73 %). **(c)** Structure of a monomeric non-repetitive amino-terminal domain from *Euprosthenoops australis* (PDB: 3LR2), illustrating a characteristic five-helix bundle.^[35] **(d)** The alignment of different NTDs from well known spider species *E. australis* (Ea_MaSp1), *Latrodectus hesperus* (Lh_MaSp1, Lh_MaSp2) and *Nephila clavipes* (Nc_MaSp2) is shown exemplarily (sequence identity: 50 %, sequence similarity: 74 %). In this study, the NTD from *L. hesperus* MaSp1 was used since the sequences of NTDs from *A. diadematus* are not known so far. H1 - H5 indicate the positions of the five helices of the different TDs. The amino-terminal groups (NH_3^+) are highlighted, at which the TD is connected to the repetitive domain. The highly conserved

charged residues (acidic: red, basic: blue), as well as cysteine residues (green) are highlighted.

Alignments were created using the software ClustalOmega.

Protein	Monomer	Theoretical MW (Monomer)	Dimer	Theoretical MW (Dimer)
eADF4 C ₁₆		47 kDa	—	—
eADF4-CTD C ₁₆ NR4		58 kDa		116 kDa
NTD-eADF4-CTD NRN1LC ₁₆ NR4		74 kDa		148 kDa
eADF3 (AQ) ₁₂		48 kDa	—	—
eADF3-CTD (AQ) ₁₂ NR3		60 kDa		120 kDa
NTD-eADF3-CTD NRN1L(AQ) ₁₂ NR3		76 kDa		152 kDa
heterodimer with CTDs only C ₁₆ NR4/(AQ) ₁₂ NR3	—	—		118 kDa
heterodimer with NTDs and CTDs NRN1LC ₁₆ NR4/NRN1L(AQ) ₁₂ NR3	—	—		150 kDa







Legend			
Terminal domains		Recombinant core domains of <i>A. diadematus</i>	
Amino-terminus of <i>L. hesperus</i>	NRN1L	Carboxyl-termini of <i>A. diadematus</i>	NR3 NR4
			
		module C	module A module Q
			 

Figure S2. Scheme of recombinant variants derived from ADF3 and ADF4 used in this study, representing the two known MaSp2 components of *A. diadematus* dragline silk. C-terminal domains are derived from either ADF3 or ADF4. Since no N-terminal sequences of ADF3 or ADF4 are identified so far, the highly homologous and well characterized N-terminus of *L. hesperus* MaSp1 was used instead.

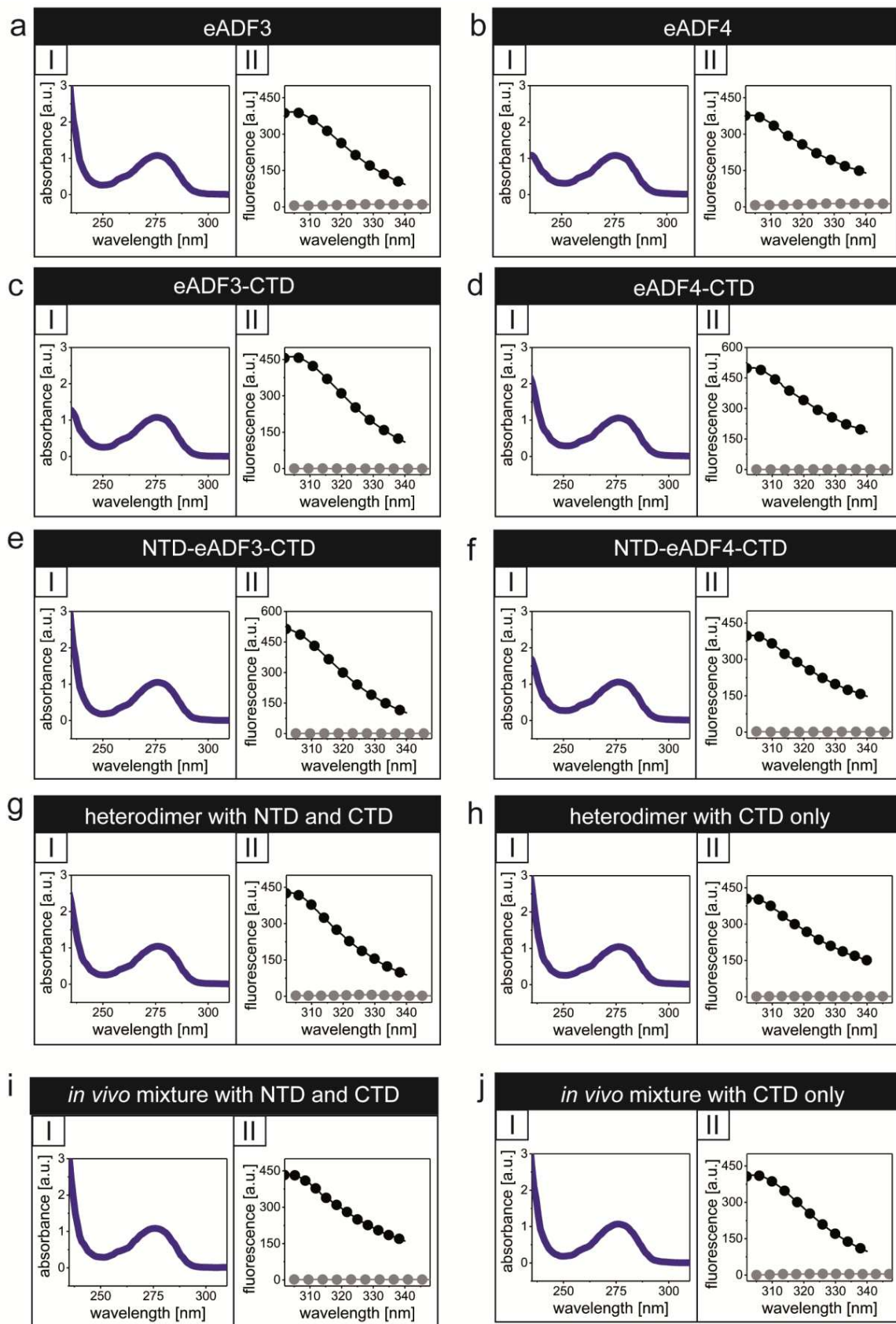


Figure S3. Analyzes of protein purity of different spidroin variants **(a)** eADF3, **(b)** eADF4, **(c)** eADF3-CTD, **(d)** eADF4-CTD, **(e)** NTD-eADF3-CTD, **(f)** NTD-eADF4-CTD, **(g)** heterodimer ADF3/4 with NTD and CTD, **(h)** heterodimer with ADF3/4 CTD, **(i)** *in vivo* mixture comprising homo- and heterodimers with NTD and CTD containing proteins, and **(j)** *in vivo* mixture comprising homo- and heterodimers with CTD containing proteins. The images show UV/Vis absorbance **(I)** and fluorescence measurements **(II)**, whereby fluorescence emission spectra of tyrosine (black) and tryptophane (grey) are presented. While tyrosine residues occur abundantly in spidroins, no tryptophanes ones are present. Tryptophane fluorescence emission is an evidence for contamination with *E. coli* proteins, which on average contain 1.5 % tryptophane.^[38] Fluorescence measurements show spectra similar to tyrosine spectra, but the absence of tryptophane emission indicated a high purity of all proteins. The purity of *in vitro* mixtures is not explicitly shown as it is based on the individual homodimeric species.

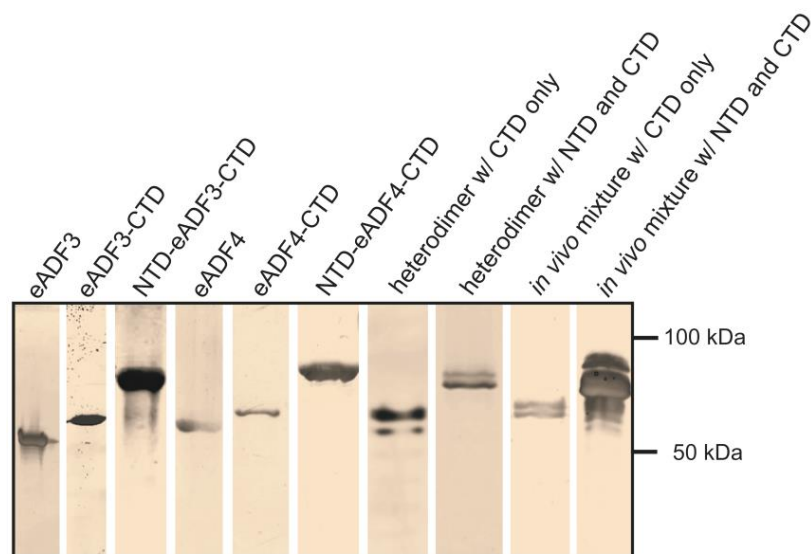


Figure S4. Analyzes of purified recombinant spider silk variants using silver stained SDS-PAGE under reducing conditions. For ADF3/4-CTDs, reducing the disulfide-bridge yielded monomers. Heterodimers and *in vivo* mixtures contained both eADF3 and eADF4 variants, which is represented by the presence of two distinct bands.

Table S1. UV/Vis absorbance of spidroin variants. 260 nm refers to nucleic acid absorbance, absorbance at 280 nm is proportional to protein concentration. Values A_{260}/A_{280} between 0.5 and 0.6 indicate high sample purity with no nucleic acid contamination.

Protein	A_{260}/A_{280}
eADF3	0.50
eADF3-CTD	0.49
NTD-eADF3-CTD	0.42
eADF4	0.51
eADF4-CTD	0.47
NTD-eADF4-CTD	0.46
CTD heterodimer	0.45
NTD/CTD heterodimer	0.46
CTD <i>in vivo</i> mixture	0.49
NTD/CTD <i>in vivo</i> mixture	0.48

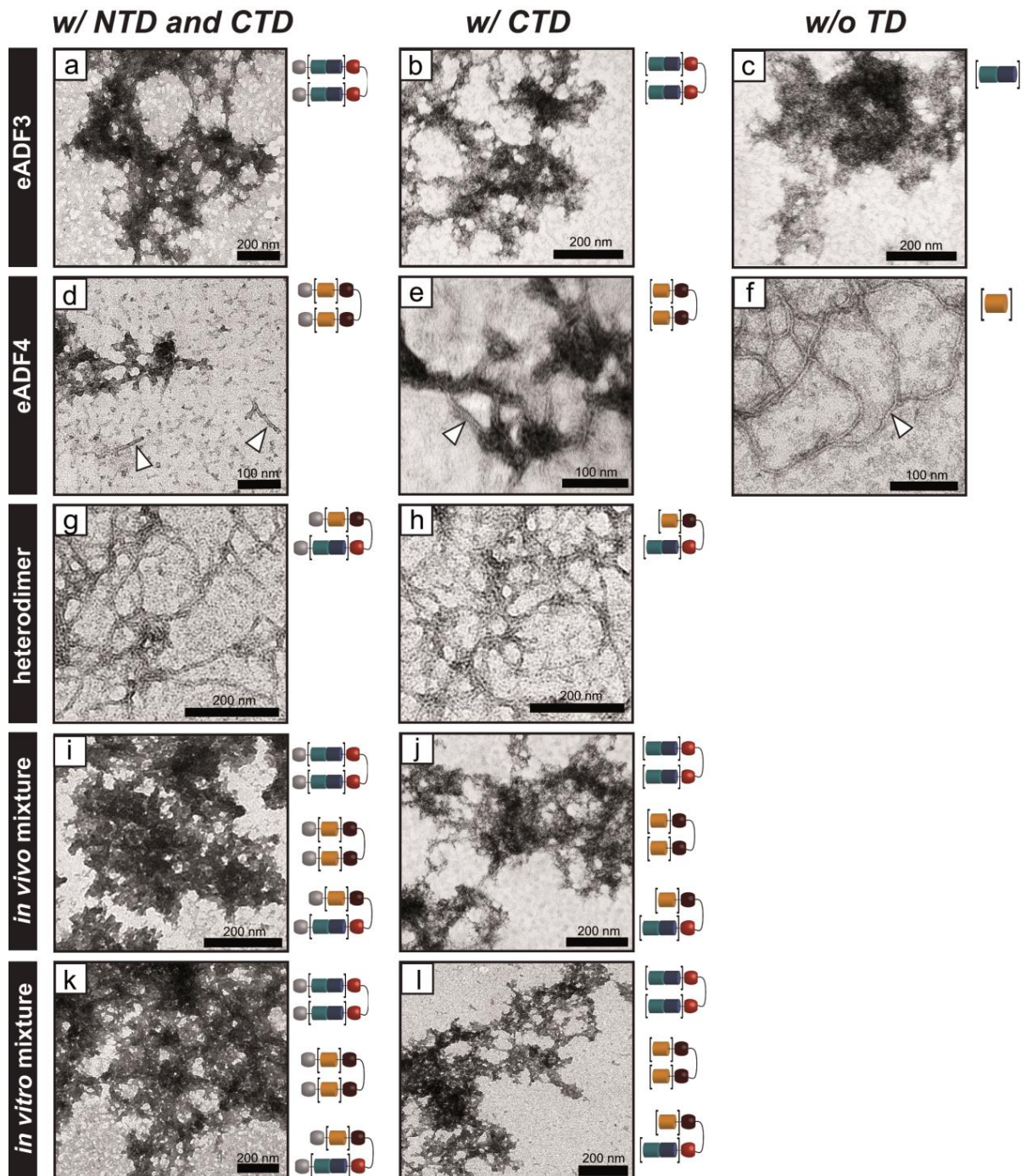


Figure S5. Self-assembly of recombinant MaSp2 variants in the presence of 50 - 150 mM phosphate ions analyzed using TEM. Spidroin variants were analyzed without terminal domains (w/o TD), with a carboxyl-terminal domain (w/ CTD) and with both amino- and carboxyl-terminal domains (w/ NTD and CTD). **(a-c)**, eADF3, **(d-f)** eADF4, arrows highlight fibrillar structures, **(g,h)** purified heterodimers (without homodimers present), **(i,j)** *in vivo* mixtures of eADF3/eADF4 homo- and heterodimers and **(k,l)** *in vitro* mixtures of eADF3/eADF4 homo-

and heterodimers. All protein samples were assembled at 20 μM in 10 mM Tris-buffer, pH 8, and 50 - 150 mM phosphate buffer. The assays were performed for 1 day at room temperature.

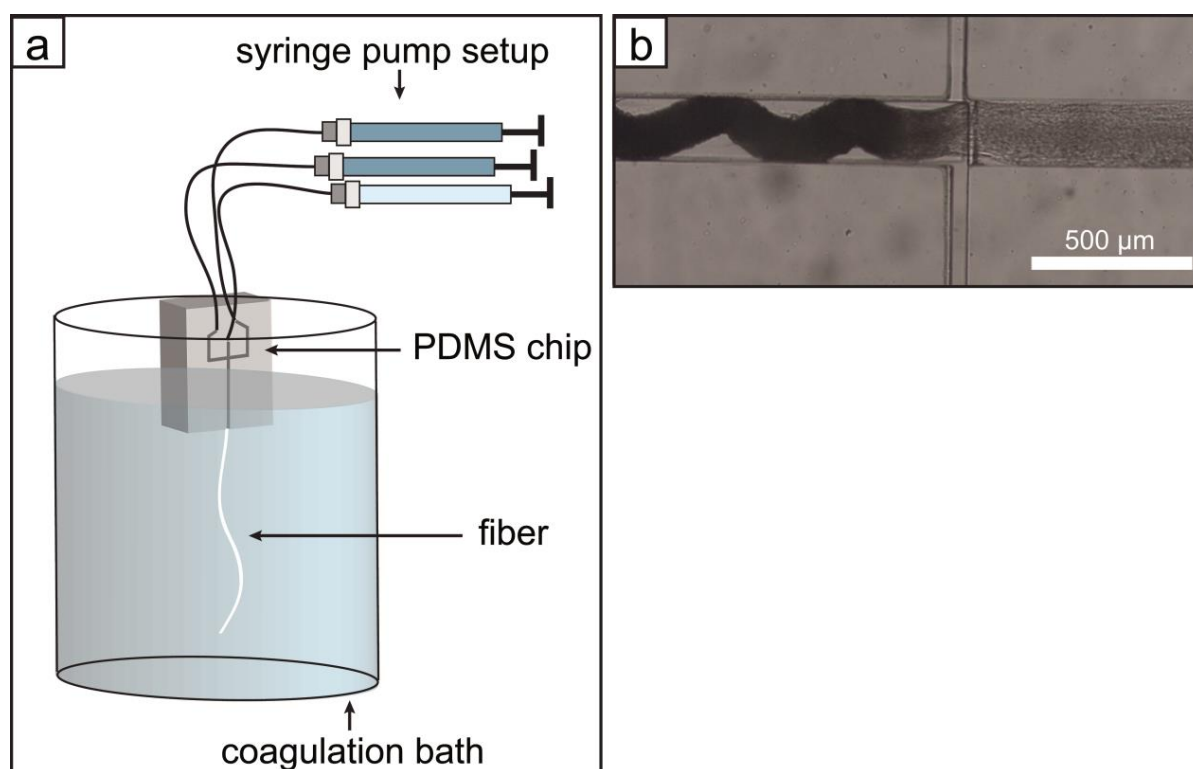


Figure S6. Microfiber production using microfluidics. **(a)** Microfluidics setup using a PDMS chip, which is connected to three syringe pumps. Simultaneous pumping of a spinning dope and two phosphate buffer solutions (30 mM, pH 8) resulted in microfiber extrusion into a coagulation bath (0.5 – 1 M potassium phosphate, pH 6). **(b)**, Zoom-in of the microchip inlet exhibiting fiber formation within the channel.

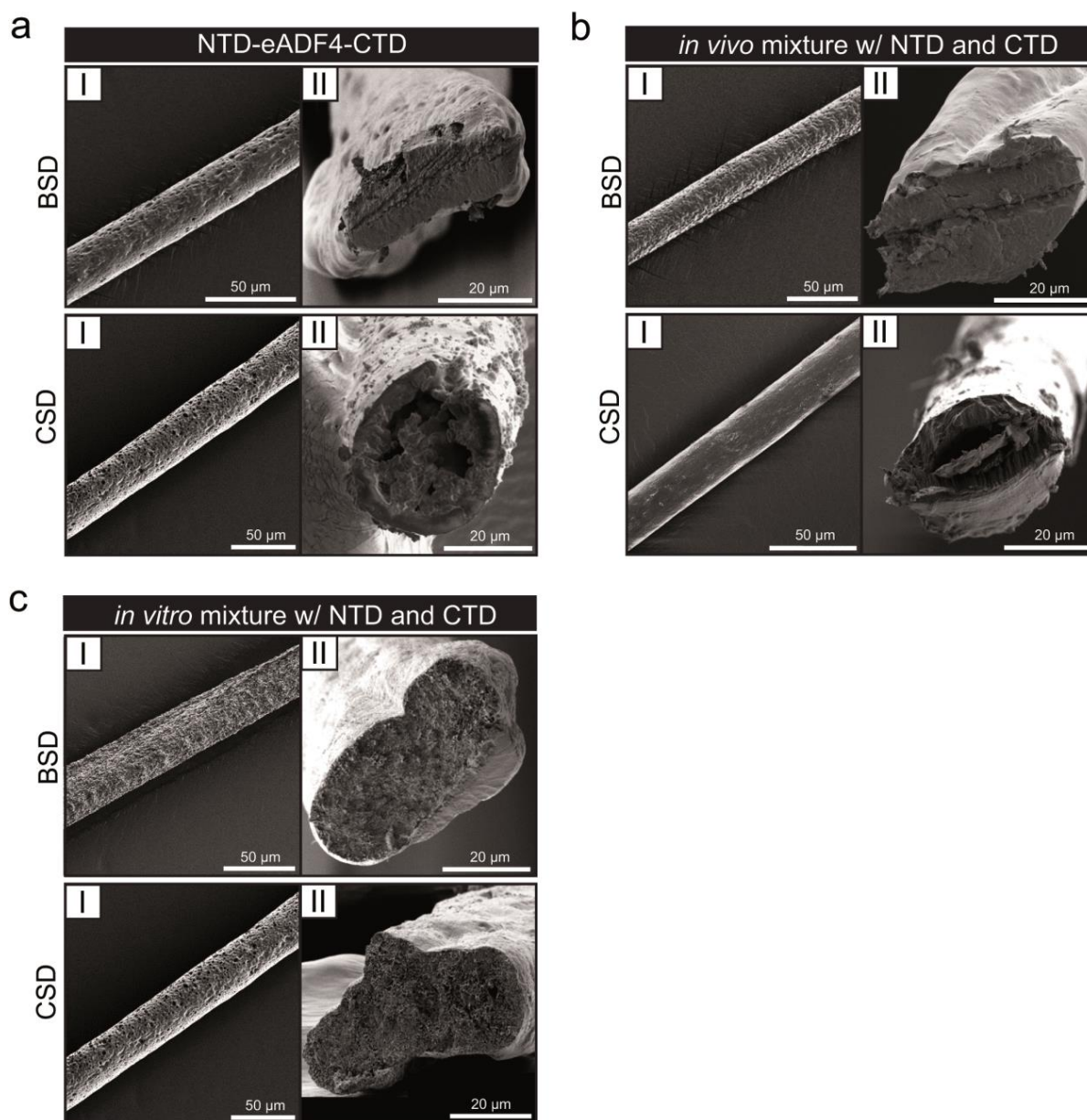


Figure S7. SEM images of CSD and BSD fibers according to Table 1 of the variants (a) NTD-eADF4-CTD (b) in vivo and (c) in vitro mixture of NTD-eADF3-CTD/ NTD-eADF4-CTD homo- and heterodimers. The images show post-stretched fibers (I) and cross-sections thereof (II). Note that the real cross-sectional area has been used to calculate engineered stress and strain.

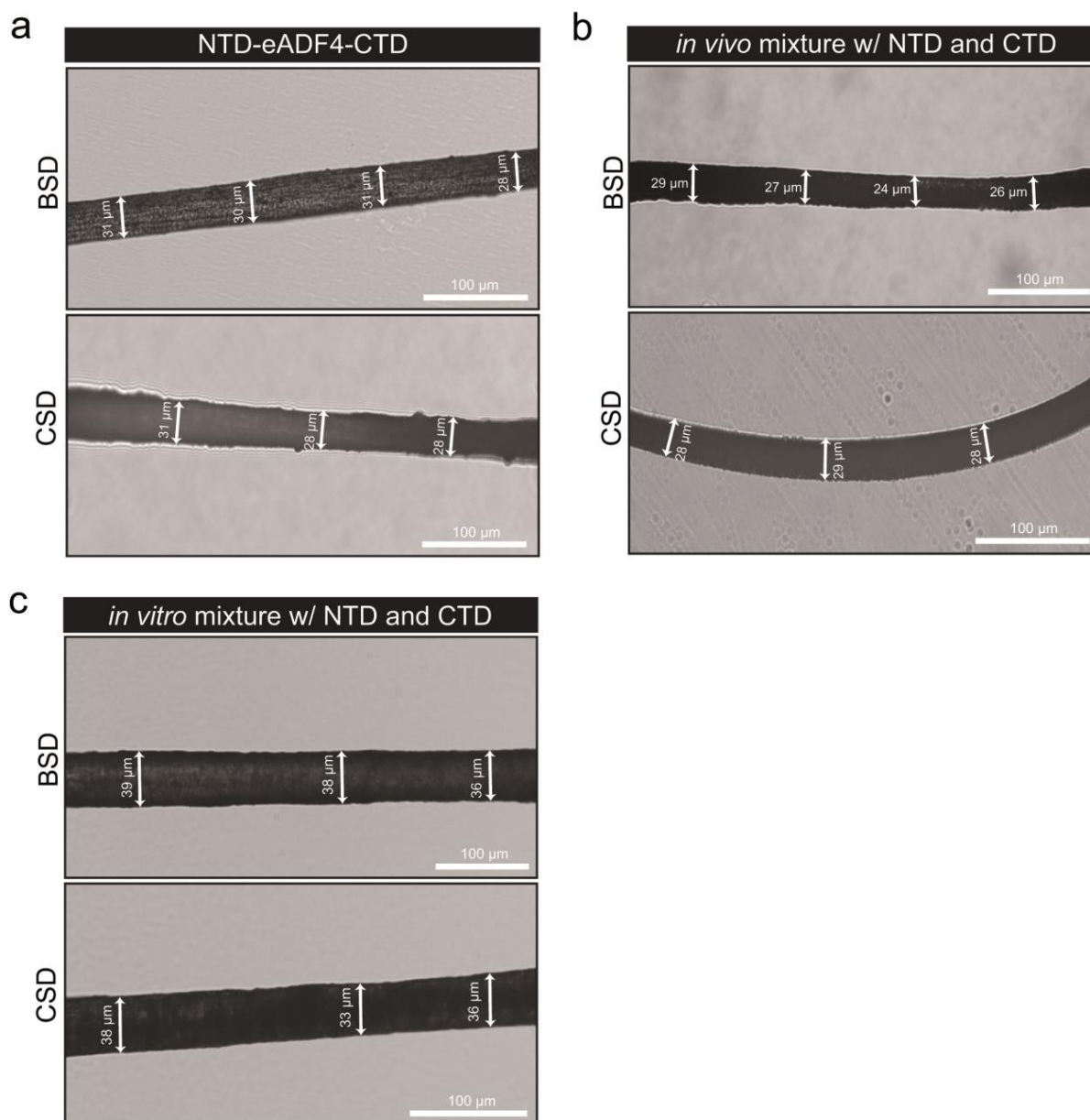


Figure S8. Light microscopy images of CSD and BSD fibers to investigate the homogeneity of the fiber diameters of the spidroin variants. **(a)** NTD-eADF4-CTD, the NTD-eADF3-CTD/NTD-eADF4-CTD homo- and heterodimers of **(b)** *in vivo* mixture and **(c)** *in vitro* mixture are shown.

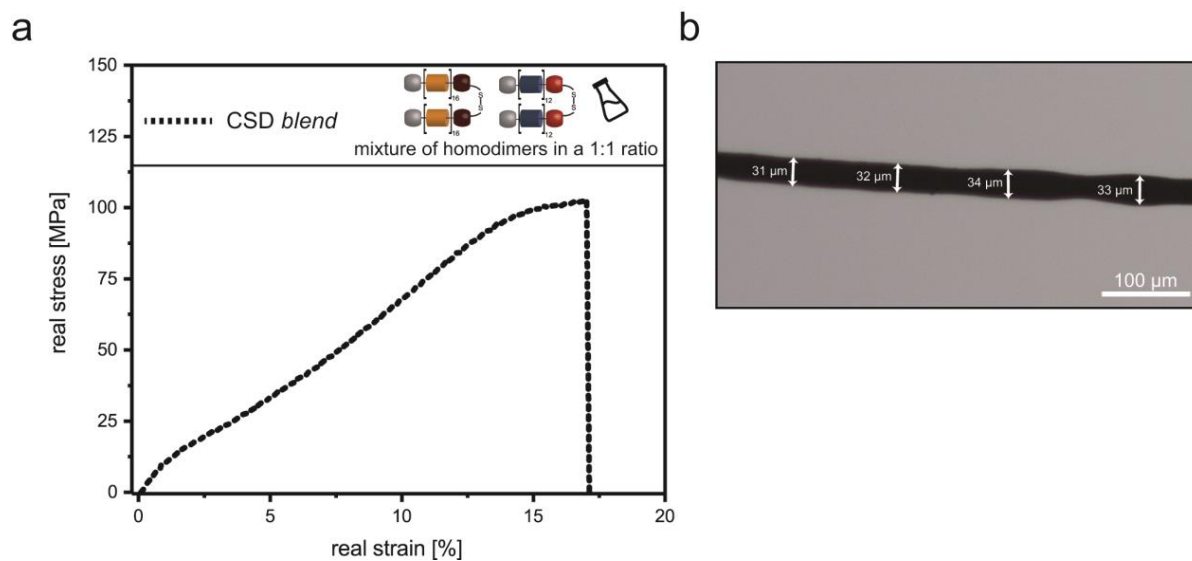


Figure S9. Real stress-strain curve of fibers spun from a CSD homodimer mixture comprising NTD-eADF3-CTD and NTD-eADF4-CTD in a 1:1 ratio. **(a)** Tensile test of post-stretched and post-treated fibers, **(b)** light microscopy image of such fibers.

Publication III

Two-In-One Spider Silk Protein with Combined Mechanical Features in All-Aqueous Spun Fibers

Saric, M. and Scheibel, T.

Biomacromolecules, 24(4), 1744-1750.

2023

Reprinted with kind permission from the publisher American Chemical Society.



pubs.acs.org/Biomac

Article

Two-in-One Spider Silk Protein with Combined Mechanical Features in All-Aqueous Spun Fibers

Merisa Saric and Thomas Scheibel*

Cite This: *Biomacromolecules* 2023, 24, 1744–1750

Read Online

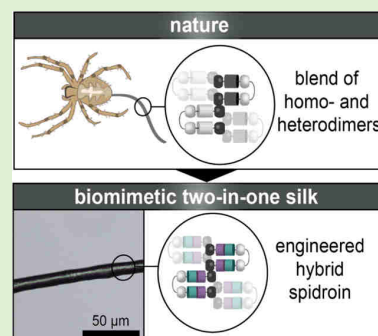
ACCESS |

Metrics & More

Article Recommendations

Supporting Information

ABSTRACT: Major ampullate (MA) spider silk reveals outstanding mechanical properties in terms of a unique combination of high tensile strength and extensibility, unmatched by most other known native or synthetic fiber materials. MA silk contains at least two spider silk proteins (spidroins), and here, a novel two-in-one (TIO) spidroin was engineered, resembling amino acid sequences of such two of the European garden spider. The combination of mechanical and chemical features of both underlying proteins facilitated the hierarchical self-assembly into β -sheet-rich superstructures. Due to the presence of native terminal dimerization domains, highly concentrated aqueous spinning dopes could be prepared from recombinant TIO spidroins. Subsequently, fibers were spun in a biomimetic, aqueous wet-spinning process, yielding mechanical properties at least twice as high as fibers spun from individual spidroins or blends. The presented processing route holds great potential for future applications using ecological green high-performance fibers.



INTRODUCTION

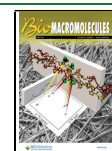
Spider silks are protein-based fibers attracting the interest of scientists for several applications, i.e., in biomedicine, electronics, and optics.^{1–3} One of the most significant challenges in fiber material research is mimicking the hierarchical self-assembly of silk proteins into fibers with multiple functionalities as found in nature. Mechanical spider silk fibers combine good tensile properties with high strains, reaching toughness values unmatched by most other fiber materials. Even though spider silks have been the focus of scientific research for decades, it is not yet possible to fabricate synthetic fibers finally mimicking the outstanding properties of their native counterparts due to their complex hierarchical architectures from the molecular to macroscopic level. A wide range of artificial spider silks exists; among them are protein fibers,⁴ non-protein fibers,⁵ hydrogel⁶/nanogel⁷ fibers, or carbon nanotube composite⁸ fibers. To imitate the characteristics of the natural blueprint, one approach is to stay as close to the natural process as possible, i.e., being biomimetic in an all-aqueous system, from spidroin to fiber. Spider major ampullate (MA) silk, also known as dragline silk, is the best investigated among spider silks.⁹ All so far analyzed MA silk threads are composed of at least two (often more) different proteins, classified as major ampullate spidroins (MaSps), varying in molecular weight, amino acid composition, and distribution within a fiber, suggesting a slightly different (mechanical) function.^{10–12} The best-characterized MaSps are MaSp1 and MaSp2 from different species, which mainly differ in their proline content, being low in MaSp1 (<1%) and high in MaSp2 (>10%).¹³ Interestingly, the MA silk of the garden spider *Araneus diadematus* contains two MaSp2 proteins,

namely, *A. diadematus* fibroin (ADF) 3 and 4.¹³ These proteins exhibit differences in hydrophobicity, with the hydrophilic ADF3 achieving high solubility, whereas ADF4 is more hydrophobic.¹⁴ All natural spider silk proteins share a similar tripartite architecture of a highly repetitive core domain, flanked by non-repetitive amino-terminal (NTD) and carboxyl-terminal (CTD) domains.¹⁵ Generally, the terminal domains (TDs) are highly conserved between different silk types and spiders, essential for storing spidroins at high concentrations and spidroin assembly upon external triggers such as shear stress, acidification, and ion exchange.^{16–19} Under non-reducing conditions, a disulfide-linked parallel oriented dimer is formed due to one conserved cysteine residue in the CTD.^{20–22} NTDs remain monomeric at neutral pH but dimerize in an anti-parallel fashion within milliseconds upon acidification.^{23–26} The properties of the natural proteins could be mimicked by engineered recombinant protein variants eADF3 and eADF4.¹⁴ Recently, we have shown that CTDs triggers heterodimerization of engineered eADFs.²⁷ Mixtures containing homo- and heterodimeric spidroins yielded high-performance fibers equaling that of natural spider silk concerning all important mechanical features such as tensile strength, elasticity, and toughness.²⁷ In contrast, blends

Received: December 19, 2022

Revised: February 5, 2023

Published: March 13, 2023



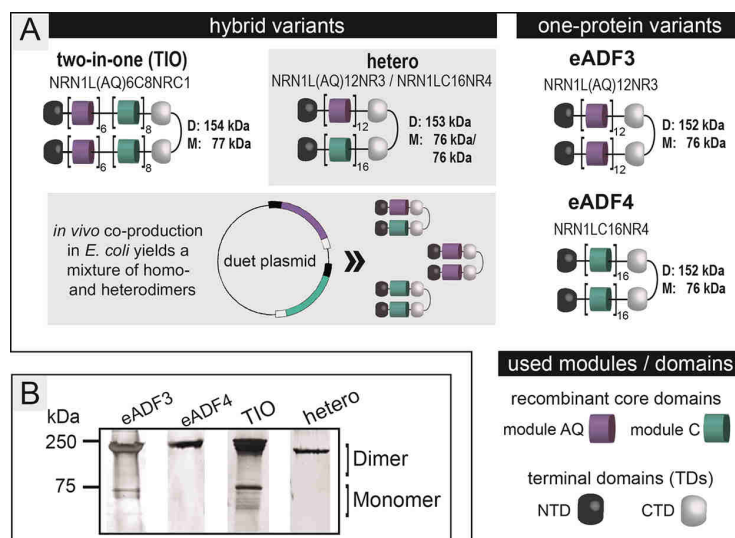


Figure 1. Design of a two-in-one (TIO) recombinant spider silk variant. (A) Sketch of ADF3 (consensus sequence module AQ) and ADF4 (consensus sequence module C), representing two different MaSp2 proteins of *A. diadematus* MA silk. Terminal domains (TDs) are highly conserved.^{16–19} Here, the C-terminal domains (CTDs) of either ADF3 (NR3), ADF4 (NR4), or MaSp1 of *Latrodectus hesperus* (NRC1) have been used. Since no N-terminal domains (NTD) of *A. diadematus* have been identified so far, the well-investigated NTD of MaSp1 of *L. hesperus* (NRN1L) was used in all cases. The respective amino acid sequences are given in Figure S1. The theoretical molecular weight of the respective proteins is shown, and further details on physicochemical properties are displayed in Table S1. Further, the molecular weights of monomers (M) and disulfide-linked dimers (D) are given. The heterodimer (hetero) was obtained upon co-production in *E. coli* using an expression vector with two multiple cloning sites. The heterodimer was isolated on-column (Figure S2) and used as a control. (B) Analysis of purified spidroins using silver-stained SDS-PAGE under non-reducing conditions.

containing individual eADF3 and eADF4 homodimers yielded fibers with significantly lower mechanical properties, highlighting that a combination of spidroin sequences in one setup has an unexpected impact on the properties of the gained fibers.²⁷ Here, it was aimed to exploit the features of both eADF3 and eADF4 in a single engineered spidroin to simplify fiber production.

MATERIALS AND METHODS

Cloning, Protein Production, and Purification. The engineered two-in-one (TIO) variant eADF(NRN1L(AQ)₆C₈NRC1), the reference spidroins eADF3(NRN1L(AQ)₁₂NR3), and eADF4(NRN1LC₁₆NR4), each containing a T7-tag, as well as the dual construct eADF(NRN1L(AQ)₁₂NR3/NRN1LC₁₆NR4) comprising both a T7- and His-Tag, were cloned using the pCS-system as previously reported.^{14,27} Amino acid sequences are given in Figure S1. Gene expression and protein purification of eADF(NRN1L(AQ)₆C₈NRC1), eADF3(NRN1L(AQ)₁₂NR3), and eADF4(NRN1LC₁₆NR4) were carried out in a column-free approach similar to the previously published strategy,^{14,27} whereas the heterodimeric protein was purified using an immobilized metal ion affinity chromatography (HisTrap HP, Sigma, USA) and an ion-exchange column (Q Sepharose FF, Sigma, USA), as depicted in Figure S2.

Protein Preparation. Freeze-dried proteins were dissolved in 6 M guanidinium thiocyanate (Carl Roth, Germany) and dialyzed against 10 mM Tris-buffer pH 6 or 8 (Carl Roth, Germany) at room temperature (RT) using dialysis tubings with a molecular weight cutoff of 6–8 kDa (Serva, Germany). Protein aggregates were separated upon centrifugation at 130,000g for 20 min at RT. Protein samples were investigated using 10–12.5% SDS-PAGE (5 μg protein) followed by silver-staining.

Analysis of Processed Spidroin Morphologies. Fibrils of different protein variants were prepared at conditions reported previously.^{28,29} Briefly, proteins assembled at 20–50 μM and 20 °C upon the addition of potassium phosphate (pH 8) at a final concentration of 75 mM. For shear-induced self-assembly assays,

100 μM spidroin samples were rotated in 75 mM potassium phosphate for 1.5 days at 25 rpm. Far-UV circular dichroism (CD) spectra were recorded in triplicate using cuvettes with 0.1 cm path lengths (Jasco J-715, Jasco, Germany) and subsequently smoothed by applying a Savitzky–Golay filter. Thermal transitions were measured at 15 μM and recorded at 222 nm with a heating rate of 1 °C min⁻¹. Chemical stability was analyzed at 15 μM with increasing concentrations of urea. Samples were incubated for 3 h and analyzed at 222 nm. For secondary structure analysis, Fourier transform infrared (FTIR) spectra were measured using attenuated total reflection (ATR) on a IFS 66s spectrometer (Bruker, USA) and scanned from 900 to 4000 cm⁻¹ with 60 accumulations averaged for each spectrum. For quantitative analysis, Fourier self-deconvolution (FSD) was employed, focusing on the peaks of the amide I band (1590 and 1705 cm⁻¹), and a baseline as well as air correction was performed. Calculations were performed using OPUS software (version 6.5, Bruker) according to a previous study.³⁰ Fluorescence spectra were monitored with a fluorescence spectrometer (Jasco FP6500, Jasco, Japan) using quartz cuvettes with 1 cm path length. For assembly kinetics, 10 μM thioflavine T (ThT) was added, and spectra were recorded in a range between 450 and 550 nm after excitation at 440 nm. For turbidity assays, spectra were recorded at 340 nm in triplicate using UV/Vis spectrometry (Varian Cary 50, Agilent Technologies, USA). Transmission electron microscope (JEOL JEM-2100, Germany) images were taken using a device camera (UltraScan 4000, Gatan Inc., USA) with Gatan Digital Micrograph software. Fluorescence, brightfield, and polarized microscopy studies were carried out using a stereomicroscope (DMI3000B, Leica, Germany) and 5×, 20×, or 40× object lenses. Birefringence was detected using a first polarizing lens at 90°, subsequently passing a second analyzer filter.

Production and Analysis of Fibers. Aqueous spinning dopes and fiber spinning were conducted as previously reported.^{4,27} Briefly, proteins in 50 mM Tris-buffer (pH 8) and 150 mM NaCl were either dialyzed against a 25% PEG (40 kDa) solution to obtain CSD or 25 mM phosphate buffer (pH 8) for BSD preparation. Further, fibers were spun in a microfluidic chip upon extrusion of spinning dopes at

flow rates of 150–300 $\mu\text{L}/\text{h}$ into a coagulation bath filled with 1 M potassium phosphate buffer (pH 6). As sheath flowed, potassium phosphate buffer (pH 8) was used at flow rates of 1000–1500 $\mu\text{L}/\text{h}$. All fibers were post-stretched to maximum, post-treated in 80% isopropyl alcohol, and analyzed by optical microscopy. Several representative images were investigated from each fiber at different sites ($n \geq 10$) to measure the quadratic mean of the fiber diameter and its standard deviation. Further, fiber sections ($n \geq 7$) were fixed on plastic sample holders with a 2 mm gap using superglue (UHU GmbH Co. KG, Germany). Tensile testing (BOSE Electroforce 3220, USA) was conducted using a 0.49 N load cell at a pulling rate of 0.005 mm/s at 30% relative humidity. Mechanical properties were quantitatively evaluated using Microsoft Excel 2016 (Microsoft Corporation, USA) or Origin 9.4 (OriginLab Corporation, USA) from real stress and real strain data.

RESULTS AND DISCUSSION

Based on the natural sequences of ADF3 and ADF4 of *A. diadematus*, a two-in-one (TIO) spidroin was engineered in the presence of TDs (Figure 1A, Figure S1). For comparison, the hetero variant was isolated from an *in vivo* (*Escherichia coli*) co-produced mixture of homo- and heterodimeric spidroins using a two-step chromatographic purification strategy (Figure S2). The TIO spidroin could be produced using a fast and inexpensive large-scale production strategy, resulting in a 25 times higher batch yield than that of the hetero one. Both purified hybrid variants were analyzed using non-reducing SDS-PAGE and compared to reference one-protein variants (Figure 1B). Theoretical biochemical properties, such as molecular weight, pI, number of charged amino acid residues, and mean hydropathicity, display high similarities between the hybrid spidroins and reference spidroins (Table S1). Next, the secondary structure of each hybrid spidroin in solution (before fiber spinning) was investigated using far-ultraviolet circular dichroism (far UV-CD) spectroscopy, displaying no significant differences (Figure 2A,B). The spectra exhibited random coil structures derived from the core domain and α -helical structures from the folded termini, resembling five-helix bundles.^{20,31} After unfolding at 90 °C, folding was fully

reversible upon cooling. The temperature-induced unfolding of the hybrid spidroins revealed melting temperatures (T_m) at 54.5 °C for the TIO variant and 59.2 °C for the hetero variant (Figure 2C). In urea-induced unfolding experiments, the hetero spidroin showed higher structural stabilities (4.6 M) compared to the TIO one (3.7 M) (Figure 2D).

Shear stress and kosmotropic salts are essential stimuli in natural spider silk fiber assembly, accompanied by an increase in β -sheet structures of the spidroins.^{32–34} In a rotation-induced experimental setup, the TIO and the hetero spidroin yielded thick insoluble fibrillary bundles in the micrometer range, comparable to the eADF3 control (Figure 3A I, IV, VII). As reported previously, eADF3 revealed a strong assembly behavior upon shearing, enhanced in the presence of TDs.^{20,35–37} Polarized light microscopy displayed assemblies made from eADF3-containing spidroins as birefringent, indicating a high β -sheet content and highly ordered crystalline structures (Figure 3A II, V, VIII). In contrast, eADF4 has been found to poorly assemble in response to elongation flow,³⁷ which could be supported by our findings (Figure 3A X, XI). The amyloid-specific dye Thioflavin T (ThT) was used to potential amyloidogenic characteristics of spidroin assemblies as ThT binds to cross- β -sheet structures.^{38,39} Here, ThT fluorescence clearly indicated the presence of cross- β -sheet structures (Figure 3A III, VI, IX, XII). Next, self-assembly was analyzed upon the addition of phosphate ions in the absence of mechanical shearing since kosmotropic ions enhance the intermolecular interaction between the hydrophobic polyalanine stretches and induce salting out.^{14,35} Previous studies have shown differences in hydropathicity of eADF3 and eADF4, playing a decisive role in the assembly performance.^{14,27,40} eADF3 is known to be more hydrophilic, whereas eADF4 appears to be more hydrophobic. Therefore, eADF3 shows a lower assembly behavior in aqueous environments and hence less ThT-specific fluorescence compared to eADF4 and TIO with eADF4 content. Here, all eADF4-comprising variants self-assembled in fibrillary structures as demonstrated by transmission electron microscopy (TEM) (Figure 3 XIII, XIV, XVI), showing similar assembly kinetics (Figure 3B). While eADF4 homodimers formed short nanofibril fragments, a highly interconnected network of branched nanofibrils was observed for the TIO and the hetero variant (Figure 3 XIII, XIV, XVI). In contrast, eADF3 showed the slowest kinetics and self-assembled yielding disordered aggregates (Figure 3 XV). In the presence of the β -sheet sensitive dye ThT, eADF4 and both hybrid variants displayed a much higher fluorescence than eADF3 (Figure 3C). The secondary structures of phosphate-induced assemblies were analyzed using Fourier transform infrared (FTIR) spectroscopy and Fourier self-deconvolution (FSD) of the amide I band between 1700 and 1600 cm^{-1} (Figure S3, Table S2). The data indicated a high content of β -sheets and, among all spidroin variants, the highest values being found in eADF4 variants.

Next, fibers were produced to investigate assembly and mechanics using a biomimetic multichannel microfluidic device and phosphate-containing coagulation baths (Figure 4A), as described previously.^{4,27} Briefly, important key factors of spiders' natural spinning process were incorporated in fiber assembly. The spidroins have been exposed to shear forces on their way from the syringe to the microfluidic chip and further pre-assembled upon addition of phosphate at low concentrations. As soon as the spidroin solution is extruded into the coagulation bath, containing high phosphate concentrations at

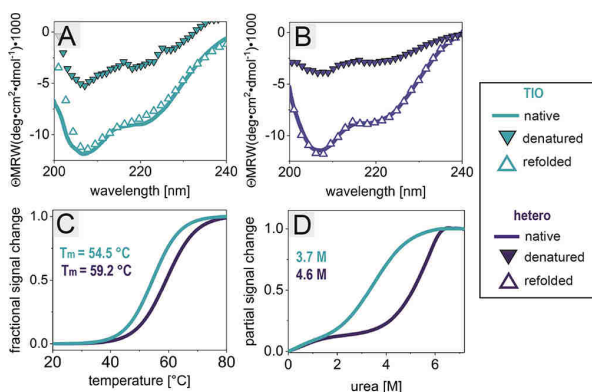


Figure 2. Structural characterization of hetero and TIO spidroins with terminal domains at pH 6, which initiated dimerization of the NTDs. (A, B) Far-UV spectra upon thermal degradation. The molar ellipticity was initially determined at 20 °C (native). Then, samples were heated to 90 °C (denatured) and again cooled to 20 °C (refolded). (C) Thermal stability and (D) chemical stability using CD ellipticity at 222 nm. The melting temperature T_m and given urea concentration refer to the condition at which half of the proteins are denatured.

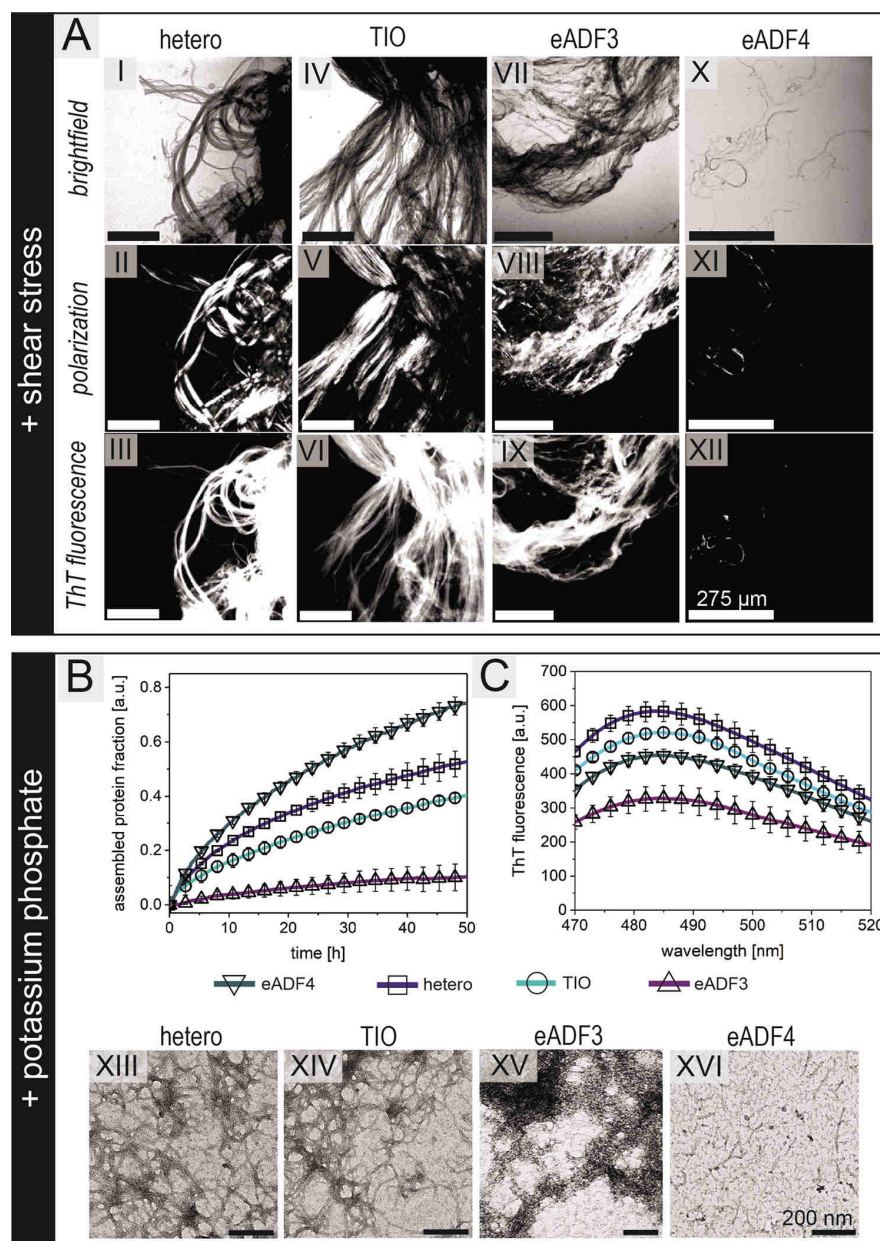


Figure 3. Self-assembly of different spidroin variants. (A) Microscopy images of macroscopic fibers formed by rotation. Samples were analyzed using brightfield (I, IV, VII, X) and polarized light (II, V, VIII, XI), highlighting locations of maximum birefringence, and further stained with Thioflavin T (ThT) (III, VI, IX, XII) to identify cross- β -sheet formation. For polarized light microscopy, the light was primarily polarized at 90° using a first polarizing lens and then passed through a second filter (analyzer). Scale bars represent 275 μm . Phosphate-induced fibril assembly kinetics by measuring (B) turbidity at 340 nm and (C) thioflavin T staining of nanofibrils indicating cross- β -sheet-rich structures. Self-assembly of the spidroin variants was investigated using TEM (XIII–XVI). Scale bars represent 200 nm.

low pH, a fiber is formed. The fibers were post-stretched to maximum and post-treated in a mixture of water and isopropanol. While isopropyl alcohol adds to the extensibility of the fiber, allowing the proteins to align along the fiber axis,⁴¹ water works as a plasticizer, rendering fibers less brittle.⁴² Highly concentrated aqueous spinning dopes (10–15% w/v) could be produced exclusively with variants comprising TDs since they considerably increase solubility and control phase transition from an aqueous spidroin dope solution to a water-insoluble solid fiber upon chemical and physical triggers. TDs

act as molecular switches by sensing changes in pH, ions, and shearing forces during spinning.^{17,20,35} In the highly concentrated dope, spidroins form micelle-like structures as hydrophilic TDs form an interface to protect the more hydrophobic repetitive core domain from the aqueous environment.^{4,35,43} Lowering the pH has contrary structural effects on the TDs. While amino-terminal domains (NTDs) form stable antiparallel dimers, carboxy-terminal domains (CTDs) induce a slight change in conformation.^{20,24,34,44} Upon the addition of kosmotropic potassium and phosphate

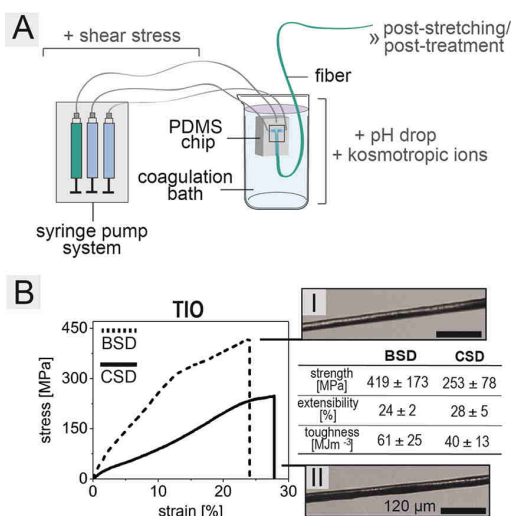


Figure 4. Bioinspired all-aqueous microfiber production. (A) Microfluidics setup using a chip connected to a syringe pump. Fibers were spun upon the extrusion of aqueous spinning dopes into a coagulation bath filled with potassium phosphate buffer. (B) True stress–strain curves of post-stretched wet-spun fibers from classical (CSD) or biomimetic (BSD) spinning dopes are shown. Light microscopic images of BSD (I) and CSD (II) fibers are displayed. Scale bars represent 120 μm . Details on mechanical properties are given in Table S3.

ions, CTDs partially refold and subsequently expose hydrophobic areas, allowing spidroins to salt-out. In combination with shearing, core domains align, and the assembly from soluble, intrinsically unfolded spidroins into solid β -sheet-rich fibers is promoted. Due to the significantly higher spidroin yields, only fibers from the TIO variant were processed but not from heterodimers. Classical spinning dopes (CSD) were prepared upon dialysis against polyethylene glycol (PEG) to remove water, which yields high protein concentrations. Biomimetic spinning dopes (BSD) could be obtained by dialysis against a phosphate buffer, inducing self-assembly of spidroins into a phase-separated viscous dope. Mechanical properties of BSD fibers spun from TIO spidroins exhibited a tensile strength of 419 ± 173 MPa, toughness of 61 ± 25 MJ m^{-3} , and Young's modulus of 4 ± 2 GPa (Figure 4B, Table S3). The BSD fibers could be post-stretched up to 400% and yielded significantly higher mechanical properties than CSD fibers (post-stretched up to 350%). They exhibit a higher molecular order due to the increased alignment of nanocrystals and amorphous structures as analyzed previously in the case of similar spidroins using SAXS and FTIR measurements.⁴⁵ The foundation for a high molecular structural order in the characteristic secondary structure elements is set in the dope preparation since phosphate buffer in the biomimetic dope initiates self-assembly and pre-structuring of the spidroins. The overall mechanical properties of BSD fibers were at least twice as good compared to blends from individual full-length eADF3 or eADF4 (Table S3) as they exhibit low processability features due to the different assembly mechanisms.²⁷ However, our previous study obtained native-like performing fibers (834 ± 34 MPa, 143 ± 6 MJ m^{-3} , 5 ± 0.2 GPa) spun from an *in vivo* co-produced spidroin mixture of three dimeric spidroin variants. In the TIO spidroin BSD fibers, similar Young's modulus properties and half the strength compared to the

spidroin mixture were obtained. Notably, compared to fibers spun using fully aqueous spinning setups in other studies, the strength of our BSD fibers spun from the TIO spidroin was consistently twice as high.^{46,47} The mechanical performance of fibers improves with a higher molecular weight of the recombinant spidroins.⁴⁸ Further, the dope preparation method has a decisive influence on the pre-assembly and fiber performance. The concentration of a protein solution by removing water leads to a different self-assembly than using a biomimetic approach with phosphate ions.⁴⁵ The coagulation bath combined important key factors of the natural spidroin assembly process such as kosmotropic ions and low pH, and obtained fibers were post-stretched as well as post-treated adding to the fibers extensibility and allowing the proteins to align along the fiber axis.

CONCLUSIONS

In summary, we utilized the characteristics and functions of both eADF3 and eADF4 to engineer a new spider silk variant with multifunctional properties (Figure 5). Here, our

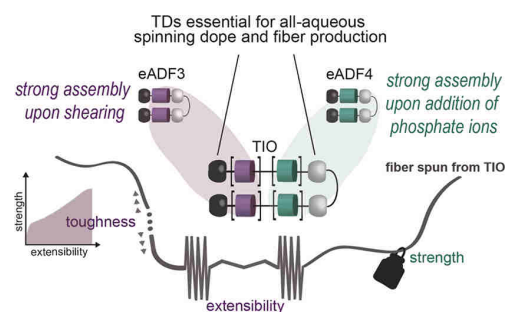


Figure 5. Illustration of the impact of individual TIO spidroin domains on self-assembly. TDs play a crucial role as solubility prerequisites, enabling spinning dope assembly up to high concentrations (10–15% w/v). The core domain of the TIO spidroin combines the biophysical and biochemical characteristics of both underlying eADF3 and eADF4 spidroins. In solution, eADF3 contributes to a strong assembly behavior upon shearing, and eADF4 facilitates nanofibrillation upon the addition of phosphate ions. Fibers spun from TIO comprise toughness and extensibility, which are provided by eADF3, as well as strength, which is provided by eADF4.

engineered two-in-one (TIO) spidroin follows the sequence-structure-function design principles of the natural blueprint regarding the self-assembly into β -sheet-rich hierarchical superstructures, which blends or one-protein variants could not achieve.^{27–29,49–51} TIO showed assembly behaviors of both underlying eADF3 and eADF4 sequences and revealed similar responses to environmental changes compared to the hetero variant. The combination of chemical and mechanical trigger features, such as shearing and salting out, is an important prerequisite for fiber formation. Further, functionalization with TDs precisely controls highly concentrated solutions' performance, yielding spinning dopes that are well suited for fiber spinning in all-aqueous approaches. We presented a strategy to conveniently produce TIO spidroins at a large scale, in decent yields, and of high quality, paving the way for green high-performance fibers made in an all-aqueous spinning process.

■ ASSOCIATED CONTENT

Supporting Information

The Supporting Information is available free of charge at <https://pubs.acs.org/doi/10.1021/acs.biomac.2c01500>.

Amino acid sequences of the used modules/domains (Figure S1), isolation strategy of heterodimers out of a spidroin mixture (Figure S2), physicochemical properties of the spidroin variants (Table S1), secondary structure content of phosphate-induced assemblies (Figure S3, Table S2), and comparison of mechanical properties of artificially spun fibers (Table S3) (PDF)

■ AUTHOR INFORMATION

Corresponding Author

Thomas Scheibel – Lehrstuhl Biomaterialien, Universität Bayreuth, 95447 Bayreuth, Germany; Bayreuther Zentrum für Kolloide und Grenzflächen (BZKG), Bayreuther Materialzentrum (BayMat), and Bayreuther Zentrum für Molekulare Biowissenschaften (BZMB), Universität Bayreuth, 95440 Bayreuth, Germany; Bayrisches Polymerinstitut (BPI), Universität Bayreuth, 95440 Bayreuth, Germany; orcid.org/0000-0002-0457-2423; Email: thomas.scheibel@bm.uni-bayreuth.de

Author

Merisa Saric – Lehrstuhl Biomaterialien, Universität Bayreuth, 95447 Bayreuth, Germany

Complete contact information is available at:

<https://pubs.acs.org/doi/10.1021/acs.biomac.2c01500>

Author Contributions

M.S. and T.S., conceptualization; M.S., investigation; M.S., writing (original draft); T.S., writing (review and editing); M.S., visualization; T.S., supervision.

Notes

The authors declare the following competing financial interest(s): T. S. is the founder and share-holder of AMSilk GmbH.

■ ACKNOWLEDGMENTS

This work was supported by the German Research Foundation (DFG) in the framework of the Collaborative Research Centre SFB 840 project A08. The authors would like to thank Anika Winkler and Dr. Tamara Aigner for transmission electron microscopy imaging.

■ REFERENCES

- (1) Liu, Y.; Ren, J.; Ling, S. Bioinspired and biomimetic silk spinning. *Compos. Commun.* **2019**, *13*, 85–96.
- (2) Strassburg, S.; Zainuddin, S.; Scheibel, T. The Power of Silk Technology for Energy Applications. *Adv. Energy Mater.* **2021**, *11*, 2100519.
- (3) Aigner, T. B.; DeSimone, E.; Scheibel, T. Biomedical applications of recombinant silk-based materials. *Adv. Mater.* **2018**, *30*, 1704636.
- (4) Heidebrecht, A.; Eisoldt, L.; Diehl, J.; Schmidt, A.; Geffers, M.; Lang, G.; Scheibel, T. Biomimetic fibers made of recombinant spidroins with the same toughness as natural spider silk. *Adv. Mater.* **2015**, *27*, 2189–2194.
- (5) Dou, Y.; Wang, Z.-P.; He, W.; Jia, T.; Liu, Z.; Sun, P.; Wen, K.; Gao, E.; Zhou, X.; Hu, X. Artificial spider silk from ion-doped and twisted core-sheath hydrogel fibres. *Nat. Commun.* **2019**, *10*, 1–10.
- (6) Wu, Y.; Shah, D. U.; Liu, C.; Yu, Z.; Liu, J.; Ren, X.; Rowland, M. J.; Abell, C.; Ramage, M. H.; Scherman, O. A. Bioinspired supramolecular fibers drawn from a multiphase self-assembled hydrogel. *Proc. Natl. Acad. Sci. U. S. A.* **2017**, *114*, 8163–8168.
- (7) He, W.; Qian, D.; Wang, Y.; Zhang, G.; Cheng, Y.; Hu, X.; Wen, K.; Wang, M.; Liu, Z.; Zhou, X.; Zhu, M. Protein-Like Nanogel for Spinning Hierarchically Structured Artificial Spider Silk. *Adv. Mater.* **2022**, *34*, 2201843.
- (8) Fang, G.; Zheng, Z.; Yao, J.; Chen, M.; Tang, Y.; Zhong, J.; Qi, Z.; Li, Z.; Shao, Z.; Chen, X. Tough protein–carbon nanotube hybrid fibers comparable to natural spider silks. *J. Mater. Chem. B* **2015**, *3*, 3940–3947.
- (9) Gosline, J.; Guerette, P.; Ortlepp, C.; Savage, K. The mechanical design of spider silks: from fibroin sequence to mechanical function. *J. Exp. Biol.* **1999**, *202*, 3295–3303.
- (10) Correa-Garhwal, S. M.; Clarke, T. H.; Janssen, M.; Crevecoeur, L.; McQuillan, B. N.; Simpson, A. H.; Vink, C. J.; Hayashi, C. Y. Spidroins and silk fibers of aquatic spiders. *Sci. Rep.* **2019**, *9*, 1–12.
- (11) Kono, N.; Nakamura, H.; Mori, M.; Yoshida, Y.; Ohtoshi, R.; Malay, A. D.; Moran, D. A. P.; Tomita, M.; Numata, K.; Arakawa, K. Multicomponent nature underlies the extraordinary mechanical properties of spider dragline silk. *Proc. Natl. Acad. Sci. U. S. A.* **2021**, *118*, No. e2107065118.
- (12) Garb, J. E.; Haney, R. A.; Schwager, E. E.; Gregorič, M.; Kuntner, M.; Agnarsson, I.; Blackledge, T. A. The transcriptome of Darwin's bark spider silk glands predicts proteins contributing to dragline silk toughness. *Commun. Biol.* **2019**, *2*, 1–8.
- (13) Guerette, P. A.; Ginzinger, D. G.; Weber, B. H.; Gosline, J. M. Silk properties determined by gland-specific expression of a spider fibroin gene family. *Science* **1996**, *272*, 112–115.
- (14) Huemmerich, D.; Helsen, C. W.; Quedzuweit, S.; Oschmann, J.; Rudolph, R.; Scheibel, T. Primary structure elements of spider dragline silks and their contribution to protein solubility. *Biochemistry* **2004**, *43*, 13604–13612.
- (15) Xu, M.; Lewis, R. V. Structure of a protein superfiber: spider dragline silk. *Proc. Natl. Acad. Sci. U. S. A.* **1990**, *87*, 7120–7124.
- (16) Garb, J. E.; Ayoub, N. A.; Hayashi, C. Y. Untangling spider silk evolution with spidroin terminal domains. *BMC Evol. Biol.* **2010**, *10*, 1–16.
- (17) Bauer, J.; Scheibel, T. Conformational stability and interplay of helical N- and C-terminal domains with implications on major ampullate spidroin assembly. *Biomacromolecules* **2017**, *18*, 835–845.
- (18) Challis, R.; Goodacre, S.; Hewitt, G. Evolution of spider silks: conservation and diversification of the C-terminus. *Insect Mol. Biol.* **2006**, *15*, 45–56.
- (19) Beckwitt, R.; Arcidiacono, S. Sequence conservation in the C-terminal region of spider silk proteins (Spidroin) from *Nephila clavipes* (Tetragnathidae) and *Araneus bicentenarius* (Araneidae). *J. Biol. Chem.* **1994**, *269*, 6661–6663.
- (20) Hagn, F.; Eisoldt, L.; Hardy, J. G.; Vendrely, C.; Coles, M.; Scheibel, T.; Kessler, H. A conserved spider silk domain acts as a molecular switch that controls fibre assembly. *Nature* **2010**, *465*, 239–242.
- (21) Spöner, A.; Unger, E.; Grosse, F.; Weisshart, K. Conserved C-termini of spidroins are secreted by the major ampullate glands and retained in the silk thread. *Biomacromolecules* **2004**, *5*, 840–845.
- (22) Ittah, S.; Michaeli, A.; Goldblum, A.; Gat, U. A model for the structure of the C-terminal domain of dragline spider silk and the role of its conserved cysteine. *Biomacromolecules* **2007**, *8*, 2768–2773.
- (23) Askarieh, G.; Hedhammar, M.; Nordling, K.; Saenz, A.; Casals, C.; Rising, A.; Johansson, J.; Knight, S. D. Self-assembly of spider silk proteins is controlled by a pH-sensitive relay. *Nature* **2010**, *465*, 236–238.
- (24) Andersson, M.; Chen, G.; Otikovs, M.; Landreh, M.; Nordling, K.; Kronqvist, N.; Westermarck, P.; Jörnvall, H.; Knight, S.; Ridderstråle, Y.; Holm, L.; Meng, Q.; Jaudzems, K.; Chesler, M.; Johansson, J.; Rising, A. Carbonic anhydrase generates CO₂ and H⁺ that drive spider silk formation via opposite effects on the terminal domains. *PLoS Biol.* **2014**, *12*, No. e1001921.

- (25) Ries, J.; Schwarze, S.; Johnson, C. M.; Neuweiler, H. Microsecond folding and domain motions of a spider silk protein structural switch. *J. Am. Chem. Soc.* **2014**, *136*, 17136–17144.
- (26) Bauer, J.; Schaal, D.; Eisoldt, L.; Schweimer, K.; Schwarzingler, S.; Scheibel, T. Acidic residues control the dimerization of the N-terminal domain of black widow spiders' major ampullate spidroin 1. *Sci. Rep.* **2016**, *6*, 1–9.
- (27) Saric, M.; Eisoldt, L.; Döring, V.; Scheibel, T. Interplay of Different Major Ampullate Spidroins during Assembly and Implications for Fiber Mechanics. *Adv. Mater.* **2021**, *33*, 2006499.
- (28) Slotta, U. K.; Rammensee, S.; Gorb, S.; Scheibel, T. An engineered spider silk protein forms microspheres. *Angew. Chem., Int. Ed.* **2008**, *47*, 4592–4594.
- (29) Humenik, M.; Magdeburg, M.; Scheibel, T. Influence of repeat numbers on self-assembly rates of repetitive recombinant spider silk proteins. *J. Struct. Biol.* **2014**, *186*, 431–437.
- (30) Hu, X.; Kaplan, D.; Cebe, P. Determining beta-sheet crystallinity in fibrous proteins by thermal analysis and infrared spectroscopy. *Macromolecules* **2006**, *39*, 6161–6170.
- (31) Rising, A.; Hjälm, G.; Engström, W.; Johansson, J. N-terminal nonrepetitive domain common to dragline, flagelliform, and cylindrical spider silk proteins. *Biomacromolecules* **2006**, *7*, 3120–3124.
- (32) Eisoldt, L.; Smith, A.; Scheibel, T. Decoding the secrets of spider silk. *Mater. Today* **2011**, *14*, 80–86.
- (33) Knight, D. P.; Vollrath, F. Changes in element composition along the spinning duct in a *Nephila* spider. *Sci. Nat.* **2001**, *88*, 179–182.
- (34) Vollrath, F.; Knight, D. P. Liquid crystalline spinning of spider silk. *Nature* **2001**, *410*, 541–548.
- (35) Eisoldt, L.; Hardy, J. G.; Heim, M.; Scheibel, T. R. The role of salt and shear on the storage and assembly of spider silk proteins. *J. Struct. Biol.* **2010**, *170*, 413–419.
- (36) Bauer, J.; Scheibel, T. Dimerization of the conserved N-terminal domain of a spider silk protein controls the self-assembly of the repetitive core domain. *Biomacromolecules* **2017**, *18*, 2521–2528.
- (37) Rammensee, S.; Slotta, U.; Scheibel, T.; Bausch, A. Assembly mechanism of recombinant spider silk proteins. *Proc. Natl. Acad. Sci. U. S. A.* **2008**, *105*, 6590–6595.
- (38) Slotta, U.; Hess, S.; Spieß, K.; Stromer, T.; Serpell, L.; Scheibel, T. Spider silk and amyloid fibrils: a structural comparison. *Macromol. Biosci.* **2007**, *7*, 183–188.
- (39) Groenning, M. Binding mode of Thioflavin T and other molecular probes in the context of amyloid fibrils—current status. *J. Chem. Biol.* **2010**, *3*, 1–18.
- (40) Zbilut, J. P.; Scheibel, T.; Hümmerich, D.; Webber, C. L., Jr.; Colafranceschi, M.; Giuliani, A. Statistical approaches for investigating silk properties. *Appl. Phys. A: Mater. Sci. Process.* **2006**, *82*, 243–251.
- (41) Albertson, A. E.; Teulé, F.; Weber, W.; Yarger, J. L.; Lewis, R. V. Effects of different post-spin stretching conditions on the mechanical properties of synthetic spider silk fibers. *J. Mech. Behav. Biomed. Mater.* **2014**, *29*, 225–234.
- (42) Doblhofer, E.; Heidebrecht, A.; Scheibel, T. To spin or not to spin: spider silk fibers and more. *Appl. Microbiol. Biotechnol.* **2015**, *99*, 9361–9380.
- (43) Exler, J. H.; Hümmerich, D.; Scheibel, T. The amphiphilic properties of spider silks are important for spinning. *Angew. Chem., Int. Ed.* **2007**, *46*, 3559–3562.
- (44) Gauthier, M.; Leclerc, J.; Lefèvre, T.; Gagné, S. M.; Auger, M. Effect of pH on the structure of the recombinant C-terminal domain of *Nephila clavipes* dragline silk protein. *Biomacromolecules* **2014**, *15*, 4447–4454.
- (45) Anton, A. M.; Heidebrecht, A.; Mahmood, N.; Beiner, M.; Scheibel, T.; Kremer, F. Foundation of the outstanding toughness in biomimetic and natural spider silk. *Biomacromolecules* **2017**, *18*, 3954–3962.
- (46) Andersson, M.; Jia, Q.; Abella, A.; Lee, X.-Y.; Landreh, M.; Purhonen, P.; Hebert, H.; Tenje, M.; Robinson, C. V.; Meng, Q.; Plaza, G. R.; Johansson, J.; Rising, A. Biomimetic spinning of artificial spider silk from a chimeric minispidroin. *Nat. Chem. Biol.* **2017**, *13*, 262–264.
- (47) Hu, C.-F.; Qian, Z.-G.; Peng, Q.; Zhang, Y.; Xia, X.-X. Unconventional Spidroin Assemblies in Aqueous Dope for Spinning into Tough Synthetic Fibers. *ACS Biomater. Sci. Eng.* **2021**, *7*, 3608–3617.
- (48) Xia, X.-X.; Qian, Z.-G.; Ki, C. S.; Park, Y. H.; Kaplan, D. L.; Lee, S. Y. Native-sized recombinant spider silk protein produced in metabolically engineered *Escherichia coli* results in a strong fiber. *Proc. Natl. Acad. Sci. U. S. A.* **2010**, *107*, 14059–14063.
- (49) Borkner, C. B.; Lentz, S.; Müller, M.; Fery, A.; Scheibel, T. Ultrathin spider silk films: Insights into spider silk assembly on surfaces. *ACS Appl. Polym. Mater.* **2019**, *1*, 3366–3374.
- (50) Neubauer, V. J.; Trossmann, V. T.; Jacobi, S.; Döbl, A.; Scheibel, T. Recombinant Spider Silk Gels Derived from Aqueous–Organic Solvents as Depots for Drugs. *Angew. Chem., Int. Ed.* **2021**, *60*, 11847–11851.
- (51) Müller-Herrmann, S.; Scheibel, T. Enzymatic degradation of films, particles, and nonwoven meshes made of a recombinant spider silk protein. *ACS Biomater. Sci. Eng.* **2015**, *1*, 247–259.

Recommended by ACS

Anisotropic Frictional Properties Induced by Cellulose Nanofibril Assembly

Koichiro Ishida and Tetsuo Kondo

APRIL 06, 2023
BIOMACROMOLECULESREAD 

Wild Silkworm Cocoon Waste Conversion into Tough Regenerated Silk Fibers by Solution Spinning

Kenjiro Yazawa, Yasuo Gotoh, *et al.*MARCH 14, 2023
BIOMACROMOLECULESREAD 

Effects of Glucose and Coagulant on the Structure and Properties of Regenerated Cellulose Fibers

Jia Wei, Yi Nie, *et al.*MARCH 03, 2023
BIOMACROMOLECULESREAD 

The Glass Transition Temperature of Heterogeneous Biopolymer Systems

Suellen Pereira Espíndola, Stephen J. Picken, *et al.*MARCH 08, 2023
BIOMACROMOLECULESREAD 

Get More Suggestions >

Supporting Information

Two-In-One Spider Silk Protein with Combined Mechanical Features in All-Aqueous Spun Fibers

*Merisa Saric and Thomas Scheibel**

Additional Figures

Terminal domains (TDs)	
Amino-terminal domain	
NRN1L	
10	20
GQANTPWSSK ANADAFINSF ISAASNTGSF SQDQMEDMSL IGNTLMAAMD NMGGTRITPSK	
70	80
LQALDMAFAS SVAEIAASEG GDLGVTTNAI ADALTSAFYQ TTGVVNSRFI SEIRSLIGMF	
130	140
AQASANDVYA SAGSGSGGGG YGASSASAAS ASAAAPSGVA YQAPAQAQIS FTLRGQQPVS	
Carboxyl-terminal domains	
NR3	
10	20
GAASAAVSVG GYGPQSSSAP VASAAASRLS SPAASSRVSS AVSSLVSSGP TNQAALSNTI	
70	80
SSVVSQVSAS NPGLSGCDVL VQALLEVSA LVSILGSSI GQINYGASAQ YTMVGGQSV	
QALAG	
NR4	
10	20
GAYGPPSPAS ASVAASRLSS PAASSRVSSA VSSLVSSGPT NGAAVSGALN SLVSQISASN	
70	80
PGLSGCDALV QALLELVSA LVAISSASIG QVNVSSVSQS TQMISQALSG	
NRC1	
10	20
GSGPGQIYYG PQSVAAPAAA AASALAAPAT SARISSHASA LLSNGPTNPA SISNVISNAV	
70	80
SQISSNPGA SACDVLVQAL LELVTALLTI IGSSNIGSVN YDSSGQYAQV VTQSVQNAFAG	
Core domains	
A-module	
10	20
GPYGPASAAA AAAAGGYGPG SGQQ	
Q-module	
10	20
GPGQQGPGQQ GPGQQGPGQQ	
C-module	
10	20
GSSAAAAAAASGPGGYGPE NQGPGSGPGGY GPGGP	

Figure S1. Amino acid sequences of the used modules/domains. The sequence motifs of the highly repetitive core domains are derived from the MaSp2 analogs ADF3 and ADF4 from *A. diadematus*. While modules A and Q represent the consensus sequence of the core domain of ADF3, module C represents the consensus sequence of the core domain of ADF4. The modules were multimerized in an arbitrary seamless manner, as previously reported.¹ The highly conserved non-repetitive terminal domains derived from either *A. diadematus* (NR3 from ADF3, NR4 from ADF4) or *L. hesperus* (NRN1L and NRC1). So far, no amino-terminal domains from *A. diadematus* have been identified.

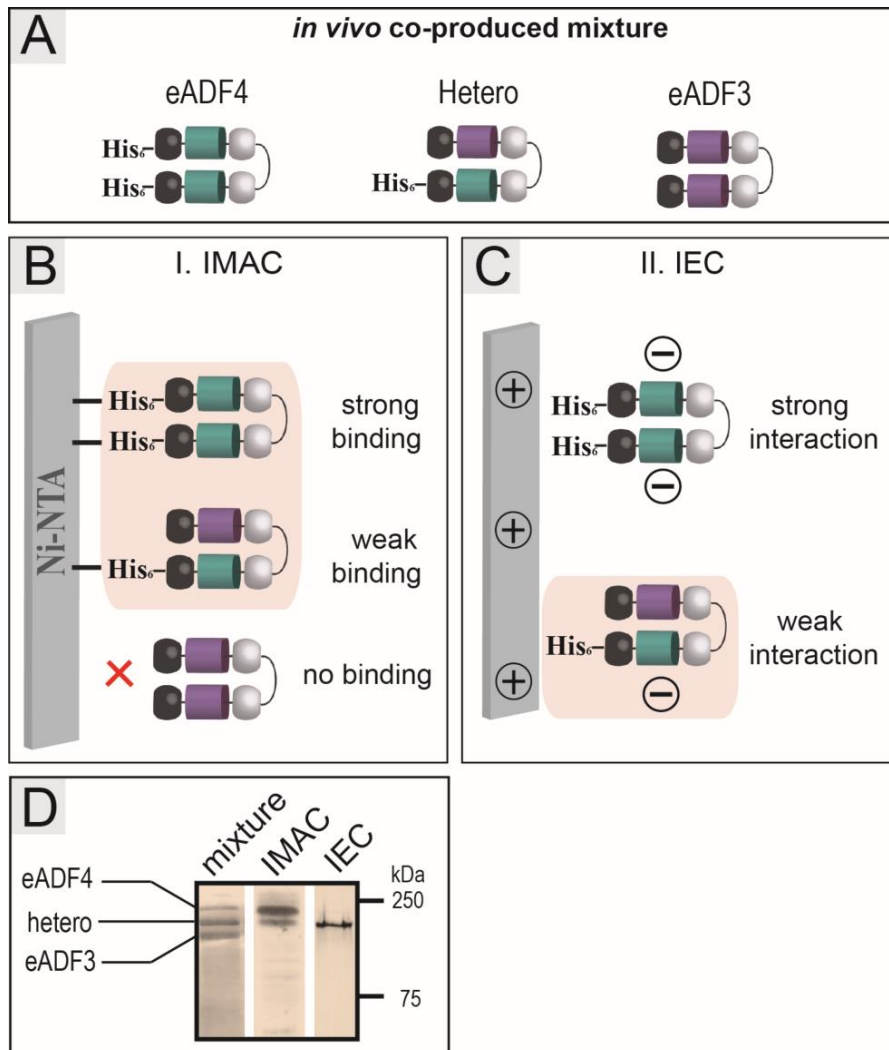


Figure S2. Schematic on-column isolation strategy of heterodimers out of a spidroin mixture. (A) The spidroin mixture containing homo- and heterodimers was obtained upon co-production in *E. coli* (*in vivo*) as depicted in Figure 1 a. To distinguish between the spidroins, eADF4 comprised a hexahistidine (His₆)-tag. (B) In an immobilized metal affinity chromatography (IMAC) using a Ni-NTA column, non-tagged eADF3 homodimers elute, while His₆-tagged eADF4 variants bind, yielding a remaining mixture of eADF4 homodimers and heterodimers. (C) Next, using an ion-exchange chromatography (IEC), heterodimers elute earlier than eADF4 homodimers since fewer negative charges result in weaker interactions. (D) Silver-stained SDS-PAGE analyzing the purification efficiency of the heterodimer isolation from a mixture containing all three dimeric eADF variants.

Table S1. Physico-chemical properties of the spidroin variants two-in-one (TIO), heterodimer (hetero), and the respective one-protein controls in the presence of TDs, the given data refers to dimeric constructs.

Protein	Physico-chemical properties			
	Molecular weight [kDa]	Theoretical pI	Number of charged amino acid residues (negative / positive)	Mean hydropathicity
TIO	154	4.0	46 / 14	-0.40
hetero	153	4.3	44 / 18	-0.39
eADF3	152	4.4	28 / 18	-0.54
eADF4	152	4.3	60 / 18	-0.24

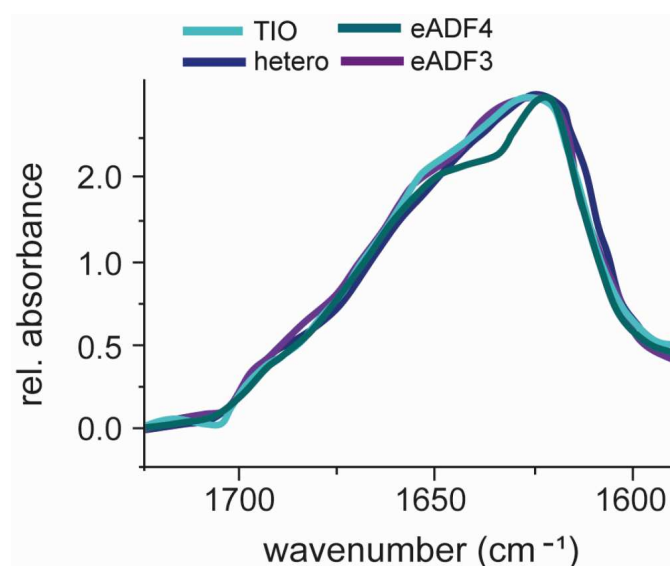


Figure S3. FTIR spectroscopy (amide I region 1595-1705 cm^{-1}) analysis of phosphate-induced assemblies of two-in-one (TIO), heterodimer (hetero), and the respective one-protein variants in the presence of TDs.

Table S2. Secondary structures of spidroins assembled in phosphate buffer. Fourier self-deconvolution (FSD) of the amide I region was used to assign particular structural elements of the proteins. Structural contents were calculated using FSD of the respective amide I bands (Figure S3). Peaks assignments were taken from literature.²

Secondary structure	TIO	hetero	eADF4	eADF3
side chain	7 ± 1	7 ± 2	7 ± 1	6 ± 1
β-sheet	39 ± 3	42 ± 3	38 ± 3	33 ± 2
random coils	23 ± 2	25 ± 2	27 ± 2	29 ± 2
α-helices	8 ± 1	8 ± 2	8 ± 1	8 ± 1
turns	23 ± 2	18 ± 2	20 ± 2	24 ± 2

Table S3. Comparison of mechanical properties of artificially spun fibers made of TIO spidroins comprising TDs. Fibers were spun in an all-aqueous biomimetic setup from classical spinning dopes (CSD) 10-13 % w/v and biomimetic (BSD) 15 % w/v spinning dopes, post-stretched and post-treated. Tensile testing was performed at room temperature and 30 % RH. Details on individual contribution of eADF3 and eADF4 in TIO are illustrated in Figure 3 b.

Protein	eADF3 ^{3, [a]}		eADF4 ³		Blend of eADF3 and eADF4 ^{3, [a]}		Two-in-one	
	CSD	BSD	CSD	BSD	CSD	BSD n. a. ^[b]	CSD	BSD
Dope	CSD	BSD	CSD	BSD	CSD	BSD n. a. ^[b]	CSD	BSD
Stretching [%]	600	600	300	300	300	-	350	400
Diameter [μm]	31 ± 0.5	23 ± 1	29 ± 0.2	33 ± 0.3	32 ± 3	-	21 ± 3	18 ± 4
Extensibility [%]	59 ± 1	80 ± 1	8 ± 0.2	10 ± 0.2	17 ± 5	-	28 ± 5	24 ± 2
Strength [MPa]	239 ± 12	329 ± 11	417 ± 15	602 ± 26	103 ± 21	-	253 ± 78	419 ± 173
Toughness [MJm ⁻³]	71 ± 3	137 ± 6	17 ± 1	32 ± 2	11 ± 4	-	40 ± 13	61 ± 25
Young's Modulus [GPa]	1 ± 0.1	3 ± 0.3	4 ± 0.4	6 ± 0.5	1 ± 0.6	-	2 ± 1	4 ± 2
Number of samples	6	7	7	7	9	-	8	8

^[a] Fibers produced in a coagulation bath comprising 80% isopropyl alcohol. ^[b] n. a.: not available

References

- (1) Huemmerich, D.; Helsen, C. W.; Quedzuweit, S.; Oschmann, J.; Rudolph, R.; Scheibel, T. Primary structure elements of spider dragline silks and their contribution to protein solubility. *Biochemistry* **2004**, *43* (42), 13604-13612.
- (2) Hu, X.; Kaplan, D.; Cebe, P. Determining beta-sheet crystallinity in fibrous proteins by thermal analysis and infrared spectroscopy. *Macromolecules* **2006**, *39* (18), 6161-6170.
- (3) Saric, M.; Eisoldt, L.; Döring, V.; Scheibel, T. Interplay of Different Major Ampullate Spidroins during Assembly and Implications for Fiber Mechanics. *Advanced Materials* **2021**, *33* (9), 2006499.

Publication IV

Tyrosine's Unique Role in the Hierarchical Assembly of Recombinant Spider Silk Proteins: From Spinning Dope to Fibers

Stengel, D., Saric, M., Johnson, H. R., Schiller, T., Diehl, J., Chalek, K., Onofrei D.,
Scheibel, T., and Holland, G. P.

Biomacromolecules, 24(3), 1463-1474.

2023

Reprinted with kind permission from the publisher American Chemical Society.



pubs.acs.org/Biomac

Article

Tyrosine's Unique Role in the Hierarchical Assembly of Recombinant Spider Silk Proteins: From Spinning Dope to Fibers

Dillan Stengel, Merisa Saric, Hannah R. Johnson, Tim Schiller, Johannes Diehl, Kevin Chalek, David Onofrei, Thomas Scheibel, and Gregory P. Holland*

Cite This: *Biomacromolecules* 2023, 24, 1463–1474

Read Online

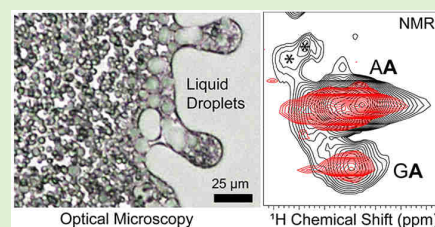
ACCESS |

Metrics & More

Article Recommendations

Supporting Information

ABSTRACT: Producing recombinant spider silk fibers that exhibit mechanical properties approaching native spider silk is highly dependent on the constitution of the spinning dope. Previously published work has shown that recombinant spider silk fibers spun from dopes with phosphate-induced pre-assembly (biomimetic dopes) display a toughness approaching native spider silks far exceeding the mechanical properties of fibers spun from dopes without pre-assembly (classical dopes). Dynamic light scattering experiments comparing the two dopes reveal that biomimetic dope displays a systematic increase in assembly size over time, while light microscopy indicates liquid–liquid-phase separation (LLPS) as evidenced by the formation of micron-scale liquid droplets. Solution nuclear magnetic resonance (NMR) shows that the structural state in classical and biomimetic dopes displays a general random coil conformation in both cases; however, some subtle but distinct differences are observed, including a more ordered state for the biomimetic dope and small chemical shift perturbations indicating differences in hydrogen bonding of the protein in the different dopes with notable changes occurring for Tyr residues. Solid-state NMR demonstrates that the final wet-spun fibers from the two dopes display no structural differences of the poly(Ala) stretches, but biomimetic fibers display a significant difference in Tyr ring packing in non- β -sheet, disordered helical domains that can be traced back to differences in dope preparations. It is concluded that phosphate pre-orders the recombinant silk protein in biomimetic dopes resulting in LLPS and fibers that exhibit vastly improved toughness that could be due to aromatic ring packing differences in non- β -sheet domains that contain Tyr.



INTRODUCTION

Spider dragline silk exhibits extraordinary mechanical properties combining high strength and moderate extensibility that result in fiber toughness that exceeds most natural and synthetic fibers.^{1–6} The proteins that comprise dragline silk are large (250–500 kDa), highly repetitive structural proteins coined spidroins. The earliest and best-known examples of these spidroins are major ampullate spidroin 1 and 2 (MaSp1 and 2) that encompass the majority of spider dragline or major ampullate (MA) silk.^{7–9} Although significant progress has been made in the production of recombinant spider silk proteins, the mechanical properties of reconstituted man-made fibers based on recombinant systems have never reached those of native dragline spider silks.^{10–14} This is due to a number of factors including challenges in producing recombinant protein with high molecular weight,¹⁵ the lack of understanding all details of silk protein assembly within the MA gland and the highly controlled subsequent fiber spinning process that occurs within the duct. The spider silk proteins experience a multitude of processing conditions in the spinning duct that include ion-exchange processes,¹⁶ an acidic pH gradient responsible for pH-triggered assembly,^{17,18} dehydration,¹⁹ and shear flow^{20,21} all of which contribute to the silk assembly process and subsequent mechanical properties of the fibers.

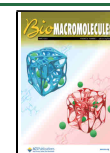
Producing recombinant spider silk fibers that exhibit mechanical properties approaching that of the natural ones suffers from several key knowledge gaps. These gaps mainly lie in understanding the atomic, molecular, and mesoscale structural regime of spider silk protein assembly and how features on these length scales correlate with macroscale material properties. On these length scales, the influence of salt content, pH, and concentration on the soluble protein plays a key role in determining the final structure of spun fibers.²² Determined efforts to understand this process have yet to yield a processing scheme to achieve large quantities of tunable silk fibers that rival their native counterparts.²³ The propensity to aggregate, high sequence repetitiveness, and complexity of the native spinning system requires a combination of biophysical techniques to properly interrogate.

Previously, recombinant spider silk fibers have been produced under aqueous native-like conditions of reasonably

Received: December 10, 2022

Revised: February 2, 2023

Published: February 15, 2023



high strength and extensibility, resulting in a toughness approaching that of native spider silk.^{5,24} This recombinant protein has been studied in a variety of iterations since it can be readily modified to include or exclude either termini and contains an adjustable number of (AQ) repeats.^{5,24} The engineered spidroin variant (AQ)₁₂NR3 is composed of 44 residue blocks repeated 12 times, followed by a non-repetitive C-terminal helical domain bringing the molecular weight to ~59 kDa (Figure 1).²⁴ It has been previously shown that the

```

GPYGPASAAAAAGGYGPGSGQQGPGQQGPGQQGPGQQGPGQQ
GPYGPASAAAAAGGYGPGSGQQGPGQQGPGQQGPGQQGPGQQ
GPYGPASAAAAAGGYGPGSGQQGPGQQGPGQQGPGQQGPGQQ
GPYGPASAAAAAGGYGPGSGQQGPGQQGPGQQGPGQQGPGQQ
GPYGPASAAAAAGGYGPGSGQQGPGQQGPGQQGPGQQGPGQQ
GPYGPASAAAAAGGYGPGSGQQGPGQQGPGQQGPGQQGPGQQ
GPYGPASAAAAAGGYGPGSGQQGPGQQGPGQQGPGQQGPGQQ
GPYGPASAAAAAGGYGPGSGQQGPGQQGPGQQGPGQQGPGQQ
GPYGPASAAAAAGGYGPGSGQQGPGQQGPGQQGPGQQGPGQQ
GPYGPASAAAAAGGYGPGSGQQGPGQQGPGQQGPGQQGPGQQ
GAAASAVSGYGPQSSAPVASAAASRLSSPAASRVSSAVSSLVSS
GPTNQAALNTISSVVSQVSAASNPGLSGCDVLVQALLEVVSALVSLGSS

```

A unit = Alanine rich unit, highlighted in blue

Q unit = Glutamine rich unit, highlighted in green

Y amino acid = Tyrosines, highlighted in yellow

Figure 1. Full primary amino acid sequence for the (AQ)₁₂NR3 recombinant spider silk protein. The last two lines correspond to the helical C-terminal domain. The A and Q units as well as the Tyr residues are highlighted.

C-terminal domain facilitates the formation of a parallel-oriented dimer which is further stabilized by one conserved disulfide bridge, creating a protein with a molecular weight of approximately 120 kDa.²⁴ The underlying sequence is inspired by MaSp2 of *Araneus diadematus*, having shorter poly(Ala)₆ runs compared to MaSp1, juxtaposed by Gln–Gln dipeptide repeats, and a number of Pro residues, the hallmark of MaSp2 derivatives.²⁴ Lyophilized (AQ)₁₂NR3 protein can be reconstituted into either a biomimetic spinning dope (BSD) containing phosphate or classical spinning dope (CSD) in Tris buffer following previously published protocols.⁵

Currently, there are several groups trying to understand the aqueous spinning process from soluble proteins to fibers using recombinant proteins. However, none have provided a detailed and holistic view regarding the hierarchical assembly process across length scales from soluble proteins in different dope preparations through the spun fiber state. Here, we utilize a combination of solution and solid-state nuclear magnetic resonance (NMR), dynamic light scattering (DLS), and light microscopy to study the differences in (AQ)₁₂NR3 spider silk dope reconstituted under both biomimetic (preassembled) and classical conditions as well as the subsequent fibers produced after aqueous wet-spinning from both dopes. Our goal is to provide a full picture, from starting protein dope to the final fiber, of how the differences in silk spinning dope preparation dictate the downstream recombinant spider silk structure and mechanical properties.

METHODS

Protein Production, Isotope Labeling, and Purification. The engineered protein (AQ)₁₂NR3 bearing a N-terminal T7-tag (ASMTGGQQMGRGSM) was produced in fed-batch fermentation in *Escherichia coli* BL21Gold (DE3) using a pET29 vector. Initially, *E. coli* were grown in a complex medium at 25–30 °C for 12–14 h until

OD₆₀₀ of 30 was reached. Cells were harvested under sterile conditions by centrifugation at 5000 rpm for 20 min at room temperature. Next, the *E. coli* pellet was thoroughly washed twice and then resuspended in M9 medium supplemented with 20 g L⁻¹ ¹³C–glucose and 1.5 g L⁻¹ (¹⁵NH₄)₂SO₄. After induction with 0.1 mM IPTG, isotopically enriched proteins were produced at 25 °C for 14–16 h. Protein purification was carried out as reported previously.⁵ Two types of labeled proteins were used throughout the NMR experiments; proteins sparingly labeled with ¹³C–glucose/(¹⁵NH₄)₂SO₄ and those fully labeled with ¹³C–glucose/(¹⁵NH₄)₂SO₄. The ¹³C enrichment varied in the sparingly labeled material, reaching a maximum of approximately 30% for specific sites as anticipated.²⁵ Fully labeled materials were ¹³C-enriched to approximately 85% for several amino acids including Gly, Ala, and Gln.

Spinning Dope Preparation. The BSD and CSD were created as reported previously.⁵ Briefly, the protein was first dissolved in 6 M GdmSCN for several hours at a concentration between 10 and 25 mg/mL, then loaded into a dialysis bag, and dialyzed three times against a 50 mM Tris/HCl and 100 mM NaCl pH 8.0 buffer. Afterward, the CSD was prepared by dialysis against 20% w/v PEG (35 kDa) solution, while the BSD was obtained by dialysis against 30–50 mM sodium phosphate buffer pH 7.2 overnight. The final solution was then centrifuged at low speed to pellet the dope, and the top phase (supernatant) was immediately separated from the BSD.

Fiber Production. Fibers spun from (AQ)₁₂NR3 were produced as described previously.²⁶ Briefly, spinning dopes were extruded at flow rates of 50–150 μL h⁻¹ through a syringe into a microfluidic chip fixed in a coagulation bath filled with 80% isopropyl alcohol. Fibers were manually post-stretched to maximum and post-treated in 70% ethanol.

DLS and Microscopy of Dopes. For time-dependent analyses, CSD samples were taken after 0, 2, 4, and 6 h during PEG dialysis. To create a BSD, a protein solution was dialyzed against phosphate buffer for approximately 3 h, facilitating the phosphate ions to enter the dialysis bag. This represented the protein start solution (0 h); after additional 2 h of further dialysis, phase separation occurred, and samples were taken after 2, 4, and 6 h from the BSD as well as the supernatant. Dope concentrations were determined in triplicates using a nanophotometer (Implen P330). Samples above a concentration of 50 mg/mL were diluted in the respective buffer system to achieve high transmittance and reliable polydispersity index (PDI) values. DLS was done using an Anton Paar LitesizerTM 500 device and a Univette low-volume cuvette. All measurements were conducted at 20 °C and 1 min equilibration time. For each sample, 60 runs (each 10 s) have been performed. The manufacturer's suggested refractive index of protein, 1.4500, was used. The data were fitted using the protein analysis model for data processing. All dopes were analyzed using a stereomicroscope (Leica DMI3000B, software Leica V4.3). Structures found in the dope solutions were monitored with 20× and 40× object lenses and images were taken thereof.

Solution NMR of Dopes. Solution NMR including 1D proton and ¹³C direct detect, 2D ¹H–¹³C and ¹H–¹⁵N HSQC were collected with a 600 MHz Bruker AVANCE III spectrometer equipped with a 5 mm TXI HCN solution probe. The temperature was 25 °C and pH 7 for all NMR experiments. High-resolution 2D and 3D solution NMR experiments were also conducted using a Bruker AVANCE III 850 MHz spectrometer with a cryogenic HCN probe on a BSD sample to obtain high-resolution data and conduct backbone assignment. Typical experimental parameters included 16 scans with 384 points in the indirect dimension collected with 16 dummy scans and a recycle delay of 1.3 s for HSQC experiments. The ¹H and ¹⁵N sweep widths were 10 and 22 ppm, respectively. For 3D HNCACB²⁷ and CBCAcNH^{28,29} experiments, 64 scans were collected with 64 points in the ¹³C dimension and 112 points in the ¹⁵N dimension with 32 dummy scans and a recycle delay of 1 s. The sweep widths for the ¹H, ¹³C, and ¹⁵N dimensions were 10, 22, and 74 ppm, respectively. Experiments used 50% non-uniform sampling (NUS). The CSD and BSD were only used for a maximum of 4 days as judged by ¹H–¹⁵N HSQC, which yielded consistent spectra up to that time. Chemical

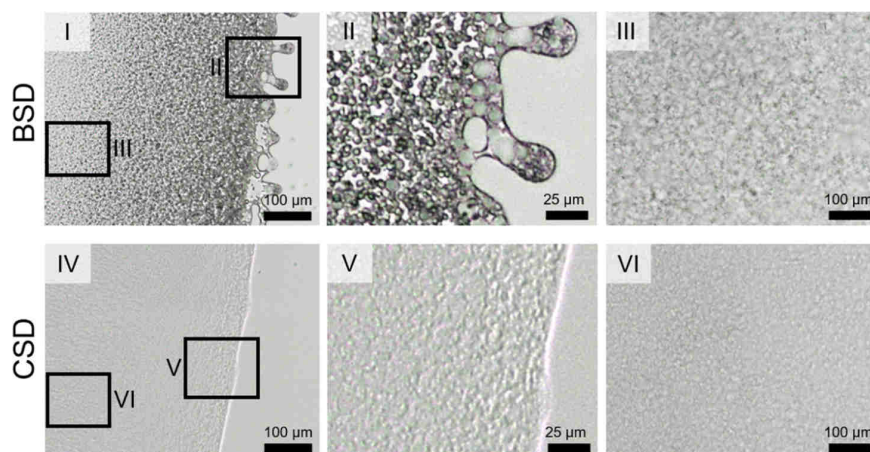


Figure 2. Light microscopy images of BSD (top, I–III) and CSD (bottom, IV–VI), both at a concentration of 100 mg/mL. Regions from (II,III,V,VI) are enlarged to see the differences between the systems, where the BSD contains large droplets indicative of LLPS.

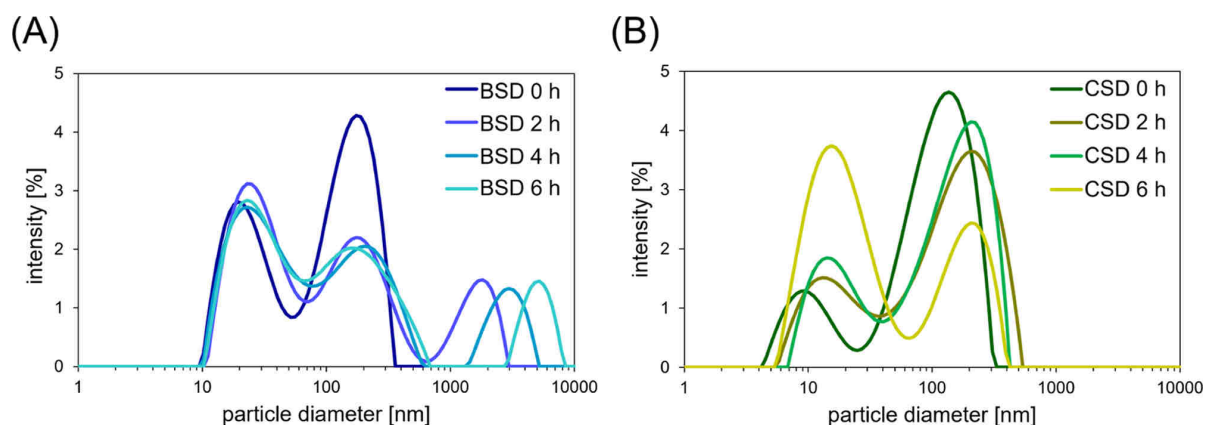


Figure 3. DLS of BSD (A) and CSD (B). Samples were taken after 0, 2, 4, and 6 h to follow the assembly process of the spinning solutions. After this, no further changes were observed, and the dope production was completed. During the assembly, the concentrations gradually increased. For the BSD, concentrations at 0, 2, 4, and 6 h were 27, 63, 96, and 177 mg/mL, respectively. For the CSD, concentrations at 0, 2, 4, and 6 h were 25, 41, 106, and 197 mg/mL, respectively. Details on spidroin diameters are given in Table S1.

shifts were referenced to sodium trimethylsilylpropanesulfonate (DSS) for ^1H and ^{13}C and externally referenced to formamide for ^{15}N . Secondary structure assignments were based on work from Jardetzky.³⁰ Approximately 300 μL of dope was used for all experiments, and the CSD and BSD concentrations were 12–20% w/v protein.

Solid-State NMR of Fibers. ^1H – ^{13}C cross-polarization magic-angle-spinning (CP-MAS) solid-state NMR (SSNMR) experiments were performed at 30 kHz MAS with 16,384 scans and a recycle delay of 3 s. Dipolar assisted rotational resonance (DARR) experiments^{31,32} were conducted at 14 kHz MAS with 256 scans, 256 points in the indirect dimension, and a recycle delay of 2.5 s with continuous wave decoupling under a rotary resonance ($\omega_r = \omega_{rf}$) of 14 kHz with a variable mixing time. Data was collected with mixing time of 50 and 500 ms to observe short- and long-range correlations, respectively. DARR difference experiments³³ were collected at 8–10 kHz MAS with either 4096 or 8192 scans using a recycle delay of 4 s. ^1H – ^{13}C HETCOR-FSLG experiments³⁴ were conducted at 30 kHz MAS with 256 scans and 256 points in the t1 dimension with a recycle delay of 2.5 s. The CP contact time for all experiments was 1 ms. Approximately 6–8 mg of sparingly $^{13}\text{C}/^{15}\text{N}$ -labeled (AQ)₁₂NR3 biomimetic and classical fibers were loaded separately into 1.9 mm rotors.

RESULTS AND DISCUSSION

Light microscopy reveals significant morphological differences between the CSD and BSD. For the BSD sample, there are clearly detectable liquid droplets between 5 and 25 μm , which are fully absent in the CSD sample (Figure 2). In the CSD sample, the droplets appear to bleed together creating a more continuous single phase. The key difference is the choice of buffer, where the BSD contains phosphate buffer and the CSD contains Tris/HCl buffer (pH 8). In the CSD, the presence of chaotropic ions promoted high interactions between the protein and the solvent. Kosmotropic phosphate ions in the BSD lead to protein assemblies and micron-scale liquid droplets by promoting protein–protein rather than protein–solvent interactions. Protein droplets arising from liquid–liquid phase separation (LLPS) may help to keep the proteins soluble until ready to be spun and could play a critical role in the pre-organization of silk proteins for the spinning process that occurs in the duct. This type of phase separation with phosphate has been recently seen in native and recombinant MaSp2 systems where the addition of phosphate produced a phase separation and subsequent fibrillization when the pH was dropped to acidic conditions.³⁵

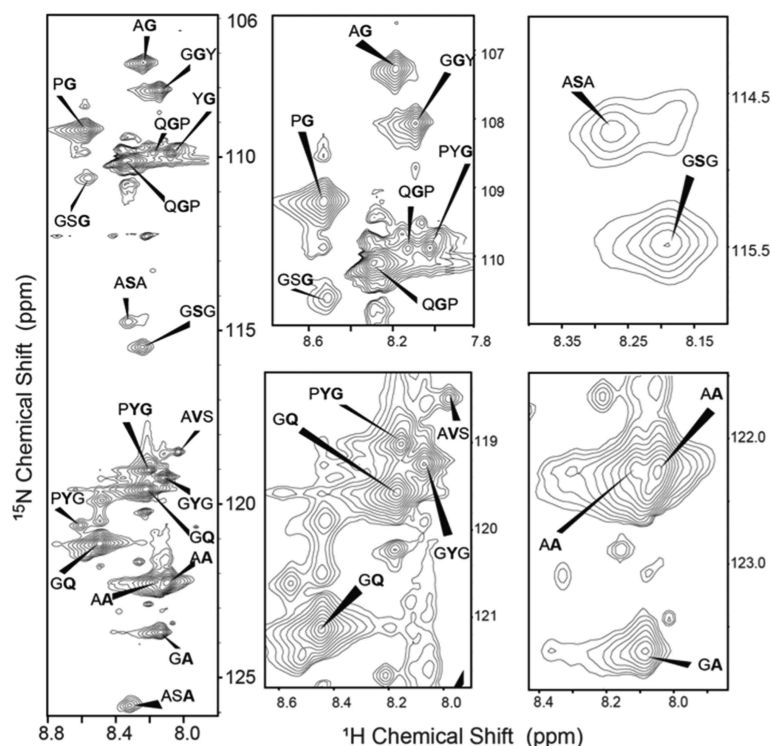


Figure 4. ^1H - ^{15}N HSQC NMR spectrum of the fully labeled $^{13}\text{C}/^{15}\text{N}$ -(AQ) $_{12}$ NR3 BSD collected at 850 MHz. Bolded amino acid indicates the resonance identity with di- and tri-peptide repeats based on 3D experiments (see the [Supporting Information](#)).

Although we see evidence of pre-assembly droplets with light microscopy, we know from previous work that this behavior also occurs at the mesoscale (100's of nm) for native systems where hierarchical silk protein micelle-like superstructures have been observed by diffusion NMR and cryoEM.³⁶ We therefore explored the size and population distributions of these proteins in solution at this length scale. Using DLS ([Figure 3](#) and [Table S1](#)), we monitored particle size over time and found that the size and population distribution of these pre-assemblies changed depending on buffer type. Typically, there were two major populations reported with DLS in the early dope formation process ([Figure 3A,B](#)). For a monomeric (653 amino acids, ~60 kDa) and dimeric (1306 amino acids, ~120 kDa) protein of this size, the predicted diameter based on the empirical relationship between the number of residues and diameter would be between ~18 and 26 nm depending on the degree of denaturation and monomer/dimer populations.³⁷ In both dopes, CSD and BSD, monomeric and dimeric proteins are present, as reflected by the small size populations ([Figure 3](#) and [Table S1](#)). The larger peak between 100 and 1000 nm is due to the formation of large, hierarchical assemblies and varies with sample and time. Since there are only two peaks in the CSD throughout the time course ([Figure 3B](#)); this suggests that during the concentration step of creating the dope, the monomer/dimer equilibrium coalesces to form pre-assemblies in one step, whereas in the BSD, this occurs gradually over time. The foundation for a high molecular structural order is set in the dope preparation. CSD samples were created by removing excess water from the protein solution, representing a forced assembly procedure. With decreasing water content,

spidroins presumably assemble over time in transient micelles (~200 nm) which dissolve again.

In the final BSD ([Figure 3A](#)), there are three predominant sizes present. The peaks at 20 and 200 nm appear consistent, suggesting that when the dope is formed, the proteins interact and form a consistent size, driven by the conditions of the buffer. Since phosphate increases the surface tension of water, hydrophobic interactions between poly(Ala) motifs cause the assembly of spidroins to larger structures, probably micelles (~200 nm), and continue to evolve micron-scale droplets (~3000 nm) over time. These results are in line with what we saw previously with light microscopy ([Figure 2](#)) that dopes prepared using a phosphate buffer create droplets larger in size than those created in the CSD. To understand the role of phosphate in creating these pre-assemblies, we used NMR to probe the atomic-level interactions that facilitate this behavior.

In order to understand atomic-level structural differences between dope preparations, we utilized 3D HNCACB and CBCAcoNH NMR experiments ([Figure S1](#)) to assign peaks in the ^1H - ^{15}N HSQC spectrum of the isotopically enriched BSD ([Figure 4](#)). In the HNCACB experiment, we found the ^{15}N chemical shift of the "i" amino acid and correlated that to the $\text{C}\alpha$ and $\text{C}\beta$ resonances of the same amino acid. This experiment also had the benefit of revealing the preceding $i - 1$ residue, which helped to further assign longer sequences of the protein together with the CBCAcoNH that provided assignment of the $i + 1$ residue. Using the primary amino acid sequence for (AQ) $_{12}$ NR3 as guidance ([Figure 1](#)), we were able to assign several di- and some tri-peptide motifs in the ^1H - ^{15}N HSQC ([Figure 4](#)). The bold letter indicates the "i" amino acid, which is assigned without ambiguity with corresponding $\text{C}\alpha$ and $\text{C}\beta$ shifts when applicable. Overall, this spectrum was

Table 1. Tabulated Solution NMR Chemical Shifts from HNCACB Strip Plots for BSD with Known Secondary Structure Assignments^{30a}

	¹⁵ N				¹³ C α				¹³ C β				¹ H (amide)			
	protein	α -helix	RC	β -sheet	protein	α -helix	RC	β -sheet	protein	α -helix	RC	β -sheet	protein	α -helix	RC	β -sheet
GGY	108.088	107.34	109.94	110.19	45.01	47.02	45.34	45.08					8.089	8.23	8.34	8.27
PG	109.204				45.184								8.524			
AG	107.329				45.211								8.194			
GSG	110.605				45.378								8.513			
YG	109.877				44.584								8.023			
QGP	110.14				44.497								8.301			
QGP	109.874				43.485								8.128			
ASA	114.748	114.78	115.94	117.44	58.713	60.86	58.35	57.14	63.465	62.81	63.88	65.39	8.277	8.11	8.26	8.57
GSG	115.467				58.69				63.94				8.192			
GQ	121.156	118.59	119.73	123.14	55.67	58.61	55.94	54.33	29.5	28.33	28.67	31.92	8.45	8.11	8.25	8.51
GQ	119.572				55.73				29.281				8.168			
PYG	119.019	119.67	120.05	122.55	57.318	61.07	57.72	56.56	38.609	38.38	38.71	40.79	8.154	8.10	7.90	8.69
PYG	120.27				57.98				39.68				8.59			
GY	119.264				57.578				38.88				8.066			
AA	122.29	121.65	123.52	125.57	52.69	54.86	52.67	50.86	18.74	18.27	19.03	21.72	8.05	7.99	8.11	8.59
AA	122.29				52.92				18.71				8.11			
GA	123.68				52.71				19.13				8.08			
ASA	125.825				53.17				18.684				8.276			
AVS	118.495	119.53	119.66	123.27	61.943	65.96	61.8	60.72	32.772	31.41	32.68	33.81	7.983	7.99	7.88	8.73

^aChemical shifts referenced to DSS.

similar to other ^1H - ^{15}N HSQCs we have collected previously on native MA silk dopes, where there are generally four regions residing near $^{15}\text{N} = 110, 115, 120,$ and 123 ppm,^{38,39} corresponding to regions where the “i” amino acid is Gly, Ser, X (X = Gln, Tyr, and Val), and Ala, respectively.

BSD chemical shifts are shown in Table 1 along with known secondary structure chemical shift perturbations. Most residues are readily assigned to random coil (RC) secondary structure, with a few exceptions where potential α -helices (AG, ASA, and GY) and β -sheets (GSG and ASA) are indicated from ^{15}N chemical shifts. However, when focus is placed on $C\alpha$ and $C\beta$ chemical shifts, all residues appear to be RC. The $C\alpha$ and $C\beta$ chemical shifts are the most reliable for secondary structure analysis because these sites cannot participate in hydrogen-bonding. Thus, it was interpreted that the differences observed in ^{15}N chemical shifts are likely an indication of hydrogen-bonding differences between the sites and are not necessarily an indicator of traditional secondary structure perturbations. Some of the ^{15}N chemical shift perturbations could be due to loop or β -turn structures due to the abundance of Pro in the sequence as can be seen with polyproline helical environments⁴⁰ and will be further expounded upon in a future publication.

Interestingly, we observed two distinct PYG sites even though there is only one PYG environment in the sequence (Figure 1). The population of the two sites has been determined (Figure S2) where the one at ^{15}N 120.3 ppm has a population of 11.4%. This is attributed to the presence of both *cis* and *trans* Pro where the Tyr following a *cis* or *trans* Pro is ascribed to ^{15}N 120.3 and 119.0 ppm, respectively. This interpretation is further supported by the ^{13}C direct detect solution NMR data discussed below. There are also unusually low Gly $C\alpha$ shifts observed for QGP that can be attributed to the following Pro in the sequence and not due to secondary structure effects.⁴¹

In order to compare the structure of the protein in the two different dopes, ^1H - ^{15}N HSQC spectra were collected for CSD and BSD and compared (Figure 5). The spectra are very similar exhibiting RC chemical shifts and low ^1H chemical shift dispersion (<0.5 ppm), which is the hallmark of intrinsically disordered proteins (IDPs).⁴² The Gly region (<110 ppm, ^{15}N) of the HSQC was nearly superimposable, showing no changes between the two dopes. However, small differences were observed in the Tyr (region 1), Gln (region 2), Ala (region 3), and Ser (region 4) environments. In the Tyr region, there was a small shift in the ^1H dimension to lower ppm for PYG units, indicating minor structural perturbations in these domains. There were also small shifts in the AV region and appearance of two new Ala environments and one new Ser environment (indicated with an *) in the BSD when compared to the CSD. The results indicated some subtle structural differences between the two dopes. However, the overall state of the protein is best defined as RC with the emergence of new Ala and Ser environments for the BSD, indicating changes in the more hydrophobic domains of the A-unit (Figure 1).

In order to examine more closely the structural differences of the protein in the two dopes, ^{13}C direct detect spectra were collected and compared for CSD and BSD, and these results are presented in Figure 6. ^{13}C direct detection experiments have been shown to provide valuable structural information with improved resolution for IDPs, as the ^{13}C dimension has a considerably larger chemical shift range compared to either ^1H or ^{15}N .^{42–46} Assignment in the ^{13}C NMR spectrum was based

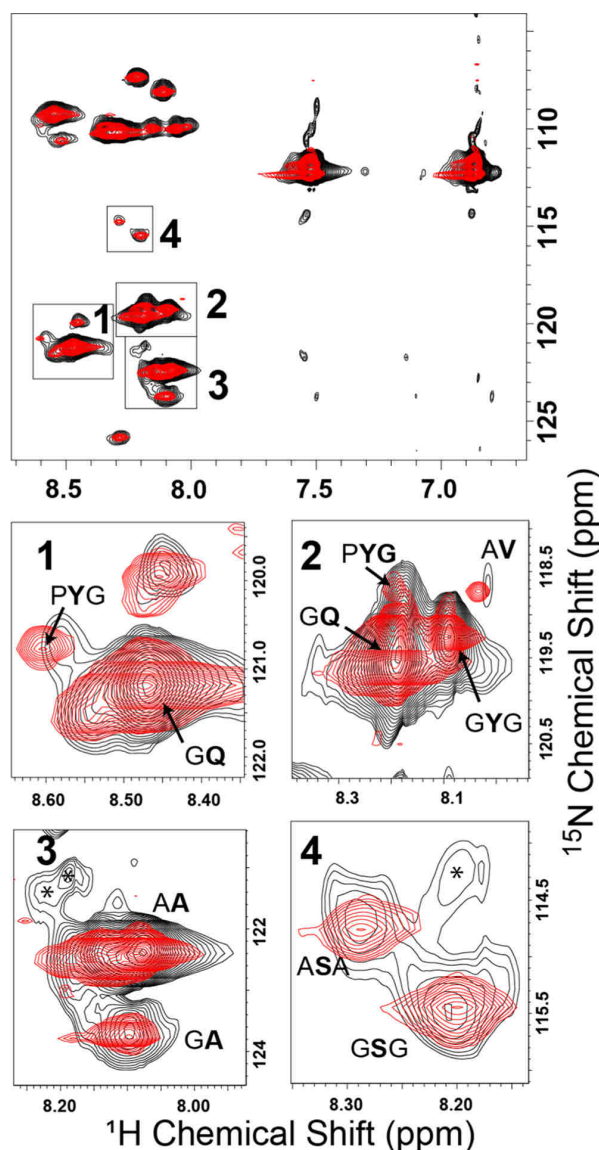


Figure 5. ^1H - ^{15}N HSQC NMR spectrum of the ^{15}N -labeled (AQ)₁₂NR3 CSD (red) and BSD (black) collected at 600 MHz. The assignment is based on the 3D experimental reports in the Supporting Information. The full HSQC is shown at the top with blowups of regions 1, 2, 3, and 4 shown below. New resonances observed in the BSD are marked with an asterisk (*) and are due to Ala and Ser environments.

on 3D (Figure S1) and ^1H - ^{13}C HSQC (Figure S3) NMR experiments. A number of subtle but interesting differences were observed between the two dopes in the ^{13}C solution NMR spectra. The first obvious difference was resonance line sharpening observed for the BSD when compared to the CSD. Line sharpening was most notable for the $C\beta$ Ala resonances GA, SA, and AA; Pro $C\alpha$ resonances GPY and GPG; and carbonyl resonances. IDPs like spider silk proteins display structural heterogeneity due to an ensemble of conformational environments. The observed line sharpening indicated that addition of phosphate in the BSD induced a degree of structural ordering. This pre-ordering of the silk protein prior

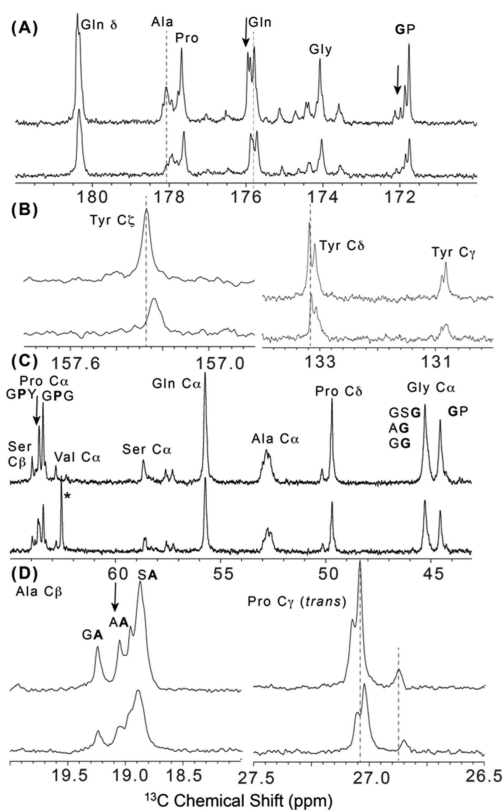


Figure 6. ^{13}C solution NMR spectrum of the $(\text{AQ})_{12}\text{NR3}$ CSD (bottom) and BSD (top) collected at 600 MHz. The carbonyl (A), aromatic (B), backbone (C), and aliphatic (D) regions of the spectrum are displayed. Resonances that exhibit notable line sharpening are indicated with arrows. Tris buffer signal is assigned an asterisk (*).

to fiber spinning in BSD suggests an important step that could lead to spun fibers with improved mechanical properties.

Other notable perturbations observed in the ^{13}C direct solution NMR spectrum of the two dopes included slight chemical shifts to higher ppm for the Pro $\text{C}\gamma$ resonances, the Tyr aromatic ring environment, and the Tyr C–OH moiety with a pronounced shift for the Ala carbonyl resonance. This indicated that these environments are the most impacted by the BSD environment. One thing that stood out was the change observed for the Tyr aromatic C–OH ($\text{C}\zeta$), which also exhibited a line width that is $\sim 2\times$ sharper in the BSD. The importance of the Tyr environment in the final spun fibers (discussed below) and differences observed in Tyr ring interactions could be traced back to some unique differences in the two dopes where the Tyr environment was significantly more ordered for the BSD likely due to hydrogen-bonding differences between the two dopes resulting in varying Tyr ring packing. The Tyr ring and hydrogen-bonding interactions have previously been implicated as a driving force in a number of protein systems that undergo LLPS including RNA-binding proteins^{47,48} and His- and Tyr-rich squid beak-derived peptides.^{49,50} The pronounced shift for Ala carbonyl resonance also indicated an increased ordering effect for this environment, showing that there is a notable effect on poly(Ala) in the BSD.

The last thing to note from the ^{13}C solution NMR data was the observation of Pro in cis/trans environments that were well resolved in the Pro $\text{C}\gamma$ region (Figure S2). Integration of these two resonances allowed an estimation of cis/trans fraction that was $\sim 12.3\%$ (CSD) and $\sim 17.5\%$ (BSD) in rough agreement with the 11.4% determined from the two different PYG environments that were attributed to Pro conformational differences (discussed above). However, fractions of cis/trans were similar in the two dopes with the only difference being a slight chemical shift to higher ppm observed in the BSD dope. Cis/trans Pro has been implicated in a number of protein folding problems, and the population of cis/trans here was quite high compared to other protein systems⁵¹ but in line with Pro-containing peptides⁵² which far exceeded those observed in other IDP-containing Pro, where the population is typically only a few %.

Using ^{13}C SSNMR, we investigated the secondary structural differences between lyophilized proteins before fiber spinning and fibers spun from CSD and BSD dopes. The ^{13}C CP-MAS SSNMR spectra of the three samples are shown in Figure 7.

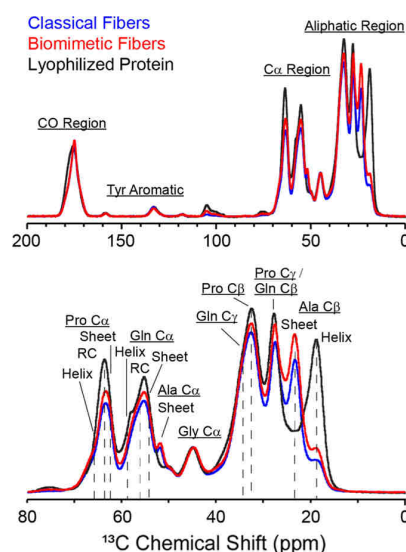


Figure 7. ^1H – ^{13}C CP-MAS SSNMR spectrum of sparsely labeled $^{13}\text{C}/^{15}\text{N}$ – $(\text{AQ})_{12}\text{NR3}$ -lyophilized protein (black) and fibers spun from the BSD (blue) and CSD (red). Full spectrum (top) and blowup of the low ppm region (bottom) are shown.

Several chemical shift differences were readily observed when comparing the lyophilized proteins and two fiber types. Most notably, both spun fiber samples displayed an Ala $\text{C}\beta$ resonance positioned at 23.3 ppm, reflecting a considerably higher amount of β -sheet structure for both spun fibers compared to the lyophilized powder that is dominated by RC conformation based on the Ala $\text{C}\beta$ resonance positioned at 18.3/18.4 ppm. In order to determine the content of Ala in the β -sheet structure, the ^{13}C CP-MAS SSNMR spectra were fit to determine that the Ala β -sheet conversion during fiber spinning which is identical for both the CSD and BSD fibers, exhibiting a 77% β -sheet content (Figure S4). When considering the primary amino acid sequence (Figure 1), 79% of Ala were present in the repetitive region as poly(Ala)₆ repeats and one Ala present in the flanking Gly–Ala–Ser unit with the remaining Ala present in the C-terminus. This result

indicated that most if not all the Ala present in the repetitive region were converted to the β -sheet structure when spun into fibers with the C-terminal Ala remaining RC.

2D ^{13}C – ^{13}C correlation spectra at both short (50 ms) and long (500 ms) mixing times were collected to extract all ^{13}C chemical shifts for the abundant amino acids (Gly, Ala, Gln, Pro, and Tyr) of spun fibers, and comparisons were made to native dragline silk fibers and known secondary structures (Figure 8 and Table 2).^{53–57} In the 2D ^{13}C – ^{13}C DARR

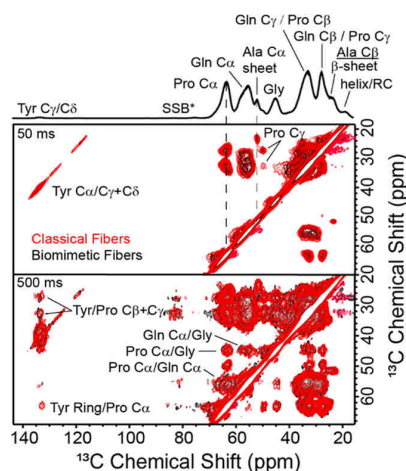


Figure 8. 2D ^{13}C – ^{13}C DARR SSNMR correlation spectra collected with 50 ms (top) and 500 ms (bottom) mixing times for CSD (red) and BSD (black) fibers.

SSNMR experiment, magnetization exchange occurs between ^{13}C nuclei that are near in space (<5 Å) via dipolar interactions.^{31,32,57} Specifically, short mixing times (50 ms)

allowed for accurate assignment of intramolecular chemical shifts, whereas long mixing times (500 ms) allowed for intermolecular contacts between amino acids that are close in space.⁵⁷ In order to confirm 2D DARR assignments, we deployed a method developed by our lab called 1D DARR difference with Gaussian pulse selection.³³ In this experiment, a ^{13}C resonance of interest is selected with a Gaussian shaped pulse, followed by a DARR mixing to allow magnetization exchange to occur between nearby nuclei. The result is a 1D spectrum where each signal corresponds to only nuclei close in space, allowing for selection of just a single amino acid site in a typically crowded spectrum if one of the amino acid site is resolvable. This experiment was used to confirm 2D DARR assignments and make some difficult assignments such as the individual CO for each amino acid site (Figure S5).

When comparing the ^{13}C chemical shifts for the spun fibers to native dragline silks, near-identical chemical shifts were observed (Table 1), reflecting the structural similarity between the recombinant fibers and native spider silks with the CSD and BSD fibers displaying nearly identical chemical shifts. Ala is dominated by a β -sheet secondary structure with Tyr and Gln residing in disordered helical domains as indicated by the observed ^{13}C chemical shifts in the RC region. Gly, similar to spider dragline silk, displayed structural heterogeneity for the CO resonance and was present in β -sheet and disordered structures. This indicated that Gly is located in regions that flank (Gly–Ala–Ser) the β -sheet forming poly(Ala) domains were likely β -sheet in the fibers with the remaining Gly in Pro-rich regions and the terminal region residing in β -turn and RC, helical structures, respectively. One notable difference is the lack of heterogeneity in the Ala C β resonance in the recombinant fibers. In dragline spider silk, there were three distinct environments observed, while in the spun recombinant fibers, only two (β -sheet and RC) environments were observed. In native dragline spider silk, there were two β -

Table 2. ^{13}C Chemical Shifts (ppm) from SSNMR of BSD and CSD Fibers, Native Dragline Spider Silk,^{5,53–557} and Known Secondary Structure Assignments.^{56a}

residue	BSD	CSD	native dragline	α -helix	RC	β -sheet
Ala C α	51.6	51.6	51.0/51.2/52.0	54.7	52.5	50.9
Ala C β	18.3/23.3	18.4/23.3	19.4/22.9/25.3	18.4	19.3	21.7
Ala CO	174.6	174.6	174.5/174.6/176.1	179.0	177.0	175.7
Pro C α	63.3	63.3	62.7	65.3	63.1	62.7
Pro C β	32.2	32.2	32.5	31.5	32.0	32.2
Pro C γ	27.5	27.5	27.4	27.7	27.2	27.3
Pro C δ	49.3	49.6	49.5	50.2	50.3	50.5
Pro CO	176.3	176.3	176.8	177.5	176.2	176.0
Gln C α	54.9	54.9	54.9	58.3	55.7	54.5
Gln C β	30.1	30.1	34.0	28.6	29.5	31.5
Gln C γ	33.8	33.8	35.2	33.8	33.7	33.8
Gln CO	175.1	175.1	174.1	177.3	175.5	178
Gly C α	44.8	44.8	45.3	46.7	45.2	45.2
Gly CO	171.5/173.4	172.0/174.2	173.0	175.3	173.8	172.1
Tyr C α			57.0	60.6	57.6	56.6
Tyr C β	40.3	40.5	40.3	38.1	39.0	41.1
Tyr C γ	133.1	133.3	129.0	130.1	127.7	129.5
Tyr C δ	133.1	133.2	132.0	132.0	132.6	132.7
Tyr C ϵ	118.2	118.0	115.7	117.8	117.9	117.8
Tyr C ζ	158.7	158.5	157.2	157.8	158.1	155.9
Tyr CO	173.0	173.0	174.2	177.0	175.1	174.3

^aChemical shifts referenced to DSS.

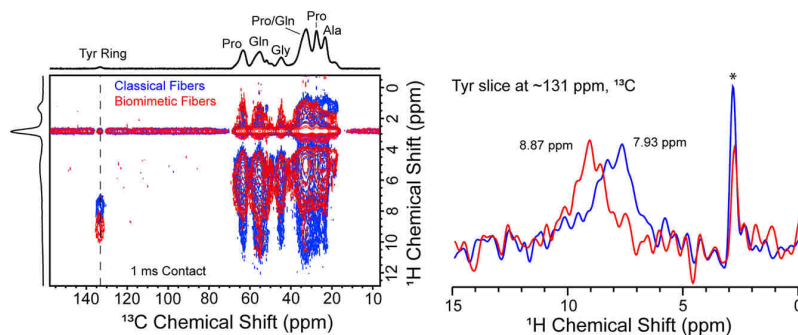


Figure 9. 2D ^1H – ^{13}C HETCOR SSNMR spectrum collected with FSLG homonuclear proton decoupling for CSD (blue) and BSD (red) fibers. Slices were extracted at the Tyr side-chain resonance (right) to illustrate the differences between the ^1H chemical shift of the Tyr aromatic ring for the two fibers. This downfield (high ppm) ^1H chemical shift in the BSD fibers is also observed in the $\text{C}\alpha$ region but not in the aliphatic region. The DC offset glitch due to FSLG homonuclear decoupling is indicated with an asterisk (*).

sheet environments that are ascribed to poly(Ala) and Ala present in Gly–Ala regions flanking the poly(Ala) runs that form β -sheets. Since the repetitive region of the recombinant protein is dominated by poly(Ala) (>80%) with the other potential Ala site residing in Gly–Ala–Ser units flanking poly(Ala), this result indicated that this Ala exhibits a similar β -sheet structure to poly(Ala). Another possibility is that it is too low in abundance to observe, which is additionally complicated by the fact that this site (~ 25.3 ppm) would overlap the Pro $\text{C}\gamma$ resonance ~ 27.5 ppm.

At longer mixing times (500 ms) in the 2D ^{13}C – ^{13}C DARR, inter-residue correlations between several residues approximately 0.3–0.5 nm away are observed.^{57,58} This allowed for the determination of several key amino acids and their correlations such as Gln $\text{C}\alpha$ /Gly $\text{C}\alpha$, Pro $\text{C}\alpha$ /Gly $\text{C}\alpha$, Pro $\text{C}\alpha$ /Gln $\text{C}\alpha$, and Tyr $\text{C}\gamma + \delta$ /Pro $\text{C}\beta + \gamma$ (Figure 8, 500 ms). Unfortunately, it was difficult to determine if inter-residue interactions (Tyr/Pro and Pro/Gln) were occurring between strands or within the same strand because these residues are neighbors in the primary sequence (Figure 1). With improved resolution from the 2D DARR, we were able to extract slices correlating the Pro $\text{C}\alpha/\beta/\gamma$ sites and determined its secondary structure (Figure S6). By calculating the difference in chemical shift between the Pro $\text{C}\beta$ and $\text{C}\gamma$ resonances, we were able to show that Pro in both CSD and BSD fibers adopted an elastin-like β -turn structure.⁵⁹ This is similar to previous reports regarding a Pro secondary structure in *A. aurantia* spider dragline silk.⁵⁴

A correlation was also observed between the Tyr ring and Pro $\text{C}\alpha$ in the fiber samples; however, this peak was on the threshold of noise in the 2D spectrum. In order to further probe this interaction, the 1D DARR difference experiment was used (Figure S7).³³ In this experiment, the ^{13}C resonance of interest (Tyr aromatic ring) was selected with a Gaussian-shaped pulse, followed by a DARR mixing period to allow magnetization exchange to occur between nearby nuclei. By conducting experiments with variable DARR mixing time, it is possible to spatially probe distances from the site of interest (in this case, the Tyr aromatic ring). This experiment was similar in principle to a 2D DARR, with added selectivity for resonances of interest in a one-dimensional fashion and benefits from improved S/N compared to 2D experiments.³³ By targeting the Tyr aromatic ring that was fully resolved in the 1D spectrum, strong contacts were observed to the other Tyr sites as expected and Pro sites as indicated from the 2D

^{13}C – ^{13}C DARR (Figure 8, 500 ms). Tyr–Pro inter-residue build-up occurs between the Tyr ring and the Pro $\text{C}\alpha$, $\text{C}\beta$, and $\text{C}\gamma$ resonances. This provided evidence for Tyr aromatic–Pro ring interactions which are well-known in proteins and typically result from interactions between the π aromatic face of Tyr and polarizable C–H bond-denoted CH/π interactions.⁶⁰ This result was not too surprising when considering that Pro–Tyr is a common repeating unit in the sequence (Figure 1). However, the possibility of long-range, inter-strand Pro–Tyr interactions should not be discounted and have been shown to be present in a number of systems.⁶⁰

SSNMR 2D heteronuclear correlation experiments (^1H – ^{13}C HETCOR) were implemented to correlate ^1H and ^{13}C nuclei close in space. Because of the strong ^1H dipole-coupling network in proteins, high MAS speeds were required to average out these effects in combination with LG ^1H homonuclear decoupling. From the 2D HETCOR spectrum, we saw two major differences between the BSD and CSD fibers (Figure 9). First, the region between approximately 50–65 ppm corresponding to the $\text{C}\alpha$ backbone of the protein appears shifted downfield (to high ppm) in the ^1H dimension for BSD (red) compared to CSD fibers (blue). The same was true for the Tyr ring region at 131 ppm, ^{13}C . In fact, the shifts downfield for the protons on the Tyr ring were more dramatic than those seen in the $\text{C}\alpha$ backbone region. This suggested that the Tyr ring and the $\text{C}\alpha$ groups in BSD are located in a more polar environment, shifting their ^1H resonances downfield. The Tyr ring is shifted nearly 1 ppm higher in the BSD compared to CSD fibers suggesting differences in Tyr ring packing between the two fibers. One possibility is that there are differences in Tyr π – π stacking or other Tyr π -related interactions (excluding the Pro–Tyr interactions which are similar in both systems, Figure S7) between the two fibers as aromatic ring interactions are known to greatly perturb aromatic ^1H chemical shifts, resulting in aromatic chemical shift shielding effects for systems exhibiting strong π stacking interactions.^{61,62} This Tyr packing difference could be traced back to the dope starting material where differences in the Tyr environment were observed (Figure 6) that might help drive LLPS, resulting in Tyr structural perturbations observed in the final spun fibers when comparing CSD and BSD systems.

CONCLUSIONS

Through a combination of biophysical methods, recombinant spider silk protein assembly was tracked from the assembly of

the dope to the final spun fiber for biomimetic and classically prepared dopes. Light microscopy and DLS revealed that these recombinant silk protein transition from a low- to high-density phase through two different processes depended on buffer conditions. Protein dopes containing phosphate buffer (BSD) transitioned from monomer/dimers to pre-assemblies gradually over time and ultimately achieved LLPS in the final highly concentrated dope. Dopes that did not contain phosphate transitioned from monomers/dimers to pre-assemblies but stopped short of forming large liquid–liquid droplets on the micron-scale. Solution NMR illustrated that the recombinant protein is present in a RC conformation in both dopes; however, subtle but distinct differences were observed when comparing the two dopes. BSD exhibits sharper resonance lines for a number of environments in ^{13}C solution NMR spectra, illustrating a protein pre-ordering in the BSD together with some distinct differences in the Tyr aromatic ring environment due to hydrogen-bonding differences at the C–OH moiety and presumably perturbations in aromatic ring packing between the two dopes. A distinct difference in the Tyr aromatic ring environment was also observed in the final fibers where a large downfield chemical shift was observed for the aromatic ^1H resonances in ^1H – ^{13}C HETCOR SSNMR spectra when comparing BSD and CSD fibers, indicating a more polar environment in the former. These results pointed to the importance of Tyr in spider silk assembly where clear differences were observed for this environment in both dopes and the spun fibers that could help explain the significant difference in the mechanical properties observed when comparing CSD and BSD spun fibers. It also highlights the importance of tracking the non- β -sheet disordered helical domains in spider silk formation as both systems display similar poly(Ala) β -sheet conversion (77%) and Pro conformations but distinct differences in the Tyr environments which are present in non- β -sheet domains. This work lays the foundation for future studies to interrogate atomic and mesoscale interactions in recombinant spider silk dope preparations and spun fibers, where a number of important interactions remain to be elucidated.

■ ASSOCIATED CONTENT

SI Supporting Information

The Supporting Information is available free of charge at <https://pubs.acs.org/doi/10.1021/acs.biomac.2c01467>.

DLS particle size analysis, strip plots for 3D solution NMR, $^1\text{H}/^{15}\text{N}$ and $^1\text{H}/^{13}\text{C}$ HSQC solution NMR, spectral fitting of ^{13}C CP-MAS SSNMR, Pro ^{13}C SSNMR analysis, and 1D ^{13}C DARR difference spectra (PDF)

■ AUTHOR INFORMATION

Corresponding Author

Gregory P. Holland – Department of Chemistry and Biochemistry, San Diego State University, San Diego, California 92182-1030, United States; orcid.org/0000-0003-3062-3391; Email: gholland@sdsu.edu

Authors

Dillan Stengel – Department of Chemistry and Biochemistry, San Diego State University, San Diego, California 92182-1030, United States

Merisa Saric – Lehrstuhl Biomaterialien, Fakultät für Ingenieurwissenschaften, Universität Bayreuth, Bayreuth 95447, Germany

Hannah R. Johnson – Department of Chemistry and Biochemistry, San Diego State University, San Diego, California 92182-1030, United States

Tim Schiller – Lehrstuhl Biomaterialien, Fakultät für Ingenieurwissenschaften, Universität Bayreuth, Bayreuth 95447, Germany

Johannes Diehl – Lehrstuhl Biomaterialien, Fakultät für Ingenieurwissenschaften, Universität Bayreuth, Bayreuth 95447, Germany

Kevin Chalek – Department of Chemistry and Biochemistry, San Diego State University, San Diego, California 92182-1030, United States

David Onofrei – Department of Chemistry and Biochemistry, San Diego State University, San Diego, California 92182-1030, United States

Thomas Scheibel – Lehrstuhl Biomaterialien, Fakultät für Ingenieurwissenschaften, Universität Bayreuth, Bayreuth 95447, Germany

Complete contact information is available at:

<https://pubs.acs.org/10.1021/acs.biomac.2c01467>

Notes

The authors declare no competing financial interest.

■ ACKNOWLEDGMENTS

D.S. and M.S. were the primary authors of the paper. All authors commented and edited the final version of the manuscript. T.S. acknowledges financial support from the Office of Naval Research Global, Office of Naval Research, and the Air Force Office of Scientific Research, contract number N62909-20-1-2068. G.P.H. acknowledges financial support from DOD-AFOSR under the award number FA9550-20-1-0103. Additional funding was received from the Bavaria California Technology Center for research-related travel under project 2[2019-1]. Technical support from Dr. Brian Cherry at Arizona State University for collection of the 850 MHz NMR data is also acknowledged.

■ REFERENCES

- Blackledge, T. A.; Swindeman, J. E.; Hayashi, C. Y. Quasistatic and continuous dynamic characterization of the mechanical properties of silk from the cobweb of the black widow spider *Latrodectus hesperus*. *J. Exp. Biol.* **2005**, *208*, 1937–1949.
- Gosline, J.; Lillie, M.; Carrington, E.; Guerette, P.; Ortlepp, C.; Savage, K. Elastic proteins: biological roles and mechanical properties. *Philos. Trans. R. Soc. London, Ser. B* **2002**, *357*, 121–132.
- Swanson, B. O.; Blackledge, T. A.; Beltrán, J.; Hayashi, C. Y. Variation in the material properties of spider dragline silk across species. *Appl. Phys. A* **2005**, *82*, 213–218.
- Lewis, R. Spider Silk: Ancient Ideas for New Biomaterials. *Chem. Rev.* **2006**, *106*, 3762–3774.
- Heidebrecht, A.; Eisoldt, L.; Diehl, J.; Schmidt, A.; Geffers, M.; Lang, G.; Scheibel, T. Biomimetic fibers made of recombinant spidroins with the same toughness as natural spider silk. *Adv. Mater.* **2015**, *27*, 2189–2194.
- Lang, G.; Neugirg, B. R.; Kluge, D.; Fery, A.; Scheibel, T. Mechanical Testing of Engineered Spider Silk Filaments Provides Insights into Molecular Features on a Mesoscale. *ACS Appl. Mater. Interfaces* **2017**, *9*, 892–900.
- Xu, M.; Lewis, R. Structure of a Protein Superfiber: Spider Dragline Silk. *Proc. Natl. Acad. Sci. U.S.A.* **1990**, *87*, 7120–7124.

- (8) Hinman, M.; Lewis, R. V. Isolation of a clone encoding a second dragline silk fibroin. *Nephila clavipes* dragline silk is a two-protein fiber. *J. Biol. Chem.* **1992**, *267*, 19320–19324.
- (9) Ayoub, N. A.; Garb, J. E.; Tinghitella, R. M.; Collin, M. A.; Hayashi, C. Y. Blueprint for a High-Performance Biomaterial: Full-Length Spider Dragline Silk Genes. *PLoS One* **2007**, *2*, No. e514.
- (10) An, B.; Hinman, M. B.; Holland, G. P.; Yarger, J. L.; Lewis, R. V. Inducing β -Sheets Formation in Synthetic Spider Silk Fibers by Aqueous Post-Spin Stretching. *Biomacromolecules* **2011**, *12*, 2375–2381.
- (11) An, B.; Jenkins, J. E.; Sampath, S.; Holland, G. P.; Hinman, M.; Yarger, J. L.; Lewis, R. Reproducing Natural Spider Silks' Copolymer Behavior in Synthetic Silk Mimics. *Biomacromolecules* **2012**, *13*, 3938–3948.
- (12) Albertson, A. E.; Teulé, F.; Weber, W.; Yarger, J. L.; Lewis, R. V. Effects of different post-spin stretching conditions on the mechanical properties of synthetic spider silk fibers. *J. Mech. Behav. Biomed. Mater.* **2014**, *29*, 225–234.
- (13) Tucker, C. L.; Jones, J. A.; Bringhurst, H. N.; Copeland, C. G.; Addison, J. B.; Weber, W. S.; Mou, Q.; Yarger, J. L.; Lewis, R. V. Mechanical and physical properties of recombinant spider silk films using organic and aqueous solvents. *Biomacromolecules* **2014**, *15*, 3158–3170.
- (14) Andersson, M.; Jia, Q.; Abella, A.; Lee, X. Y.; Landreh, M.; Purhonen, P.; Hebert, H.; Tenje, M.; Robinson, C. V.; Meng, Q.; Plaza, G. R.; Johansson, J.; Rising, A. Biomimetic spinning of artificial spider silk from a chimeric minispidroin. *Nat. Chem. Biol.* **2017**, *13*, 262–264.
- (15) Bowen, C. H.; Dai, B.; Sargent, C. J.; Bai, W.; Ladiwala, P.; Feng, H.; Huang, W.; Kaplan, D. L.; Galazka, J. M.; Zhang, F. Recombinant Spidroins Fully Replicate Primary Mechanical Properties of Natural Spider Silk. *Biomacromolecules* **2018**, *19*, 3853–3860.
- (16) Knight, D. P.; Vollrath, F. Changes in element composition along the spinning duct in a *Nephila* spider. *Naturwissenschaften* **2001**, *88*, 179–182.
- (17) Dicko, C.; Kenney, J. M.; Knight, D.; Vollrath, F. Transition to a β -Sheet-Rich Structure in Spidroin in Vitro: The Effects of pH and Cations. *Biochemistry* **2004**, *43*, 14080–14087.
- (18) Askarieh, G.; Hedhammar, M.; Nordling, K.; Saenz, A.; Casals, C.; Rising, A.; Johansson, J.; Knight, S. D. Self-assembly of Spider Silk Proteins is Controlled by a pH-sensitive Relay. *Nature* **2010**, *465*, 236–238.
- (19) Tillinghast, E. K.; Chase, S. F.; Townley, M. A. Water Extraction by the Major Ampullate Duct During Silk Formation in the Spider, *Argiope Aurantia* Lucas. *J. Insect Physiol.* **1984**, *30*, 591–596.
- (20) Eisoldt, L.; Hardy, J. G.; Heim, M.; Scheibel, T. R. The role of salt and shear on the storage and assembly of spider silk proteins. *J. Struct. Biol.* **2010**, *170*, 413–419.
- (21) Koski, K. J.; McKiernan, K.; Akhenblit, P.; Yarger, J. L. Shear-induced rigidity in spider silk glands. *Appl. Phys. Lett.* **2012**, *101*, 103701.
- (22) Vollrath, F.; Knight, D. P. Liquid crystalline spinning of spider silk. *Nature* **2001**, *410*, 541–548.
- (23) Johansson, J.; Rising, A. Doing What Spiders Cannot—A Road Map to Supreme Artificial Silk Fibers. *ACS Nano* **2021**, *15*, 1952–1959.
- (24) Huemmerich, D.; Helsen, C. W.; Quedzuweit, S.; Oschmann, J.; Rudolph, R.; Scheibel, T. Primary Structure Elements of Spider Dragline Silks and Their Contribution to Protein Solubility. *Biochemistry* **2004**, *43*, 13604–13612.
- (25) Lundström, P.; Teilum, K.; Carstensen, T.; Bezsonova, I.; Wiesner, S.; Hansen, D. F.; Religa, T. L.; Akke, M.; Kay, L. E. Fractional ^{13}C enrichment of isolated carbons using $[1-^{13}\text{C}]$ - or $[2-^{13}\text{C}]$ -glucose facilitates the accurate measurement of dynamics at backbone α and side-chain methyl positions in proteins. *J. Biomol. NMR* **2007**, *38*, 199–212.
- (26) Saric, M.; Eisoldt, L.; Döring, V.; Scheibel, T. Interplay of Different Major Ampullate Spidroins during Assembly and Implications for Fiber Mechanics. *Adv. Mater.* **2021**, *33*, No. e2006499. From NLM PubMed-not-MEDLINE
- (27) Meissner, A.; Sørensen, O. W. Sequential HNCACB and CBCANH protein NMR pulse sequences. *J. Magn. Reson.* **2001**, *151*, 328–331.
- (28) Grzesiek, S.; Bax, A. Amino acid type determination in the sequential assignment procedure of uniformly $^{13}\text{C}/^{15}\text{N}$ -enriched proteins. *J. Biomol. NMR* **1993**, *3*, 185–204.
- (29) Muhandiram, D. R.; Kay, L. E. Gradient-Enhanced Triple-Resonance Three-Dimensional NMR Experiments with Improved Sensitivity. *J. Magn. Reson., Ser. B* **1994**, *103*, 203–216.
- (30) Wang, Y.; Jardetzky, O. Probability-based protein secondary structure identification using combined NMR chemical-shift data. *Protein Sci.* **2002**, *11*, 852–861.
- (31) Takegoshi, K.; Nakamura, S.; Terao, T. ^{13}C - ^1H dipolar-assisted rotational resonance in magic-angle spinning NMR. *Chem. Phys. Lett.* **2001**, *344*, 631–637.
- (32) Takegoshi, K.; Nakamura, S.; Terao, T. ^{13}C - ^1H dipolar-driven ^{13}C - ^{13}C recoupling without ^{13}C rf irradiation in nuclear magnetic resonance of rotating solids. *J. Chem. Phys.* **2003**, *118*, 2325–2341.
- (33) Addison, B.; Stengel, D.; Bharadwaj, V. S.; Happs, R. M.; Doeppke, C.; Wang, T.; Bomble, Y. J.; Holland, G. P.; Harman-Ware, A. E. Selective One-Dimensional (^{13}C) - (^{13}C) Spin-Diffusion Solid-State Nuclear Magnetic Resonance Methods to Probe Spatial Arrangements in Biopolymers Including Plant Cell Walls, Peptides, and Spider Silk. *J. Phys. Chem. B* **2020**, *124*, 9870–9883.
- (34) van Rossum, B. J.; Förster, H.; de Groot, H. J. M. High-Field and High-Speed CP-MAS ^{13}C NMR Heteronuclear Dipolar-Correlation Spectroscopy of Solids with Frequency-Switched Lee–Goldburg Homonuclear Decoupling. *J. Magn. Reson.* **1997**, *124*, 516–519.
- (35) Malay, A. D.; Suzuki, T.; Katashima, T.; Kono, N.; Arakawa, K.; Numata, K. Spider silk self-assembly via modular liquid-liquid phase separation and nanofibrillation. *Sci. Adv.* **2020**, *6*, 1–12.
- (36) Parent, L. R.; Onofrei, D.; Xu, D.; Stengel, D.; Roehling, J. D.; Addison, J. B.; Forman, C.; Amin, S. A.; Cherry, B. R.; Yarger, J. L.; Gianneschi, N. C.; Holland, G. P. Hierarchical spidroin micellar nanoparticles as the fundamental precursors of spider silks. *Proc. Natl. Acad. Sci. U. S. A.* **2018**, *115*, 11507–11512.
- (37) Wilkins, D. K.; Grimshaw, S. B.; Receveur, V.; Dobson, C. M.; Jones, J. A.; Smith, L. J. Hydrodynamic Radii of Native and Denatured Proteins Measured by Pulse Field Gradient NMR Techniques. *Biochemistry* **1999**, *38*, 16424–16431.
- (38) Xu, D.; Yarger, J. L.; Holland, G. P. Exploring the backbone dynamics of native spider silk proteins in Black Widow silk glands with solution-state NMR spectroscopy. *Polymer* **2014**, *55*, 3879–3885.
- (39) Onofrei, D.; Stengel, D.; Jia, D.; Johnson, H. R.; Trescott, S.; Soni, A.; Addison, B.; Muthukumar, M.; Holland, G. P. Investigating the Atomic and Mesoscale Interactions that Facilitate Spider Silk Protein Pre-Assembly. *Biomacromolecules* **2021**, *22*, 3377–3385.
- (40) Treviño, M. A.; Pantoja-Uceda, D.; Menéndez, M.; Gomez, M. V.; Mompeán, M.; Laurents, D. V. The Singular NMR Fingerprint of a Polyproline II Helical Bundle. *J. Am. Chem. Soc.* **2018**, *140*, 16988–17000. From NLM PubMed-not-MEDLINE
- (41) Schwarzynger, S.; Kroon, G. J. A.; Foss, T. R.; Chung, J.; Wright, P. E.; Dyson, H. J. Sequence-Dependent Correction of Random Coil NMR Chemical Shifts. *J. Am. Chem. Soc.* **2001**, *123*, 2970–2978.
- (42) Brutscher, B.; Felli, I. C.; Gil-Caballero, S.; Hošek, T.; Kümmerle, R.; Piai, A.; Pierattelli, R.; Solyom, Z. NMR Methods for the Study of Intrinsically Disordered Proteins Structure, Dynamics, and Interactions: General Overview and Practical Guidelines. In *Intrinsically Disordered Proteins Studied by NMR Spectroscopy*; Felli, I. C., Pierattelli, R., Eds.; Springer International Publishing, 2015; pp 49–122.
- (43) Felli, I. C.; Pierattelli, R. *Advances in Experimental Medicine and Biology*; Springer, 2014.

(44) Barbet-Massin, E.; Pell, A. J.; Knight, M. J.; Webber, A. L.; Felli, I. C.; Pierattelli, R.; Emsley, L.; Lesage, A.; Pintacuda, G. ^{13}C -detected through-bond correlation experiments for protein resonance assignment by ultra-fast MAS solid-state NMR. *Chemphyschem* **2013**, *14*, 3131–3137.

(45) Bertini, I.; Felli, I. C.; Kümmerle, R.; Moskau, D.; Pierattelli, R. ^{13}C – ^{13}C NOESY: An Attractive Alternative for Studying Large Macromolecules. *J. Am. Chem. Soc.* **2004**, *126*, 464–465.

(46) Felli, I. C.; Pierattelli, R. ^{13}C Direct Detected NMR for Challenging Systems. *Chem. Rev.* **2022**, *122*, 9468–9496. From NLM Medline

(47) Murthy, A. C.; Dignon, G. L.; Kan, Y.; Zerze, G. H.; Parekh, S. H.; Mittal, J.; Fawzi, N. L. Molecular interactions underlying liquid–liquid phase separation of the FUS low-complexity domain. *Nat. Struct. Mol. Biol.* **2019**, *26*, 637–648. From NLM Medline

(48) Lin, Y.; Currie, S. L.; Rosen, M. K. Intrinsically disordered sequences enable modulation of protein phase separation through distributed tyrosine motifs. *J. Biol. Chem.* **2017**, *292*, 19110–19120. From NLM Medline

(49) Gabryelczyk, B.; Cai, H.; Shi, X.; Sun, Y.; Swinkels, P. J. M.; Salentinig, S.; Pervushin, K.; Miserez, A. Hydrogen bond guidance and aromatic stacking drive liquid-liquid phase separation of intrinsically disordered histidine-rich peptides. *Nat. Commun.* **2019**, *10*, 5465. From NLM Medline

(50) Lim, J.; Kumar, A.; Low, K.; Verma, C. S.; Mu, Y.; Miserez, A.; Pervushin, K. Liquid-Liquid Phase Separation of Short Histidine- and Tyrosine-Rich Peptides: Sequence Specificity and Molecular Topology. *J. Phys. Chem. B* **2021**, *125*, 6776–6790. From NLM Medline

(51) Alderson, T. R.; Lee, J. H.; Charlier, C.; Ying, J.; Bax, A. Propensity for cis-Proline Formation in Unfolded Proteins. *Chembiochem* **2018**, *19*, 37–42. From NLM Medline

(52) Sarkar, S. K.; Young, P. E.; Sullivan, C. E.; Torchia, D. A. Detection of cis and trans X-Pro peptide bonds in proteins by ^{13}C NMR: application to collagen. *Proc. Natl. Acad. Sci. U.S.A.* **1984**, *81*, 4800–4803. (accessed 2022/10/18)

(53) Holland, G. P.; Jenkins, J. E.; Creager, M. S.; Lewis, R. V.; Yarger, J. L. Quantifying the fraction of glycine and alanine in beta-sheet and helical conformations in spider dragline silk using solid-state NMR. *Chem. Commun. (Cambridge, U. K.)* **2008**, 5568–5570.

(54) Jenkins, J. E.; Creager, M. S.; Butler, E. B.; Lewis, R. V.; Yarger, J. L.; Holland, G. P. Solid-state NMR evidence for elastin-like β -turn structure in spider dragline silk. *Chem. Commun. (Cambridge, U. K.)* **2010**, *46*, 6714–6716.

(55) Izdebski, T.; Akhenblit, P.; Jenkins, J. E.; Yarger, J. L.; Holland, G. P. Structure and Dynamics of Aromatic Residues in Spider Silk: 2D Carbon Correlation NMR of Dragline Fibers. *Biomacromolecules* **2010**, *11*, 168–174.

(56) Fritzsche, K. J.; Yang, Y.; Schmidt-Rohr, K.; Hong, M. Practical use of chemical shift databases for protein solid-state NMR: 2D chemical shift maps and amino-acid assignment with secondary-structure information. *J. Biomol. NMR* **2013**, *56*, 155–167. From NLM Medline

(57) Holland, G. P.; Creager, M. S.; Jenkins, J. E.; Lewis, R. V.; Yarger, J. L. Determining Secondary Structure in Spider Dragline Silk by Carbon–Carbon Correlation Solid-State NMR Spectroscopy. *J. Am. Chem. Soc.* **2008**, *130*, 9871–9877.

(58) Hong, M.; Schmidt-Rohr, K. Magic-Angle-Spinning NMR Techniques for Measuring Long-Range Distances in Biological Macromolecules. *Acc. Chem. Res.* **2013**, *46*, 2154–2163.

(59) Kricheldorf, H. R.; Mueller, D. Secondary structure of peptides. 3. Carbon-13 NMR cross polarization/magic angle spinning spectroscopic characterization of solid polypeptides. *Macromolecules* **1983**, *16*, 615–623.

(60) Zondlo, N. J. Aromatic-Proline Interactions: Electronically Tunable CH/ π Interactions. *Acc. Chem. Res.* **2013**, *46*, 1039–1049.

(61) Venkataramana, G.; Sankararaman, S. Synthesis and Spectroscopic Investigation of Aggregation through Cooperative π – π and C–H \cdots O Interactions in a Novel Pyrene Octaldehyde Derivative. *Org. Lett.* **2006**, *8*, 2739–2742.

(62) Nandy, R.; Subramoni, M.; Varghese, B.; Sankararaman, S. Intramolecular π -Stacking Interaction in a Rigid Molecular Hinge Substituted with 1-(Pyrenylethynyl) Units. *J. Org. Chem.* **2007**, *72*, 938–944.

Recommended by ACS

Injectable Colloidal Hydrogels of N-Vinylformamide Microgels Dispersed in Covalently Interlinked pH-Responsive Methacrylic Acid-Based Microgels

Xuelian Wang, Brian R. Saunders, *et al.*

APRIL 07, 2023
BIOMACROMOLECULES

READ 

Controlling the Trimerization of the Collagen Triple-Helix by Solvent Switching

Qi Zhang, Yang Li, *et al.*

MARCH 27, 2023
BIOMACROMOLECULES

READ 

Composition and Charge Compensation in Chitosan/Gum Arabic Complex Coacervates in Dependence on pH and Salt Concentration

Philipp Schröder, Comelia Cramer, *et al.*

FEBRUARY 13, 2023
BIOMACROMOLECULES

READ 

Direct and Efficient Incorporation of DOPA into Resilin-Like Proteins Enables Cross-Linking into Tunable Hydrogels

Ya-Jiao Zhu, Xiao-Xia Xia, *et al.*

MARCH 23, 2023
BIOMACROMOLECULES

READ 

Get More Suggestions >

Supporting Information:

**Tyrosine's Unique Role in the Hierarchical Assembly of Recombinant Spider
Silk Proteins: From Spinning Dope to Fibers**

Dillan Stengel¹, Merisa Saric², Hannah R. Johnson¹, Tim Schiller², Johannes Diehl², Kevin Chalek¹, David Onofrei¹, Thomas Scheibel², Gregory P. Holland^{1,}*

¹Department of Chemistry and Biochemistry, San Diego State University, 5500 Campanile Dr. San Diego CA, 92182-1030 USA

²Lehrstuhl Biomaterialien, Fakultät für Ingenieurwissenschaften, Universität Bayreuth, Prof.-Rüdiger-Bormann-Str.1, 95447 Bayreuth, Germany

Tab S1: Overview of dynamic light scattering (DLS) results for particle size analysis of different (AQ)₁₂NR3 spinning dopes. Spidroin concentration, the average particle sizes (Peak 1 to 3) and their respective standard deviations (SD 1 to 3), as well as polydispersity index (PDI) are given.

Sample Name	Concentration [mg/ml]	Peak 1 [nm]	SD 1 [nm]	Peak 2 [nm]	SD 2 [nm]	Peak 3 [nm]	SD 3 [nm]	PDI [%]
BSD 0 h	27	26	8	163	83	-	-	29
BSD 2 h	63	18	5	148	56	1608	1121	28
BSD 4 h	96	23	8	214	118	2430	653	22
BSD 6 h	177	17	6	203	124	5032	1553	25
CSD 0 h	25	7	2	172	169	-	-	27
CSD 2 h	41	17	6	191	141	-	-	29
CSD 4 h	106	18	6	176	122	-	-	28
CSD 6 h	197	25	11	244	118	-	-	24

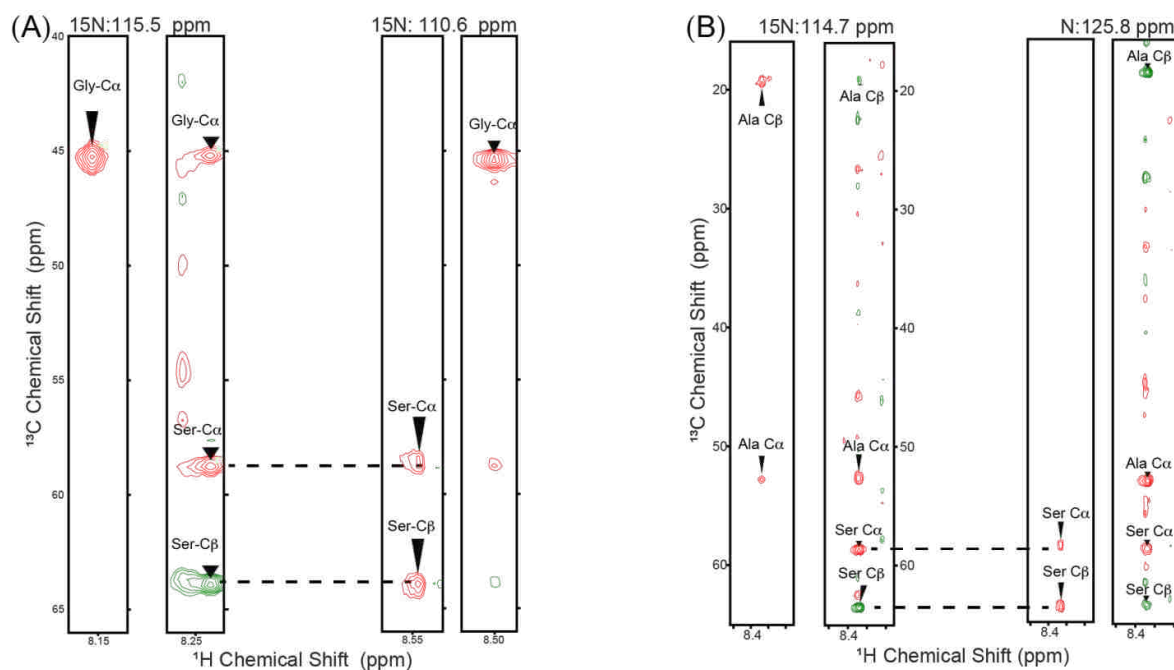


Fig. S1. Strip plots showing a representative strategy used to assign di- and tri-peptide sequences for the recombinant spider silk protein, (AQ)₁₂NR3. Paired CBCAcoNH (left) and HNCACB (right) are shown for the assignment of Gly-Ser-Gly (A) and Ala-Ser-Ala (B).

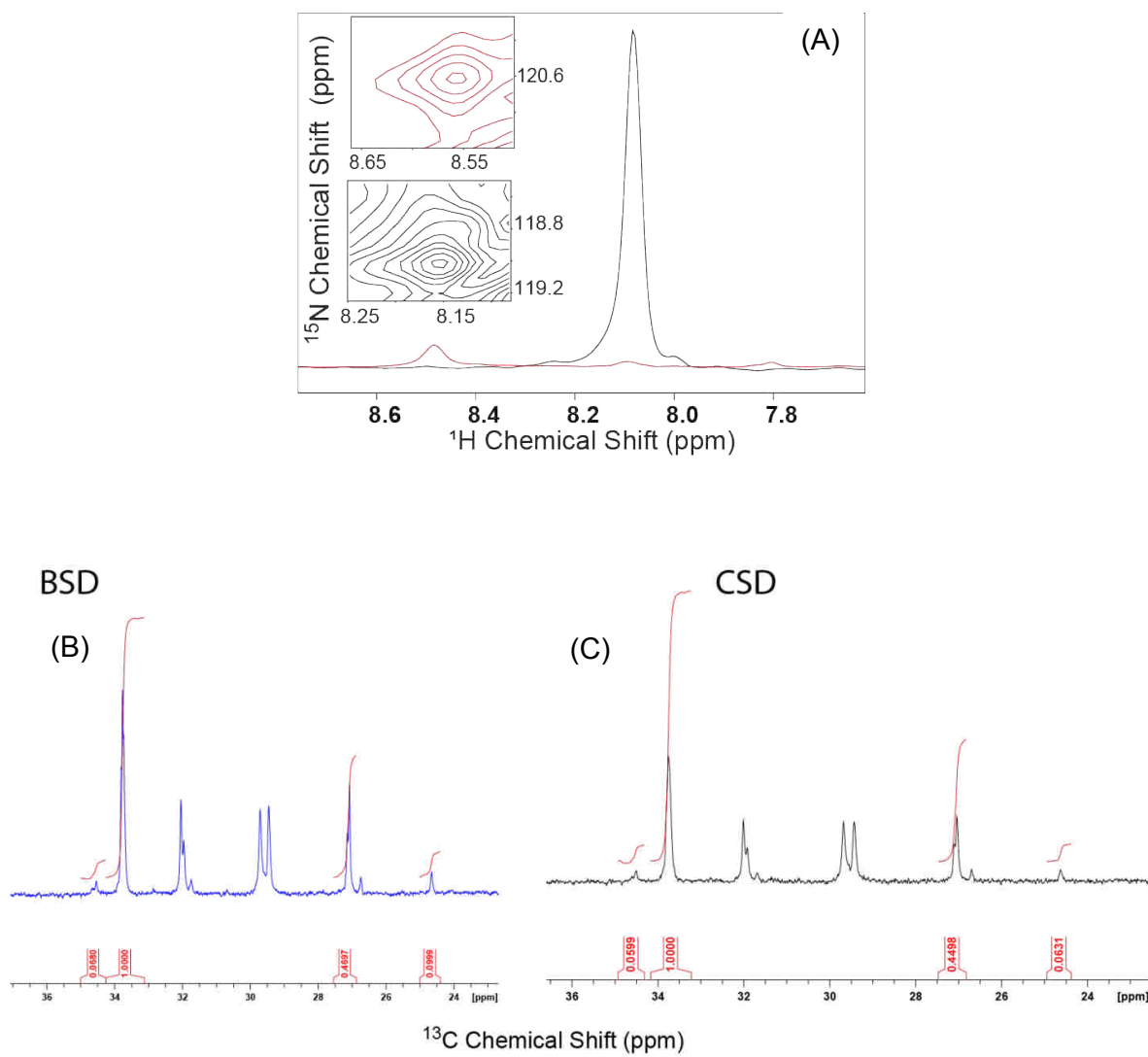


Fig. S2. ^1H - ^{15}N HSQC solution NMR spectrum BSD showing two PYG sites, the low population site is 11.4% and attributed to Tyr following *cis* Pro (top). The ^{13}C solution NMR spectrum of (B) BSD and (C) CSD. The Pro C γ resonance was used to quantify the *cis/trans* ratio for Pro that is 12.3% and 17.5% for CSD and BSD, respectively.

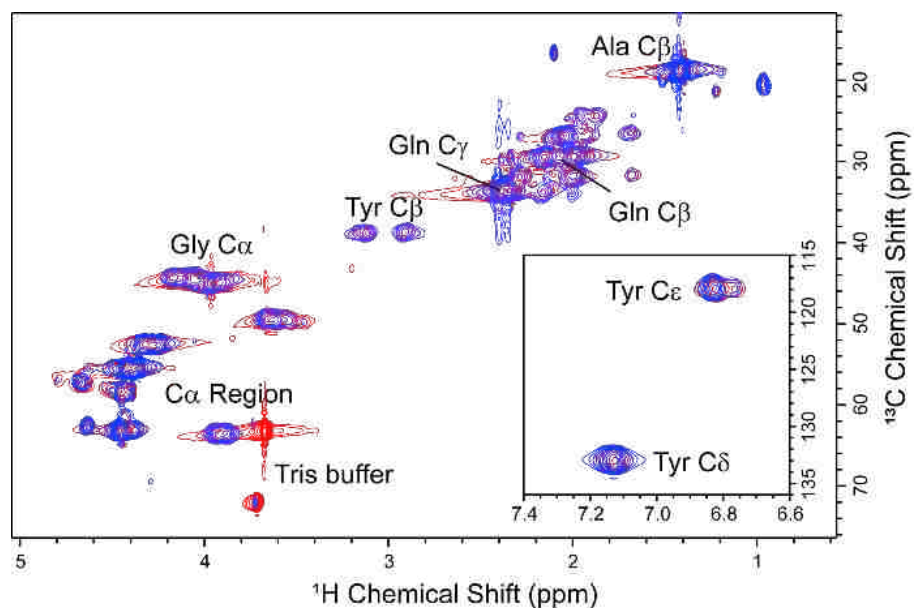


Fig. S3. ^1H - ^{13}C HSQC solution NMR spectrum CSD (red) and BSD (blue). This spectrum was used to confirm some assignments of the ^{13}C NMR spectrum presented in the main text. The protein here was sparingly labeled with ^{13}C glucose.

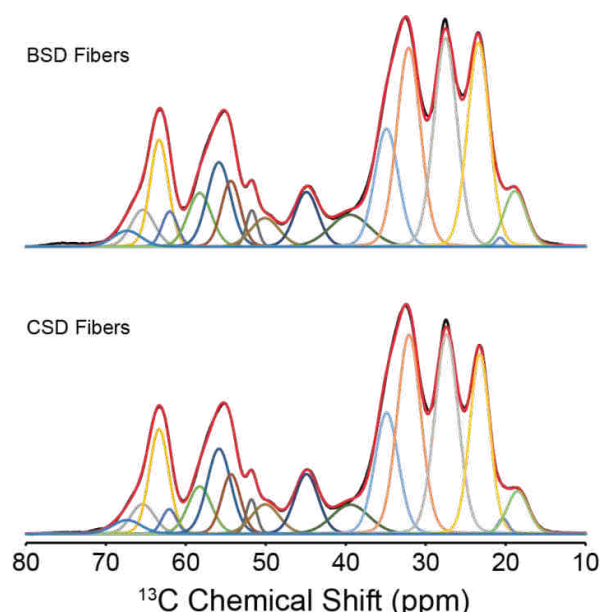


Fig. S4. Spectral fitting of BSD (top) and CSD (bottom) ^{13}C CP-MAS SSNMR spectra of spun fibers. The fraction of poly(Ala) in β -sheet conformation was determined from the Ala C β resonance (15-25 ppm) to be 77% for both fiber types.

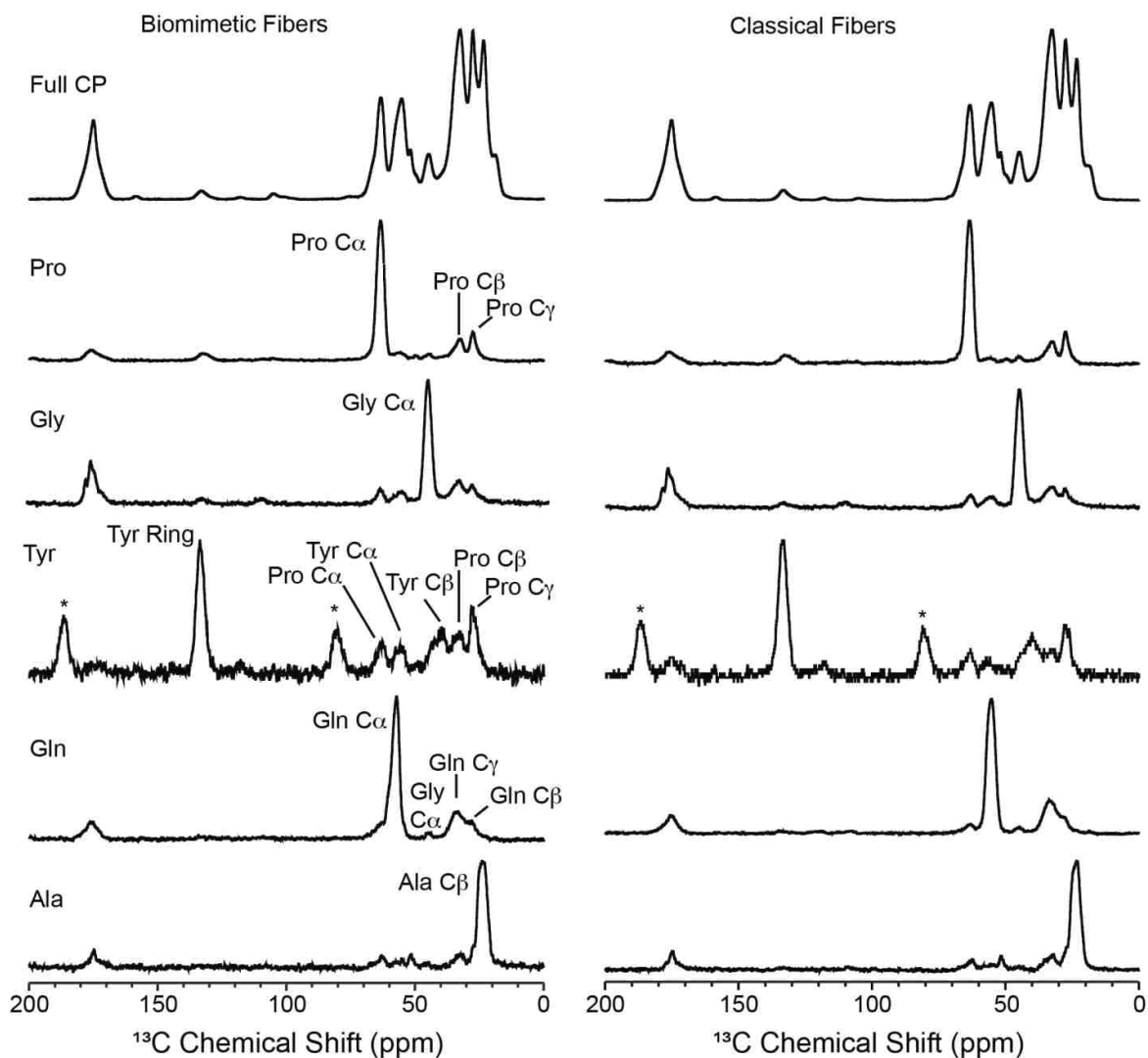


Fig. S5. Through-space ^{13}C 1D DARR difference SSNMR experiment with gaussian selection pulse applied on well resolved site for each amino acid. The selected site is the strongest signal in each the spectrum (Pro $\text{C}\alpha$, Gly $\text{C}\alpha$, Tyr ring, Gln $\text{C}\alpha$ and Ala $\text{C}\beta$). Spectra were collected at 10 kHz MAS (8 kHz for Tyr) with a DARR mixing time of 500 ms to probe long range contacts. This enables the detection of all sites within in a given amino acid and long-range inter-residue contacts. BSD and CSD fibers are displayed to the left and right, respectively. Spinning sidebands (SSBs) are assigned an asterisk (*). Strong inter-residue dipolar contacts are observed between a number of sites as discussed in the main text. The full standard ^{13}C CP-MAS spectrum is shown at the top for comparison purposes.

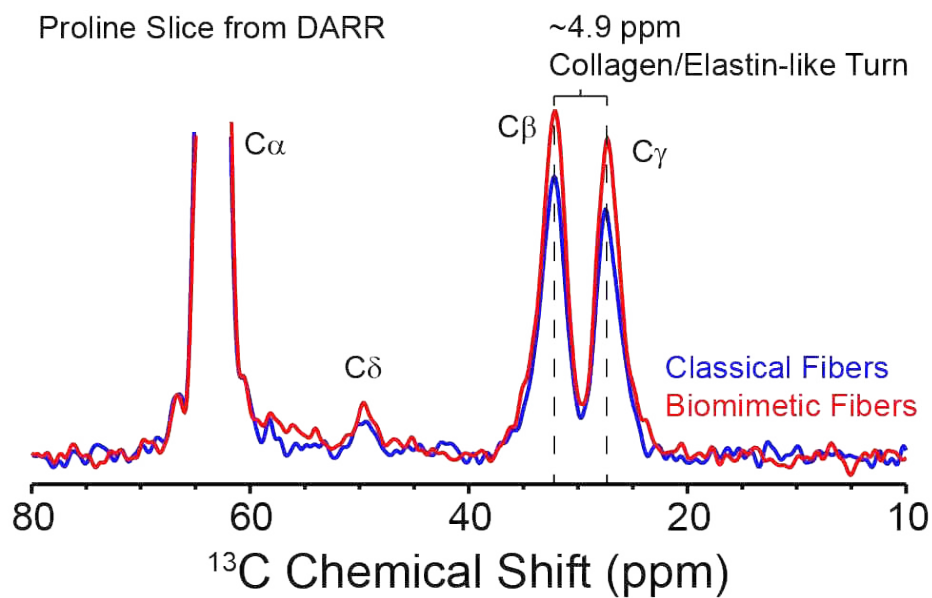


Fig. S6. Slice extracted from DARR spectra at Pro $\text{C}\alpha$ resonance (~ 63 ppm) for both CSD (blue) and BSD (red) fibers. By taking the difference in chemical shift between the Pro $\text{C}\beta$ and $\text{C}\gamma$ resonances, it is possible to determine the secondary structure of Pro. The results indicate that Pro in both CSD and BSD fibers have an elastin-like type II β -turn secondary structure.

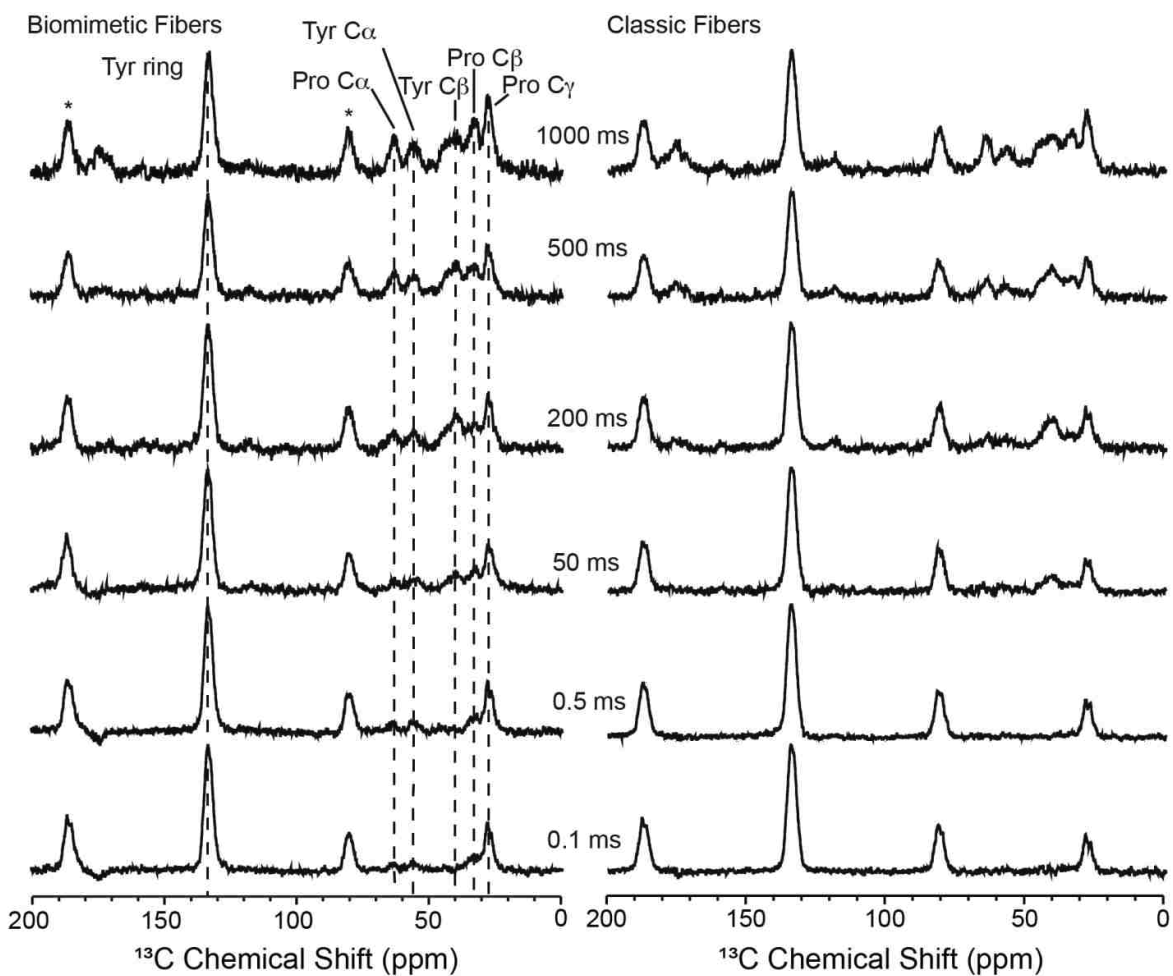


Fig. S7. Through-space ^{13}C 1D DARR difference SSNMR experiment with gaussian selection pulse applied on the Tyr ring resonance. Spectra were collected at 8 kHz MAS as a function of DARR mixing time as indicated in the figure. BSD and CSD fibers are displayed to the left and right, respectively. Spinning sidebands (SSBs) are assigned an asterisk (*). Strong inter-residue dipolar contacts are observed between the Tyr ring and Pro sites. Buildups are nearly indistinguishable between the two fibers.

DANKSAGUNG

An dieser Stelle möchte ich mich bei allen bedanken, die mich auf unterschiedliche Art und Weise unterstützt und somit zu dieser Arbeit beigetragen haben.

Zuerst geht ein großer Dank an meinen Doktorvater Prof. Dr. Thomas Scheibel, der mir ermöglicht hat auf diesem interessanten Projekt zu promovieren. Danke für die wissenschaftlichen Diskussionen und Anregungen, aber auch für die Freiheiten meine Ideen umzusetzen, was maßgeblich zu meiner wissenschaftlichen sowie persönlichen Entwicklung beigetragen hat.

Weiterhin möchte ich mich bei Herrn Prof. Dr. Holger Kress und Frau Prof. Dr. Birte Höcker für die Übernahme meines Mentorats bedanken.

Außerdem möchte ich mich bei meinen Kooperations- und Publikationspartnern bedanken:

- › Dr. Lukas Eisoldt, Volker Döring, Tim Schiller und Johannes Diehl
- › Prof. Dr. Gregory Holland, Dr. Dillan Stengel, Dr. David Onofrei, Dr. Kevin Chalek und Hannah Johnson

Bei meinen lieben Kollegen möchte ich mich für die großartige Unterstützung bedanken:

- › Dem gesamten (T)A-Team Johannes Diehl, Andreas Schmidt, Nicole Pittel, Alexandra Pellert, Claudia Stemmann, Eva Möller und Heike Haase für die Hilfe im Laboralltag.
- › Dem „gewissenhaftesten TA der Welt“ Johannes Diehl und dem „schnellsten TA der Welt“ Andreas Schmidt für die Hilfe bei Fermentation und Reinigung, aber auch für eure Ratschläge, Motivation (u.a. auch in Form von Energie-haltigen Getränken) und besonders für euren Humor!
- › Andrea Bodner, Sabrina Schwägerl und Christa Vogl für die Bewältigung unzähliger organisatorischer Herausforderungen.
- › Dr. Hendrik Bargel und Claudia Stemmann für REM Aufnahmen.
- › PD Dr. Martin Humenik und Dr. Sarah Lentz für AFM Aufnahmen.
- › Anika Winkler und Dr. Tamara Aigner-Bogner für TEM-Aufnahmen.
- › Dr. Christian Haynl für die Einweisungen in die Mikrofluidik.

- › PD Dr. Martin Humenik für sein wissenschaftliches Coaching - angefangen mit meinem Forschungsmodul, über die Masterarbeit hinweg bis hin zur Doktorarbeit.
- › Meiner Arbeitsgruppe *Protein Folding & Modification* für den wissenschaftlichen Input.
- › Meinen Praktikantinnen Angelika Häussermann, Yeldem Koç-Köhler, Leonie Veh, Tiziana Nicola und Michelle Schäper für die Unterstützung innerhalb meiner Projekte.
- › Dem gesamten Admin-Team, insbesondere Kai Mayer, Julia Jasinski, Shakir Zainuddin, Dr. Thomas Gruhn, Dr. Sarah Lentz und Dr. Vanessa Neubauer für die Überwindung vieler IT Hürden.
- › Allen aktuellen und ehemaligen Kollegen des Lehrstuhls Biomaterialien für den einmaligen Zusammenhalt, die tolle Arbeitsatmosphäre, die Mittagspausen und die vielen unvergesslichen Erinnerungen.
- › Dr. Stephen Strassburg und Dr. Elise Liensdorf fürs Korrekturlesen von Manuskripten.
- › Stefan Bindereif, Dr. Stephen Strassburg und dem Jungle Office für das Korrekturlesen dieser Arbeit.

Ein besonderer Dank gilt meinen „Jungle Office“ Freunden Anika (+ Charly), Vanessa (+ Viby), Annika, Sarah und Wicki für die unzähligen interessanten, tiefsinnigen und vor allem lustigen Gespräche sowie die erlebnisreiche Zeit #Soulmates #Hangouts #CoffeeTime #Brennpunkte. Speziell bedanke ich mich auch bei meinen TAO-Bürokolleginnen: Anika für den unvergesslichen Teamspirit all die Jahre (!) und Kim für den mentalen Endphasen-Mindset-Meme-Support. Tim danke ich für die gewissenhafte Ausübung seines wöchentlichen Wahlrechts #GottaCatch‘EmAll

Zuletzt möchte ich mich aus tiefstem Herzen bei meiner gesamten Familie bedanken, allen voran bei meiner bewundernswerten Mutter Jasmina – du bist meine beste Freundin und mein Vorbild! Danke, für deine endlose Unterstützung, Kraft und Liebe in allen Lebenslagen, du hast mir das beste Fundament für mein Leben bereitet.

Ein ganz besonderer Dank geht an meinen Schatz Stefan - Vielen Dank für deine Liebe, für die unzähligen wertvollen Momente und dafür, dass du mein nie endender Brunnen für Motivation, Glück und Freude bist!

EIDESSTATTLICHE VERSICHERUNGEN UND ERKLÄRUNGEN

(§ 9 Satz 2 Nr. 3 PromO BayNAT)

Hiermit versichere ich eidesstattlich, dass ich die Arbeit selbständig verfasst und keine anderen als die von mir angegebenen Quellen und Hilfsmittel benutzt habe (vgl. Art. 64 Abs. 1 Satz 6 BayHSchG).

(§ 9 Satz 2 Nr. 3 PromO BayNAT)

Hiermit erkläre ich, dass ich die Dissertation nicht bereits zur Erlangung eines akademischen Grades eingereicht habe und dass ich nicht bereits diese oder eine gleichartige Doktorprüfung endgültig nicht bestanden habe.

(§ 9 Satz 2 Nr. 4 PromO BayNAT)

Hiermit erkläre ich, dass ich Hilfe von gewerblichen Promotionsberatern bzw. -vermittlern oder ähnlichen Dienstleistern weder bisher in Anspruch genommen habe noch künftig in Anspruch nehmen werde.

(§ 9 Satz 2 Nr. 7 PromO BayNAT)

Hiermit erkläre ich mein Einverständnis, dass die elektronische Fassung meiner Dissertation unter Wahrung meiner Urheberrechte und des Datenschutzes einer gesonderten Überprüfung unterzogen werden kann.

(§ 9 Satz 2 Nr. 8 PromO BayNAT)

Hiermit erkläre ich mein Einverständnis, dass bei Verdacht wissenschaftlichen Fehlverhaltens Ermittlungen durch universitätsinterne Organe der wissenschaftlichen Selbstkontrolle stattfinden können.

Bayreuth, den